DEVELOPMENT OF RELIABLE AND SECURE LAST-MILE CONNECTIVITY MODEL FOR RADIO OVER FIBER-BASED WIRELESS ACCESS NETWORK

Thesis submitted for the Award of Degree of

DOCTOR OF PHILOSOPHY

in

Computer Science and Engineering

By

Irfan Ahmad Rather

Registration Number: 41900625

Supervised by:
Dr. Gulshan Kumar (16865)
Computer Science and Engineering (Professor)
Lovely Professional University, Punjab

Co-Supervised by:
Dr. Rahul Saha (18818)
Computer Science and Engineering (Professor)
Lovely Professional University, Punjab

LOVELY PROFESSIONAL UNIVERSITY, PUNJAB

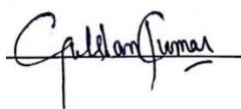**2024**

i

_____

DECLARATION

I, hereby declare that the presented work in the thesis entitled "Development of Reliable and Secure Last-mile Connectivity Model for Radio over Fibre-based Wireless Access Network" in fulfilment of degree of Doctor of Philosophy (Ph. D.) is outcome of research work carried out by me under the supervision of Dr. Gulshan Kumar working as Professor, in the School of Computer Science and Engineering (SCSE) of Lovely Professional University, Punjab, India and Co-Supervision of Dr. Rahul Saha working as Professor, in the School of Computer Science and Engineering (SCSE) of Lovely Professional University, Punjab, India. In keeping with general practice of reporting scientific observations, due acknowledgements have been made whenever work described here has been based on findings of another investigator. This work has not been submitted in part or full to any other University or Institute for the award of any degree.

Irfan Ahmad Rather
School of Computer Science and Engineering
Lovely Professional University
Jalandhar –
Delhi G.T. Road (NH-1)
Phagwara, Punjab – 144411
India
Date: 21st Aug. 2024
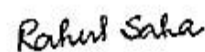
_____

CERTIFICATE

This is to certify that the work reported in the Ph. D. thesis entitled "Development of Reliable and Secure Last-mile Connectivity Model for Radio over Fibre-based Wireless Access Network" submitted in fulfillment of the requirement for the award of degree of **Doctor of Philosophy (Ph.D.)** in the School of Computer Science and Engineering Lovely Professional University, Punjab, India is a research work carried out by Irfan Ahmad Rather, 41900625 is bonafide record of his/her original work carried out under my supervision and that no part of thesis has been submitted for any other degree, diploma or equivalent course

Dr. Gulshan Kumar	Dr. Rahul Saha
Professor	Professor
SCSE	SCSE
Lovely Professional University	Lovely Professional University
Jalandhar	Jalandhar
Delhi G.T. Road (NH-1)	Delhi G.T. Road (NH-1)
Phagwara, Punjab – 144411	Phagwara, Punjab – 144411
India	India
Date: 21st Aug. 2024	Date: 21st Aug. 2024

_____

DEDICATION

I would like to dedicate this to my father, Mr. A G Rather and my mother who have been the guiding force and encouragement for this work.

_____

ACKNOWLEDGEMENT

LIST OF PUBLICATIONS

Rather, I. A., Kumar G. & Rahul S. (2021). Survey on RoF technology and the mitigation schemes over the challenges in the RoF network. In *Optik, Volume 247, 2021, 168007, ISSN 0030-4026.*

Rather, I. A., Kumar G. & Rahul S. (2022). Analog and Digital RoF Spatial Mux MIMO-LTE System based on A2 (arithmetic Aquilla) optimization model for 5G Network. In *Algorithms, Computing and Mathematics (ACM) Conference 2022.*

Rather, I. A., Kumar G. & Rahul S. (2023). Improved aquila optimization-based parameter evaluation framework and meta-heuristic algorithm in radio-over-fiber SpatialMux multi-input multi-output long-term evolution system. In *Int J Commun. Syst. 2023; 36(9): e5473.*

Rather, I. A., Kumar G., Rahul S. & Kim, Th. (2023). Enhancement of Security in GFDM Using Ebola-Optimized Joint Secure Compressive Sensing Encryption and Symbol Scrambling Model. In *The 3rd International Conference on Artificial Intelligence and Computer Vision (AICV2023), March 5–7, 2023. AICV 2023. Lecture Notes on Data Engineering and Communications Technologies, vol 164. Springer, Cham.*

Rather, I. A., Kumar G. & Rahul S. Physical Layer Security in Generalized Frequency Division Multiplexing-passive Optical Network Using Optimization Based Encryption Technique. Under Review in *Int J Wireless Personal Communications.*

_____

ABBREVATIONS

_____

Abbreviations	Description

_____

Abbreviations	Description
2D-LSCM	2-Dimensional Logistic-Sine-Coupling Map
ABC	Artificial Bee Colony
ACI	Adjacent Channel Interference
ACLR	Adjacent Channel Leakage Ratio
ADC	Analogue To Digital Converter
AHHO	Aquila-Harris Hawk Optimization
AO	Aquila Optimizer
ATM	Asynchronous Transfer Mode
BBoF	Baseband Over Fibre
BER	Bit Error Rates
CAP	Clustering Mapping Principles
CCDF	Complementary Cumulative Distribution Function

CCDM	Constant Composition Distribution Matching
CLSM	Closed Loop Spatial Multiplexing
CNN	Convolutional Neural Networks
CP	Cycle Prefix
CS	Compressive Sensing
CS	Cycle Suffix
DAC	Digital To Analogue Converter
DAS	Distributed Antenna System
DCT	Discrete Cosine Transform
DML	Directly Modulated Laser
DPD	Digital Pre-Distortion
DSB-FT	Double Sideband Frequency Translation
DSB-OCS	Dual-Sideband Optical Carrier Suppression
DSL	Digital Subscriber Loop
DSP	Digital Signal Processing
DWDM	Dense- Wavelength Division Multiplexing
EAM	Electro Absorption Modulator
EMI	Electromagnetic Interference
EOP	Eye Opening Penalty
ESOA	Ebola Search Optimization Algorithm

EVM	Error Vector Magnitude
FBG	Fibre Bragg Gratings
FEC	Forward Error Control
FFO	Firefly Optimization
FiWi	Fibre Wireless
FrFT	Fractional Fourier Transform
FWA	Fixed Wireless Access
FWM	Four-Wave Mixing
GFDM	Generalized Frequency Division Multiplexing
GWO	Grey Wolf Optimization
HHO	Harris Hawk Optimization
HL-TDMA	Hybrid Link Time Division Multiple Access
ICI	Inter-Carrier Interference
IF	Intermediate Frequency
IFoF	Intermediate Frequency Over Fibre
IM	Intensity Modulation
IM-DD	Intensity Modulation And Direct Detection
ISI	Inter-Symbol Interference
ISP	Internet Service Provider
LMMSE	Linear Minimum Mean-Squared Error

LTE	Long Term Evolution
MBM	Measurement Basis Matrix
MIMO	Multi-Input And Multi-Output
MQAM	M-Ary Quadrature Amplitude Modulation
MUD	Multiuser Detection
MZI	Mach Zehnder Interferometer
MZM	Mach Zehnder Modulator
NGN	Next Generation Network
NSP	Network Service Providers
OFDM-MDM	Orthogonal Frequency Division Multiplexing-Mode Division Multiplexing
OLSM	Open Loop Spatial Multiplexing
OLT	Optical Line Terminal
OMP	Orthogonal Matching Pursuit
ONUs	Optical Network Units
OOB	Out Of Band
OSTBC	Orthogonal Space-Time Block Code
OTDM	Orthogonal Time Division Multiplexing
OVSF	Orthogonal Variable Spreading Factor
PAPR	Peak-To-Signal Noise Ratio

PLC	Power Line Communication
PLS	Physical Layer Security
PMI	Pre-Coding Matrix Indicator
PON	Passive Optical Networks
PRBS	Pseudo-Random Binary Sequence
QAM	Quadrature Amplitude Modulation
RAU	Remote Antenna Unit
RFoF	Radio Frequency Over Fibre
ROF	Radio-Over-Fibre Technology
RRC	Root Raised Cosine
SBM	Sparse Basis Matrix
SC-FDE	Single Carrier Frequency Domain Equalization
SCM	Sub-Carrier Multiplexing
SD-ROF	Sigma Delta Radio Over Fiber
SER	Symbol Error Rate
SINR	Signal-To-Interference Plus Noise
SISO	Single Input Single Output
SMF	Single-Mode Fibre
SPM	Self-Phase Modulation
SRS	Stimulated Raman Scattering

SSO	Slap Swarm Optimization
SSSB	Single Sideband Frequency Translation
STBC	Space Time Block Code
TCM	Trellis-Coded Modulation
TSHO-PTS	Twin Symbol Hybrid Optimization Partial Transmit Sequence
TWDM-PON	Time And Wavelength Division Multiplexing-Passive Optical Network
UAV	Unmanned Aerial Vehicles
URLCC	Ultra-Reliable Low Latency Communications
VCSEL	Vertical-Cavity Surface-Emitting Laser
VLC	Visible Light Communication
WDM	Wavelength Division Multiplexing
WI-FI	Wireless-Fibre Networks
WiMAX	Worldwide Interoperability For Audio Broadcast And Digital Video And Microwave Access
W-LAN	Wireless Local Area Network
XPM	Cross Phase Modulation
ZF	Zero Forcing

_____

CONTENTS

LIST OF TABLES

LIST OF FIGURES

ABSTRACT

An emerging technology for the next-generation wireless network, including 5G, is multiple input multiple output-long-term evolutions (MIMO-LTE) using a Radio over Fiber (RoF) connectivity. The data transmission via a wireless channel in a next-generation (NG) network demands extremely high data rates. As a result, a MIMO system's primary requirements include efficient transmission and a high data rate. To increase the dependability of 5G wireless communication, RoF technology is introduced (WC). Each antenna in this study deals with a 64-bit quadrature amplitude-modulated (QAM) 800 MHz 5G signal, which has a total frequency of 3.2 GHz. For distributed applications and the conveyance of broadband wireless signals, a 70 Km standard single-mode fiber (SSMF) is also introduced. Moreover, bandpass sampling is used, and the methodology for reducing the bandwidth demand in RoF links is defined. Analyses of the performance are conducted for both traditional digital RoF (D-RoF) and analog RoF (A-RoF). The analysis is also done on the RoF front haul system's ideal transmission circumstances in MIMO systems. The Arithmetic Aquila optimization approach is used to optimize the bias power and current transmission to improve the transmission condition of the link RoF. All of the work is done using the MATLAB program. Both D-RoF and A-RoF systems are examined in terms of performance indicators such as the eye-opening penalty (EOP), error vector magnitude (EVM), and signal-to-noise ratio (SNR). The D-RoF and A-RoF in the experimental scenario had EVMs of 1.45% and 1.13%, EOPs of 51.19dB and 51dB, SNRs of 27dB and 26dB, and calculation times of 0.14s, respectively. To determine the efficiency of the suggested approach, the experimental analysis is contrasted with existing methodologies such as the particle swarm optimization algorithm, chimp optimization, remora optimization, and Aquila optimizer (AO).

Radio-over-fiber (RoF) methodology is used to fully use the MIMO system. While communicating wideband Long-Term Evolution (LTE) MIMO signals, the unique system can handle a variety of services. Several nonlinear effects can be used to examine the RoF fronthaul system in MIMO systems. It is probable to lessen the cause of nonlinear circumstance effects that the RoF mechanism causes by regulating several transmission factors, like input signal power or the laser bias current. To improve the broadcast conditions in a MIMO RoF method, this research suggests

adopting the Improved Aquila Optimization (IAO). With this method, the correct bias current for RF and laser signal power may be determined quickly. In a MIMO IM/DD (Intensity Modulation and Direct Detection) RoF system, wavelength-multiplexed MIMO signals were used in the investigations. Transmissions and carrier frequency are governed by the LTE standard. Results are acquired after the suggested system is put into practice in MATLAB. A good balance between noise and non-linearity may be achieved for a variety of bandwidths, according to experiments, which also demonstrate quick convergence. By employing properly input signal power and biased current, it is possible to lower system distortions and enhance Error Vector Magnitude (EVM) values. The maximum EVM of 3.14 for quadrature phase shift keying (QPSK) and 1.88 for QAM was achieved as lowest among various existing approaches. The signal-to-noise ratio (SNR), which was achieved at about 3.20 for QPSK and 2.69 for the QAM modulation which was highest among the various other approaches. Attained complexity of computation 0.137s for 200 repetitions. The results of the experiments demonstrate that our suggested strategies produce better results than other approaches.

Due to their energy efficiency, low cost, and high capacity, Passive Optical Networks (PONs) have drawn a lot of attention in recent decades as a potential solution for supplying the growing demand for broadband services. Data sent through the PON is more susceptible to being intercepted by an unauthorized Optical Network Unit since there is a broadcasting structure in downstream traffic (ONU). As a result, data transmission security issues in PON get harder. So, this work suggests a method to boost optical generalized frequency division multiplexing (GFDM) transmission in PON while also improving physical layer security. The suggested chaotic compressive sensing (CS) method aims to compress the transmitted data. Bitstream transmission using CS has several limitations because it cannot satisfy sparsely in both the temporal and frequency domains. Multimedia transmissions run the risk of making the sent data sparse. With a sensor, the data can then be recognized as multimedia. If so, the sensor output is recorded as side data in the pilot and simultaneously sent to the terminal, using the CS technique. To encrypt the system, pseudo-random variables are produced for the measurement matrix's first row using a 2-dimensional Logistic-Sine-Coupling Map (2D-LSCM). Image security is achieved via hybrid Aquila-Harris hawk optimization (AHHO) with the best key selection. The Discrete Cosine Transform (DCT) is employed to implement the CS method since data transmission is constrained in the physical layer.

Using GFDM-PON systems with this chaotic CS encryption method decreases bandwidth while enhancing security. The suggested work is employed in MATLAB, and the effectiveness is estimated against currently used OFDM-PON methods. To determine the effectiveness of the proposed system, performance metrics like entropy, peak-to-signal noise ratio (PSNR), complementary cumulative distribution function (CCDF), encryption time, decryption time, Mean Square Error (MSE), and Bit Error Rate (BER) are examined.

Orthogonal frequency division multiplexing (OFDM), which is frequently utilized, is established as a generalized form of Generalized Frequency Division Multiplexing (GFDM). The security of the data is a difficult challenge to do, and the data transfer across the Passive Optical Network (PON) is highly vulnerable. To solve this issue, GFDM systems are given a symbol scrambling and joint secure compressive sensing encryption approach in this study work. The chaotic measurement matrix and chaotic sparse matrix that depend on the DCT are then used to produce a high compression rate in the Compressive Sensing (CS) phase after the binary sequence is first divided into sub-blocks. The suggested system is improved for high security in the second stage by converting the received CS data to Binary Phase Shift Keying (BPSK) symbols and using the SHA-256 approach for key selection and key creation. For the best key selection procedure, the Ebola meta-heuristic system is recommended. The objective function (OF) of this suggested key selection is the maximum Peak-to-Signal Noise Ratio (PSNR), which is used to find the best secret key from a set of random numbers. The safety of the CS data is improved by performing a symbol scrambling operation on the resulting BPSK symbols. Finally, this suggested system's performance is related to some of the existing approaches based on encryption time (ET), decryption time (DT), BER, and Complementary Cumulative Distribution Function (CCDF). These methods include Chaos-DNA encrypting, chaotic CS, Brownian motion-chaos, Feedforward neural network-based chaos encryption and High-security three-dimensional optical mechanism in OFDM-PONs. According to PSNR, entropy, and MSE, the planned methodology is also related to other optimization strategies, including Particle Swarm Optimization (PSO), Hive optimization Algorithm (HOA), and Spark Optimization Algorithm (SOA). The suggested GFDM-attained PON's values for PSNR are 57.86319, MSE is 0.004114, Entropy is 9.495201, encryption time is 0.054, and decryption time is 0.048.

CHAPTER 1

INTRODUCTION

1.1 Overview

The capacity of today's communication systems has been worn down by the increasing demand for wireless applications and the rapid increase in the amount of connected users. High throughput, excellent spectrum efficiency, and wide connectivity with minimal latency are among the growing demands of wireless applications. Recent developments in 5G wireless communication show the importance of integrating various communication topologies, vehicular proximity, and switching methods. The MIMO approaches to improve communication performance by increasing channel capacity, bit rate, and transmission speed. When MIMO is used, multiple antennas are typically enabled on both the transmitter and reception sides. Power Line Communication (PLC) [1] is a major broadband access technology. Data is transported over power line infrastructure in PLC. Signals are transmitted using electromagnetic waves that are transported via Medium Voltage (MV) and Low Voltage (LV) and are mixed with electric power. Nowadays, the evolution of Internet users is accelerating, as is the evolution of data communication. The Next Generation Network (NGN) [2] is developed as the primary issue to meet the bandwidth requirement. It is separated into the Next Generation Access Network and Next Generation Core Network. The transmission of a network for data rate has grown because of the participation of photonic methodology and the utilization of optical fibers. The front haul link among the base station and central station in a broadband wireless access network is called Radio-Over-Fibre technology (ROF) [3]. Transmission direction in this technology is accomplished by transforming an optical signal into a radio signal. The capability of Fiber Wireless (FiWi) [4] Internet access networks has increased the combination of fiber and wireless networks. Edge computing is a major issue for FiWi because it does not rely on the backhaul network for end-to-end data delivery. Polling is used in wireless broadband access networks to give the highest possible service quality.

The communication network must be industrialized with high real-time speed to access information anytime and anywhere. Both optical fiber communication and wireless communication are critical for data transmission. ROF technology is one of the important advancements in future wireless networks. Radio over fiber has recently advanced to transmit radio frequency communications over large distances. The RoF technology improves wireless access coverage by including a basic antenna. The data transmission from optical to radio

signals is delivered at high speed and with flawless convergence utilizing millimeter (mm) waves. The mm-wave is produced in an optical fiber by the complexity of both phase modulation and stimulated Brillouin scattering. The ROF technology consists of a base station, a central station, and the signal processing at the base station includes modulation, frequency conversion, and multiplexing. Signal processing and de-multiplexing are carried out in the central station. The optical signal is routed across the fiber to the base station, where the RF signal is retrieved by photodetectors, amplified, and finally radiated to the antenna. The remote antenna unit (RAU) [5] is installed to transmit radio frequency communications to end users without distortion via broadband access. RAU includes fewer components, lowering the cost of installation.

The RoF intensity modulation includes external and optical modulation, data modulation, and internal modulation. The modulation systems are used to modify the electrical and optical signals. Existing transmission lines did not transfer mm-waves due to their large frequency range; therefore, frequency up-conversion at reception and frequency down-conversion at transmission are required. The conversion process allows for additional cost increases at the Base Station. Methodologies such as orthogonal time division multiplexing (OTDM), dense-WDM (DWDM), and wavelength division multiplexing (WDM) [6] have increased optical transmission capacity while also allowing for more bandwidth in optical fibers. There are numerous problems with the fiber link connected to the RoF availability in the Intermediate Frequency (IF), baseband frequency, and Radio Frequency (RF). Chromatic dispersion and non-linear distortion are problems affected by the fiber link. Since these problems relate to the technology's connection performance, they will impact long-distance transmission. The issues are most prevalent with the analog RoF, which operates very frequently. The nonlinear distortion, which is made up of harmonic distortion and intermodulation distortion, results from signal deterioration at the fiber. The optical modulator's nonlinear properties bring on these kinds of distortions.

The nonlinear properties of the modulator, as well as the high Peak-to-Average Power Rate (PAPR) induced due to the power amplifiers, cause chromatic dispersion and nonlinearity distortion in RoF technology [7]. Furthermore, when the RoF method is merged with the PON, it will provide a large user capacity; nevertheless, the PON method with multiplexing has uncertainty issues at the physical layer, as well as the large PAPR brought by OFDM signals. In order to improve the data rate, all the above-mentioned effects must be minimized, including a low EVM and a large user capacity.

Passive optical networks (PON) [8] provide an optimal method for transmitting data from the antenna to end users for last-mile access. In a PON network, the Optical Line Terminal is terminated in the central base station to transfigure the optical signal to an electrical signal. Because radio over fiber manages the stations using optical fiber, it may provide better solutions than optical fiber and wireless communication. Wavelength division multiplexing (WDM) [9] can reduce high bit error rates (BER) by maximizing Q-factor values. Subcarrier multiplexing has been investigated in WDM to boost bandwidth efficiency while maintaining high dispersion tolerance. Sigma Delta Radio over Fiber (SD-ROF) [10] is an empowering technology that combines analog and digital RoF technologies. The performance of (SD-ROF) is measured in the evaluation of EVM and Adjacent channel leakage ratio (ACLR) [11].

1.2 Radio over Fiber (RoF)

The RoF framework found in 1990 for cordless telephone service modulates optical signals using a Radio Frequency (RF) signal via an optical link. It consists of a Central Station (CS) where all frequency component operations and processing of RF signal are performed, such as multiplexing, carrier modulation, and frequency up-conversion. An optical fiber network connects the CS to numerous Base Stations (BS), emitting into the antenna. Modulated RF signals are transferred from the base station (BS) to the Remote Antenna Unit (RAU) via optical fiber cable (OFC) with a RoF scheme [12]. The BS uses E/O and O/E converters to convert optical to electrical signals.

The modulation of light from an RF signal before being transmitted as an optical signal through OFC refers to RoF. To fundamentally have a communication system with subcarrier frequency, rising capacity, and wide bandwidth, this technology supports optical and wireless access networks. In the meantime, this system has the potential to develop into a strong contender for integrating with a variety of communication standards, including WiMAX, digital subscriber loop (DSL), video digital, and Wi-Fi, which offers speeds of up to 100 Mbps for both fixed and mobile applications. For mobile communication systems that allow data sharing and high-speed information transfer between two vehicles, IEEE 802.16, and more recently, at frequencies between 2 and 66 GHz [13]. Figure 1.1 shows the architecture of basic RoF
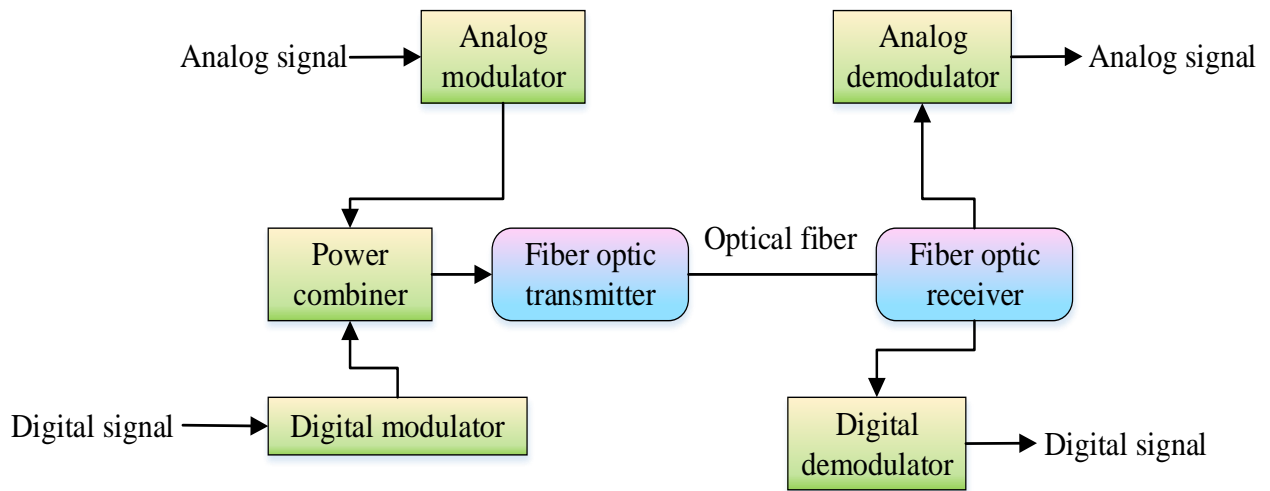
Figure 1. 1: Basic RoF Architecture

Most network providers use it now to support network reliability even in poor weather conditions and unreachable zones. It allows the modulation of electrical signal to optical signal and its traversal to long-distance antenna locations, the RoF system is appropriate for lower costs and less power consumption. When an optical connection is used, a modulated RF signal is sent there, and the power used is released through the antenna side's strong RF carriers. One way to explain the RoF technology cost reduction is through the central station (CS), which offers resources that a group of base stations (BSs) can share. Another way is through the fact that these BSs have accomplished very simple functions that are tiny in size and have low power requirements.

Radio over fiber systems is an RF and optical network integration technique that increases the channel capacity of mobile and application systems while lowering cost and power requirements. The radio access that the RoF system offers can be combined in a variety of ways with both current and next-generation wireless systems. Over a RoF networking system, the optical wave transmission among CS and BS can be accomplished. Signal broadcast among the user, mobile units, and base station occurs using an antenna positioned at the BS unit, as shown in Figure 1.2.
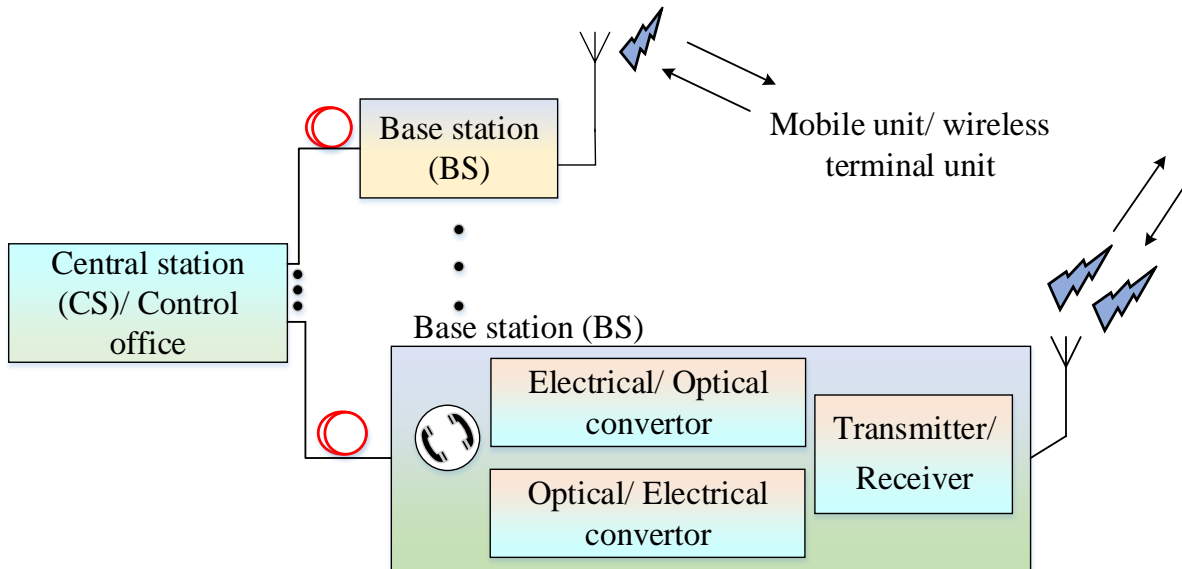
Figure 1. 2: Radio over Fiber block diagram

Optical source with fluctuating output power can make a modulated RF signal, which is then transmitted over an OFC. This could be accomplished either by external modulation of laser source via intensity modulation, such as a Mach Zehnder Modulator (MZM), Electro Absorption Modulator (EAM) [14], or otherwise through direct modulation. Furthermore, the later modulation approach is known as Intensity Modulation (IM), where the amplitude of a laser beam is directly modified by an RF signal. The optical carrier phase is manipulated by a scheme such as MZM in the External modulation method. It is preferred because direct modulation is better for low-cost transmitters; nonetheless, it is the basis of an undemanding wavelength chirp that generates limitless chromatic dispersion at high speeds. Numerous advantages include a refractive index that changes parallel with practical voltage and normal electronic stability working temperatures. However, the drawbacks of external modulation include its complex mechanism and high cost.

1.2.1 Architecture of RoF

Depending on the transmitted signal frequency, radio over communication systems are classified as Radio Frequency over Fibre (RFoF) and Intermediate Frequency over Fibre (IFoF) [15]. Before transmission via fiber optical connection, a strong RF signal is forced on an optical carrier in RFoF. Additionally, the air-interface carrier is transmitted concurrently with the signal via the optical link of fiber. The identified signal is then directly transferred to confirmation air transportation, simplifying remote unit conformation. Therefore, there is no

need for up/down conversion of frequency at the base station, resulting in a simple and cost-effective circuitry application. However, to transcend the Mm wave band, photonic devices such as Photodetectors (PDs) and MZM [16] along a large bandwidth, which is highly expensive must be used.

In contrast, an Intermediate Frequency (IF) signal [17] is used in IFoF architecture to modulate the light signal and transmit the modified signal via an OFC. So, before radiating over the air, the signal processing at the BS is required, such as amplification circuits, and frequency up-conversion, and the signal must be converted to the RF signal by up-conversion. In comparison, IFoF implementation will be accomplished using a low-speed photonic mechanism such as PIN photodetectors and Directly Modulated Laser (DML) [18]. It also allows for deploying bandwidth-efficient communication methods based on channel aggregation. As a result, IFoF systems will be bandwidth-efficient and highly cost-effective for Mm wave service than RFoF schemes.
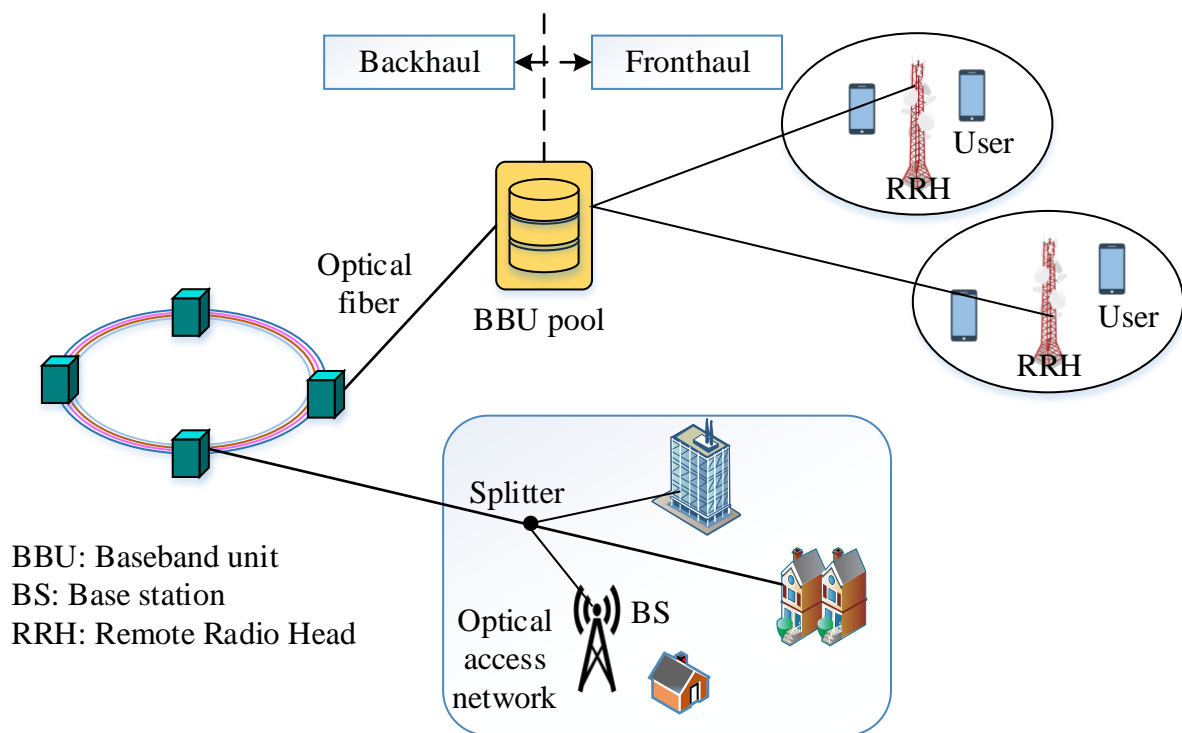
Figure 1. 3: Radio-over-Fiber (RoF) system architecture,

High RF usage also brings additional difficulties. The free-space propagation loss in the high RF band is significantly higher than in the lower RF band. One possible solution is the RoF scheme, which combines the greatest features of optical fiber with wireless communications. As depicted in Figure 1.3, these systems use optical fibers to deliver wireless signals, using

6

their high bandwidth and low loss characteristics. RoF technology has been extensively studied for many application scenarios and coupled with other technologies, including wavelength-division-multiplexing (WDM) networks and/or traditional passive optical networks (PONs) [19]. Additionally, due to 5G and beyond-5G wireless communications, the RoF technology has been researched recently for mobile front haul to provide better speed and system throughput.

1.2.2 Classification of RoF

According to the carrier signal frequency, RoF was categorized. Based on the microwave signal's maximum frequency, the carrier frequency was used to modulate. Baseband over Fibre (BBoF), IFoF, and RFoF are the three categories under which RoF technology is classified [20]. Although in RFoF the RF signal was sent via an OFC and in IFoF, the RAU produced microwave signals that were sent over an up-conversion link.

1.2.2.1 RFoF

RFoF is mentioned to analog RoF, it can transmit electrical signals at frequencies between 10GHz and 40GHz. Before being sent across the optical fiber link, high-frequency signal data was converted into a light wave. Because of this, radio signals were transmitted to the BS at incredibly elevated frequencies, transformed to electrical impulses, and then amplified and broadcast by the aerial. The replacement of coaxial cables with RFoF for potential usage in the radar system. The link generates less noise than the other links since it consists of three semiconductor-based components. The RFoF system is simple and inexpensive because it does not require frequency up- or down-conversion. The long-distance transmission and system link performance is impacted by the chromatic dispersion and nonlinear distortion on the RFoF.

1.2.2.2 IFoF

The term digital RoF or IFoF was also used to describe the digitalized FoF. The signal was modulated by the low-frequency signal at the CS and transferred to the BS because IFoF operates in the 10MHz to 100MHz frequency region. Before delivering the signal to the aerial unit, frequency up and down conversions are necessary due to the low operational frequency. By the use of bandpass signaling techniques, the expensive frequency conversion procedure lowers the chromatic dispersion of the OFC. The applications had a crucial role in determining the condition for weight loading at the aerial stage (e.g. flying devices). Under such situations,

the cable's thickness and screening coatings could be increased to provide protection against disturbance. The additional safeguarding keeps the cable heavier and has an inverse relationship with flexibility. Implementing the IFoF with an antenna from the generator to the heterodyne receiver was the remedy for this issue.

1.2.2.3 BBoF

Radio broadcasts were transmitted at CS at frequencies between 20Hz and 20 KHz during the BBoF, commonly known as the digital RoF. An OFC is used to transmit the signal to the BS. After being up-converted to RF via IF, the mobile unit receives the electrical signal at BS. Although the chromatic dispersion was modest in those systems, the BS model was expensive, making it possible to acquire the performance connection. In that kind of design, the CS and BS both used an additional digital-to-analog converter (DAC) and analog-to-digital converter (ADC) [21]. The usage of converters causes jitter in the communication process, which the all-photonic DRoF architecture could decrease.
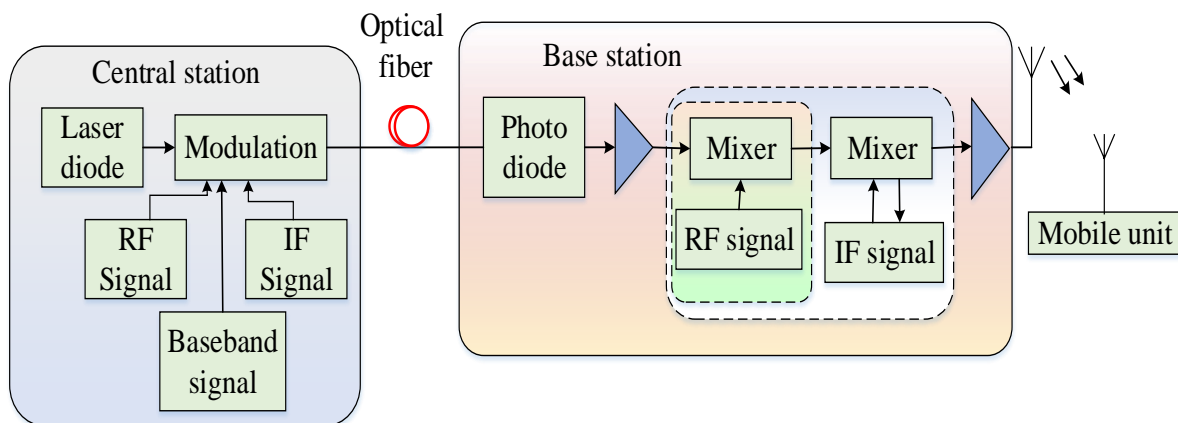
Figure 1. 4: System architecture downlink for BBoF, IFoF and RFoF

The three sets of frequency based on the RoF system are shown as being processed downlink in Figure 1.4. In contrast to IFoF processing, which is shown by the blue line, RF frequency processing is represented by the red line. The BS had to process the IF signal in IFoF, which necessitated frequency up-conversion. IF and RF for signal up-conversion are used in baseband signal processing. As a result, the system is quite expensive.

1.2.3 Modulation in ROF

The growth of optical fiber communication in the modern period has been exponential, and fiber optical communications now can handle significantly higher data speeds [22]. These

systems' complexity is rising daily. The most reliable and quick method of satisfying customer needs and reliability is an optical fiber connection. With a little bit of error, it sends data over large distances. The non-Gaussian noise sources and non-linear devices used in the optical communication system are labor- and time-intensive [23]. Additionally, an error code was generated when the signal was changed from an optical to an electrical one, resulting in a long-distance transmission failure.

1.2.4 Transmission Techniques of RoF

The transformation of electrical and optical signals necessitated the employment of two modulation techniques in RoF technology. As a result, both external and internal modulation techniques were employed [24]. These modulation techniques were referred to as data modulators and optical modulators, respectively, because they both require the conversion of optical to electrical and electrical to optical signals. The optical signal and RF signal would be combined by the external modulator to create light, which would then be transmitted to the internal modulator for the conversion of an electrical signal.

1.2.4.1 External and Direct Modulation

The photodetector was utilized to retrieve the initial signal after the RF signal varied the light signal's intensity. RoF technology's modulation techniques are shown in Figure 1.5. For optically disseminating radio signals, direct modulation was a straightforward and affordable technique. The modulation technique was reliable enabling low-dispersion fiber and producing linear outcomes. This modulation system didn't function at greater microwave frequencies due to the laser diode's modulation bandwidth which was its drawback; however, this limitation could be circumvented using external modulation techniques.

The constraints of direct modulation could be overcome by external modulation because it provides a simple solution. An external modulation method that could function at mm-wave frequencies utilized the optical modulator. The linear chirp was generated by the optical communication technology. An external modulation approach using an optical recirculation frequency shift loop and an optical frequency sweep was employed to lessen the effect of the chirp. It uses the MZM [25] for external modulation and the Vertical-Cavity Surface-Emitting laser (VCSEL) for direct modulation. The modulation approaches for QAM were evaluated, and the sub-carrier signal was produced using OFDM.

(a)

(b)
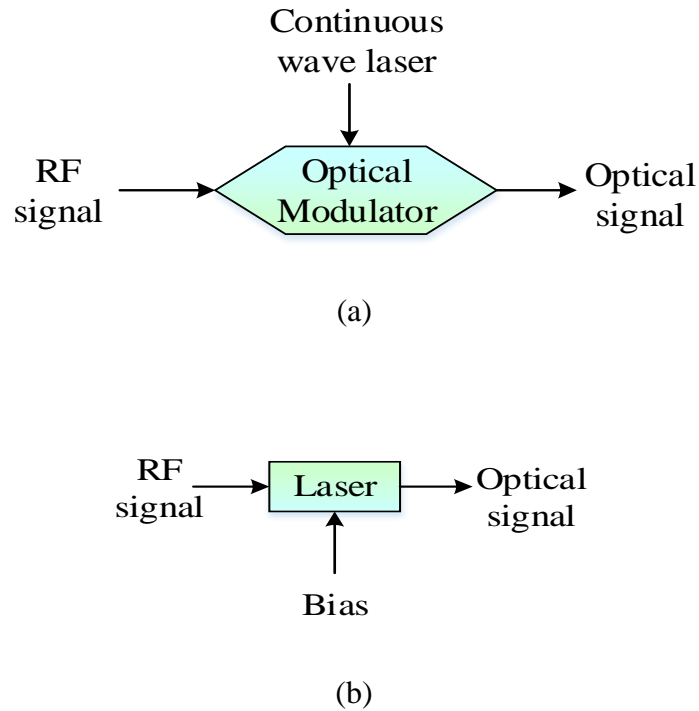
Figure 1. 5: RoF Modulation a) external modulation b) direct modulation

1.2.5 Advantages and Limitations of RoF Technology

Low loss, large bandwidth, resistance to radio frequency interference, cost-effective, simple system, multi-service, maximizing channel capacity, low power consumption and multi-operation capability, simple installation and dynamic resource allocation, maintenance, and improved cellular coverage make RoF distribution suitable for wireless communication network requirements [26]. Furthermore, using RoF offers several advantages for giving radio access, such as modules of cost-effective remote antenna, flexibility to connect tiny ones, and simplicity of update for future possible inquiries. RoF performs to be a favorable nominee that will be widely used for various communication networks standards such as worldwide interoperability for audio broadcast, digital video, and microwave access standards, Wireless-Fibre networks (WI-FI), Digital Subcarrier Loop (DSL), which provide low power consumption and high bandwidth while reducing the cost of wireless network deployment and maintenance.

However, when the RF signal is transported across an OFC, many anomalies occur due to fiber properties such as dispersion, attenuation, and fiber nonlinearity, which decreases the whole performance of the system. Accordingly, the fiber optic acts as a linear medium for low power levels and non-linear for high power levels, influencing the OFC with nonlinear impacts that reduce system performance. The Kerr nonlinearity and scattering influence that is affected by

the alteration of the refractive index owing to signal strength is the main fiber nonlinear influence in the primary fiber optical communication setup.

When an optical signal is distributed by fiber, attenuation tends to reduce its power, and the maximum communication distance of the optical signal can be established. Dispersion refers to the broadening of pulse length as it travels along the fiber. Inter-symbol interference (ISI) [27] is also caused when the expansion of pulses slowly begins to overlay with one another. After a certain range, the pulses become unrecognizable, and the pulses lose their information and definition if the signal transmits further. Nonlinear phenomena in optical fibers such as Stimulated Raman Scattering (SRS) caused by inelastic scattering [28], Kerr effect, and the Brillouin scattering. Some of the transmitted light power is absorbed by the optical medium via the scattering effect.

Nonlinearity is caused by the Kerr effect. The said effect modifies the silica Refractive Index (RI) due to fluctuations in the intensity of the optical signal. These results in numerous irregularities depending on the nature of the input, such as Cross Phase Modulation (XPM), Four-Wave Mixing (FWM) for numerous channels [29], and Self-Phase Modulation (SPM) for a single channel. Furthermore, signal flaws such as distortion and noise are essential in both RoF technology and analog transmission. RoF link's Noise Figure (NF) and Dynamic range (DR) are reduced due to impairments. RoF systems may limit fiber link lengths while increasing RF carrier phase noise based on Single-Mode Fibre (SMF) [30]. Furthermore, in Multi-Mode Fibre (MMF), these deficiencies minimize the bandwidth, available link, and distance.

1.3 GFDM

Regarding the Out of Band (OOB) complexity and emission, the GFDM [31] can be offered as a favorable 5G option. A waveform of non-orthogonal is employed for conveying M-ary quadrature amplitude modulation (MQAM) symbols, subcarriers, and sub-symbols. Another significant feature of GFDM is its adaptability; to support 4G technology, this waveform may be modified. The designed GFDM transceiver uses Forward Error Control (FEC) to boost data strength in the face of channel transfer interference. Convolutional, Polar, and check parity of poor density can be used at rates of 5/6, 3/4, 2/3, and 1/2. Two correlated types of signals are created while the modulated signal is subjected to a time-reversal of space-time coding system.

A flexible multicarrier modulation method known as GFDM also can be recommended for the 5G network air interface. As special examples, because of the flexibility of GFDM, CP-OFDM and single carrier frequency domain equalization (SC-FDE) can be encompassed by it. GFDM is related to the independent block(s) modulation, wherein every block involves several sub-symbols and subcarriers. The prototype filter which is circularly shifted in the time and frequency domain filters the subcarriers. These OOB emissions are minimized by such technique allowing dynamic spectrum and fragmented spectrum distribution without interfering with other customers or incumbent services. Non-orthogonal subcarriers, as well as ISI and Inter- Inter-Carrier Interference (ICI), can be a result of subcarrier filtering.

This approach could feed two antennas separated by certain wavelengths, with a multi-route channel providing the receiver to use diversity gain. A Cycle Prefix (CP) and Cycle Suffix (CS) are also applied to the signals to increase their strength in contrast to the multipath channel. The application of the Digital Pre-Distortion (DPD) system eliminated nonlinear distortions caused by the electrical amplifier at the RF Front End. In other words, DPD recognizes the electrical amplifier transfer function and induces an opposite response, aimed towards the linear action of output. The receiver's automatic gain control will equalize the input level, and the transmitter will reverse after synchronization and channel estimate. As shown in Figure 1.6, the QAM demodulator performs the QAM de-mapping and transfers obtained bits to the channel decoder, which delivers only associated information to the Ethernet interface.
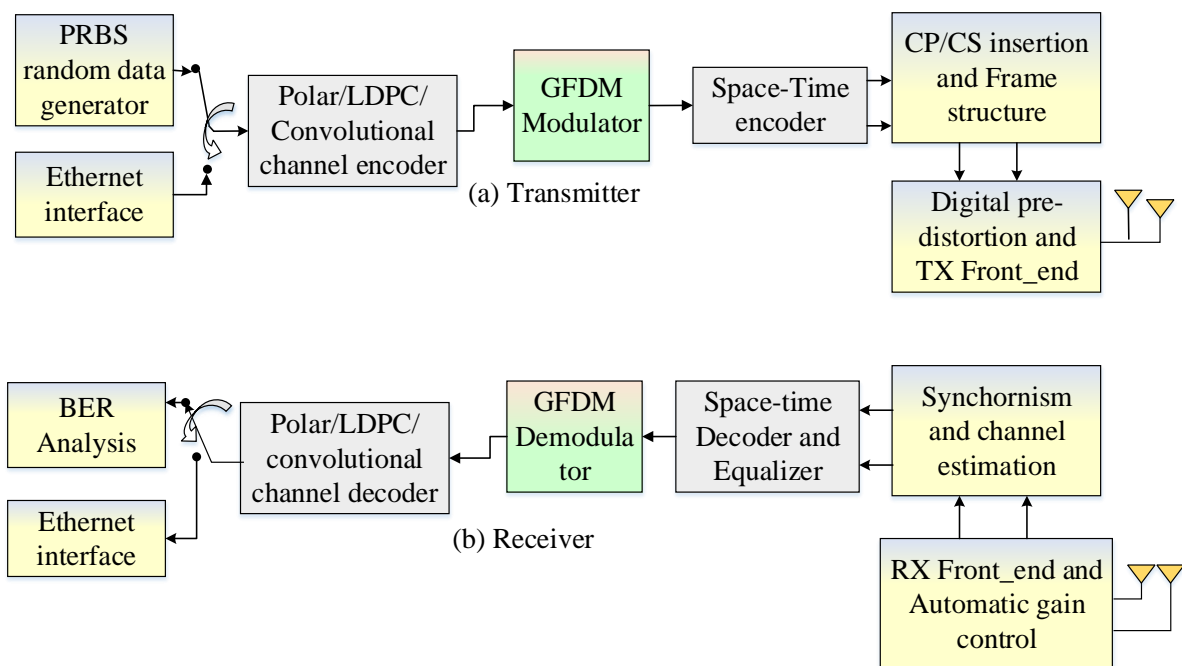
Figure 1. 6: Block diagram of GFDM based 5G transceiver

The development of a fibre-wireless 5G network based on multi Gbit/s and GFDM was revealed. DD-MZM was used to broadcast two RF signals at the same time while using two 5G nomination bands, specifically: the 700 Mega Hertz band for supercell rural access and 26GHz spectrum for femtocell with 2 Gbit/s capability. A vector signal generator was also used to produce the broadband 26 GHz signal. The Brazilian 5G transceiver based on GFDM produces a low-frequency signal with lesser out-of-band emission. The primary advantage of using DD-MZM is that it reduces interference among RF1 and RF2, which is caused by nonlinearity in the modulation process. Clear RF signals are modified independently with top and bottom arms using cleared and optimized bias voltages.

Air interface of the upcoming 5G networks has been suggested to use the flexible MCM technology known as GFDM. Independent blocks in GFDM schemes are made up of several subcarriers and sub-symbols that are modified individualistically. When sub-carrier filtering is used, the GFDM sub-carriers may lose their orthogonally, leading to ICI or ISI. The following is a discussion of a few recent GFDM techniques. To minimize the system overhead and counteract the effects of ICI and ISI, the CP is appended to a complete GFDM block. Carrier frequency offsets (CFO) are believed to be unaffected by GFDM and FBMC waveforms like UFMC and filter bank OFDM-OQAM [32]. GFDM is therefore categorized as a non-orthogonal MCM based on the block approach. GFDM is being used as an access method in hybrid analog-digital MU equalizer for wideband mm Wave-m MIMO systems. They demonstrate that GFDM outperforms OFDM in terms of better management of OOB emissions, increased spectrum efficiency, and lower PAPR.

Out-of-band (OOB) emission is filtered out in each sub-carrier of GFDM-based transceivers to reduce the adverse impacts. Prototype filters that are circularly shifted in both the frequency and temporal domain are used for this. The outcomes in an AWGN channel of the suggested filter is related to that of the Xia filters and Root Raised Cosine (RRC) in terms of power spectral density concerning various sub-carriers and Symbol Error Rate (SER) vs signal to noise ratio. It is suggested that SCMA and GFDM be combined using two different methods. Block Expectation Propagation (BEP), a type of soft equalizer, is combined with a Multiuser Detection (MUD) strategy using a sum-product technique in the first (SPA). The receiver complexity is significantly increased; however, this method yields the best SER outcome.

DFT-based channel estimation is demonstrated for the GFDM system. By eliminating the impulse of channel replies that aren't actual impulse responses, the suggested technique can

increase the Least Square (LS) channel estimation method. To obtain channel response for all GFDM blocks, the frequency and time domains are interpolated. The system's functionalities have been altered for a suitable tactile internet application.

1.4 PON

The majority of the time, telecommunications network providers use a passive optical network (PON) to deliver fiber optic cabling and messages to the end user. The system can be classified as fiber to the home, fiber to the building, etc. depending on where the PON terminates. A PON system is composed of several Optical Network Units (ONUs) close to end users and an Optical Line Terminal (OLT) [33] at the communication of the central office. A single OLT typically supports connections for up to 32 ONUs. The term passive simply refers to the point that optical transmission requires no power and has no active electronic components once the signal has been sent over the network. Active optical networks, on the other hand, need electrically powered switching hardware for transmitting frames or cells across fiber optic cable. Figure 1.7 shows a diagram of a Passive optical network.
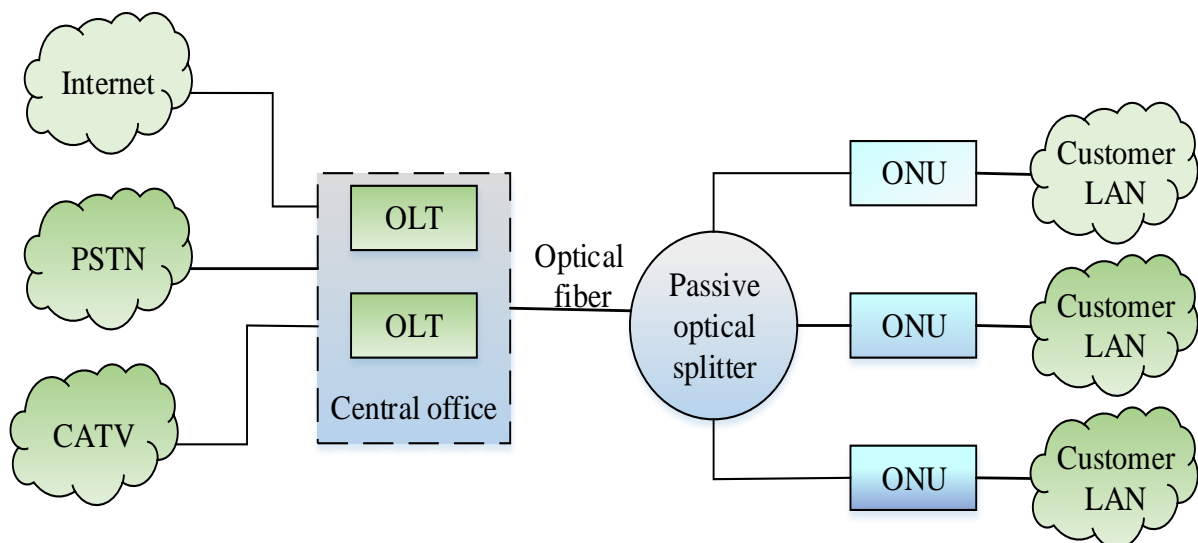
Figure 1. 7: Passive optical network

The central office of the communications service provider can be seen housing redundant OLT hardware in this photograph. A passive optical splitter is then used to divide the fiber connection into several ONUs and terminate it near the customer's demarcation point. Fiber cabling is disseminated up to 20 kilometers from the central office. Customers can then easily join their pre-existing Local Area Networks (LANs) and help ONU transfer the network handoff over fiber or copper ethernet wires.

Theoretically, the optical level capacity of all PON systems is effectively the same. The upper and lower limits for downstream and upstream bandwidth are set by the electrical overlay, the protocol used to control the connection and divide the capacity. With an electrical layer based on asynchronous transfer mode (ATM) or cell switching protocols, the first PON systems to achieve significant commercial deployment were known as APON. Although they are now referred to as broadband PON or BPON, these are still in use today. Downstream capacities for APON or BPON networks are typically 155 Mbps or 622 Mbps, with the latter being the more typical. With 155 Mbps cell bursts, upstream transmission is possible. Through the use of wavelength division multiplexing and optical splitter methods, different PON users could be given access to different portions of this bandwidth. Another use for a PON is as a coaxial cable network trunk uplink between a bigger system, like a community antenna television system, and a home Ethernet network, a building, or a neighborhood.

Ethernet-based PONs are the replacement for ATM-based PONs in PON architecture. For instance, gigabit PON (GPON) deals with a range of speed possibilities, from symmetrical 622 Mbps (equal downstream and upstream capacity) to asymmetric 2.5 Gbps download and 1.25 Gbps upload capacities. GPON is a hybrid network that sends data over Ethernet and voice over ATM. In general, GPON is used in fiber-to-the-home networks.

1.4.1 PON Security

Eavesdropping and service theft pose two different security risks to PONs. Potential eavesdropping situations are caused by the point-to-multipoint downstream architecture of TDM PONs [34]. Users are stopped from accessing frames that are not intended for a typical PON by a filter. By turning off the filter at the first ONU, eavesdropping can be carried out. The user will have access to all of the network's frames when the filter has been turned off.

The other user's ONU or that user's input to the splitter would need to be physically accessible for eavesdropping to take place upstream of the PON. This issue arises as a result of a PON's multipoint-to-point architecture, which is inherently more secure than the downstream. Due to the possibility of eavesdropping in TDM PONs, encryption measures are used to discourage prospective eavesdroppers. For each OLT and user in the network to have a point-to-point connection, encryption is implemented at or above the MAC layer.

1.5 Last Mile Technologies

The end-to-end communication network link comprises various modules that address various functions to deliver a diversified collection of services. The needs and preferences of a service-using end-user influence the range and quality of these services. Internet service providers (ISPs) and Network service providers (NSPs) are the two key businesses that provide services that allow end-users to communicate with one another (ISPs). NSPs build worldwide networks and lease bandwidth to regional Service Providers, who then sell the capacity to local ones. Local ISPs distribute the services to end consumers. As a result, the complete network is kept as discrete blocks, and different technologies can be employed in every block. This framework allows the Internet backbone, ISP network, and end-user last-mile network to be developed and controlled practically independently.

When considering a communication system as an entire block between sender and recipient, several distinct mediums are used. However, the communication process can be divided into minor parts for simpler study. In commercial mobile networks, the backhaul transmits communication signals through a very dependable bandwidth-rich physical medium. This necessitates the usage of a wired setup of infrastructure, such as OFC. In order to establish final connectivity between Service providers and end users, a standard is used known as last mile technology. Unlike backhaul, last-mile technology is also dependent on end-user requirements, where coverage and budget may become more essential than reliability and data transmission velocity. Wireless technologies are strong contenders for last-mile technology [35]. They offer a good settlement due to user mobility and convenience of use, both of which are critical in new-generation technologies in mobile networks. The use of mobile devices and mobile communications is quickly expanding among technology users. The fact that wireless technologies cannot match the reliability and data transmission rate of their wired counterparts becomes secondary apprehension.
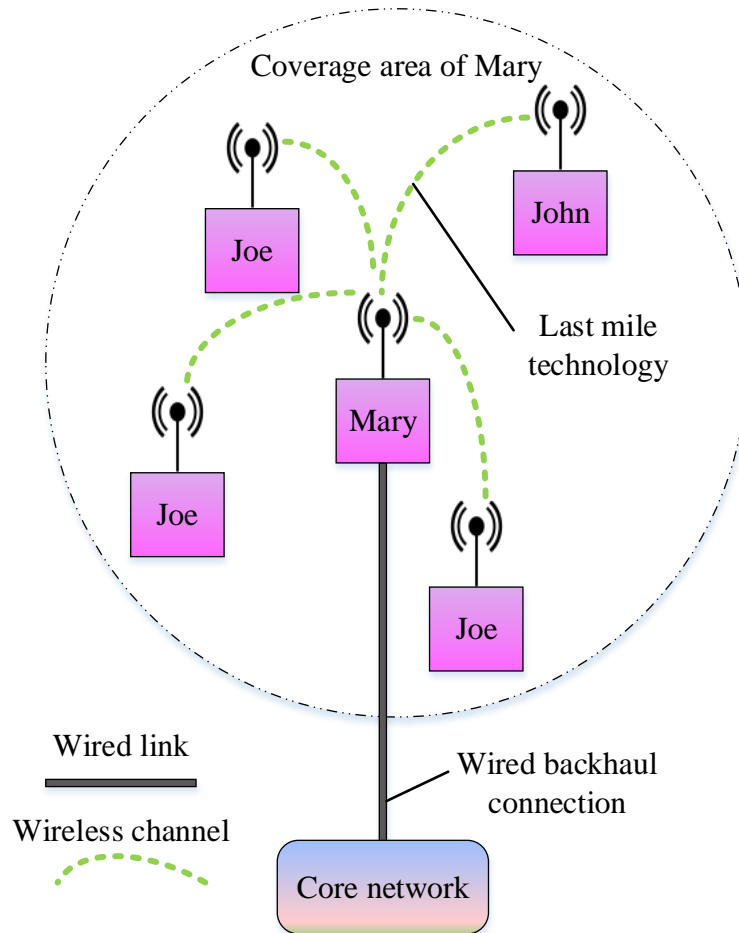
Figure 1. 8: Wireless Network as a last mile technology

The open nature of the wireless channel makes it more vulnerable to security concerns. In Figure 1.8, Mary, a genuine wireless transmitter, is shown using a wired connection to connect to the main network and using wireless for the last mile link to interact with John, a legitimate receiver. Due to the open nature of wireless technology, unauthorized receivers can also pick up Mary's transmissions. The strength of the signal received on John varies with distance and is influenced by channel characteristics like multipath fading and shadowing. The same method of reception is used for interference from other resources.

1.5.1 Selecting Wireless as a last mile technology

Wireless networks are now a significant part of telecommunication networks, and they shall also be a significant part of future network developments in future. A significant portion of broadband users use the family of IEEE 802.11 technologies in addition to 4G and 5G mobile systems to associate their PCs to the Internet final mile. The use of wireless technologies as the last mile technology is therefore extremely likely to continue in the future. Mobility and

simplicity of use are the major factors influencing the choice of wireless technology. In reality, when compared to desktop with 42%, the percentage of time spent on mobile digital media in the US is already greater at 51%. The usage of wireless technologies has drawbacks, including limited bandwidth and security concerns. While the increased data rates of more recent wireless technologies make up for the disadvantage of lower data transmission rates, the open nature of wireless communications makes security concerns with wireless technologies a serious concern. Using wireless technology exposes the physical layer to specific vulnerabilities in addition to security risks from the OSI model's upper layers.

1.5.2 Importance of last mile for security

The open nature of the wireless channel, as was previously discussed, is what poses the biggest security problem for wireless technologies as the final mile. In traditional cable networks, cables make up the physical layer medium, and signal communication via a cable amid two nodes is regarded as secure. This assumption is true since it would be simple to make a cable physically impossible to access, for as by employing subterranean cables or secured server rooms. When the cables are inaccessible, it becomes exceedingly difficult for unauthorized users to carry out eavesdropping attacks to listen to the link and collect data. Instead of requiring wires to transfer signals, antennas are utilized in wireless communications to both transmit and receive signals. After sendoff from the transmitter antenna and before they reach the receiving antenna, the signals undergo some strength and phase shifts. But when wireless channels are used to send signals, the latter can go anywhere as there is a sufficient level of Signal-to-Interference plus Noise (SINR), i.e., within the transmission range. A requirement for effective signal reception on the receiver side is that service providers maintain the SINR over a threshold that is acceptable to their consumers.

However, the SINR level for unauthorized users could be sufficient to successfully intercept the sent data, which raises serious safety concerns when taking into account the eavesdropping assault. There is a spatial pattern to how signals are disseminated when they are emitted from an antenna, and the next part will go into more detail on how signal strength varies with distance. The antenna range is the spatial characterization of a signal's presence above a certain threshold. The areas where the signal can be successfully received are specified by this. All users within the broadcast range, including unauthorized receivers like eavesdroppers, can receive and receive the transmitted signals. The wireless transmitter antenna, named Mary in the diagram, is linked to the main network through a wired link. Mary is the authorized

transmitter, sending signals to an authorized receiver John, but the signals are also received by unauthorized users, also known as Joe. As a result of the intrinsic characteristics of wireless channels, such as route loss and shadowing, the received power of signals from the transmitter antenna as a function of distance is also depicted in the image. The following section will go into great detail about these attributes. It is obvious from the context that the security of the last mile has an impact on network security overall. Even though the main network security risks may be handled by established security solutions, the security of the wireless last mile is still a problem that needs to be handled with physical layer security procedures that are specifically tailored to the wireless channel.

1.6 Aquila Optimization

Motivated by the natural behavior of Aquila in the prey-capturing method, the Aquilla Optimization AO is a revolutionary meta-heuristic optimization method. To capture a wide range of prey, most notably squirrels, deeps, rabbits, marmots, hares, and other ground animals, the Aquilla bird has agility and speed with powerful broad and feet, pointed nails. Therefore, numerous hunting methods rely on the prey's natural behavior. The conditions of hunting and the bird's capability to transition back and forth between chasing techniques neatly and quickly impact the choice of hunting tactics. The improved AO (IAO) Algorithm has been improved to identify the highest result for transmission conditions in the RoF link, which also includes power transmission and bias current. AO is related to the Aquila's natural hunting behaviors. General AO has a modest convergence rate and struggles to maintain stability. According to the results, IAO is suggested together with a propagation factor. This has the potential to increase AO's performance. Therefore, the proposed optimization methods of the algorithm are distributed into four classifications: selecting the hunt space with a vertical stoop and high soar, determining within a deviated hunt area with a short glide assault and contour flight, looking to exploit within a converged hunt area with a slow descent assault and low journey, and swooping with a snatch and walk victim.

1.7 Harris Hawk Optimization

Originating in southern Arizona, USA, Harris Hawks are the greatest intellectual birds as per the survey by Louis Lefebvre in 1997. Harris Hawks' stocking behavior differs greatly from other birds, as they continue to feed with other family members of the same species. They assault their prey using a tactic known as the "surprise pounce," often called the "seven kills"

strategy. While attacking, a few other hawks possibly ambush in various converge and directions on the target e.g. rabbit, completing the attack in a small seconds. Harris Hawks employ several hunting techniques dependent on the escape behavior of the prey and vigorous situation changes. Working in a group and found that the prey is trying to escape from the leader hawk after the leader hawk dives swiftly to attack it, for instance, hawks will alter tactics and send another hawk in the team for the pursuit. Such alternating strategies aim to exhaust the identified prey and enhance its hazard while confusing the intended prey. Finally, fatigued creatures cannot elude the hawk squad, as one of the powerful hawks kills and shares the exhausted prey with the group.

The cooperative behavior and surprise pounce hunting technique of the Harris Hawk in nature serve as HHO's primary sources of inspiration. The HHO mathematical approach provides behaviors and dynamic patterns to create an optimization method. The effectiveness of an HHO optimization procedure is assessed by contrasting it alongside various prevailing metaheuristic methods, 29 benchmark limitations, and numerous real-life engineering problems.

1.8 Ebola optimization

Disease modeling frequently takes the procedure of a Susceptible Infected and Recovered (SIR) approach. Attempts had been made to test such methods on Ebola virus disease. This modified prior SIR-based approaches such that the important parts are captured, making the transmission of EVD appropriate for optimization difficulties. An external agent or unclean environment helps as a reservoir of the quarantine population, virus, and population that is vaccinated, all designated by Q, V, and PE, respectively. The addition of PE is justified by agents that operate as virus reservoirs; Q and V are acceptable by the enthusiasm they bring to the afflicted and prone population. The SEIR+HVQD model is the result of a SIR-based model design, that now includes the exposed section and a mix of Vaccinated (V), Quarantine (Q), Dead (D), and Hospitalized (H) cases. More inspired by the construction of suggested optimizers with a special means that mimics the virus's ability to linger in the human body fluid of improved instances, thereby preventing the possibility of affecting vulnerable cases.

1.9 Benefits of RoF Technology

The following list includes a few advantages of RoF technology over electronic signal distribution.

1.9.1 Low Attenuation Loss

It is difficult and expensive to distribute electrical power for high-frequency microwave transmissions across transmission lines or in free space. Losses from absorption and reflection in open space grow with frequency. In transmission lines, impedance increases with frequency, resulting in extremely high losses. As a result, electrically transmitting high-frequency radio signals over large distances needs a costly regeneration apparatus. It is impossible to distribute mm waves across short distances using transmission lines. Distributing baseband or low intermediate frequency (IF) [36] signals from the switching center to the BS is another solution. At every base station, up-conversion of the baseband or IF signals to the necessary microwave or mm-wave frequency are amplified, and broadcasted. The system configuration used to distribute narrowband mobile communication systems is the same as this one. This configuration results in complicated base stations with stringent performance requirements because high-performance LOs are needed for up-conversion at each base station. However, because OFC has such a low loss, therefore RoF technology can be utilized to simultaneously simplify RAUs and distribute mm-waves with minimal loss. Commercially available standard Single Mode Fibres (SMFs) manufactured of glass (silica) [37] with attenuation losses < 0.2 dB/km and 0.5 dB/km in the 1550 nm and 1300 nm windows, respectively. In the 500–1300 nm range, Polymer Optical Fibres (POFs), a more contemporary type of optical fiber, show increased attenuation that ranges from 10–40 dB/km. These losses are far less than, for example, those in coaxial cable, which are three orders of magnitude larger at greater frequencies. For frequencies above 5 GHz, the attenuation of a 12-inch coaxial cable (RG-214) is greater than 500 dB/km. As a result, transmission distances are multiplied by multiple, and the required transmission powers are significantly decreased when microwaves are transmitted in optical form.

1.9.2 Large Bandwidth

The bandwidth provided by OFCs is huge. The wavelengths of 1550 nm, 1310 nm, and 850 nm are the three main transmission windows that provide low attenuation. The total bandwidth of the three windows for a single SMF optical fiber is greater than 50 Tera Hz. Modern commercial systems just use a small portion of this capability, though, therefore this is a problem (1.6 THz). However, research to utilize greater optical capacity per fiber is currently ongoing. The main forces behind extracting ever-increasing amounts of bandwidth from optical fiber are the availability of Erbium Doped Fibre Amplifier for the 1550 nm window, low

dispersion fiber, and the usage of specifically Optical Time Division Multiplexing in conjunction with Dense Wavelength Division Multiplex (DWDM) techniques, advanced multiplex techniques. Apart from having a great size for carrying microwave signals, the vast bandwidth provided by OFCs has other advantages. The extreme optical bandwidth allows for high-speed signal processing, which may be more challenging or even impossible in electrical systems. In other words, it is possible to perform multiple challenging microwave operations, such as mixing, filtering, and up/down conversion, in the optical domain. For example, it is possible to perform mm-wave filtering by first converting the electrical signal to be filtered into an optical signal, filtering the optical signal with optical devices like the, then transforming the filtered signal back into electrical form and Fibre Bragg Gratings (FBG) or Mach Zehnder Interferometer (MZI). A further benefit of optical domain processing is the ability to handle large bandwidth signals while using less expensive low-bandwidth optical components, including modulators and laser diodes.

Since electronic devices serve as the main transmitters and receivers of data transmission, their limited bandwidth significantly restricts the use of optical fibers' enormous bandwidth. The term electronic bottleneck refers to this issue. Inefficient multiplexing is the cause of the electronic bottleneck. Digital optical systems use the OTDM and DWDM methods that were previously stated. Sub-Carrier Multiplexing (SCM) is used to enhance optical fiber bandwidth utilization in analog optical schemes, which includes RoF methods. In SCM, several microwave subcarriers that have been modulated (analog or digital) are merged and utilized to modulate an optical signal which is then transmitted through a single fiber, hence making RoF systems economical.

1.9.3 Immunity to Radio Frequency Interference

The capability of optical fiber communications to be insusceptible to electromagnetic interference (EMI), predominantly for microwave transmission, is quite an alluring feature. This is correct since the signals are transferred through fiber in the form of light. Fibre cables are selected even for transitory connections at mm-waves because of their immunity. The immunity to eavesdropping is related to EMI immunity and is a crucial feature of optical fiber communications since it offers security and privacy.

1.9.4 Maintenance and Easy Installation

In RoF systems, expensive and complicated apparatus is maintained at the head end, simplifying the RAUs. For example, the majority of RoF methods do away with the requirement for a LO and associated equipment at the RAU. The RAU in these circumstances is made up of an RF amplifier, a photodetector, and an antenna. The head end is where the switching and modulation hardware is sustained and shared by numerous RAUs. This arrangement results in RAUs that are smaller and lighter, which efficiently decreases the cost of maintenance and implementation. Because there are so many RAUs needed for mm-wave systems, they must be simple to install and inexpensive to maintain. The decrease in maintenance requirements results in significant operational cost savings in applications where RAUs are not readily available. Environmental effect is also lessened as a result of smaller RAUs.

1.9.5 Reduced Power Consumption

Having simplified RAUs with less equipment results in reduced power centralized head end is where most of the sophisticated equipment is maintained. The RAUs are used in passive mode in various applications. They may be used in passive mode for instance, in some 5GHz Fibre-Radio systems using pico-cells. Given that RAUs are occasionally located in off-grid, rural areas, the RAU's decreased power consumption is noteworthy.

1.9.6 Multi-Service Operation and Multi-Operator

RoF provides flexibility in how a system is operated. It is possible to make the RoF distribution system signal arrangement clear depending on the microwave generation method. The Intensity Modulation and Direct Detection (IM-DD) [38] method, for instance, can be designed to function as a transparent and linear system. Low-dispersion fiber and RF subcarriers that have been pre-modulated can be used to accomplish SCM. The distribution of traffic from many operators and services can then be done using the same RoF network, which will result in significant financial savings. Due to its chromatic dispersion tolerance, the thesis's main idea is that when combined with either WDM or SCM, the optical frequency multiplication (OFM) can also provide multi-service operation.

1.9.7 Dynamic Resource Allocation

Dynamically allocating capacity is possible because modulation, switching, and other RF operations are carried out at a centralized head end. For instance, in a RoF distribution scheme for GSM traffic, greater capacity can be provided to a location at peak hours and redistributed to other locations during non-peak hours. By using Wavelength Division Multiplexing (WDM), it is possible to allocate optical wavelengths as needed. A permanent allocation of capability, which will be a resource waste in situations where there is frequent traffic load variation and by wide margins, can be avoided by allocating capacity dynamically as needed. Additionally, having the centralized head end makes combining various tasks like mobility and macro diversity transmission easier.

1.10 Drawbacks of RoF Technology

RoF is principally an analog transmission system because it uses analog modulation and light detection. As a result, signal flaws like distortion and noise, which are crucial in analog communication schemes, are also crucial in RoF systems. These flaws frequently restrict the DR and NF of the RoF links. Because the power received at the BS from MUs varies greatly, DR is a crucial metric for mobile (cellular) communication systems like GSM. In other words, the RF power established from a MU that is close to the BS may be significantly larger than the RF power established from a MU that is several kilometers away but still in a similar cell. Relative intensity noise (RIN), shot noise, phase noise, thermal noise, and fiber dispersion are some noise sources in analog optical fiber communications. Chromatic dispersion may restrict the fiber connection lengths in Single Mode Fiber (SMF) based RoF systems. It can also produce phase de-correlation, which results in higher RF carrier phase noise. Modal dispersion significantly reduces Multi-Mode Fiber-based RoF systems' link range and bandwidth. It must be noted that the RoF transmission technique is equivalent, the distributed radio method need not be equivalent as well (for example, WLAN, UMTS), but rather can use complete multi-level signal modulation formats like OFDM or xQAM

1.11 Applications of RoF Technology

Generally speaking, the Rothe F scheme is unsuited for solutions where large Spurious Free Dynamic Range (SFDR = maximum output signal strength for which the power of the third-order intermodulation product is similar to the noise floor) is essential due to the minimum DR. This is particularly correct for mobile phone networks with vast coverage, such GSM which

demand SFDR values greater than 70 dB and this high SFDR is not necessary for the majority of indoor use cases. For example, GSM's necessary (uplink) SFDR drops from greater than 70 dB to roughly 50 dB for indoor applications. As a result, wireless signals from mobile and data communication (such as WLAN) systems may be easily distributed inside buildings using RoF distribution systems [39]. As a result, the RoF system is transformed into a distributed antenna system (DAS).

Due to immense losses over the walls in high-frequency applications like WPAN, cell size will be tiny, taking the benefits of RoF stated above. The fiber infrastructure installed within the building can be used for wired and wireless use cases. Using MMF or POF fibers to feed the RAUs instead of SMF fibers may lower maintenance costs and system installation, especially for indoor applications. MMF is commonly used in in-building data communication LANs. RoF schemes are also appealing for other current and future use cases that do not require a high SFDR. For example, UMTS MUs must manage their transmitter power so that the base station receives equal power levels. As a result, because UMTS does not require the high SFDR needed by GSM, RoF distribution systems can be employed for interior and outdoor UMTS signal distribution. Another area of application is in Fixed Wireless Access (FWA) schemes, such as WiMAX, where RoF technology can be used to optically carry signals over long distances optically. Broadband first/last mile access can be accomplished cost-effectively by bringing greatly shortened RAUs closer to the end user from which wireless links can be established.

1.12 Problem Statement

Analyzing the literature reveals the main drawbacks of current methods for transmitting safe data. The current research has certain significant limitations, including bandwidth usage and achieving minimum data rates. Therefore, the following is considered:

- Review on RoF Technology and mitigation Schemes over challenges in RoF Network.

- Propose Optimization Approaches to improve the transmission conditions in the Radio Over Fiber Network.

- Physical layer security (PLS) and transmission performance issues in RoF.

- Processing time complexity due to key generation.

- Weak encryption and excessively attenuated optical fibers. Due to high BER and high computational complexity, existing approaches suffered in GFDM modulation in heterogeneous networks for 5G.

- The lengthy encryption and decryption processes severely hampered OFDM and GFDM in 5G wireless communication. Due to high noise and inaccuracy, device-to-device schemes based on GFDM- in 5G cellular networks suffered.

- The existing approaches have poor performance metrics in both D-RoF and A-RoF systems, including eye-opening penalty (EOP), EVM, encoding and decoding time, bit error rate, PSNR, and SNR.

1.13 Motivation

The PON's broadcasting nature in downstream traffic makes the data it transmits more susceptible to interception by unauthorized Optical Network Unit (ONU). With physical layer security, data transport, and header information can be safeguarded. Recently, numerous strategies for enhancing physical layer security have been put out, but most have neglected transmission efficiency. Optical orthogonal frequency division multiplexing (O-OFDM) was lately hailed as a viable modulation method for the next PONs due to its many advantages, including resistance to fiber dispersion, cost-effectiveness, and high spectrum efficiency. The primary disadvantage of the O-OFDM signal is its high PAPR, which leads to optical receiver saturation and nonlinear distortion. These significant shortcomings drove to improve the GFDM-PON strategy by safeguarding the physical layer. So this work suggested a way of encryption for GFDM-PONs to improve physical layer security. Given the inherent benefits, such as high spectrum efficiency, cost-effectiveness, variable allocation of resources, and good tolerance to fiber dispersion, GFDM-PON has received a lot of attention in next-generation PON research. The GFDM block receives less Cyclic Prefix (CP) than an OFDM block. As a result, the GFDM system's general spectral efficiency is enhanced.

According to the emerging trend in next-generation wireless communication, transport options, integrating diverse communication designs, and switching technologies would be crucial. By enhancing channel capacity, transmission speed, and bit rate, MIMO technology enhances the performance of wireless communication systems. MIMO uses several antennas for reception

and transmission to benefit from multipath propagation. By enabling its antenna array to focus tiny beams onto a user, 5G technology, which was already commercialized in 2020, helps to boost capacity and spectral efficiency. MIMO was added to LTE to take advantage of multiple path propagation and enhance signal quality. The RoF link is an ideal option owing to the large losses of a coaxial cable with signals of high frequency. The capability of the MIMO system can still be increased, although it will be challenging. So, an efficient strategy is unavoidable for data transmission in the MIMO system. Although there is an ancillary study in this area, the greater power consumption resulting from transmission conditions hurts the performance of existing MIMO approaches. These significant shortcomings push to create a better strategy for addressing the transmission challenges in the MIMO system.

1.14 Research Objectives

- To study and analyze the existing radio over fiber technologies for last-mile connectivity.
- To design an optimal framework for radio frequency to optical signal conversion.
- To develop a meta-heuristic algorithm for the proposed framework
- To enhance the security of last-mile connectivity

1.15 Thesis Organization

Chapter 1: Introduction

This chapter addressed the history of RoF, GFDM, and PON and their roles in diverse applications. In addition, information on the many forms of RoF, problem definition, research objectives, motivation, and thesis proposal will be offered.

Chapter 2: Literature survey

This chapter includes the relevant works of RoF Technology and Mitigation Schemes provided by various writers. This chapter also discusses the work's benefits and drawbacks. The paper below is also included in the literature review.

Chapter 3: Analog and Digital RoF Spatial Mux MIMO-LTE System-based arithmetic Aquila optimization model for 5G network

This chapter discussed the Aquila optimization model for the 5G network based on the Analog and Digital RoF Spatial Mux MIMO-LTE System. A detailed, step-by-step walkthrough of the

suggested methodology is provided. This chapter also provides comparison charts as well as information on the implementation tool. Many techniques currently in use are used to analyze the effectiveness of the work offered and this chapter is concluded with a summary.

Chapter 4: Improved Aquila Optimization based Parameter Evaluation Framework and Meta-heuristic Algorithm in RoF SpatialMux MIMO-LTE System

This chapter discusses the Improved Aquila Optimization-based parameter estimation framework and Meta-heuristic method in the RoF SpatialMux MIMO-LTE system. The proposed methodology is thoroughly explained step by step. It contains information on the dataset, the implementation tool, comparison tables, and graphs. Many methodologies that are now in use are used to assess the effectiveness of a supplied work. Finally, a summary concludes the chapter.

Chapter 5: Physical Layer Security in Generalized Frequency Division multiplexing-passive Optical Network using Optimization-based Encryption Technique

This chapter discussed physical layer security in a generalized frequency division multiplexing-passive optical network utilizing an optimization-based encryption approach. The proposed methodology is thoroughly explained step by step. It includes information about the implementation tool as well as comparison tables. Many methodologies that are now in use are used to assess the effectiveness of a supplied work. This chapter comes to a close with a summary.

Chapter 6: Enhancement of security in GFDM using Ebola-optimized joint secure compressive sensing encryption and symbol scrambling model

This chapter addresses the Ebola-optimized joint secure compressive sensing encryption and symbol scrambling model for GFDM security enhancement. In-depth, step-by-step instructions are provided for the suggested methodology. Numerous techniques now in use are used to evaluate the effectiveness of a work offered. The chapter ends on a breezy note.

Chapter 7: Conclusion and future work

This chapter offers an overview and conclusions for the suggested works. This chapter also quantifies the significant findings that were made. This chapter also discusses the potential for carrying out future work.

1.16 Summary

Passive Optical Networks (PONs) have received much attention in recent decades as a potential technology for fulfilling the increased demand for broadband services due to their high capacity, lower cost, and energy efficiency. Data delivered over the PON is more vulnerable to eavesdropping through an unauthorized Optical Network Unit (ONU) since it is a broadcasting structure in downstream traffic. As a result, data transmission security concerns in PON become more onerous. This chapter discusses RoF, GFDM, PON, last mile connectivity, benefits of RoF technology, limitations, and applications. This chapter also covers the problem statement, research objective, and thesis organization.

CHAPTER 2

LITERATURE SURVEY

2.1 Overview

The number of Internet users and data communication speed is growing fast in the modern world [40]. The Next Generation Network (NGN) is created as the primary concern. It is divided into two segments, the Next Generation Core Network and Next Generation Access Network, to meet the bandwidth need [41]. Photonic technology and the installation of optical fibers have boosted the network's transmission data rate [42]. The communication network's real-time, high-speed industrialization is required to provide access to information from any location. Data transmission relies heavily on wireless and optical fiber networks [43]. The key advancement for wireless networks in the future is ROF technology. Recent developments in radio over fiber have made it possible to transmit radio frequency signals over great distances [44]. Wireless access coverage is boosted by including a basic antenna in the RoF technology. The communication from optical to radio signals is delivered at high speed with flawless convergence utilizing millimeter (mm) waves [45].

The part of the ROF technology in the base station, signal processing occurs through modulation, frequency conversion, and multiplexing. The signal processing and de-multiplexing procedure happens in the central station [47]. The optical signal is delivered via fiber to the base station, where the RF signal is retrieved by photodetectors, amplified, and then transmitted to the antenna [48]. Broadband access is used to broadcast radio frequency communications to end users without interference using a Remote Antenna Unit (RAU). RAU includes fewer components, lowering the installation cost [49]. A passive Optical Network (PON) is the best method for transmitting data from the antenna to end users for last-mile connectivity. The optical line terminal is terminated in the central base station to transform the optical signal into an electrical signal in a PON network [50]. Because radio over fiber uses optical fiber to operate the stations, it may offer superior solutions to wireless communication and optical fiber [51]. Based on the above-mentioned systems, the literature survey distinguishing the various techniques, performance analysis, advantages, and disadvantages are covered in this chapter.

2.2 Various research based on security in the RoF system

Singh M. *et al.* [52] advised a unique design for a Radio over Free Space Optical (RoFSO) transceiver based on Orthogonal Frequency Division Multiplexing-Mode Division Multiplexing (OFDM-MDM) that was resistant to the effects of dust. To establish an 80 GHz 5G communication link 40 Gbps single-channel, two different 20 Gbps-40 GHz 4-QAM data-bearing optical beams were transmitted via two discrete Hermite-Gaussian modes, HG01 and HG00. The SNR and total power were used as the main assessment metrics to examine the connection availability and performance under the influence of a clear climate. The various dust circumstances, including very moderate dust and dense dust, light dust, and light. Additionally, they had established the longest link distance that can be reached while still meeting suitable performance standards, i.e., SNR 20 dB for each desert weather scenario.

Elbir A. M. *et al.* [53] presented a Deep Learning (DL) method for hybrid beamforming and channel estimate in frequency-selective wideband mm-Wave schemes. A massive MIMO Orthogonal FDM (MIMOOFDM) system offers three dissimilar DL procedures of Convolutional Neural Networks (CNNs), which receive raw data of a conventional signal as input and produce channel evaluations and hybrid beam formers at output. Furthermore, they present offline and online prediction algorithms. This approach offers higher tolerance, larger spectral efficiency, fewer pilot signals, and lower computational cost against variances in the received pilot data, propagation environment, and corrupted channel matrix according to numerical experiments comparing it to the most advanced optimization and DL methods currently available.

Yichuan L. *et al.* [54] proposed a photonics-assisted beamforming method to replace the large electronic phase shifters and the beam-squinting effect while offering a low-cost RAN setup. They use an Analogue Radio over Fiber (A-RoF) assisted design to support current and future mobile network availability. This photonics-assisted beamforming was combined with a reconfigurable multi-user MIMO method, allowing users to use beamforming joined with diversity, stand-alone beamforming, or beamforming joined with multiplexing dependent on resources presented, the user channel information, and the quality of service necessities.

M. Vinoth K. & Vinod K. [55], had suggested creating a millimeter wave for radio over fiber. By achieving the frequency range, Wavelength Division Multiplexing (WDM) was assessed to increase channel capacity and bandwidth. By enhancing both the direct and indirect modulated waves at the transmitter side and using the Mach-Zehnder Modulator (MZM) and Phase

Modulator (PM), the millimeter wave was produced in this instance. Due to its lighter weight and low transmission loss, optical fiber had been utilized to transport signals, and an optical fiber network had also connected the base station and the central.

Jaswinder K. & Vishal S. [56], had suggested a higher order spatial diversity QAM schemes enabled MIMO-OFDM-RoF system that was Orthogonal Space-Time Block Code (OSTBC) prepared. The proposed work handled both LOS (Line of Sight) and NLOS (Non-Line of Sight) states. The exhibited work also explains relative QoS studies of sixth (3*2 antenna package) and ninth-order spatial diversity (3*3 antenna package). It suggests the best antenna suite based on the demands of a suggested combined scheme in the established circumstances.

Anastasios V. *et al.* [57] proposed a hybrid link TDMA HL-TDMA Mac protocol that was supplied to them for convolutional and RoF links in Wireless Local Area Networks (RoF-WLAN). Optical fiber and a wireless network were combined to form RPOF. The performance had been predicted to be improved by Hybrid Link Time Division Multiple Access (HL-TDMA). In convolutional WLAN, the separation between the mobile station and the central station was many meters, whereas, in ROF-WLAN, it was many kilometers. Only the throughput performance in both ROF and convolutional WLAN had been enhanced by HL-TDMA.

Weile Z *et al.* [58] suggested a ROF link (or APL) with multidimensional optimization, which can achieve nonlinearity mitigation, dispersion-induced power fading correction, and CSR optimization all at once. For a 50-km SMF transmission, the link gain, SFDR, and NF were increased by 11.9, 14.5, and, 5.8 dB, respectively, over a traditional quadrature-biased link according to MZM. The working frequency of a system was only constrained by the modulator and PD's combined bandwidth since other components were frequency-independent. Initially, only one bias voltage needs to be steadied for the system to be stable and automatically organized. This can be done with commercial bias controllers for the MZM (plug tech, MBC-MZM-01).

Tingwei W. *et al.* [59] provided chaotic Compressive Sensing (CS) encryption techniques to reduce the amount of sent data and boost data security for an Orthogonal Frequency Division Multiplexing Passive Optical Network (OFDM-PON). Owing to its incapability to fulfill the sparseness in neither the time domain nor the frequency domain, direct CS bitstream transmission was limited. While the sparsity of data transmission can be created when sending multimedia. The data is then categorized as multimedia using a sensor. If so, the sensor output

is set as side information simultaneously communicated to the terminal and entered into the pilot via the CS approach. A 2D-LSCM was used for encryption processing to create pseudo-random integers to build the first row of a measurement matrix that encrypts the scheme. After that, four transform formats were used to create the transmitted data's sparseness. The DCT was used to implement the CS approach since data transmission was constrained at the physical layer.

R. Anil K. & K. Satya P. [60], had proposed the work to create a cluster-based approach that creates the greatest number of node contacts in a heterogeneous wireless network. Further, provided effective development in Multi-User Generalized FDM implementation in the physical layer for wireless communications. Disconnected nodes Base Stations (BS) decreased the efficiency and coverage capacity of the wireless network. Anytime a wireless front/endpoint is linked to at least one isolated neighbor node, it functions as a virtual clustered head based on the node's shortest path and residual energy.

Rizwana A. & Anand S. [61], had proposed an Optical GFDM (O-GFDM) scheme for VLC against its O-OFDM equivalent for various performance parameters. The proposed O-GFDM scheme performs better in terms of experimental outcomes of PAPR, SER, and subcarrier frequency shift tolerance, which were used to construct the analytical formula for the SER of O-GFDM. One of the proposed scheme's variations was discovered to use less power and have greater spectral efficiency than its O-OFDM counterpart. The GFDM-based VLC system was anticipated to operate extremely well with next-generation wireless systems to offer smooth services. It will enable more elasticity using software-defined networking since GFDM was being investigated for 5G wireless networks.

Siva V. *et al.* [62] developed a block circulant nature of the GFDM modulation matrix to reduce the difficulty of a GFDM. They simplify the calculation of an inverse for the minimum MSE receiver by expressing the modulation matrix as the sum of permutation matrices. The DFT, which they refer to as the extension of DFT to the modulation matrix, was used in conjunction with the theory of circular arrays to get the inversion formula. A set-up was created utilizing LabVIEW software and National Instruments Universal Software Radio Peripheral (USRP) 2953R hardware to verify the suggested algorithm's non-distorting nature.

Mohammad U. H. & Ghulam M. [63], had developed a DAS (distributed antenna) system network based on RoF which can support both sixth-generation terahertz and fifth-generation millimeter wave services. A 10 km single-mode OFC was used to test the experimental

broadcast of a single-carrier modulated 6G signal utilizing 256-QAM and a 5G new radio signal. Additionally, at the 6G RAU, a 3 m wireless medium was used to receive the 6G signal. The distance of wireless transmission of the 6G THz link was required to be 3 m due to the restrictions of the experimental environment, resulting in a net loss of 7 dBm in power. EVM and CSR were used to evaluate performance. A vital tool for the coexistence of 6G and 5G services, which can be implemented using silicon photonics, was photonic integration, also employed in this experiment to combine many photonic components.

Adnan H. A. *et al.* [64] investigated and assessed an optical (Orthogonal Frequency Division Multiplexing) OFDM-RoF-based Wireless Local Area Network (W-LAN) system. Microstrip patch antenna and the OFDM-RoF technology, both used in the Opti system communication tool, offered the framework for merging optical and wireless technologies into a single system. To accommodate mm-wave services and multi-standard operations, the suggested OFDM-RoF system was designed in this manner. The suggested system can work with several modulation techniques, such as 4.16 and 64QAM, which can be connected to OFDM, support multi-data speeds of up to 5 Gbps, and operate on various RF bands. The outcomes show the integrated optical wireless link's sturdiness in transmitting OFDM-RoF-based WLAN signals through optical fibers.

Meet K., *et al.* [65] proposed and experimented with a symmetrical and bidirectional Time and Wavelength Division Multiplexing-Passive Optical Network (TWDM-PON) system. The upstream and downstream transmission was accomplished using OFDM and 4-level quadrature amplitude modulation. To support the cost-effective high transmission rate fiber/VLC optical network, a 625 nm red light-emitting diode was also used for Visible Light Communication (VLC) via a radio link. For variable fiber-wireless connection range, downstream and upstream channels for the TWDM-PON using OFDM with the VLC scheme had been examined. In the proposed link, the impacts of a large transmission rate and the use of a Digital Signal Processing (DSP) unit to lower losses caused by fiber nonlinearity effects have also been studied.

Jinnan Z. *et al.* [66] suggested a three-dimensional (3D) carrier-less amplitude and phase modulation approach for Trellis-Coded Modulation (TCM) that was suitable for Passive Optical Networks (PON) and relied on Clustering Mapping Principles (CAP). This technique expands the TCM's coding gain while combining the constellation shaping and TCM mapping processes, performing a multi-level mapping of the coded signal under the classification label to improve constellation shaping gain. Chua's chaotic model for rotation encryption was

adopted by the 3D constellation produced by the multi-level mapping, which enhances the optical access network's capacity to fend off hostile attacks at the physical layer. Experiments demonstrate that the approach suggested in this study allows for 70 Gb/s (710 Gb/s) transmission on a 2 km weakly connected seven-core OFC.

Mrinmoy S. *et al.* [67] presented a Twin Symbol Hybrid Optimization that would be the foundation of the Cyclic Prefx-OFDM (CP-OFDM) method known as Partial Transmit Sequence (TSHO-PTS). This said method met the demands of 5G communications standards. Furthermore, the rigorous search for ideal phase components may raise PTS's computing expense. A hybrid version of the Bald Eagle Search (BES) and Slap Swarm Optimization (SSO) algorithms was presented to solve this issue and examine the phase factor by the PTS approach as effectively as possible. The DFT Spread OFDM (DFT-S-OFDM) subcarrier allocation data transmission technique uses chaotic digital sequences to maintain the physical layer security. Different performance metrics were used to assess the performances, such as the Bit Error Rate (BER), Complementary Cumulative Distribution Function (CCDF), and computational complexity. Several current approaches and earlier research were compared to the performance of a suggested model.

Joarder J. S. *et al.* [68], had loped the combined effect of a 3D fractional-order Liu chaotic system and a 3D fractional-order Li chaotic system in the physical layer security of the UAV-to-ground communication network. Additionally, effective Orthogonal Variable Spreading Factor (OVSF) codes were used with a Zero Forcing (ZF) scheme to lessen Multi-User Interference (MUI). Additionally, a combined MUI signal discrimination and ZF signal detection strategy were presented to reduce the Bit Error Rate (BER). Various channel coding methods with multi-user beamforming weighting were provided in this method. The numerical results demonstrate the suggested system's effectiveness in physical layer security (PLS) and data rate improvement with a signal-to-interference-plus-noise ratio. With this method, 119 dB less out-of-band emission was produced.

Syamsuri Y. *et al.* [69] produced the Dual-sideband Optical Carrier Suppression (DSB-OCS) approach was used to generate an optical millimeter-wave (mm-wave) signal in Radio over Fibre (RoF) systems. The suggested system uses a Dual-Electrode Mach-Zehnder Modulator (DE-MZM) with a carrier of 40 GHz mm-wave for data transmission across the RoF systems. Characteristics that affect the system's performance include the modulation index, phase imbalance, and dispersion parameters. The system output tests demonstrate that when the

modulation index is increased, the mm-wave signal output power follows the MZM's transfer function. Additionally, phase imbalance and optical splitting ratio impacted the generated optical mm-wave signal power. The DSB-OCS system was observed to be affected by optical fiber dispersion, which reduces the amplitude of the mm-wave and SNR.

Mohit B. & Manoj S. [70], had presented an inexpensive radio over fiber system with mm-wave generation based on Stimulated Brillouin Scattering (SBS). A stimulated Brillouin scattering-based, dispersion-tolerant millimeter-wave signal that spans the frequency range of 20 GHz to 80 GHz was demonstrated. The proposed design differs from earlier works because it uses a null-biassed modulator and an all-optical SBS approach to generate improved frequency shifts in the mm-wave region. A remote optical local oscillator system was suggested for radio over fiber systems. Both the central station and the base station produce high-frequency signals. High carrier signals were produced by SBS in the central station and by heterojunction bipolar transistors at the base station. The overhead of a large-frequency or traditional oscillator was reduced when a radio-frequency signal was used as the local oscillator.

Xiaorong X. *et al.* [71] suggested a bidirectional link resource allocation technique, GFDM-based multiuser SWIPT systems, to increase system energy efficiency. Each SWIPT user employs Power Splitting (PS), receiver structure for Information Decoding (ID), and non-linear Energy Harvesting (EH) in the downlink channel. The electricity used for information transmission in the uplink channel was produced from the energy that had been gathered. Through bidirectional link power allocation, subcarrier and subsymbol scheduling, and weighted sum ID attainable rates, an optimization problem was created to maximize these rates in the downlink and uplink channels. The Lagrange duality approach, the sub-gradient-based method, and the greedy algorithm were each used to tackle this non-convex optimization problem.

Deepthi S. & Visalakshi P. [72], had proposed (Enhanced OFDM) EO-OFDM approach for (Single Input Single Output) SISO and MIMO internal communication in VLC with regards to BER, channel gain, PAPR, and average received power. They conclude that MIMO performs significantly better than the SISO system model in indoor VLC communication. The wireless community was investigating the usage of EO-OFDM in 5G systems for various advantages, such as a flexible structure, straightforward sending and receiving of waveforms, and reduced power utilization through a decrease of PAPR.

Joarder J. S. *et al.* [73], had suggested a cooperative (Cyclic Prefix) CP-less mmWave downlink GFDM system. The emphasis was on physical layer security for (mMTC) massive Machine-Type Communication users in such a network when UAVs (Unmanned Aerial Vehicles) and a terrestrial cellular network were joined. In this study, using MU-MIMO (Multi-User Multiple-Input Multiple-Output) Gyre precoding and an effective low-complexity T-transformation spreading code led to a decrease in MUI (Multi-User Interference) and an increase in the achievable ergodic rate. By removing the impacts of a fading channel at mmWave, using null subcarriers at both ends of a GFDM block for sub-time symbols and a Better than better-than-raised cosine (BTRC) filter led to a large decrease in the OOB power of spectrum.

Zhiyi W. *et al.* [74], had proposed a novel constellation encryption system based on probabilistic shaping (PS), where two bit-level encryption operations are initially carried out using chaotic sequences and hash values. The hyperchaotic system creates the chaotic sequences, while SHA-512 calculates the hash values. Then PS was used to improve gearbox efficiency. Constellation encryption was used after PS-16- QAM with the goal of maintaining the overall shape distribution's consistency and enhancing security. In this experiment, it successfully broadcasted an encrypted PS-16-QAM OFDM) signal over a 50 km standard single-mode fiber (SSMF) and a 5 m wireless channel. The outcomes show that a key space of 10^{121} has been attained to protect against malicious attempts.

Yaoqiang X. *et al.* [75], had proposed a safe RoF system using feedback neural network (FNN) and key nested polar code. The original key for the nested polar code was chosen at random from the created codebook, and the index of the key was encoded by the inner polar code, which was placed at the location where the frozen bit of the outer polar code had better channel quality. The information bits for the other portion of outer polar code were encrypted by a chaotic sequence produced by 4-D cellular neural network. For orthogonal frequency division multiplexing (OFDM), the polar coded sequence was mapped to the 16-QAM symbol.

Archa C. & Joseph Z. J. [76], had suggested coherent detection (CD) uses an optical local oscillator (OLO) source to maintain the phase and magnitude of the transmitted signals. The same OLO was used in the design of a full duplex system. Digital signal processing techniques were used to rationally cancel the phase noise in CD systems. Analysis shows that any coherent RoF system can be created with acceptable error vector magnitude (EVM) and log (BER) values, resulting in a full duplex system.

Muhammad U. H. *et al.* [77], had suggested an architecture of Open Radio Access Network (O-RAN) specifications, and Radio over Fiber (RoF) systems were the main topics of this paper's exploration of current developments in optical communication for sixth generation (6G) networks. Using 60 GHz and 28 GHz carriers over 10 km single mode fiber, an experimental study of 6G Analog RoF shows how effective Digital Pre-Distortion (DPD) linearization was in lowering Error Vector Magnitude (EVM). Even though EVM had been shown to increase with bandwidth, DPD helps to somewhat enhance performance. This highlights how important it was to keep making progress in reducing obstacles and utilizing 6G Analog RoF (A-RoF) technology to the fullest for future O-RAN.

Shakir S. A. *et al.* [78], had suggested a new quantum MAC technique that addresses the propagation latency Quantum Teleportation was used in the Quantum Entanglement-based MAC protocol (QE-MAC). Data is transferred via the classical channel and four entanglement states were used to represent the control packets of the classical MAC protocol. State transitions were utilized as an alternative to control packets like acknowledgement, request to transmit, and Clear to send. The network performance was significantly improved by this method, which eliminates the latency and collision problems related to control packets. It formulate and determine the proposed QE-MAC protocol's latency, duty cycle (DC), and power consumption. Ji W. *et al.* [79], had proposed a wireless positioning mechanism and a radio-over-fiber distributed antenna system (ROF-DAS). Reflective Semiconductor Optical Amplifier (RSOA), ROF network based on star topology, optical switch array, and modified Medium Access Control (MAC) frame were used in the system design. To maximize signal transmission efficiency, the system uses a Sigma Delta Modulator (SDM).

The comparison table for various research based on security in the RoF system is given in Table 2.1 below.

Table 2.1: Comparison table for various research based on security in the RoF system

Author and References	Method	Objectives	Merits	Demerits
Singh. *et al.* [52]	OFDM-MDM	• The link availability and performance	• It gives a significant increase in the rate of	• Multiplexing in wavelength and polarization dimensions

		were examined under the influence of varied dust conditions and a clear climate.	information transfer.	needs to be improved. • It needs to improve the quality of the signal and the performance of the link overall.
Elbir. *et al.* [53]	CNNs	• This proposed method was utilized to evaluate the limited coherence and lack of fully digital beamforming in hybrid architectures.	• Higher spectral efficiency • Lower computational cost • Fewer pilot signals • Higher tolerance against variances in the pilot data that is received.	• Propagation environment and corrupted channel matrix
Yichuan L. *et al.* [54]	A-RoF	• This architecture aimed to support the current and future mobile network requirements.	• It created a low-cost RAN solution by developing a photonics-assisted beamforming method that does away with the heavy electronic phase shifters and the effect of beam-squinting.	• Cost was high

			• It increased throughput or improved performance for each user depending on the channel quality and user needs.	
M. Vinoth K. & Vinod K. [55]	PM, WDM, MZM	• Generate millimeter wave in RoFfibere	• Improved operating frequency • Results demonstrate acceptable increases in output power for sine wave ranges applied to modulators that were greater	• Transmission loss
Jaswinder K. & Vishal S. [56]	MIMO-OFDM-RoFThe	• Alamouti algorithm was used to implement MIMO-OFDM-based RoF to arrange spatial diversity.	• It was a trusted and spectrally efficient system • It had higher-order spatial diversity in combination with QAM systems. • It improves EVM performance with a significantly smaller power overhead.	• Spectral efficiency issues

Anastasios V. *et al.* [57]	HL-TDMA MAC protocol	HL-TDMA MAC protocol was proposed to enhance the functionality of RoF and regular WLANs.	• To improve the performance of conventional and RoF WLANs • The findings show that the probability of transmitted symbol errors decreased when several antennas were used in spatial diversity mode on both sides (transmitter and receiver).	• Only throughput has enhanced the performance using this method.
Weile Z. *et al.* [58]	ROF	• The objective was to develop a multidimensional radio over fiber link optimization.	• Commercial bias controllers for the MZM can achieve the necessary bias voltage stabilization. • It enhances the noise figure and the gain. • The signal can be transmitted without power fading.	• Only a small portion of the IMD3 components can be suppressed.
Tingwei W. *et al.* [59]	Chaotic compressive	• The objective was to compress data	• The chaotic encryption method was used	• The extra 5 to 8 times compression

				ratio on images was the only disadvantage and unacceptable.
	sensing, OFDM PON, 2D-LSCM	to transmit more valuable information using the same bandwidth.	to increase security. • OFDM works well with mobile fronthaul, other 5G communication protocols, and MIMO; it was selected as the transmission format.	
R. Anil K. & K. Satya P. [60]	Cluster-based algorithm and effective Multi-User GFDM	• The goal was to create a cluster-based method that creates the most node connections possible in a heterogeneous wireless network	• It demonstrates the performance improvement of the network. • Significant improvement in spectral efficiency with a 99.98% error rate reduction for GFDM at K=5. • Gains in efficiency of network energy, capacity, spectral efficiency, channel, and network capacity for GFDM at cluster iterations K=5 were 336%,	• There will be computational complexity for future communications. • PAPR needs to be reduced

			203%, 79.68%, and 190%, respectively.	
Rizwana A. & Anand S. [61]	O-GFDM	• The purpose of O-GFDM was used for indoor visible light communicatio n	• The subcarrier frequency shift tolerance and SER validated increased performance. • The proposed scheme's variations use less power and have greater spectral efficiency • Using software-defined networking increases flexibility.	• BER performance needs to be enhanced
Siva V. *et al.* [62]	OFDM and GFDM for 5G wireless communi cations	• The objective was to reduce the complexity using OFDM and GFDM	• Better resource distribution and intercession management • GFDM modulation matrix for GFDM system's receiver to decrease receiver complexity.	• The parameters of a system need to be optimized

			• To make the inverse computation for the minimum mean square error receiver less complex.	
Mohammad U. H. [63]	RoF-based DAS network	• The goal was to make future mobile networks more usable.	• The immanent benefits of RoF technology include enhanced DAS network usage and transmission performance.	• The suggested fiber wireless distributed antenna system would be more difficult for RAU since it had increased photonic constituents than the MHU. • Due to the experimental setup's limitations, the wireless transmission distance was limited to 3 m with a 7 dB clear loss. • Increased clear losses resulting from the longer wireless range could be

44

				compensated by using THz amplifiers.
Adnan H. A. *et.al.* [64]	OFDM-RoF	• OFDM-RoF approach aimed to give better efficiency for RF interferences and little multipath distortion	• A hybridized optical OFDM-active microstrip antenna system can increase system reliability by expanding the service coverage area. • It was appropriate for implementation in small-cell concepts and unified management. • It can cover a length of around 100 km on SMF and approximately 10 meters on a wireless platform.	• It addresses the hassle of elasticity and large throughput in 5G small cell transport systems.
Meet K *et al.* [65]	TWDM-PON, OFDM	• The Objective of the system is to improve high bandwidth requirements.	• The influence of large broadcast rate and usage of DSP units to decrease losses.	• Increasing the free space link reduces the optical power of the signal.

			• Decreases error rate • High transmission rate • The recommended TWDM-PON method can provide a next-generation access network from rural to urban ranges. • The technology can be put to use to deliver long-range, fast, cost-effective wired-wireless link services from rural to urban locations.	
Jinnan Z. *et al.* [66]	TCM method-based CAP	• The objective was to increase the optical access network's capacity to counter malicious attacks at the physical layer.	• The chaotic spherical constellation receiver had a sensitivity of approximately 6.98 dB higher than the 2D shaping constellation receiver.	• It needs to increase the transmission capacity at short distances.

			• It increases short-reach transmission capacity while providing dependable security performance • It attained error-free transmission	
Mrinmoy *et al.* [67]	CP-OFDM, TSHO-PTS	• The system was suggested to meet the needs of 5G telecommunication standards.	• The suggested approach achieved less PAPR • Minimum BER • Less processing time than the current systems • very low complexity	• Cost was high
Joarder J. S. *et al.* [68]	OVSF-encoded OW-DFTs-OFDM system	• The system led to a decrease in multi-user interference (MUI) and an increase in user data rate.	• Multi-user beamforming weighted mixed MUI signal discrimination and ZF signal detection strategy was presented to lessen BER and strengthened by a variety of channel coding approaches	• It had an impact on multiple eavesdroppers. • Difficulty in the use of massive MIMO • Need to improve the efficacy of a PLS technique.

			• Increases effectiveness and data rate with a low signal-to-interference-plus-noise ratio.	
Syamsuri Y. *et al.* [69]	DSB-OCS	• Data transmission over the RoF systems was accomplished by the suggested method using a DE-MZM and a carrier of 40 GHz mm-wave.	• According to the system's performance evaluations, the output mm-wave signal power increases as the MZM's modulation index is enhanced. • The optical fiber dispersion affects the system's performance by lowering mm-wave amplitude and SNR as fiber length increases.	• Needraiserise the transmission capacity of the method.
Mohit B. & Manoj S. [70]	Stimulated Brillouin Scattering (SBS)	• The method was developed to reduce the degrading effects.	• Low cost • Lower sidebands (LSBs) produced by the system under test had high power and strong SNR.	• Need to increase the efficiency of the system

Xiaorong Xu. *et al.* [71]	GFDM-based multiuser SWIPT systems	• The objective was to enhance the system's energy efficiency	• Examined the achievable weighted sum rates for bidirectional links by allocating subcarriers and subsymbols. • Increased system energy efficiency	• Computational complexity
Deepthi S. & Visalakshi P. [72]	EO-OFDM	• To decrease band energy usage and increase spectrum efficiency.	• Simple waveform transmitting and receiving, adaptable structure, and low power consumption due to PAPR reduction.	• Computational complexity
Joarder J. S. *et al.* [73]	GFDM, BTRC	• The method was used to improve BER performance and decrease OOB power emission	• It reduces computational complexity and MUI • Improves the performance of BER	• The BER performance was not exactly satisfactory.
Zhiyi W. *et al.* [74]	PS, OFDM	• Radio-over-fiber (RoF) system physical layer security was	• BER and security performance were dominant.	• Combining PS with PS-based encryption should be more effective.

		provided for future communicatio n.		
Yaoqiang X. *et al.* [75]	FNN, OFDM	• It was suggested to use a safe RoF system based on FNNs with key nested polar codes.	• The resistance to chosen-plaintext attacks and the resistance to brute-force attacks are covered. • It can assurance accurate information transmission while also significantly enhancing system security.	• Repeating mechanism can greatly increase time.
Archa C. & Joseph Z. [76]	CD using OLO	• To maintain the transmitted signals' phase and amplitude an OLO source was utilized considering CD.	• The suggested approach provides an efficient method to send four distinct signals back-to-back without phase noise interfering.	• Maximum received power
Muhammad U. H. *et al.* [77]	A-RoF technolo gy	• To modify throughout the course of several	• Providing increased dependability, efficiency, and	• Very less higher carrier frequencies

		development phases, motivated by real-world experiences with CRAN technologies.	speed to satisfy the ever-changing demands of the digital landscape	
Shakir S. A. *et al.* [78]	QE-MAC	• To suggest a novel IoT-RoF architecture based on quantum entanglement, where sensors gather data from their environment and send it to a decision-making section.	• It performed better when measured for delay, DC, and power consumption when compared to the traditional RoF MAC protocol.	• It was unable to concentrate on figuring the best way for distributing power and formulate throughput when there are collisions.
Ji W. *et al.* [79]	ROF-DAS	• To maximize signal transmission efficiency for downlink transmission.	• It can attain optimal results in terms of power usage and positioning precision.	• There was a slight variation in the positioning accuracy between 4 and 5 antennas.

In the mentioned literature study, this chapter covers performance analysis, the different methodologies' literature reviews, and their merits and weaknesses. The previous techniques suffered greatly from major limitations such as heavily attenuated optical fibers, low encryption

51

capability, high BER, high computational complexity, low encryption capability, and temporal complexity, according to a thorough examination of the aforementioned linked work. An innovative strategy is required to address these drawbacks.

2.3 Summary

Internet users and data communication speeds are increasing rapidly in the modern world. The Next Generation Network (NGN), divided into the Next Generation Core Network and Next Generation Access Network, was developed as the key issue to accommodate the bandwidth requirement. The communication network must be industrialized with high real-time speed to access information anytime and anywhere. The transport of data requires both wireless and optical fiber connections. This chapter comprises the pertinent writings on RoF Technology and Mitigation Schemes supplied by different authors. The objectives, methods, superiority, and drawbacks of the work remain too covered in this chapter

Chapter 3

Analog and Digital RoF Spatial Mux MIMO-LTE System-based A^2 (arithmetic Aquila) optimization model for 5G network

3.1 Overview

Regarding achieving high data rates in both uplink and downlink channels, 4G Long Term Evolution (LTE) systems rely heavily on MIMO technology. The capability of a MIMO-LTE system is increased by using multiple antennae on the transmitter and reception sides. Also, compared to SISO communication systems, the MIMO system avoids the excessive use of bandwidth and electricity. C-RAN, or cloud radio access network, is strongly advised in MIMO-LTE systems to boost system capacity. The baseband unit (BBU), which processes signals using a variety of standards, is the foundation upon which the C-RAN system operates. Typically, MIMO-LTE systems employ RoF links to improve connectivity between BBU and distant radio heads (RRH). As a result of some non-linear distortions, MIMO-LTE with RoF links employs a very broad bandwidth with little power loss. However, this distortion is caused by fiber dispersion and change from optical-to-electrical and electrical-to-optical. This disadvantage causes failure in spectrum redevelopment and is referred to as adjacent channel interference (ACI). The use of OFDM-based LTE or LTE-A systems now makes significant breakthroughs in reducing wireless channel distortions. However, it is very susceptible to distortion because of the high peak-to-signal noise ratio (PAPR) during signal addressing. Several research has recently been conducted to better understand the effectiveness of MIMO-LTE systems, focusing on transceiver signals.

Some quadrature-phase imbalance (I/Q) is common in space temporal diversity systems. This can be evaluated without using nonlinearity in the transmitter section at the previous step. Some typical crosstalk occurs before data transmission and must be thoroughly studied utilizing MIMO methods. Crosstalk is continuously examined in the RF transmitter using couplers instead of the real framework of the MIMO schemes. Data transmission in MIMO systems generally uses the same local oscillator (LO), which reduces power usage significantly. The single sideband frequency translation (SSSB) and double sideband frequency translation (DSB-FT) approaches are used for cost reduction in MIMO RoF systems. This method operates based on 2 MIMO channels sharing the same LO. A filtering mechanism is used in the SSB frequency translation system to reduce power loss in the LSBs and USBs. The recent 5G wireless communication trend demonstrates that integrating various communication architectures,

vehicle proximities, and switching mechanisms has become increasingly crucial. The MIMO approaches improve communication performance by rising speed of transmission, bit rate, and channel capacity. MIMO typically employs multipath propagation by utilizing several antennas on both the transmitter and receiver sides. However, 5G technology was introduced in late 2020 and primarily improved the capacity and spectral efficiency of MIMO-LTE systems. MIMO is being introduced into the LTE system to improve signal performance and speed of transmission. High data losses may occur in standard coaxial cable; hence, adopting RoF links in MIMO-LTE systems is the ideal solution. Additionally, the existence of optical fiber results in a wide bandwidth and resilience to electromagnetic interference. Only limited studies have been conducted to improve the carrying capacity of the MIMO-LTE RoF link. However, these techniques fail to provide transmission capacity in a MIMO system. As a result, an effective result is imperative to soar the transmission capacity of the MIMO-LTE system.

The ushering and commercialization of the 5G mobile network is a major shift in how people and things are connected. The characteristic of a 5G network is that several standards are recommended based on usage scenarios. Furthermore, the original 5G specification released by 3GPP specifies two separate usage situations based on applications: (i) improved mobile broadband (eMBB) that provides peak download rates of >20 Gb/s, 4 ms latency of user-plane, and a dependable data rate for users of 100 Mb/s in metropolitan regions, and (ii) Ultra-reliable low latency communications (URLCC) ensures sub-1 ms latency as well as extremely high availability/reliability, and protection for enabling applications like autonomous cars and portable healthcare.

Therefore, ad hoc deployment of small cell solutions using upgraded MIMO technology might provide very limited coverage or improved capacity in constrained areas. To facilitate the use of a single wireless carrier, however, small cells are constructed using a single wireless communication method. As a result, small cells face compatibility issues with sector strategies and cell deployment for supporting varied services (like LTE, 5G, 3G, etc.). Moreover, because of the shortage of multiple Operators support for small cells, each mobile operator must set up and maintain their base station for every technology in each cell, necessitating a sizable machinery implementation area at the antenna location.

3.2 Analog and Digital RoF Spatial Mux MIMO-LTE System Model

The data rates in a WC system can be increased by raising the signal power received in the communication channel. However, by including a MIMO system in the WCs, the signal power received can be boosted. Several present standards, like LTE-A or LTE, are primarily responsible for maximizing rates of data. In an LTE system, each antenna contributes to the resource grid by generating and sending OFDM symbols and signals. Data speeds can be increased by extending the numerous antennas to eliminate modes in the MIMO system. The LTE specifications define four transmission modes: receiver combination, spatialMux, TxDiversity, and beam forming. The signal is transmitted individually on different antennas in spatial mux. TxDiversity transmits redundant data over many antennas deprived of raising the data rate. The data rate may be increased by the spatialMux mode in direct proportion to the amount of antennas that transmit.

Furthermore, the layer mapping procedure is conducted, which turns the data into layers. This step is repeated until the layer de-mapping is the same as with a single MIMO antenna. Following the demodulation procedure, the MIMO system undergoes a pair of processes. When one of the signals becomes distorted, the other signals are likewise affected during demodulation.

3.3 Proposed methodology

Massive data rates are required in the 5G communication system to transfer data in the MIMO-LTE system. As a result, the MIMO RoF system experiences more transmission scenarios. So, the main aim of this work is to improve the RoF Spatial Mux MIMO-LTE System's transmission performance. A MIMO LTE system with a 3.2GHz 5G signal and 64-QAM over 70 km of SSMF is introduced for signal transmission. Bandpass sampling is also emphasized to reduce the total amount of BW required in the RoF link. The transmitted power and bias current must be optimized to get the optimal value for the transmission condition. Here, a strategy for optimizing the current of bias and transmitted power is described. The performance is analyzed under A-RoF and D-RoF using MATLAB tool.

3.3.1 MIMO-LTE system

MIMO offers three operational modes that single-antenna systems do not: transmit diversity, beamforming, and spatial multiplexing. This work focuses on spatial multiplexing, for which

LTE enables up to 4 spatial layers (i.e., a maximum rank of 4) and up to 2 code words per scheduled user, where a code word is a transport block of information bits covering all RBs allocated to a user. The number of spatial layers (i.e., the transmission rank) determines how code words are mapped onto different spatial layers. LTE imposes the following practical limits to reduce feed-forward control signaling overhead and user feedback overhead.

1) The number of users scheduled in a subframe cannot exceed a specific number.
2) All RBs assigned to the same user must have the same MIMO operational mode, rank, and pre-coding matrix.
3) The MCS must be the same for each code word that spans all RBs assigned to a user in a sub-frame.

3.3.2 MIMO-RoF system

It has been recognized that Radio-over-fiber (RoF) technology, which comprises of a fiber network with the lowest propagation loss and affordable base stations, might be used to increase the transmission range of 60-GHz broadcasts. For 60-GHz RoF systems, several methods contingent on optical frequency multiplying are put forth. MIMO technology has sparked tremendous interest in increasing the capacity of data in fiber-wireless systems. With a 60-GHz RoF system, double-sideband single-carrier (DSB-SC) modulation with a 2x2 MIMO setup resulted in transmissions of 27.15 Gbps.

3.3.3 Aquila Optimization

Aquilla is a well-known raptor in the Northern Hemisphere. The most prevalent species of Aquila is the Aquila. Like other birds, Aquila is an affiliate of the "Accipitridae" family. The rear of the neck of an Aquila generally has lighter Golden-brown feathers. Juvenile Aquilas in this group have mostly whitetails with little white markings on their wings. Their agility and speed, combined with large sharpened nails and sturdy feet permit them to catch prey, marmots, deeps, primarily rabbits, squirrels, hares, and other animals in the ground. In nature, Aquila and their obvious behavior can be perceived. Aquila has domains that can extend up to 200 kilometers. They establish enormous nests at various places and mountains, that are high. Being monogamous and can remain jointly for many years, if not their whole lives, and breed in the spring. The incubation period is six weeks, and a female can lay a maximum of four eggs. At around 12 weeks, one or two infants often make it to fledge. These juvenile Aquila typically reach a point of complete certainty in the fall, at such a point they scatter to claim their area.

Aquila is one among the most researched birds on the planet due to its hunting valor. When male Aquila hunts alone, he fixes more prey. Aquila pursues rabbits, squirrels, and other animals with their pace and acute talons. Ground squirrels are a major animal in their diet. These birds have even been recognized as a danger to mature deer. The Aquila uses four hunting strategies, with several unique differentiations and largely Aquila's capacity to intelligently and swiftly switch among hunting approaches dependent on the situation. The following points express Aquila's hunting methods. Figure 3.1 shows the flow chart of an AO algorithm.
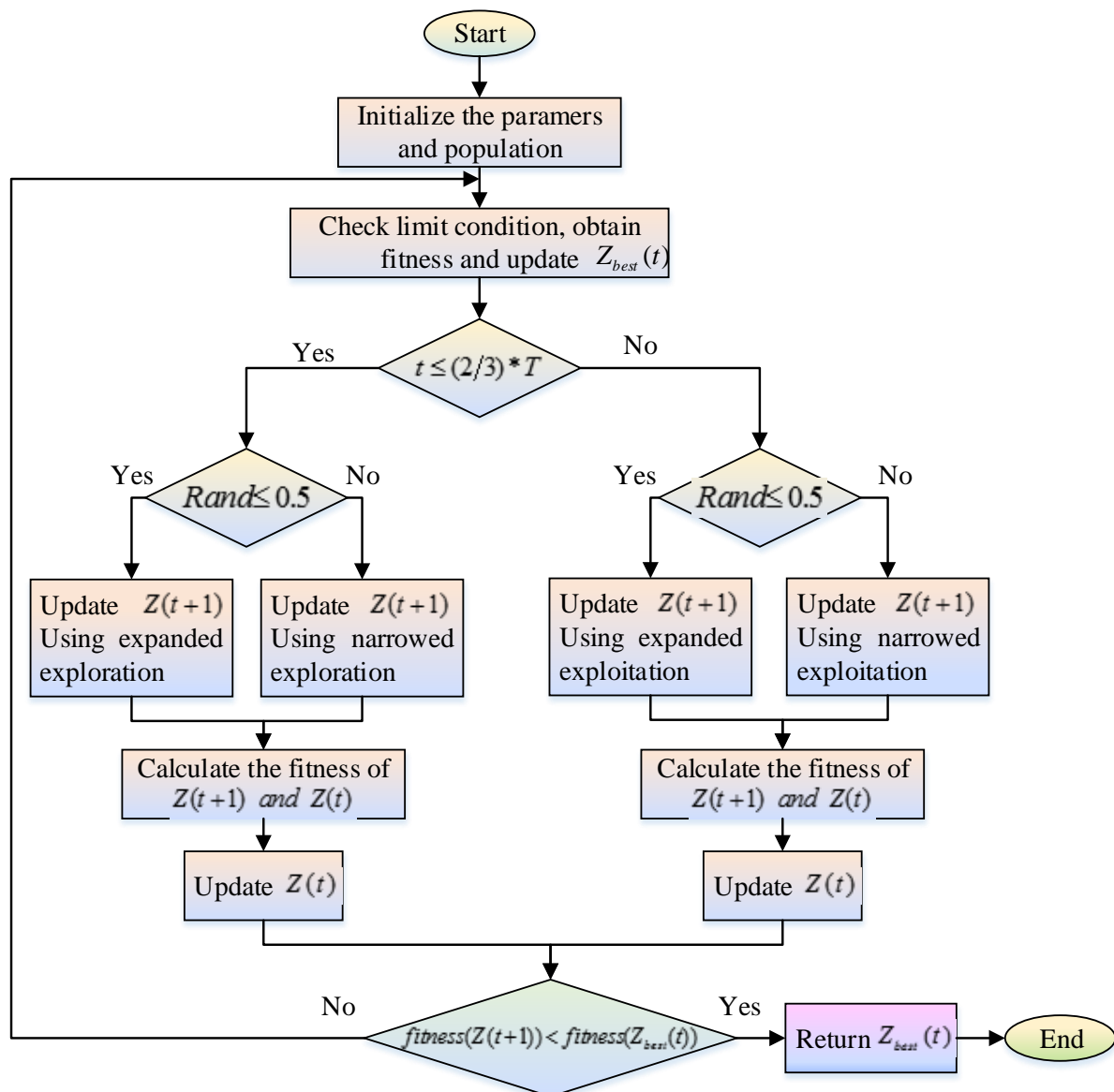
Figure 3. 1: Flow chart of AO algorithm

- High soar by a vertical stoop is the first strategy during a flight to hunt, in which Aquila ascends high above the ground. The Aquila begins a protracted glide at a low angle after

57

exploring prey, increasing speed as the wings close farther. For this strategy to succeed, the Aquila must be taller than its prey. Just before the confrontation, the wings and tail are spread out to mimic a thunderclap, thereafter the feet are impelled frontward to grab the prey.

- The subsequent second mode, contour flying with a momentary glide attack, is the most commonly used by Aquila, in which the bird upsurges at a lower level over the ground. Whether the prey is flying or running, it is then chased cautiously. This technique is useful for catching nesting grouse, ground squirrels, or seabirds.

- Then another third option is a low fly having a slow ancestry attack. In this case, they dive to the ground before launching an offensive on prey. They choose their target and land on their neck and back, seeking to enter. This hunting tactic is used for sluggish prey such as hedgehogs, rattlesnakes, tortoises, foxes, and any wildlife with no escape response.

- The fourth way is walking and grabbing prey, in which they walk on the ground and attempt to draw with their prey.

3.3.4 AOA

Population-based systems generally begin their improvement procedures (optimization processes) with randomly generated candidate solutions. A series of optimization rules incrementally improve the resulting solutions and are iteratively assessed by a specified objective function; this is the spirit of optimization approaches. Finding a solution in just one execution is not guaranteed by population-based algorithms since they stochastically look for the best answer to optimization issues. Yet, many random solutions and optimization rounds increase the possibility of finding the optimal global solution for a provided problem. The population-based optimization process is split into exploration and exploitation, regardless of the variations between the meta-heuristic methods used to avoid local solutions, the latter refers to thorough search space coverage utilizing search agents of an algorithm. The latter speaks about improving the accuracy of conclusions obtained at the time of the exploration phase.

Arithmetic, algebra, geometry, and analyses are fundamental components of number theory and one of the fundamental elements of contemporary mathematics. Arithmetic operators (multiplication, subtraction, division, and addition) are the basic computation measures to understand numbers. It employs these simple operators as a method of mathematics to select the best component from a list of potential choices according to specific criteria (solutions). Optimization issues arise in all quantitative disciplines, from computer sciences, engineering,

and economics to research procedures and industry. The advancement of solution methodologies has piqued the interest of mathematicians for millennia. Figure 3.2 shows the flow chart of AOA.
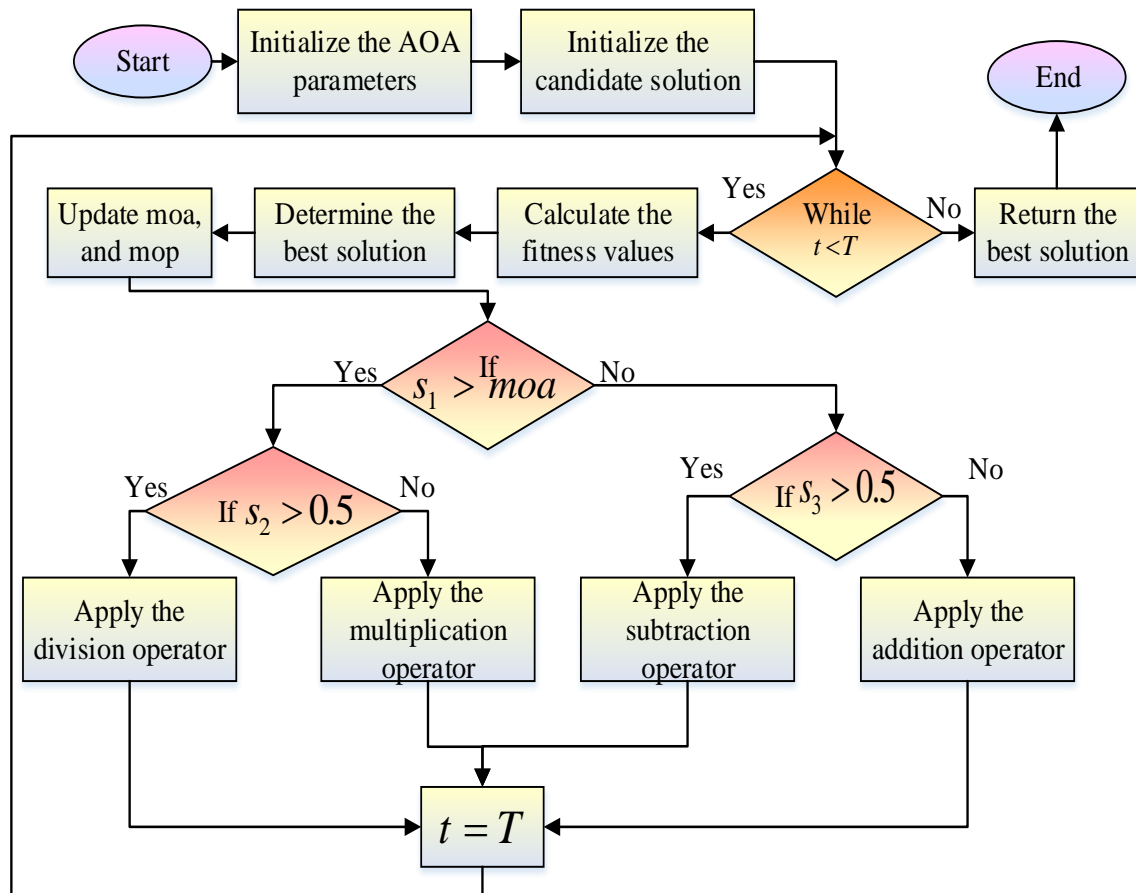
Figure 3. 2: Flow chart of AOA

3.3.5 Hybrid A^2 algorithm

During the exploration phase, the AO swarm's members hunt and fly quickly in search space. The location of each individual is modified by the global best solution, which results in increased convergence and powerful searching capabilities. However, the person's ability to escape the local optima is limited. The person is thus easily drawn into the local optima. The exploration stage of an experimental scenario's multiplication and division operator is set at a level that is too low, which leads to a lack of population diversity. Also, the exploitation and exploration switching mechanisms must be improved, which calls for hybridizing the AO and AOA algorithms. Each Aswarmms catches the target according to the four stages of predation.

3.3.5.1 First stage

In this stage, the Aquila will be flying at a great height in the hunting region. This makes it easier to efficiently search for the target's food. Following the discovery of prey, it will fly vertically to capture the prey, and its behavior is described mathematically as,

$$Z(t+1) = Z_{best}(t) * (1 - \frac{t}{T}) + (Z_M(t) - Z_{best}(t) * Rand) \tag{3.1}$$

In this case, $Z(t+1)$ stands for the individual position at iteration $(t+1)$, and $Z_{best}(t)$ the current best solution globally at t^{th} iteration. Also, the variables $t\ and\ T$ provide the current t^{th} iteration's number and the maximum number of iterations, $Z_{M(t)}$ show the current individual's average position throughout this iteration, and $Rand$ stand for a random Gaussian distribution across 0 and 1.

3.3.5.2 Second stage

The Aquila will now change its course from a high height to elevate its victim's head. This aids in getting the Aquila ready for natural predatory behavior. The revised position is articulated mathematically as,

$$Z(t+1) = Z_{best}(t) * L_F(U) + Z_s(t) + (v - w) * Rand \tag{3.2}$$

Thus, $Z_s(t)$ denotes the Aquila's random position, U denotes the width size, L_F denotes the levy flight function, and $v\ and\ w$ denote the search shape. This is mathematically articulated as,

$$\begin{cases} w = (m_1 + 0.0056 * U_1) * \sin(-\lambda * U_1 + \frac{3\pi}{2}) \\ v = (m_1 + 0.0056 * U_1) * \cos(-\lambda * U_1 + \frac{3\pi}{2}) \end{cases} \tag{3.3}$$

$$L_F(w) = 0.001 * \frac{\alpha\beta}{|\omega|^{\frac{1}{\mu}}}, \beta = \left(\frac{\left(\Gamma(1+\mu) * \sin\left(\frac{\mu\pi}{2}\right) \right)}{\left(\Gamma(\frac{1+\mu}{2}) * \mu * 2^{\left(\frac{\mu-1}{2}\right)} \right)} \right)^{\frac{1}{\mu}} \tag{3.4}$$

60

In this case, m_1 denotes the count of search cycles, ranging from 1 to 20, U_1 denotes the random integer, ranging from 1 to width U and λ is the constant, with a value of 0.005

3.3.5.3 Third stage

In this phase, the Aquila start to identify and pinpoint the general location of their prey. Next, to slow down its target, the Aquila will descend vertically for its primary attack. The following is the mathematical expression for the initial predation behavior:

$$Z(t+1) = \left(Z_{best}(t) - Z_M(t)\right) * \phi - Rand + \left(\left(U_L - L_L\right) * Rand + L_L\right) * \vartheta \tag{3.5}$$

In this case, ϕ and ϑ stands for adjustment parameters with a fixed value of 0.1, and U_L and L_L signify the upper and lower bounds of search space, respectively.

3.3.5.4 Final stage

The Aquila has arrived in the land region and is ready to pursue and attack its target. This is a mathematical formulation of the Aquila's predatory behavior:

$$Z(t+1) = \left(Q_F * Z_{best}(t)\right) - \left(N_1 * Z(t) * Rand\right) - N_2 * L_F(U) + Rand * N_1 \tag{3.6}$$

$$Q_F(t) = t^{\frac{2Rand-1}{(1-t)^2}} \tag{3.7}$$

$$\begin{cases} N_1 = 2Rand - 1 \\ N_2 = 2 \times \left(1 - \dfrac{t}{T}\right) \end{cases} \tag{3.8}$$

Here, N_1 stands for the random movement used to track the prey of an Aquila under the range [-1, 1] and N_2 stands for the gradient flight used to track the prey of an Aquila. Q_F Represents the quality function of a search strategy.

Four arithmetic operations are used in the AOA method to optimize the exploration and exploitation phase. According to the Arithmetic operators, the mathematical calculations using either Subtraction or Addition got high-dense results which refer to the exploitation search mechanism. However, these operators can easily approach the target due to their low

dispersion, unlike other operators. Subtraction or addition search strategy is modelled with the following equation.

$$Z(t+1) = \begin{cases} Z_{best}(t) \div (mop + \gamma) * (U_L - L_L) * \rho + L_L & if \ s_2 < 0.5 \\ Z_{best}(t) * mop * ((U_L - L_L) * \rho + L_L) & otherwise \end{cases} \qquad (3.9)$$

$$\begin{cases} mop(t) = 1 - \dfrac{t^{\frac{1}{\sigma}}}{T^{\frac{1}{\sigma}}} \\ moa(t) = \min + t * \left(\dfrac{\max - \min}{T} \right) \end{cases} \qquad (3.10)$$

For controlling the control parameter of the search process, here ρ is used and has a constant value of 0.5. γ stands for the compact integer. Additionally, the acronym MOP stands for mathematical optimizer probability, σ for sensitive coefficient, which helps to represent development accuracy and has a fixed value of 5, moa for mathematical optimizer acceleration, which aids in selecting the search space; and $\max$ *and* $\min$ for the maximum and the minimum values for the acceleration function.

Within this context of an evaluated system, the hybrid A^2 algorithm provides the ideal transmission conditions that fulfill arg min $EVM(I_{bias1}, I_{bias2}, Q_{in})$. To stay clear of the threshold limit and the saturation zone, the input signal power Q_{in} is adjusted between -35 and -20 dBm, and the I_{bias1} *and* I_{bias2} currents for both branches are set between 20 and 80 mA.

$$fitness \ value = \text{arg min} \ EVM(I_{bias1}, I_{bias2}, Q_{in}) \qquad (3.11)$$

Assuming the differences for equations (3.1), (3.2), (3.8), and (3.9), the individuals of AO swarms would process more random searches than the individuals of AOA. Equations (3.5), (3.8), and (3.10) give the mathematical calculations for an exploitation phase. According to these calculations, AO swarm members perform worse than AOA. The individual AOA swarms have a lower exploitation capacity than individuals in AO swarms. Combining the AO swarm exploration and exploitation phases with the AOA swarm exploitation phases would be preferable. The pseudo-code for the hybrid A^2 algorithm is specified in the Table 3.1 given below.

Table 3. 1: Pseudo-code for hybrid A^2 algorithm

Pseudo-code for hybrid A^2 algorithm
Step 1: Set population size as N
Step 2: Set the maximum quantity of iterations as T
Step 3: Set the width as U
Step 4: Initialize the individual position as $Z_y(y=1,2,....N)$
While $(t \leq T)$
Update *mop and moa* with the aid of equation (3.10)
Update, $v\ and\ w$ with the aid of equation (3.3)
Step 5: For $y = 1 : N$
If $|\varepsilon| \geq 1$
Step 6: If $Rand < 0.5$
Update the position of $Z(t+1)$ with the aid of equation (3.1)
Else
Update the position of $Z(t+1)$ with the aid of equation (3.2)
End if
Step 7: If $Rand > moa$
If $Rand > 0.5$
Update the position of $Z(t+1)$ with the aid of equation (3.9)

Else

Update the position of $Z(t+1)$ with the aid of equation (3.9)

End if

End if

End if

Step 8: End for

For $y = 1 : N$

Check if the position reaches out of the search space limit and returns back

Calculate the fitness of $Z(t)$

Update $Z_{best}(t)$

Step 9: End for

$t = T + 1$

Step 10: End while

Return $Z_{best}(t)$

3.3.6 Utilization of bandpass sampling

In many sensors and systems that employ modulated signals, bandpass signals are typical. Next, the teacher can quiz the class on what the minimal sample rate needed for distortion-free reconstruction is. When the Nyquist rate is used, 200,000 samples per second are produced at a minimum. If each sample requires 16 bits of quantization, then 3.2 Mbits/sec are needed to store the sampled signal or deliver it as a digital stream. The necessary transmission or storage rate is increased even further due to practical considerations (sampling at higher rates to account for less-than-ideal filters). The modulated RF signal with a carrier frequency of f_c, a bandwidth of b_w, and a GHz range must always be digitalized using a sampling Nyquist/Shannon with a higher sampling frequency. To do this, high-speed electronics must be used for at least twice as long as $(f_c + b_w/2)Hz$. At a carrier frequency f_c of 2.475 GHz and 3.2 GHz of BW, the symbol rate is set to 16M symbols per second. To prevent spectral aliasing among RF signals during bandpass sampling, the sampling frequency f_s must guarantee the following.

$$2\frac{f_{max}}{N} \leq f_s \leq 2\frac{f_{min}}{N-1} \tag{3.11}$$

$$1 \leq N \leq f_f \left[\frac{f_n}{f_{max} - f_{min}} \right] \tag{3.12}$$

In this case, f_{max} stands for the maximum frequency, f_{min} for the minimum frequency, N for the integer, $f_{max} - f_{min}$ for the bandpass signal BW, and f_f for the floor function that generates the upper rounding to an integer of the ratio $\dfrac{f_n}{f_{max} - f_{min}}$. Duplicate bandpass signals are often produced during bandpass sampling. To avoid spectral aliasing, a long guard band of 13 MHz is therefore positioned on either side of the center frequency. Critical bandpass sampling causes spectral aliasing most frequently, and the entire channel's BW reaches 46MHz. Hence, the realistic values for f_{max} and f_{min} are taken to be 2.49GHz and 2.45GHz, respectively. Obtaining $2*46 = 92MSa/s$ as the optimal sampling frequency N can use any integer number between 1 and 54 according to equation (3.12). If N is 2, then the sampling

frequency f_s is $24.95MSa/s$ higher than the critical sampling level. Given the 8-bit ADC's low cost and low power consumption, the resulting bit rate was roughly 1.024Gbps.

3.3.7 D-RoF Analytical Model

Using the VPI transmission technique, the D-RoF link model has been identified. An ADC of n bits that accomplishes digitalization using the bandpass sampling technique is given a 64-bit QAM RF signal. Moreover, this section includes operations for quantization and coding. Continuous signals are discretized in discrete time and amplitude domains based on ADC resolution in quantization. The suggested method's systematic block diagram is shown in Figure (3.3).
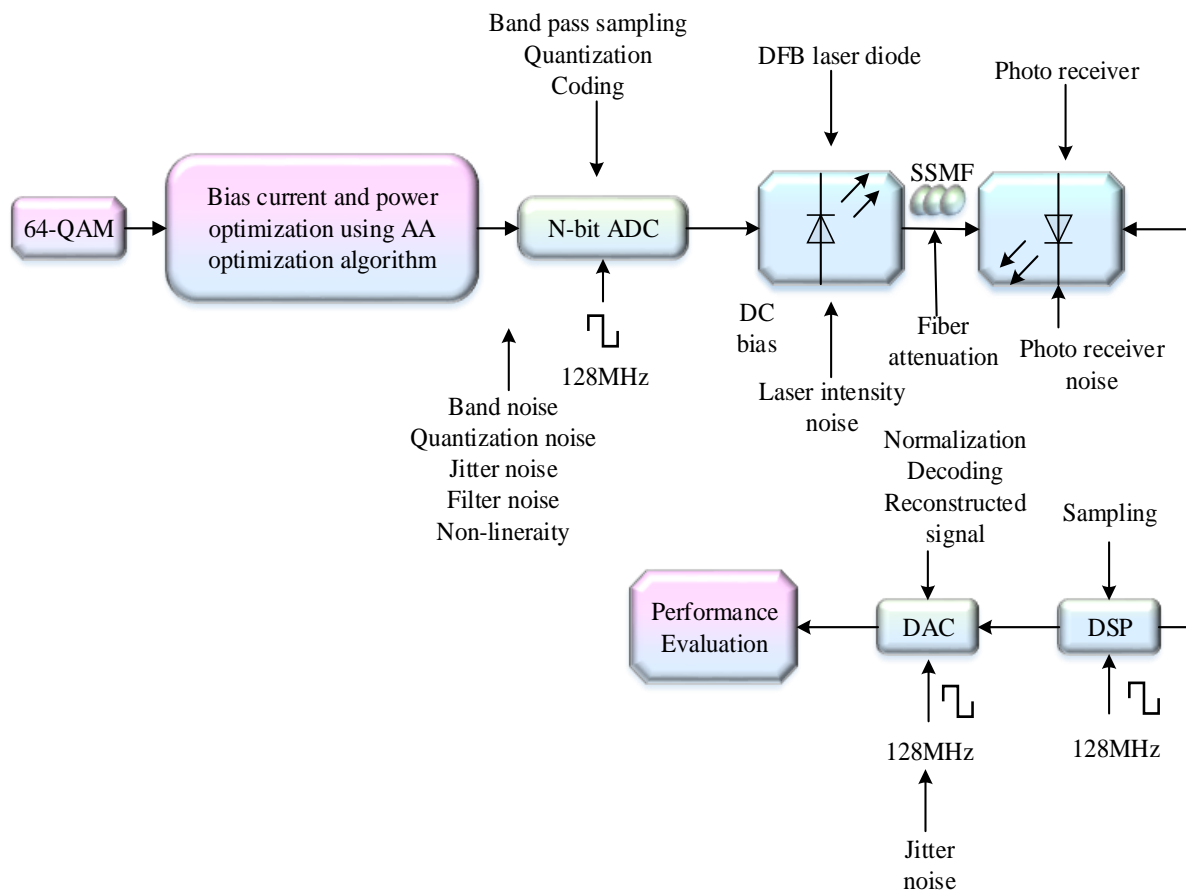
Figure 3. 3: Systematic block diagram of the proposed method

The signal is quantized, translated into a binary sequence, and encoded utilizing a Miller encoder. The resulting signal can modulate the distributed feedback (DFB) laser diode. In this step by using an electrical signal, the optical signal is created. Following generation, the resulting optical signal is transferred over SSMF's optical channel. The broadcast signal is then

picked up by a photo receiver equipped with a PIN-free photodetector. The digital signal processor (DSP) is then given the final output signal, and the optical signal is transformed into a digital signal. The digitalized signal is subsequently supplied into the DAC for signal reconstruction, normalization, and decoding processes. The performance of SNR, EVM, and EOP are then evaluated using the signal that has been rebuilt. The Nyquist region handles the band noise when the bandpass signal is resampled. In addition, the ADC presents quantization noise and jitter into the RoF link. The resolution of bits in the ADC causes the quantization sounds to be produced. Moreover, the sampling clock and the ADC itself also experience jitter noise. The DAC on the receiver side is heavily affected by jitter noise, which is mostly brought on by clock phase noise. Using a DAC, a digital input signal is transformed into an analog output signal. The digital signal is denoted by the binary code through the bits 0 and 1.

Signal deterioration, clock jitter noise, and quantization noise are all produced due to bandpass sampling. Due to the RoF link's weak correlation, the generated noise sources are considered independent. Bandpass sampling, quantization noise, and jitter averages are zero. The optical link and the ADC are also believed to be independent of a clock jitter induced by the DAC jitter noise. Mathematical manipulations are made to the SNR for an ADC jitter noise as,

$$S_{NR\_Jitter ADC}(dB) = -20\log_{10}(2\pi f_c \mu_{ADC\ Jitter})$$

(3.13)

In this case, $f_c = 2.4GHz$; $\mu_{Jitter} = 0.8ps$ whereas μ_{Jitter} modifies the ADC RMS jitter. The mathematical formulation of the SNR for an ADC quantization noise is;

$$S_{NR\_quantization}(dB) = -20\log_{10}((PAPR) + 6.02n + 10\log_{10}(3))$$

(3.14)

Here,

$$PAPR = \frac{3(\sqrt{M} - 1)}{(\sqrt{M} + 1)}; M = 64; n = number\ of\ bits$$

(3.15)

Mathematically, the SNR for band noise aliasing is represented as,

$$S_{NR\_band\ noise\ aliasing}(dB) = \frac{2Q_o}{Nf_s KT}$$

(3.16)

N the integer of a Nyquist region, Q_o Denotes the output power of a modulated RF signal, f_s the sampling frequency, κ the Boltzmann constant, and T the manipulation of a Kelvin temperature.

Signal degradation occurs in DACs because of jitter noise, which can be mathematically adjusted as follows:

$$S_{NR\_JitterDAC}(dB) = -20\log_{10}(2\pi f_c \mu_{DAC\ Jitter})^{-2}\left[\sin b\left(\frac{f_c}{f_s}\right)\right]^{-2}$$

(3.17)

Here, $f_c = 2.4GHz;\ \mu_{jitter} = 0.8ps$ and $f_s = 128MHz$

The ADC resolution should be aware that quantization noise is distributed uniformly. This demonstrates that the SNR of quantization noise is higher than the SNR of jitter noise.

$$S_{NR\_quantization} > S_{NR\_Jitter}$$

(3.18)

The above equation can be expanded as follows:

$$-20\log_{10}((P_{APR}) + 6.02n + 10\log_{10}(3)) > -20\log_{10}(2\pi f_c \mu_{Jitter})$$

(3.19)

P_{APR} Stands for PAPR and has a value of 8.1dB. It achieved the values of $f_c = 2.4GHz;\ \mu_{Jitter} = 0.8ps$. Here, $n = 8$ is taken for the best ADC solution.

Certain non-linearity leads ADC to perform poorly. As a result, the ADC must be built with the correct hardware and include various types of noise. Hence, non-linear blocks in the ADC can be utilized to reduce distortion. The non-linear blocks use experimental analysis to investigate ADC behavior. The DFB laser intensity noise was defined as the optical link that exhibits certain non-ideal behavior. The intensity noise is caused by the optical fiber and photo detector's attenuation, chromatic, dispersion, shot, and thermal noise.

3.4 Result and Discussion

The suggested is evaluated using the MATLAB Simulink tool. The investigation is performed in a 4×4 MIMO LTE system with a 3.2GHz 5G signal and 64-QAM over 70 km of SSMF. The A^2 optimization approach is introduced here to maximize the power transmission and bias current of the MIMO RoF system. However, the MIMO system requires a high BW; hence bandpass sampling is used to reduce the BW in the system. The suggested work's performance is evaluated using the traditional A-RoF and D-RoF systems.

3.4.1 Performance metrics

The EVM is the difference among the complex nominal value of a received signal and the demodulated signal. It can more precisely measure the signal BW and modulation defects. The spatialMux transmission in MIMO architecture is always influenced by one another. The effectiveness of an A-RoF and D-RoF is calculated using EVM and is theoretically formulated as follows:

$$E_{VM}(\%) = \sqrt{\frac{\frac{1}{M}\sum_{m=1}^{M}|y_m - y_{0,n}|^2}{\frac{1}{M}\sum_{m=1}^{M}|y_{0,n}|^2}} \tag{3.20}$$

In this equation, y_m denotes the normalization of the mth symbol, $y_{0,n}$ is the normalized ideal constellation point in the mth symbol, and M denotes the quantity of unique constellation symbols. Eye diagrams for transmitting signals can be used to analyze the effectiveness of D-RoF and A-RoF. The EOP, also known as eye-opening amplitude (EOA), is the ratio of a non-distorted reference eye to the distorted eye's eye-opening height (EOH). It is mathematically expressed as follows:

$$E_{OP}(dB) = 10\log\left(\frac{E_{OA}}{E_{OH}}\right) \tag{3.21}$$

The signal-to-noise ratio (SNR) is expressed in decibels (dB). It is mathematically stated as follows:

$$S_{NR} = 10\log_{10}\left(\frac{q_{signal}}{q_{noise}}\right) \tag{3.22}$$

q_{signal} Denotes signal power, and q_{noise} denotes noise power.

3.4.2 Performance evaluation of A-RoF and D-RoF system

The performance of D-RoF and A-RoF systems is estimated using EVM, SNR, and EOP while altering the input power, fiber length, and resolution bits. The graph shows that the suggested systems i.e. D-ROF and A-ROF perform better with lower attenuation.
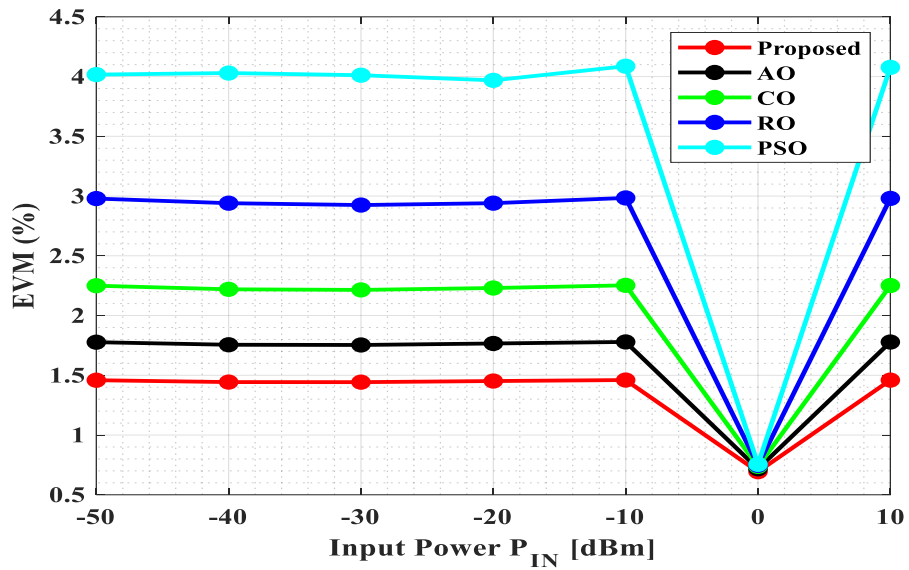
(a)
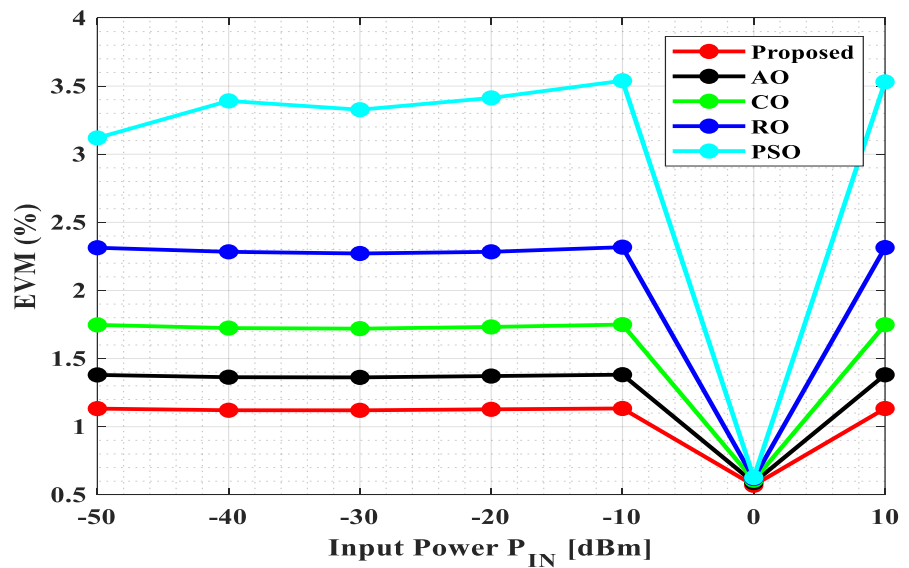
(b)

Figure 3. 4: EVM Vs Input Power, (a) EVM performance for A-RoF, (b) EVM performance for D-RoF

Figure 3.4 depicts the performance of EVM with varying input power. Figures 3.4 (a) and 3.4 (b) show the EVM performance for A-RoF and D-RoF. The graph shows that both systems generate similar results with variable input power. In general, increasing the input power reduces the EVM. The signal power is increased based on the noise power. The suggested algorithm achieves EVMs of 1.13% and 1.45% for D-RoF and A-RoF, respectively, at 10dBm input power. Because of the improved PAPR, the modulated signal results in the DFB laser falling below the threshold depending on the distortion of an optical carrier signal. Because of nonlinearity in the ADC system, the EVM in a D-RoF link increases whilst the input power is 0dBm. The dynamic range of an A-RoF link is -15dBm to 0dBm. For the D-RoF link, the dynamic range is -22dBm to 5dBm. The dynamic range of an analog RoF system is determined by the 3GPP limit, which is about half that of a digital RoF system. The graphical representation demonstrates that the received symbol for the D-RoF meets the 3GPP limit of 8% at 5dBm input power. According to a detailed graph examination, an analog RoF signal produces more noise than a digital RoF link with the same input power.

Table 3. 2: EVM for A-RoF comparison of the various approaches.

Approaches	EVM performance under A-RoF under varying input power						
AO [21]	1.776	1.755	1.753	1.766	1.779	0.717	1.778
CO [22]	2.249	2.219	2.214	2.230	2.252	0.737	2.251
RO [23]	2.978	2.940	2.924	2.940	2.984	0.746	2.980
PSO [24]	4.016	4.029	4.011	3.968	4.086	0.754	4.077
Proposed	1.458	1.443	1.442	1.451	1.460	0.69	1.459

Table 3. 3: EVM for D-RoF comparison of the various approaches

Approaches	EVM performance under D-RoF for varying input power						
AO [21]	1.380	1.363	1.362	1.371	1.381	0.590	1.381
CO [22]	1.747	1.723	1.719	1.732	1.749	0.606	1.748
RO [23]	2.313	2.283	2.271	2.283	2.317	0.619	2.314
PSO [24]	3.119	3.391	3.326	3.413	3.539	0.626	3.530
Proposed	1.132	1.120	1.120	1.127	1.134	0.570	1.133

Initially, the input power P_{in} is set to 0dBm. Yet, contingent on the length of a RoF link, the D-RoF link keeps the EVM value below 3%. According to a thorough graph examination, the 64-bit QAM receives its constellation for both D-RoF and A-RoF links with a length of 70 km. However, the received outcome is more dispersed in the case of an A-RoF link and confirms that the latter is badly influenced by specific impairments existing in the system. For 70km length, the suggested algorithm achieves an EVM of 1.44% for A-RoF and 1.12% for D-RoF. EVM is used to determine the change in volume for both systems by adjusting the input powers. The graph shows that the EVM for 0dBm input power achieves a value of more or less than 8% at a length of 70 km. Tables 3.2 and 3.3 show the value obtained for both D-RoF and A-RoF compared to existing approaches such as AO, CO, RO, and PSO.
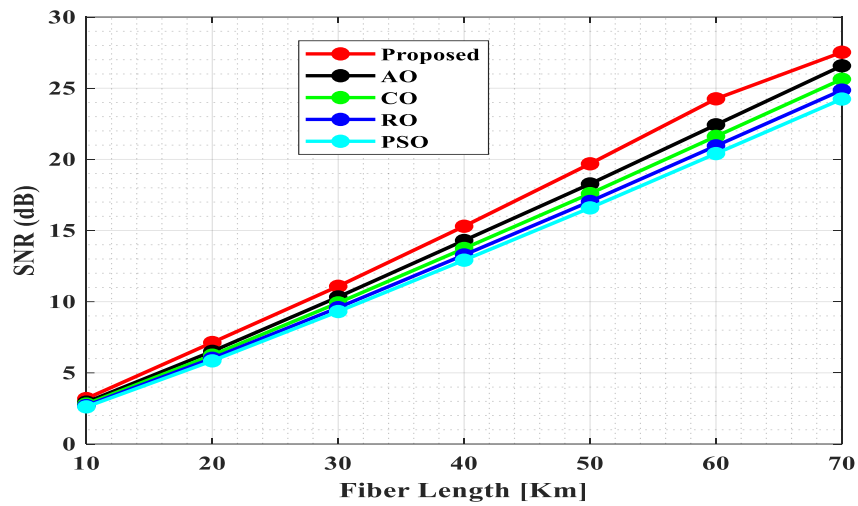
(a)
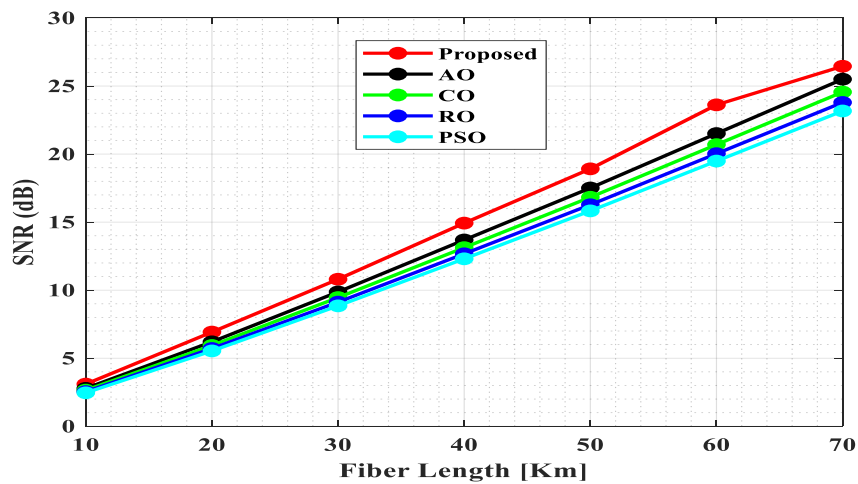
(b)

Figure 3. 5: SNR versus fiber length, (a) SNR performance of A-RoF, (b) SNR performance of D-RoF

Table 3. 4: Comparison of existing methods in terms of SNR for A-RoF

Approaches	SNR performance under A-RoF for varying fiber length						
AO [21]	2.940	6.510	10.331	14.300	18.274	22.427	26.574
CO [22]	2.808	6.242	9.918	13.737	17.593	21.613	25.632
RO [23]	2.700	6.022	9.581	13.284	17.041	20.948	24.865
PSO [24]	2.611	5.842	9.307	12.917	16.591	20.405	24.238
Proposed	3.194	7.131	11.083	15.301	19.688	24.254	27.525

Table 3. 5: Comparison of existing methods in terms of SNR for A-RoF

Approaches	SNR performance under D-RoF for varying fiber length						
AO [21]	2.787	6.204	9.872	13.688	17.508	21.509	25.502
CO [22]	2.654	5.935	9.458	13.125	16.828	20.695	24.560
RO [23]	2.546	5.716	9.122	12.672	16.276	20.030	23.79
PSO [24]	2.458	5.536	8.848	12.305	15.826	19.487	23.166
Proposed	3.100	6.921	10.80	14.92	18.91	23.617	26.454

Figure 3.5 shows the performance of SNR with changing fiber length. Figures 3.5(a) and 3.5(b) show the SNR of a D-RoF and an A-RoF, respectively. From the graph, it is revealed that the performance of D-RoF is superior to A-RoF. It is demonstrated that the D-RoF strategy outperforms the A-RoF approach. According to a detailed graph examination, as the fiber length rises, so does the SNR. For the A-RoF and D-RoF, the proposed algorithm achieves EVMs of 27dB and 26dB for 70km length, respectively. Hence, the quantization noise of an ADC does not affect the SNR value of both designs. The noise from an optical receiver begins to control the quantization noise when the length increases. As a result, substantial fiber loss occurs, restricting the overall link performance. Signal attenuation may occur in the A-RoF system due to continual SNR decrease in the RoF link.
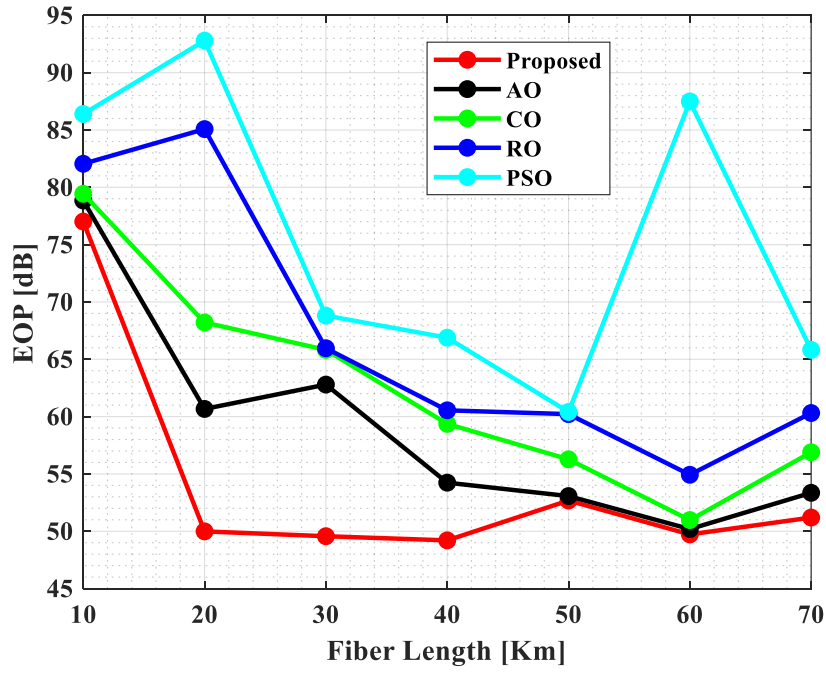
(a)
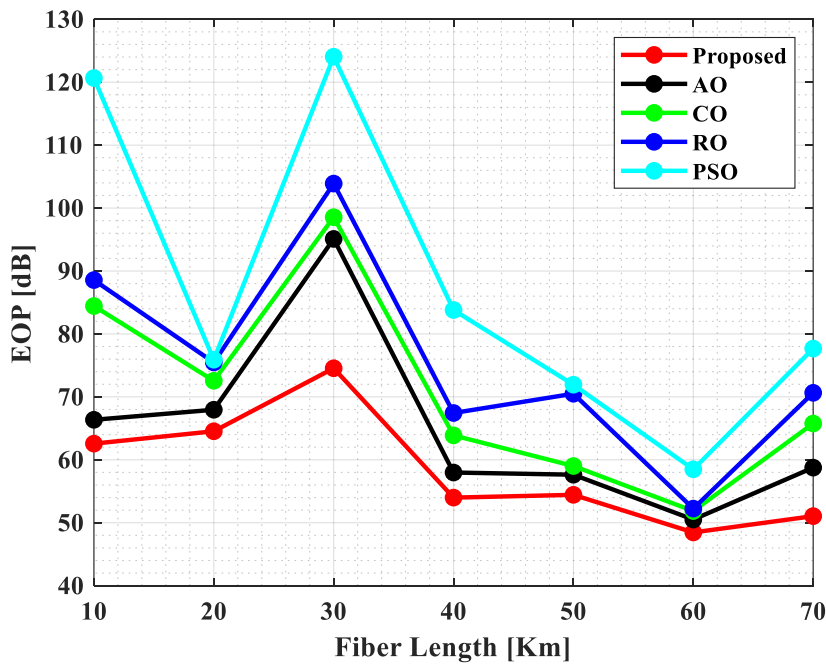
(b)

Figure 3.6: EOP versus fiber length, (a) EOP performance of A-RoF, (b) EOP performance of D-RoF

Table 3. 6: EOP for A-RoF comparison of the various approaches

Approaches	AO [80]	CO [82]	RO [81]	PSO [83]	Proposed
EOP performance under A-RoF for varying fiber length	78.846	79.433	82.05	86.39	77.01
	60.66	68.212	85.078	92.79	49.98
	62.79	65.81	65.960	68.8	49.56
	54.23	59.364	60.546	66.88	49.20
	53.06	56.274	60.213	60.40	52.67
	50.187	50.97	54.92	87.49	49.72
	53.351	56.88	60.312	65.8	51.19

Table 3. 7: EOP for D-RoF comparison of the various approaches

Approaches	AO [80]	CO [82]	RO [81]	PSO [83]	Proposed
EOP performance under D-RoF for varying fiber length	66.35	84.436	88.56	120.65	62.56
	67.95	72.557	75.46	75.904	64.53
	95.099	98.54	103.89	124.04	74.54
	57.97	63.87	67.44	83.802	53.992
	57.63	59.01	70.49	71.93	54.434
	50.504	51.85	52.244	58.48	48.459
	58.756	65.76	70.647	77.67	51.051

In the case of an A-RoF system, the EOH is closed after 70 kilometers. As a result of this, the EOP between the RoF linkages reaches infinity. The EOH remains open within the fiber limit in the event of a D-RoF scheme (70 km). When the distance is 70 km, the suggested algorithm achieves nearly comparable EOP values for the D-RoF and A-RoF systems. For shorter distances of 10 km, the suggested method achieves an EOP of 77dB for A-RoF and 62dB for D-RoF. Performance of EOP and EVM enables evaluation of the received signal's quality. Tables 3.6 and 3.7 show the value obtained for D-RoF and A-RoF compared to existing techniques like AO, CO, RO, and PSO.

Table 3. 8: EVM for A-RoF comparison of the various approaches

Approaches	PSO [83]	CO [82]	RO [81]	AO [80]	Proposed
EVM performance under A-RoF for varying fiber length	3.93	2.181	2.88	1.730	1.425
	4.08	2.257	2.99	1.782	1.46
	4.056	2.25	2.98	1.776	1.45
	3.96	2.18	2.87	1.737	1.43
	4.15	2.280	3.030	1.796	1.47
	4.194	2.280	3.05	1.792	1.46
	4.11	2.24	2.98	1.769	1.4

Table 3. 9: EVM for D-RoF comparison of the various approaches

Approaches	AO [80]	RO[81]	CO[82]	PSO [83]	Proposed
EVM performance under D-RoF for varying fiber length	1.343	2.239	1.694	3.129	1.107
	1.384	2.322	1.753	3.675	1.136
	1.379	2.321	1.748	3.232	1.132
	1.349	2.230	1.697	3.607	1.112
	1.395	2.353	1.771	3.740	1.143
	1.392	2.368	1.771	3.52	1.139
	1.374	2.317	1.742	3.457	1.127

The amount of bits increases and the EVM of the method decreases. When the input power is 0dBm, a 70Km fiber is selected. An 8-bit ADC is used for improved performance, which helps to shrink the EVM more efficiently. When a single-bit ADC is used, the suggested technique achieves an EVM of 1.4% for A-RoF and 1.10% for D-RoF. The suggested method achieves an EVM of 1.45% for the 8-bit ADC and 1.12% for the 16-bit ADC. When the number of bits is increased to more than 8, the performance of an EVM remains unchanged. However, if the ADC has a low bit resolution, excessive error may occur, and the EVM is automatically

increased. Tables 3.6 and 3.7 show the value gained for A-RoF and D-RoF compared to existing approaches such as AO, CO, RO, and PSO.
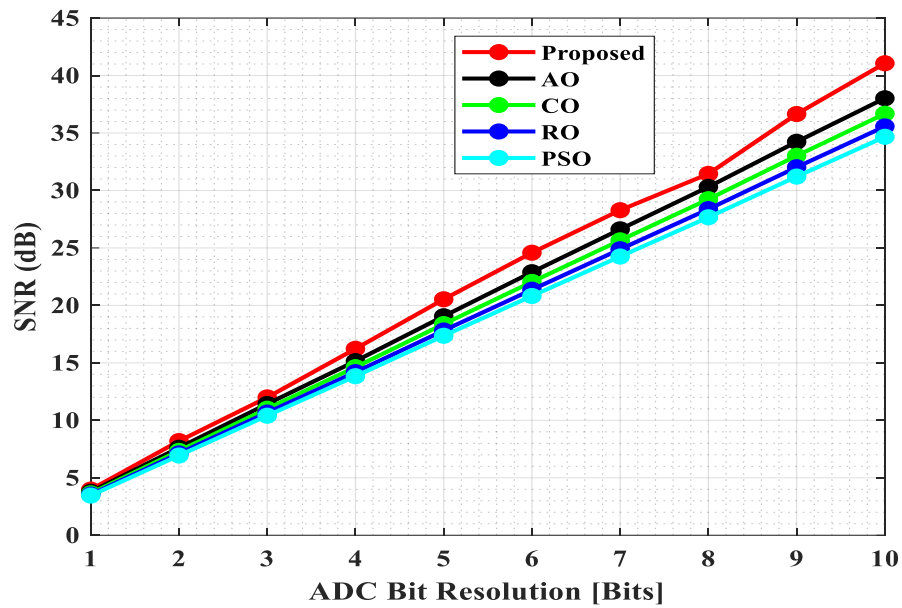
(a)
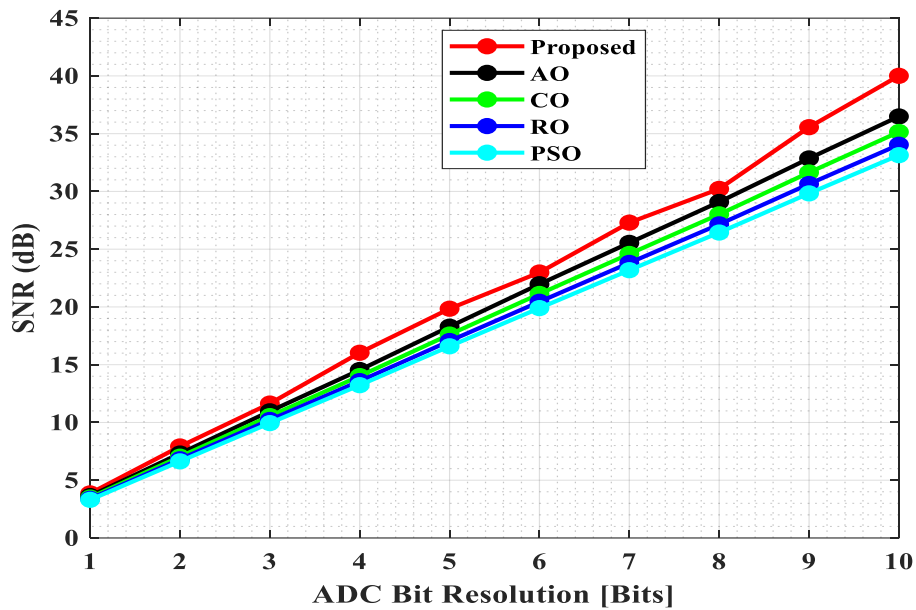
(b)

**Figure 3.7: SNR versus ADC bit resolution, (a) SNR performance for A-RoF, (b) SNR performance for D-RoF**

Figure 3.7 represents the outcomes of SNR by altering the number of ADC resolutions. Figures 3.7 (a) and 3.7 (b) show the SNR performance of the D-RoF and A-RoF, respectively.   In 8-bit ADC, the suggested algorithm achieves SNRs of roughly 28dB for A-ROF and 27dB for

D-RoF. The SNR value is not modified if the number of bits is larger than 8. A thorough examination of the graph shows that the chosen ADC has a higher SNR than the other ADCs.
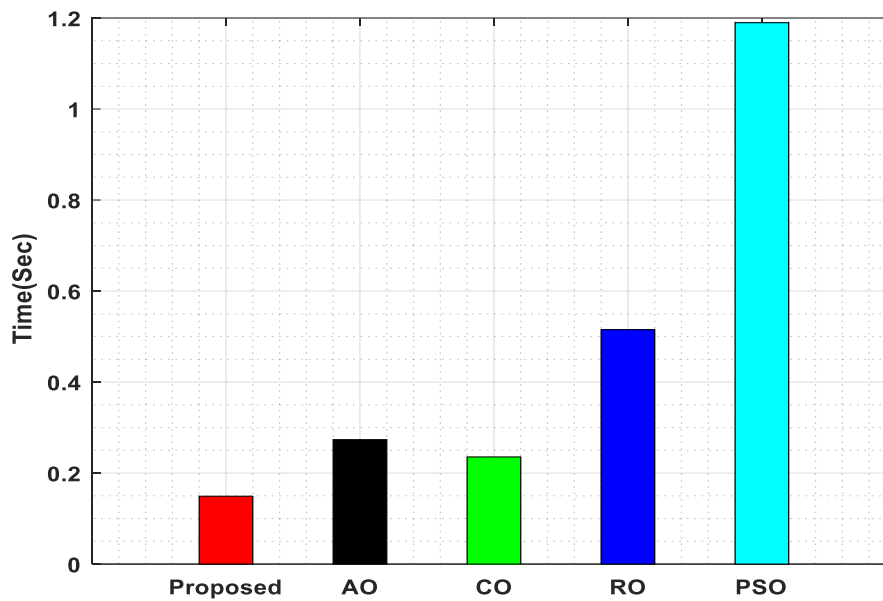
Figure 3.8: Comparison of overall computation time (sec)

Figure 3.8 manipulates the comparison of total computation time (sec). The proposed technique has low computational complexity based on a thorough examination of the above graph. The efficiency of the proposed method is demonstrated. To exhibit the effectiveness of the proposed method, its computational performance is compared to those of other current techniques such as AO, CO, RO, and PSO. The existing AO, CO, RO, PSO, and suggested algorithms achieve values of 0.27s, 0.23s, 0.51s, 1.18s, and 0.14s, respectively. Due to the imbalance of ADC and DAC operation, the existing technology has a significant computational complexity. As the fiber length rises, the performance of an ADC and DAC degrades, resulting in heavy traffic among the MIMO system. Due to the use of greatly increased ADC and DAC in the MIMO system, the suggested method achieves reduced computation time.

3.5 Summary

MIMO-LTE RoF link is an emerging technology in the 5G WC system. This study aims to improve the transmission condition of a RoF Spatial Mux MIMO-LTE system. Each antenna deals with an 800 MHz 5G signal with 64-QAM over 70Km SSMF and is regarded to transmit the signal over scattered applications. Unfortunately, the MIMO system necessitates a large BW to broadcast the signal via the RoF link. As a result, bandpass sampling is used. The proposed method's performance is examined for both A-RoF and D-RoF systems with respect

to performance measures like EVM, SNR, and EOP. The transmission condition of the MIMO system is also examined. In addition, the A2 optimization approach is developed to optimize the bias current and power transmission in the MIMO RoF system. In the experimental case, the A-RoF and D-RoF have EVMs of 1.45% and 1.13%, EOPs of 51.19dB and 51dB, SNRs of 27dB and 26dB, and calculation times of 0.14s. The proposed MIMO system is a very beneficial wireless LAN network for increasing the network efficiency of an LTE system.

CHAPTER 4

IMPROVED AQUILA OPTIMIZATION-BASED PARAMETER EVALUATION FRAMEWORK AND META-HEURISTIC ALGORITHM IN ROF SPATIALMUX MIMO-LTE SYSTEM

4.1 Overview

Broadband wireless connectivity installation is necessary due to the current telecommunications infrastructures [84]. Comparing MIMO transceivers to SISO transceivers, the throughput of an information system can be practically doubled [85]. The placement of several antennas can boost the network quality by gaining spatial diversity to increase the throughput of the data. Due to the substantial losses in coaxial cable, RoF links are the best option for high-frequency transmissions. This level of Internet traffic will be challenging for network operators to support in the coming days [86]. The demand must be met by increasing network capacity for mobile devices. In an LTE system, every antenna builds the resource grid, creates symbols of OFDM, and transfers data. In a MIMO-LTE system, many transmitters use the resource-grid translation and OFDM encoding method [87], [88]. Frequency modulation (FM) provides higher sound quality and noise immunity but uses more bandwidth than amplitude modulation (AM), which is a straightforward, bandwidth-saving technique that modifies a carrier signal's amplitude dependent on the information stream. The techniques that follow are examples of digital modulation: pulse position modulation (PPM), pulse width modulation (PWM), pulse amplitude modulation (PAM), quadratic amplitude modulation (QAM), and phase shift keying (PSK) are current modulation techniques. Every technique has pros and cons of its own, including noise, bandwidth consumption, immunity to noise, resistance to noise, complexity, and the possibility of producing high-frequency noise.

A RoF system exploits the MIMO) system. When broadcasting wideband Long-Term Evolution (LTE) MIMO signals, a unique system can handle a variety of services. Several nonlinear effects can be used to examine the RoF fronthaul system in a MIMO system. Changing transferring constraints for example input signal power or laser bias current can help to lessen the effects of nonlinear caused by the RoF system. The IAO method is recommended in this study for optimizing transferring environments in a MIMO RoF method. This method can quickly determine the suitable lasers' bias current and power of RF signal. Wavelength multiplexed MIMO signals were used in the experiments in a MIMO IM/DD (Intensity Modulation and Direct Detection) RoF method. The LTE standard manages transmissions and

frequency of carriers. The suggested approach has been developed in MATLAB, and outcomes have been collected. Tests demonstrate that quick convergence may be reached for different bandwidths, causing a favorable balance of nonlinearity and noise. Employing properly input signal power and biased current can eliminate method alterations and increase EVM results.

4.2 MIMO system model

In theory, raising the signal power that is received is the most effective way to increase the speed of data in a communication channel. Employing several antennas in MIMO structures is an appropriate way to boost received power. These technologies use standards like LTE-A or LTE to achieve maximum data speed. Each antenna produces the OFDM symbols, resource grid, and transfers the data of signal using a mechanism of LTE transmission. Many broadcast antennas in a MIMO-LTE structure perform OFDM modulation and resource-grid mapping. This multi-antenna expansion may increase current data throughput depending on the MIMO mode chosen.

The four MIMO communication modes utilized in the LTE standard are beamforming, spatial multiplexing, receiver combining, and Tx Diversity (Spatial Mux). In comparison to the TX Diversity approach, it will send redundant data on distinct antennas, Spatial Mux sends independent data on multiple antennas. By using transmit antennas in spatial Mux Mode, the data rates can be increased proportionally. The layer-mapping technique separates data into layers, and everything is similar as in the case of single-antenna till the de-mapping of the layer. The demodulation procedure is then performed in two of a kind. Therefore, if any of the MIMO signals exhibit distortion, the demodulation procedure may also affected. Transmission strategies that use diversity and spatial multiplexing increase spatial as well as acquisition of multiplexing. SM and TxD are methods for increasing diversity gains and multiplexing.

4.2.1 Transmit Diversity Encoder

The LTE-Advanced technology employs space frequency block coding (SFBC) to transmit diversity. In fact, when the user equipment (UE) moves quickly, SFBC outperforms the space-time block code (STBC), making it simple to ensure the transmission link's integrity. Figure 4.1 shows the TxD.
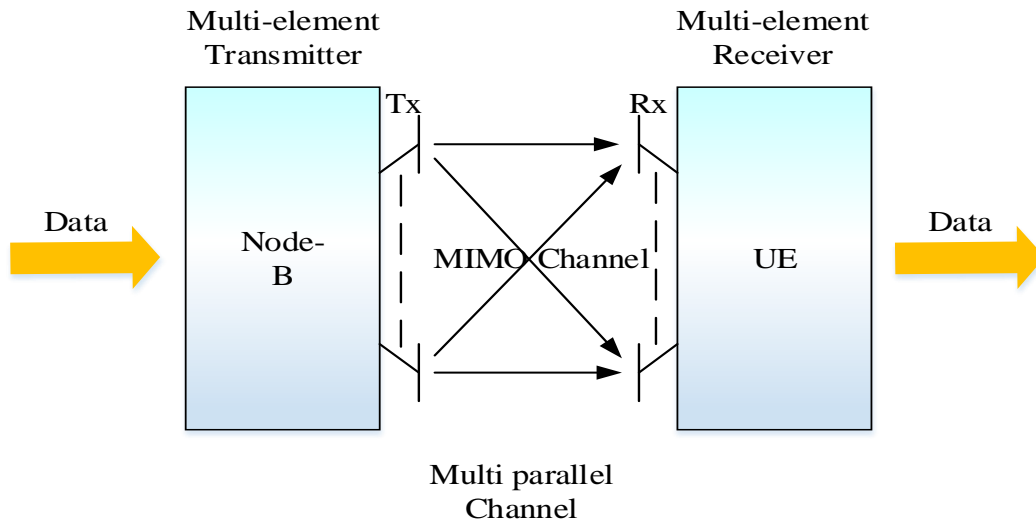
Figure 4. 1: Diagram of MIMO using Transmitter diversity

4.2.1.1 Ports with two antenna encoders

The output SFBC is attained using the Alamouti code, followed by a simple change to the STBC outcome. Every second is initially modulated using the conjugate approaches, bargaining, and STBC is done using the alamouti code. This section contains efficient executions that use the alamouti code and the STBC.

4.2.1.2 Ports with four antenna encoders

The SFBC is coupled with LTE in this part using the FSTD (frequency-switched transmit diversity) technique. Primarily, the SFBC is useful to every pair with modulated signal (n_1, n_2), and the results are placed in either two examples of antenna that is transmitting (T_A).

By applying SFBC in 1st and 3rd T_As with modulated symbols (n_3, n_4), the result is placed on 3rd and 4th samples at systematic intervals.

4.2.2 Transmit antenna decoder

The receiver component organizes the transmit decoder to the transmit diversity in order to calibrate the send-modulated signals, and the result is the opposite of a transmit diversity encoder.

Assume a 2×2 MIMO channel and use a system linear equation to derive the received signal at the receiving antenna (R_A). The formula for the matrix of the MIMO channel is as follows:

$$\begin{bmatrix} b_1(n) \\ b_2(n) \end{bmatrix} = \begin{bmatrix} a_{11}(n) & a_{12}(n) \\ a_{21}(n) & a_{22}(n) \end{bmatrix} * \begin{bmatrix} c_1(n) \\ c_2(n) \end{bmatrix} \tag{4.1}$$

Here, n denotes the transmitted signal function and $(n+1)$ denotes the representation for the next time index, which is provided by,

$$\begin{bmatrix} b_1(n+1) \\ b_2(n+1) \end{bmatrix} = \begin{bmatrix} a_{11}(n+1) & a_{12}(n+1) \\ a_{21}(n+1) & a_{22}(n+1) \end{bmatrix} * \begin{bmatrix} c_1(n+1) \\ c_2(n+1) \end{bmatrix} \tag{4.2}$$

The receiving antennas $\begin{bmatrix} b_1(n+1) \\ b_2(n+1) \end{bmatrix}$ are adjusted in the context of paired sequential symbols as follows:

$$\begin{bmatrix} b_1(n+1) \\ b_2(n+1) \end{bmatrix} = \begin{bmatrix} a_{11}(n)*c_1(n) + a_{12}(n)*c_2(n) \\ a_{11}(n+1)*c_1(n+1) + a_{12}(n+1)*c_2(n+1) \end{bmatrix} \tag{4.3}$$

When the transmit diversity encoder is given to modulate the input signal (n_1, n_2) with alamouti code and STBC, and the 2×2 is mapped as,

$$\begin{bmatrix} b_1(n+1) \\ b_2(n+1) \end{bmatrix} = \begin{bmatrix} a_{11}(n)*n_1 + a_{12}(n)*n_2 \\ -a_{11}(n+1)*\tilde{p}_1 + a_{12}(n+1)*\tilde{p}_2 \end{bmatrix} \tag{4.4}$$

For two samples, the channel gain is similar and it is denoted by $a_{11}(n) \approx a_{11}(n+1) \approx a_{11}$ and $a_{12}(n) \approx a_{12}(n+1) \approx a_{12}$. By conjugating on together sides, the above equation becomes,

$$\begin{bmatrix} d_1 \\ \tilde{d}_2 \end{bmatrix} = \begin{bmatrix} a_{11}(n)*n_1 + a_{12}(n)*n_2 \\ -\tilde{a}_{11}*n_2 + \tilde{g}_{12}*n_1 \end{bmatrix} = \begin{bmatrix} a_{11} & a_{12} \\ \tilde{a}_{12} & -\tilde{a}_{11} \end{bmatrix} * \begin{bmatrix} n_1 \\ n_2 \end{bmatrix} \tag{4.5}$$

The greatest value achieved on the receiver side is modified by changing the value of $A = \begin{bmatrix} a_{11} & a_{12} \\ \tilde{a}_{12} & -\tilde{a}_{11} \end{bmatrix}$, as follows:

$$\begin{bmatrix} n_1^* \\ n_2^* \end{bmatrix} = \begin{bmatrix} a_{11} & a_{12} \\ \tilde{a}_{12} & -\tilde{a}_{11} \end{bmatrix}^{-1} \begin{bmatrix} b_1 \\ \tilde{b}_2 \end{bmatrix} = \frac{\begin{bmatrix} a_{11} & a_{12} \\ \tilde{a}_{12} & -\tilde{a}_{11} \end{bmatrix} \begin{bmatrix} b_1 \\ \tilde{b}_2 \end{bmatrix}}{(a_{11} \times \tilde{a}_{11} + a_{12} \times \tilde{a}_{12})} \tag{4.6}$$

The transmitted signal is altered using the MRC algorithm, and designed signals are finally delivered to the receiver side. The finest signal that can be transmitted is stated numerically as,

$$n^* = \sum_{n=1}^{N} \eta_m \bar{n}_n = \sum_{n=1}^{N} \frac{u_m}{\sum_{i=1}^{N} U_i} \frac{1}{U_n} A_n \bar{b}_n = \frac{\sum_{n=1}^{N} A_n \bar{b}_n}{U_n} \qquad (4.7)$$

At every point in time, $\bar{n}_n = \begin{bmatrix} n_1^* \\ n_2^* \end{bmatrix}_n$ at the receiver side, the channel matrix $A = \begin{bmatrix} a_{11} & a_{12} \\ \tilde{a}_{12} & -\tilde{a}_{11} \end{bmatrix}$,

, and received signal are denoted by, $\tilde{b}_n = \begin{bmatrix} b_1 \\ \tilde{b}_2 \end{bmatrix}$ and the channel matrix's energy efficiency is

indicated by $U_n = \left(a_{11} \times \tilde{a}_{11} + a_{12} \times \tilde{d}_{12} \right)$ and η_m denotes the result of a channel matrix that splits all channel matrix transmitted signals.

Open Loop Spatial Multiplexing (OLSM):

As shown in Figure 4.2, In the OLSM design, a Pre-coding Matrix Indicator (PMI) response, which indicates codebook MM (matrix measurement) for pre-coding, is still provided while a Rank Indicator (RI) response is delivered to an upgraded Node B to assess user's transmission layer.
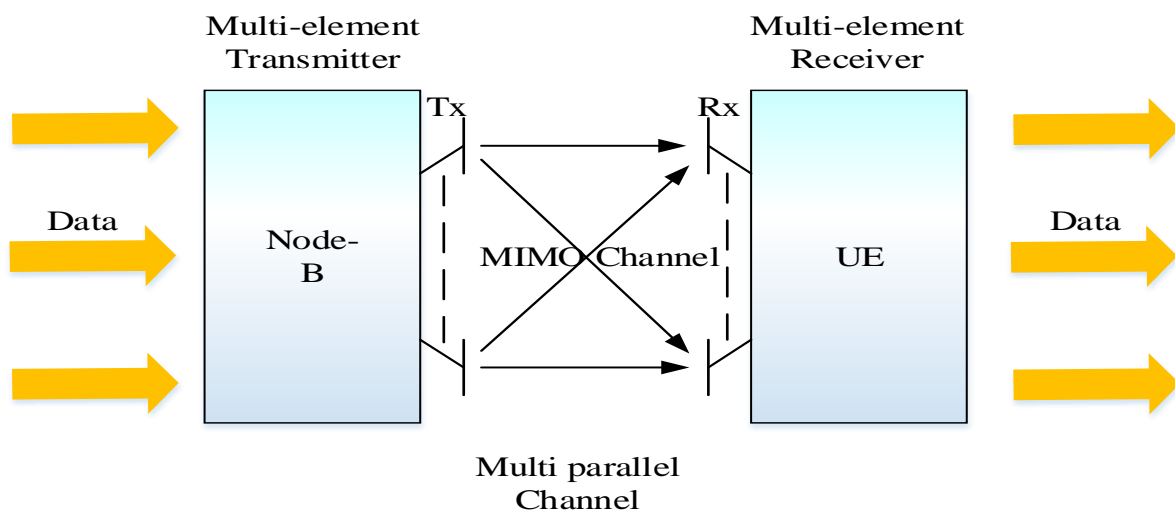
Figure 4. 2: Diagram of a MIMO using OLSM

The following is how the MIMO channel matrix with additive white noise is written:

$$B = AC + n \tag{4.8}$$

In this case, 'm' modifies the additive white noise, $'C'$ modifies the broadcast signal, and $'B'$ modifies the received signal. Multiplication of Matrix happens at the receiver section that helps to pre-coding approach. Following pre-coding, MIMO representation is written as follows:

$$B = AUC + n \tag{4.9}$$

Where, U indicates pre-coding matrix.

Closed Loop Spatial Multiplexing (CLSM):

CLSM is a transfer technology that combines beamforming with spatial multiplexing. Figure 4.3 depicts how UE obtains an RI and PMI response and communicates it to eNode-B.
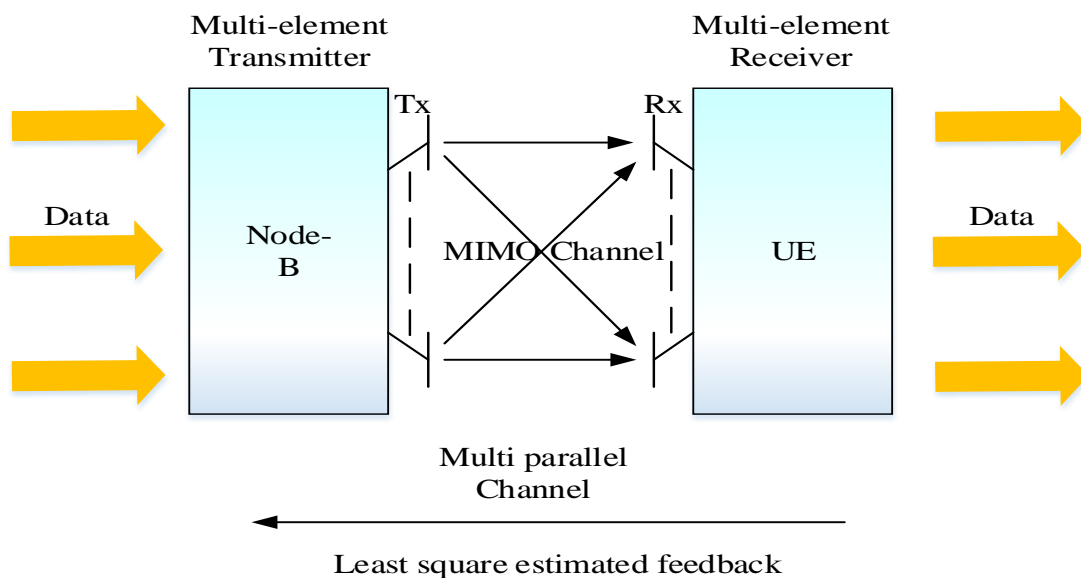
Figure 4. 3: Illustration of MIMO using CLSM

Studies have examined 2 different analog ROF systems employing frequency translation procedures Double Side Band (DSB) and frequency translation procedures of Single Side Band (SSB) to decrease the cost of MIMO-enabled ROF methods. These double systems function similarly to a typical SCM system, excluding that 2 MIMO channels partition the same LO, reducing the number of LOs by half. A notch filter with a small band is also essential for the DSB frequency translation system, causing the network to only carry a single service.

Mathematically, the signal received can be produced by the receiver side addition of additive white Gaussian noise (AWGN) as follows:

$$k(n) = B(n) - \tilde{n}(n) \tag{4.10}$$

Here, $B(n)$ manipulates the received signal vector in this case, while $\tilde{n}(n)$ manipulating the AWGN. The amount of R_{AS} must be more than that of transmitting antennas to invert the signal received. The predicted vector of the transmit signal is written mathematically as,

$$\tilde{c} = W^A k \tag{4.11}$$

In this case, k manipulates the terminal signal, and $\tilde{c}$ represents the evaluated transmitted signal 'c'. The whole estimated received signal is mathematically expressed as follows:

$$\begin{bmatrix} \tilde{c}_1 \\ \tilde{c}_2 \end{bmatrix} = (A^A A)^{-1} A^A \begin{bmatrix} d_1 \\ d_2 \end{bmatrix} \tag{4.12}$$

Here, $\tilde{c}_1$ and $\tilde{c}_2$ are calculated c_1 and c_2 of the signal transmitted.

4.3 Proposed methodology

Before transferring the RF signal via the optical fiber, the RoF technique modulates the light with the RF signal. Additionally, an optical fiber link can be used by a RoF system to transfer an RF signal. RoF can support more devices than conventional wireless communication systems because it makes extensive use of OFC bandwidth. The RoF technology allows for the transmission of signals over long distances and over heavily populated areas. In this paper, a strategy for improving the transmission conditions in a MIMO RoF system is proposed called Improved Aquila Optimisation (IAO). By using this method, the correct bias current for laser and RF signal power can be promptly determined. MIMO IM/DD RoF (Intensity Modulation and Direct Detection) signals that were wavelength-multiplexed were used in the trials. The carrier frequency and transmissions are governed by the LTE standard. This study used 70kilometerss of Standard Single Mode Fibre (SSMF) for the Digitised Transmission of a 20 MHz LTE data signal with 64 Quadrature Amplitude Modulation (QAM) for greater bandwidth signal transmission and allotment.

The main performance barrier to achieving high transmission rates over very long distances is nonlinear impacts caused by optical transmission systems (OTSs). Backbone optical networks

are fronting new issues as the need for system capacity, coverage area, and user numbers grows fast due to the advent of mobile broadband. To address such issues, a framework based on meta-heuristic algorithms is created, which exploits the entire performance of a design. In the experiment, the results of QAM and QPSK modulation were evaluated using SNR and EVM while altering the fiber length and several iterations. Furthermore, the performance of QPSK and QAM is studied and compared to current methodologies such as GWO, FFO, ABC, and AO. Comparing the suggested study with present methods is also calculated separately for QPSK and QAM modulation. Also, the computational complexity of the suggested technique is discussed.

4.3.1 Improved Aquila optimization algorithm

This paper suggests Improved Aquila Optimization (IAO) to discover the highest rate for transmission circumstances in a RoF link, comprising of power transfer and bias current. AO [89] is represented by the natural behaviors of Aquila when catching prey. The AO has a low speed of convergence and has problems keeping stability. As a result, IAO is suggested with a propagation factor; which can increase AO's performance. This has the potential to increase AO's performance. As a result, the procedures for optimization suggested algorithm is distributed into 4 classes: selecting the hunt space utilizing a vertical stoop and greater soar, determining within a deviated hunt area providing a short glide and contour flight attack, observing to exploit within a converge hunting area providing a low expedition, slow descent attack and pouncing utilizing a walk and seize prey. The recommended IAO optimization is detailed below;

IAO starts by computing the initial value L for a group of M people utilizing the expression given below:

$$L_{x,y} = \hbar \times s_1 \times (V_y - D_y) + D_y \ , \ \ x = 1, 2, ..., M \ \ \ y = 1, 2, ..., R^{'} \tag{4.13}$$

In this case, s is a random value from the range $\in [1, 0]$. At dimension y, V and D are upper and lower bounds, respectively. The dimension of a test problem is denoted by $R^{'}$. In the general AO procedure, the value $\hbar$ is fixed. As a result, the propagation factor $\hbar$ can improve the AO's performance. The following calculation can be utilized to compute the parameter $R^{'}$ for managing position changes. This value is fixed in the original AO algorithm.

$$\hbar = \frac{1.5 \cdot (Max_{iter} - f + 1)}{Max_{iter}} \qquad (4.14)$$

This parameter influences Aquila's IAO position and facilitates exploitation and exploration. The IAO has 2 steps for updating current people exploitation and exploration. At $f \leq \left(\frac{2}{3}\right) * F$, the exploration phase begins, and it has two techniques; the first is determined using the equation below.

$$L_1(f+1) = L_{best}(f) \times \left(\frac{1-f}{F}\right) + (L_N(f) - L_{best}(f) * Rand\_value) \qquad (4.15)$$

Where F is the total number of iterations, L is the best individual obtained at the current iteration f, and $\left(\frac{1-f}{F}\right)$ is used to guide search throughout the phase of exploration. Furthermore, the L is an individual average of dimensions, and is computed as follows:

$$L_N(f) = \frac{1}{M} \sum_{x=1}^{M} L(f) , \qquad (4.16)$$

The IAO uses the Levy flight distribution in the second exploration strategy to change the existing person, as described in the following equation;

$$L_2(f+1) = L_{best}(f) \times levy(R) + L_S(f) + (i-j) * Rand\_value \qquad (4.17)$$

Where, L_S represents a person chosen at random. $levy(R)$ stands for Levy flight distribution, that is defined as,

$$levy(R) = g \times \frac{v \times \vartheta}{|w|^{\frac{1}{\mu}}}, \quad \vartheta = \left(\frac{\hbar(1+\mu) \times \sin\left(\frac{\pi\mu}{2}\right)}{\hbar\left(\frac{1+\mu}{2}\right) \times \mu \times 2^{\left(\frac{\mu-1}{2}\right)}} \right) \qquad (4.18)$$

Here, $p = 0.01$ and $\mu = 1.5$ are constant values, while v and W are random numbers chosen from [0, 1]. In equation 4.5, the variables i and j are engaged to replicate the spiral shape as follows:

$$i = s \times \cos(\theta), \quad i = s \times \sin(\theta) \tag{4.19}$$

$$\text{Where, } s = s_1 + V \times R_1, \quad \theta = -u \times R_1 + \theta_1 = \frac{3 \times \pi}{2} \tag{4.20}$$

Where, $s_1 \in [0, 20]$ is a random number. $u = 0.005$ and $V = 0.00565$ represent tiny values.

A condition is necessary to break the cycle. The centroid of each iteration is denoted as $\overline{E}_F = \sum_{x=1}^{M} \frac{E_x}{M}$, where E_x are the vertex of a current simplex and M is the number of vertices excluding the finest. It's important to keep in mind that a highly "flat" function could display almost identical function values over a wide domain, making the solution susceptible to tolerance. The AO approach determines the best transmission conditions in the evaluated system's environment, satisfying arg min $EVM(i_{Bias1}, i_{Bias2}, P_{Input})$. To eliminate the saturation zone and the threshold limit, the input power of the signal P_{Input} is set among -35 and -20 dBm, and the bias currents i_{Bias1}, i_{Bias2} of both branches are set between 20 and 80 mA.

$$Fit_{value} = \arg\min EVM(i_{Bias1}, i_{Bias2}, P_{Input}) \tag{4.21}$$

Throughout the searching phase, two strategies are employed to replicate individuals' exploitation capacity. The first technique is based on using the best answer $\left(I_{Best}\right)$ and the average individual's location $\left(I_N\right)$, and it is written as $i_{Bias} \ P_{Input}$

$$J_3(f+1) = \left(J_{Best}(f) - J_N(f)\right) \times \partial - Rand\_value + \left(\left(V_y - D_y\right) \times Rand\_value + D_y\right) \times \lambda \tag{4.22}$$

Here, ∂ and λ stands for the exploitation adjustment parameters, while rand stands for a random number.

$I_{Best}, levy,$ and the quality function of $F\_quality$ is required for the second exploitation technique.

$$J_4(f+1) = F\_quality \times J_{Best}(f) - \left(H_1 \times J(f) \times Rand\_value\right) - H_2 \times levy(R) + Rand\_value \times H_1 \tag{4.23}$$

Where the primary goal of employing $F\_quality$, to balance the search strategies is defined as,

$$F\_quality(f) = f^{\frac{2 \times F\_quality(\ ) - 1}{(1-F)^2}} \qquad (4.24)$$

H_1, which stands for various motions used to track the ideal solution, and it is stated as,

$$H_1 = 2 \times Rand\_value\ () - 1 \qquad (4.25)$$

$\boldsymbol{H_2}$ is reduced from 2 to 0, and it is stated as follows:

$$H_2 = 2 \times \left(1 - \frac{f}{F}\right) \qquad (4.26)$$

Where random value is denoted by $Rand\_value$. The proposed algorithm's flowchart is shown in Figure 4.4. The proposed algorithm's pseudocode is displayed below.

Pseudo code for the proposed algorithm
Step 1: Input Related parameters (i.e. λ, ω etc.) and Aquila population I:
Step 2: While $(f < F)$
Determine the highest best solution (I_{Best}), and fitness values of the population
Update the parameters such as i, y, $F\_quality$, H_1, H_2 etc.
if $f \leq (2\ 3) * F$
if $Rand\_value \leq 0.5$
Step 3: Expanded exploration (I_1):
Based on Equation (4.15) update the current solution
Replace, $I(f)$ by $I_1(f+1)$, when $Fit(I_1(f+1)) < Fit(I(f))$
else

Step 4: Narrowed exploration (I_2):

      Based on Equation (4.17) update the current solution

      When $Fit(I_2(f+1)) < Fit(I(f))$, replace $X(t)$ by $X_2(t+1)$

      end

      if else

Step 5: if $Rand\_value \le 0.5$

      Expanded exploitation (I_3):

      Based on Equation (4.22) update the current solution

      When $Fit(I_3(f+1)) < Fit(I(f))$, replace $I(f)$ by $I_3(f+1)$

      else

Step 6: Narrowed exploitation (I_4):

      Based on Equation (4.23) update the current solution

      When $Fit(I_4(f+1)) < Fit(I(t))$, replace $X(t)$ by $X_4(t+1)$

      end if

Step 7: end if

      $f = f+1$

      End While

Output: Optimal value $Fit(I_{Best})$
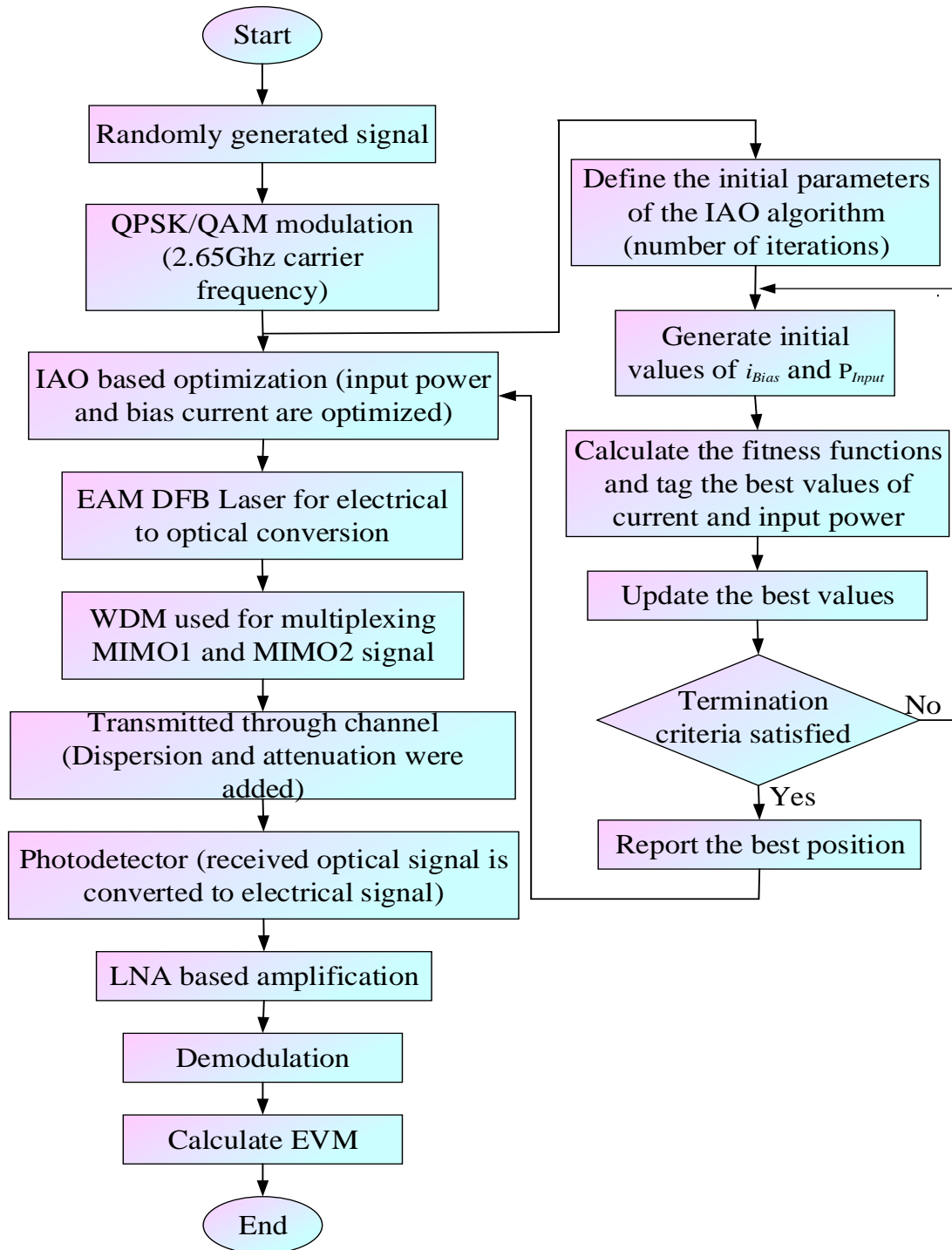
Figure 4. 4: Flowchart of the algorithm proposed

4.4 Results and Discussion

On a computer with an Intel Core i5, 2.2 GHz CPU, 16 GB of RAM, and the MATLAB 2018 platform, the EVM is calculated, and the resulting signals are recorded. In both branches, the RF carrier frequency is 2.65 GHz, which falls inside the LTE standard's Band 7 range. Each MIMO signal intensifies and modulates an optical carrier utilizing an EAM-DFB (electro-

absorption modulator distributed feedback laser). The modulations for the 2 MIMO signals are $\lambda_1 = 1550nm$ and $\lambda_2 = 1531nm$. The BBU and RRH are connected by a single mode fiber (SMF) with a dispersion of attenuation of 0.25 dB/Km, a length of 10 km, and 18 ps/(mm). The parameters for information-bearing power, DC bias, sampling time, and frequency bandwidth are respectively set to 5, 10, 15, 15 ns, 100, and 33.3 MHz. The proposed IAO uses 100 iterations, 30 search agents, 10 boundaries, 2 limits per dimension, 100 upper and lower bounds, and 0.1 exploitation adjustment parameter. To perform the optical-to-electrical transformation two photodetectors (PD) are provided. Two low noise amplifiers increase the signal power because it is so low just after the optics-to-electrical conversions (LNA). The experimental configuration for the suggested MIMO RoF Fronthaul system is exposed in Figure 4.5.
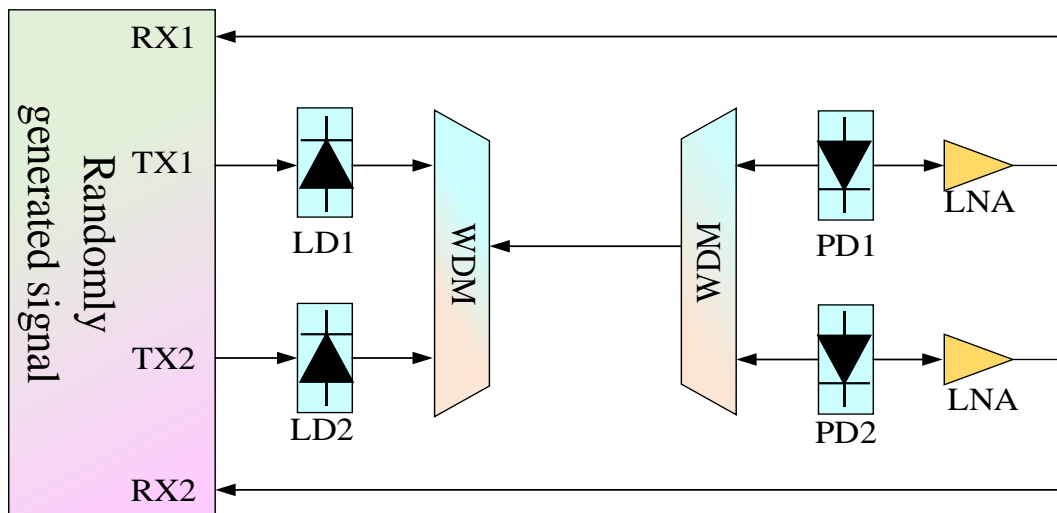
Figure 4. 5: MIMO RoF fronthaul system

4.4.1 Performance metrics

Imperfections brought on by self-phase modulation (SPM), SBS, positive frequency chirp (PFC), and CD (chromatic dispersion), during PD and fiber transmission may be avoided by controlling the MIMO input signal strength and bias current of lasers. The EVM can measure signal bandwidth and modulation flaw effects. Moreover, using the Spatial Mux transmission method, each demodulation branch may be impacted by the activities of others in a MIMO architecture. EVM recognizes the difference among the measured and nominal complex results of decoded symbols and is used to report the performance of RoF. EVM is expressed as.

$$\mathrm{E}V\mathrm{M}\left(\%\right)=100\sqrt{\frac{1}{Z}\frac{\sum_{x=1}^{Z}\left\|j_x-i_x\right\|^2}{\sum_{x=1}^{Z}\left\|i_x\right\|^2}} \qquad (4.27)$$

Z is the quantity of complex data points utilized in the computation, i_x and j_x are the corresponding transmit and receive symbols.

4.4.2 Analysis of EVM and SNR Performance

The EVM outcome of RoF techniques for the length of fiber is shown in Figure 4.6. Regarding EVM, MIMO2 and MIMO1 signals are contrasted with the length of the fiber. In the case of QPSK modulation, the value of EVM is less than 7.5, while in the case of QAM, it is smaller than 14. It also shows that the signal is less affected by the reasons for system limitations. Figures 4.6 (a) and 4.6 (b) play with the graphical representation of QAM and QPSK modulation, respectively. Figure (a) demonstrates how the EVM grows with the fiber length. The EVM reached roughly 7.21 while the length of fiber was extended to 100 km.

However, the current MIMO1 method achieves an EVM of approximately 7.04. The EVM reaches a small value of approximately 6.95 at 20 Km of the length of the fiber. However, the MIMO2 method achieves an EVM of 7.15. EVM aids in the performance examination of a MIMO system's transmitting and receiving components. According to the graph, the suggested MIMO2 achieves a higher EVM than the current MIMO1 method. High transmission conditions are due to excessive interference when the signal is broadcast across a MIMO system. However, the proposed system exhibits strong interference resistance, greatly reducing transmission conditions. Figure 4.6 (b) shows that the EVM decreases as the fiber length rises. The suggested method achieved an EVM of approximately 11.8 for a 100 km fiber length. The MIMO1 technique achieved the EVM of approximately 10.7 and 12.2 when the length of fiber was 20 km and 100 km respectively. However, the MIMO2 technique achieves the EVM of approximatlely 12.2 and 11.8 for corresponding fiber lengths of 20 km and 100 km respectively. This demonstrates that QPSK modulation outperforms QAM.
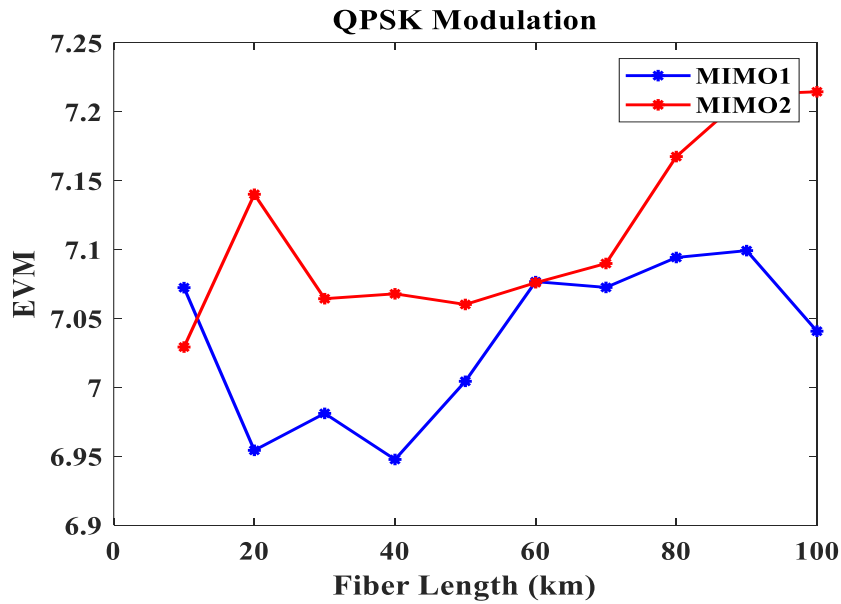
(a) QPSK modulation
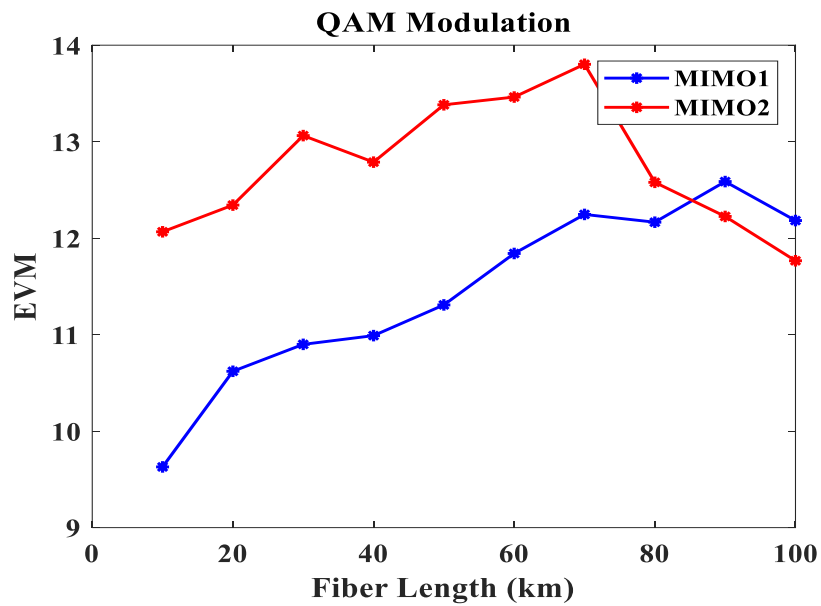
(b) QAM modulation

Figure 4. 6: Values of EVM vs fiber length

QAM and QPSK modulation are manipulated graphically in Figures 4.7 (a) and 4.7 (b). The graph demonstrates how EVM lowers as the amount of iterations rises. 4.7 (a) figure represents that the EVM reached the value of 6.95 with 20 iterations. But for the 20 iterations, the current MIMO1 achieves the EVM of 6.8. This is because the current QPSK modulation is not very stable. High attenuation and a loss of signal power may occur during signal processing. Yet by increasing the modulation process more efficiently, the suggested technique lowers the

attenuation in the transmission channel. According to graph 4.7 (b), the EVM reached roughly 12 iterations when there were 100. Nevertheless, the current system only achieves the EVM of 9.5 after 100 iterations. The suggested approach achieves the EVM of 9, useful for real-time applications, with 20 iterations. However, after 20 iterations, the current method achieved an EVM of 10.9 percent. It can be visualized from the graph that QPSK performs superior to QAM modulation.
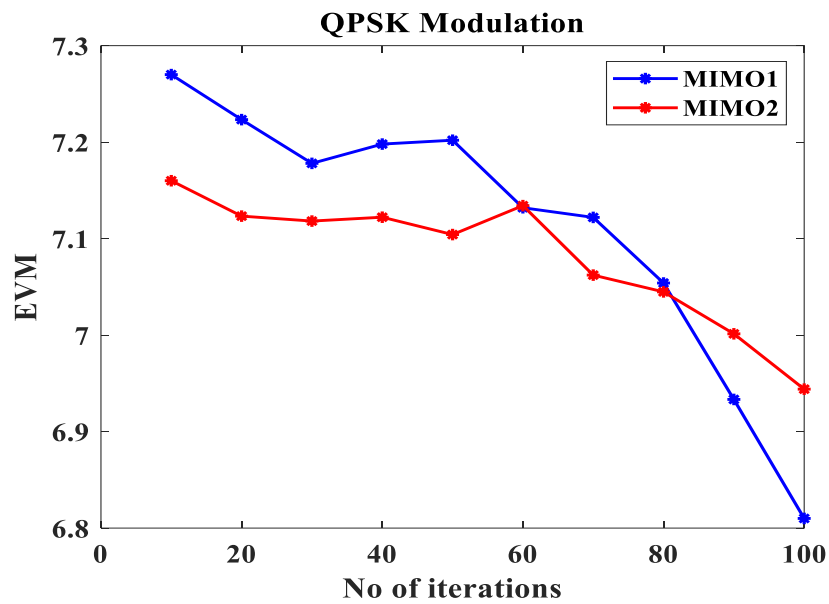
(a) QPSK modulation
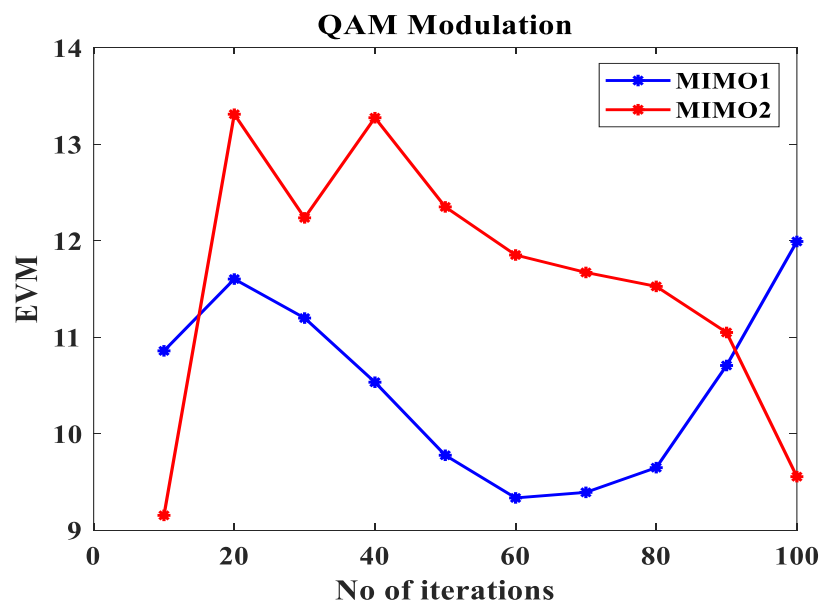
(b) QAM modulation

Figure 4. 7: Value of EVM vs number of iterations

Figure 4.8 shows the SNR performance for every signal under QAM and QPSK modulation concerning fiber length. The SNR value of QPSK modulation for MIMO2 and MIMO1 signals decreases with fiber length. While using QAM, the SNR outcomes are abruptly raised till the length of fiber reaches 20, at which point it starts to fall. The acquired noise at the optical recipient component causes noise quantization over longer distances due to the increased fiber loss, lowering connection performance overall. Here, the suggested method aids in improving the SNR value. Figures 4.8 (a) and 4.8 (b) show a graphic representation of QPSK and QAM modulation, respectively. Figures 4.8 (a) and 4.8 (b) illustrate that the SNR for QAM and QPSK modulation drops as the fiber length increases. Figure 4.8 (a) shows the suggested method's SNR at 100km of fiber, about 19.8 dB. Yet, the current method achieves an SNR of roughly 19dB for a 100km fiber length. This results from an increase in fiber length. The noise increases, which causes the MIMO channel to fade. Figure 4.8(b) shows that the suggested system achieves an SNR of roughly -3.5dB, 30% lower than the prior method when the length of fiber is increased to 10km for QAM. The existing technique achieves an SNR of around 1.5 dB and -1.5 dB for the proposed 20 km fiber length approach. High noise collection in the fiber causes a decrease in SNR for the current method. The proposed system increases the possibility of MIMO system SNR by eliminating the noise during effective modulation.
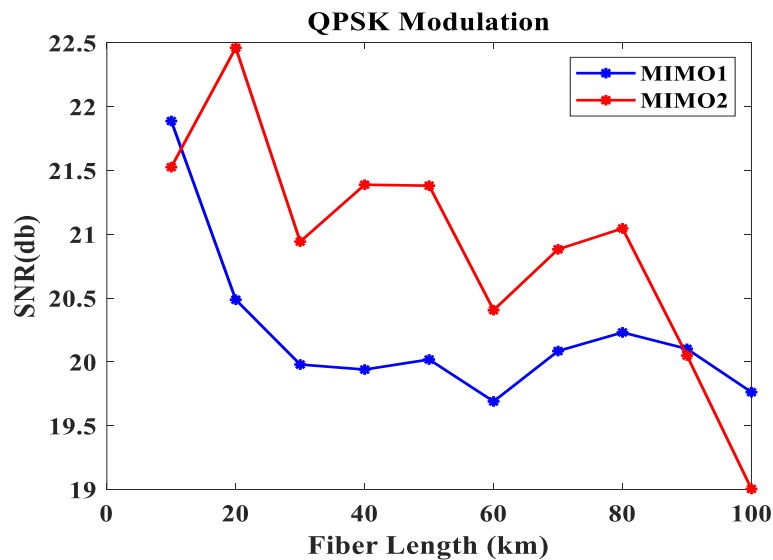
(a) QPSK modulation
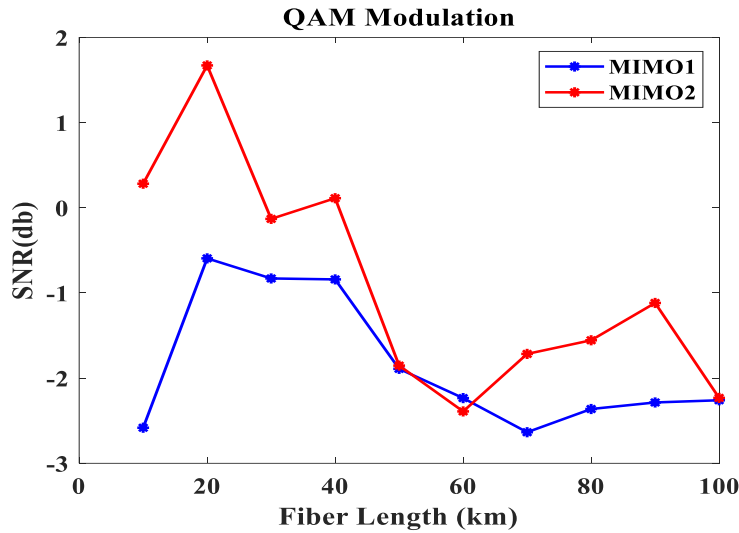
(b) QAM modulation

Figure 4. 8: Value of SNR vs fiber length

An experimental performance that is quantitatively comparable for both systems is possible. The performance of a RoF system has been thoroughly examined. In order to demonstrate the use of an improved Broadband wireless signal transmission and propagation utilizing a RoF method, it provided a bandpass sampling method for an LTE signal of 20 MHz with a format of 64 QPSK and QAM modulation. The outcomes of an experimental study agree with the theoretical model based on optimization. As compared to other strategies, the suggested strategy performs better. Figures 4.6, 4.7, and 4.8 show the direction of curves changing from upward to downward while the length of a fiber is lengthened. This is because there are irregular data packets present during signal transmission. If the base station has many antennae but little room, irregular 3D arrays are necessary. An array manifold limited complex-valued tensor decomposition issue is related to handling irregular 3D arrays under missing data. The obtained data include 3D tensors with missing values after padding zero values from the base station and re-indexing observed values. That results from a change in the received signal's SNR.

4.4.3 Comparison of existing techniques

A comparison of current techniques like AO, GWO, FFO, and ABC identifies the performance evaluation of the suggested system (Artificial Bee Colony Optimization). For QAM and QPSK modulation, the performance can be evaluated regarding SNR and EVM. The performance of SNR and EVM is examined with a 10 km fiber length and 100 iterations.

(a) *Aquila Optimization (AO)* [90] - It is an optimization technique that is based on population and motivated by Aquila's natural hunting behaviors. Thus, the optimization techniques for the proposed AO algorithm can be divided into four groups: higher soar with a vertical stoop to choose the area of search, contour flight with a short glide assault to investigate within the area of divergence search space, Slor descent attack based on low flight to exploit within the convergence search space and walk-and-grab victim to swoop. Four different predation techniques would be used by individuals of AO swarms to capture their target are given below,

- ➢ Aquila will first search and locate the target by flying across the hunting area at a high height. When prey is discovered, the animal will plunge vertically in its direction.
- ➢ Aquila will alternate between flying at a high height and hovering over the head of prey to get ready for its natural predatory behavior.
- ➢ Aquila locates the prey at first and establishes its general location. If the prey is observed to be moving more slowly, Aquila then descends vertically for introductory predation.
- ➢ Aquila travels to the land to track and attack the prey by following its flight course.

(b) *Firefly Optimization (FFO)* [91] - The bio-inspired optimization movement was inspired by firefly flashing behavior. The system states their attraction and light intensity. A species' particular flash pattern is frequently found. A bioluminescent method leads the flashing light, and the precise purposes of such signaling schemes are still up for debate. The firefly algorithm was developed and centered on idealizing the flashing performance of fireflies. The three principles are as follows:

- ➢ Every firefly is said to be unisex, and they are all drawn to each other regardless of their sexual orientation.
- ➢ Since their attractiveness is inversely correlated with their brightness, any two flashing fireflies will travel from the less attractive to the more attractive one. If neither is more attractive than the other, they will move arbitrarily. Also, they both get smaller as the distance between them grows.
- ➢ The geography of an objective function directly influences the illumination of the firefly.

(c) *Grey Wolf Optimization (GWO)* [92] - The optimization algorithm is bio-inspired and depends on the actions of a grey wolf. The hierarchy of wolf leadership and predation is modeled by the grey wolf optimization algorithm. The goal of optimization is then achieved

by using the grey wolf's skills to search, encircle, hunt, and engage in other predation-related actions.

➢ Grey wolves primarily conduct their searches based on the alpha, beta, and delta positions.

➢ During hunting, grey wolves encircle their prey. Grey wolves can change their location anywhere in the area surrounding their prey.

➢ Grey wolves can locate their surrounding prey. Typically, the alpha leads the hunt. The beta and delta may occasionally do hunting. Assume that the beta, delta, and alpha have greater knowledge regarding the possible position of prey to replicate the hunting behavior of grey wolves mathematically.

➢ The grey wolves finish the hunt by attacking the victim after it stops moving.

(d) *Artificial Bee Colony Optimization (ABC)* [93] - The ABC algorithm was developed by monitoring how actual bees search for food, also recognized as nectar, and informing bees in the nest about potential food sources. The artificial bee colony in the ABC algorithm comprises three types of bees: workers, observers, and scouts. The working artificial bees comprise the first half of a colony, and the observers make up the second.

➢ The quantity of food sources close to the hive corresponds to the amount of bees who are working. The hired bee gets changed into a scout after the other bees neglect its food supply.

➢ The quality (fitness) of the associated solution is indicated by the nectar content of a food source. The location of a food supply, on the other hand, indicates a potential resolution to the optimization issue. The population's total number of actively working bees or observers equals the total amount of solutions.

The comparison of the suggested method with known techniques is shown in Figure 4.9.

QPSK Modulation
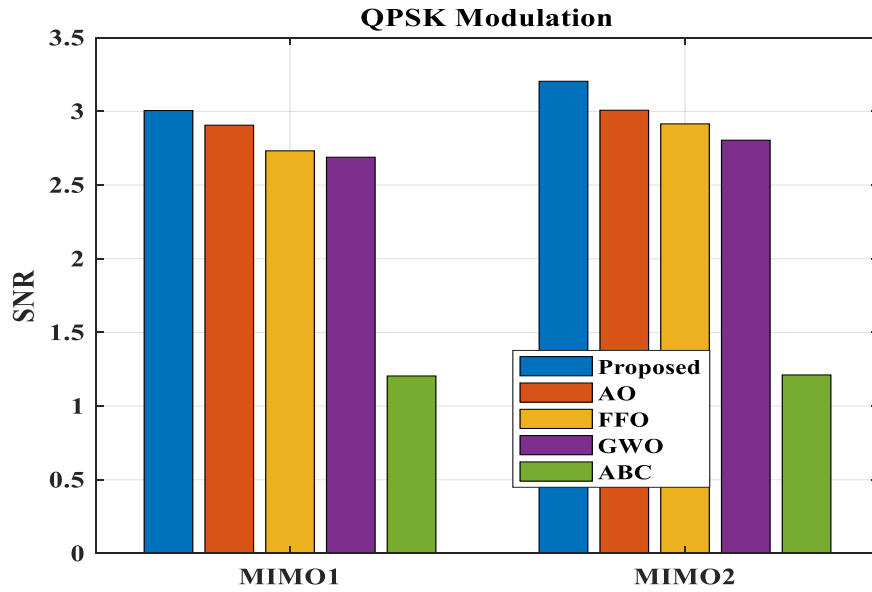
(a) QPSK modulation
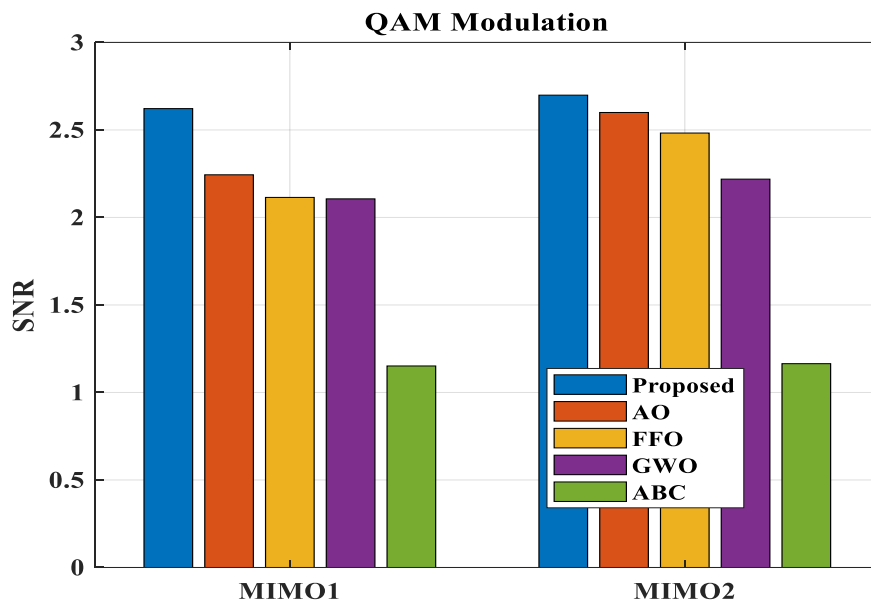
QAM Modulation

(b) QAM modulation

Figure 4. 9: SNR comparison between suggested and existing approaches.

Figures 4.9 (a) and 4.9 (b) show graphical representations of QPSK and QAM modulation, respectively. The existing techniques, including FFO, GWO, AO, ABC, and the suggested IAO, achieved SNRs of 2.906, 2.688, 2.732, 1.204, and 3.005 in the MIMO1 system, according to graph 4.9 (a). Existing strategies like FFO, GWO, AO, ABC, and the new IAO achieved SNRs of 3.007, 2.804, 2.914, 1.211, and 3.204 for the MIMO2 system, respectively. According to Figure 4.9 (b) in the MIMO1 system, the SNR was achieved by the existing techniques FFO,

GWO, AO, ABC, and the suggested IAO, respectively, with values of 2.114, 2.106, 2.243, 1.151, and 2.621. Existing methods for the MIMO2 system, including FFO, GWO, AO, ABC, and suggested IAO, achieved SNRs of 2.482, 2.218, 2.599, 1.164 and 2.698 respectively. The suggested MIMO system achieves a higher SNR than the current approach, and fiber loss is reduced, according to a detailed graph analysis. As a result, the MIMO system experiences transmission issues.

Table 4.1: Comparison of proposed approaches based on QPSK modulation with known methods in terms of SNR

Approaches	QPSK modulation	
	MIMO 1	MIMO2
IAO (Proposed)	3.005	3.204
ABC [90]	1.204	1.211
FFO [91]	2.732	2.914
GWO [92]	2.688	2.804
AO [93]	2.906	3.007

Table 4.2: Comparison of proposed approaches based on QAM modulation with known methods in terms of SNR

	QAM modulation	
Approaches	MIMO 1	MIMO 2
IAO (Proposed)	2.621	2.698
ABC [90]	1.151	1.164
FFO [91]	2.114	2.482
GWO [92]	2.106	2.218
AO [93]	2.243	2.599

The comparison of present approaches in SNR with suggestions based on QAM and QPSK is given in Tables 4.1 and 4.2. The proposed method's SNR value is contrasted with already-in-use methods, including AO, FFO, GWO, and ABC. Both QPSK and QAM modulation are used for the performance analysis. The investigation shows that the suggested methodology produces the highest results compared to current methods. Figure 4.10 compares the proposed method with current methods with regard to EVM.
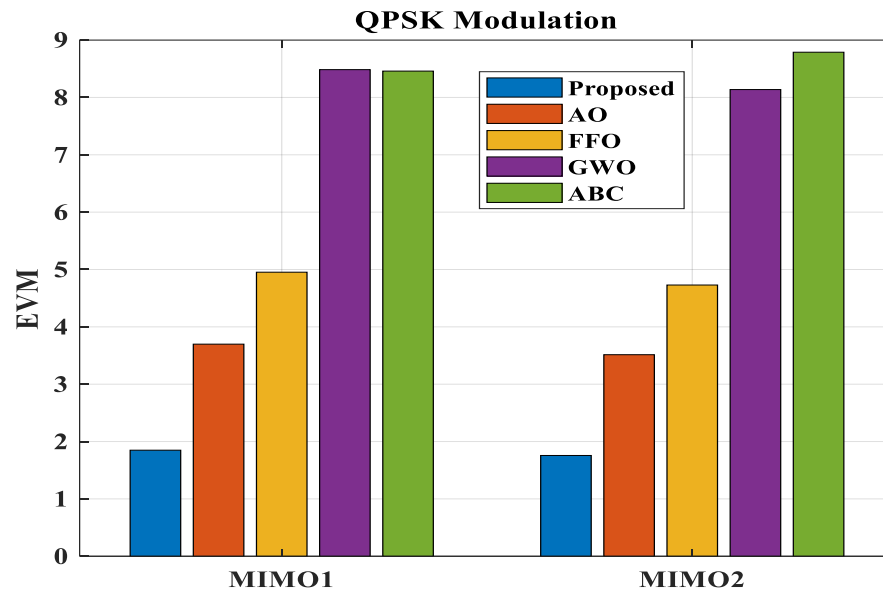
(a) QPSK modulation
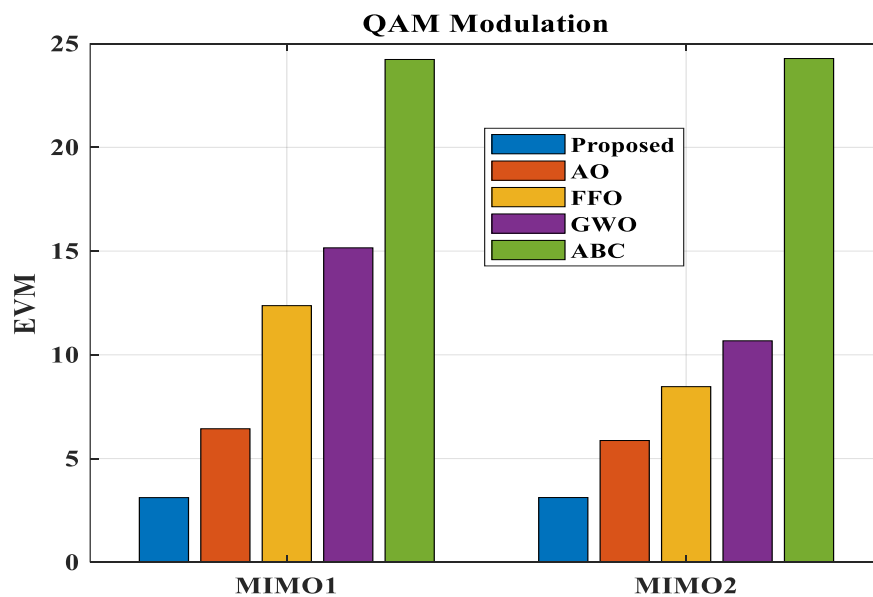
(b) QAM modulation

Figure 4. 10: Comparison of existing in terms of EVM with proposed

Figures 4.10(a) and 4.10(b) depict QPSK and QAM modulation, respectively. The previous techniques, including ABC, FFO, GWO, AO, and the suggested IAO, achieved the EVM of 8.3, 5.0, 8.2, 3.8, and 1.9, respectively, according to graph 4.10 (a) for the MIMO1 system. Existing strategies like ABC, FFO, GWO, AO, and the suggested IAO achieved the EVM of 8.8, 4.8, 8.08, 3.3, and 1.88 for the MIMO2 system. According to Figure 4.10 (b) in the MIMO1 system, the EVM was achieved by the existing techniques ABC, FFO, GWO, AO, and the suggested IAO, respectively, with values of 24.7, 12.6, 15.4, 7.4, and 3.3. Existing methods for the MIMO2 system, including ABC, GWO, FFO, AO, and the proposed IAO, achieved SNRs of 24.4, 10.7, 8.5, 5.5, and 3.14, respectively. The suggested optimization algorithm achieves low EVM compared to other current algorithms, according to the detailed study of a graph. Due to the possibility of interference and an increase in error magnitude, this occurs. The suggested approach reduces the interference, resulting in effective MIMO system transmission. Tables 4.3 and 4.4 show how the proposed and current methods in terms of EVM are compared.

Table 4. 3: Comparison of proposed approaches based on QPSK modulation with known methods in terms of EVM

Approaches	QPSK modulation	
	MIMO2	MIMO 1
IAO (Proposed)	1.88	1.9
ABC [90]	8.8	8.3
FFO [91]	4.8	5.0
GWO [92]	8.08	8.2
AO [93]	3.3	3.8

Table 4. 4: Comparison of proposed approaches based on QAM modulation with known methods in terms of EVM

Approaches	QAM modulation	
	MIMO2	MIMO1
IAO (Proposed)	3.146	3.393
ABC [90]	24.477	24.736
FFO [91]	8.53	12.625
GWO [92]	10.757	15.466
AO [93]	5.571	7.45

The proposed technique is contrasted with current methodologies, including AO, FFO, GWO, and ABC. Analyzes are done on the EVM values for MIMO1 and MIMO2 for QAM and QPSK modulation. The research study showed that the suggested outperforms the current methods.

4.4.4 Computational complexity of IAO

The amount of time to execute is measured in part by the computational complexity of an algorithm that requires Initialization, calculating the fitness function, and updating the solution make up most of the algorithm's computing complexity. Assume, $C(M)$ represents the computing complexity of initialization procedures for the solutions, and M represents the total number of solutions. The updating positions of all solutions and search for optimal placements make up the solution updating procedures, which have a computational complexity of $C(F \times M) + C(F \times M \times D_{im})$, where F denotes the overall number of iterations and A' signifies the dimension size of a mentioned issue cum problem. The proposed IAO consequently has a total computational complexity of $C(M \times (F \times A + 1))$. Figure 4.11 compares the computational complexity of the suggested strategy.
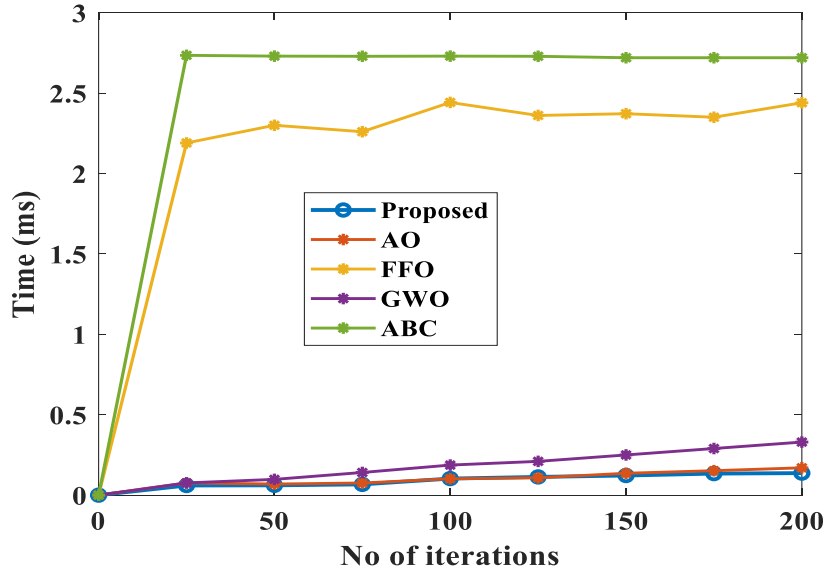
Figure 4. 11: Comparison of computational complexity with proposed

The comparison of the complexity of computation is shown in Figure 4.11. The graph demonstrates how the computational complexity rises as the number of iterations does. Table 4.5 compares the computing difficulties of the suggested technique.

Table 4. 5.: Comparison of existing approaches in terms of computational complexity with proposed

Approaches	Number of iterations			
	200	**150**	**100**	**50**
Proposed (IAO)	0.137	0.122	0.1030	0.061
ABC [90]	2.72	2.72	2.73	2.73
FFO [91]	2.44	2.372	2.442	2.3
GWO [92]	0.33	0.25	0.187	0.098
AO [93]	0.170	0.136	0.1018	0.069

For the 50 iterations, the complexity of existing techniques ABC, GWO, FFO, and AO is 2.73, 0.098, 2.3, and 0.069 respectively. Existing techniques like ABC, GWO, FFO, and AO reach levels of complexity of 2.73, 0.187, 2.442, and 0.1018 when there are 100 repetitions. The

proposed method achieves 0.061 for 50 iterations and 0.1030 for 100 iterations. In suggested approach, when compared to other existing approaches, achieves minimal computing complexity from the in-depth study of the graph. Due to undesirable transmission situations occurring throughout execution time, other existing techniques reach higher computational complexity.

4.5 Discussion

This paper suggests that the IAO be used to enhance the transmission conditions in a MIMO RoF system. This method can quickly find the correct lasers and RF signal power bias current. Other population-depend metaheuristic optimization techniques can be employed in place of IAO to produce results closer to the results. A few constant variables enhance the proposed optimization. Because of this, using different approaches would not be able to achieve the same goal. The bias current and transmission power are optimized in this suggested work using the multi-objective optimization technique. It emphasizes many goals; hence the usage of multi-objective optimization is taken into account. The investigations used wavelength-multiplexed MIMO signals in a MIMO with IM/DD RoF system. The LTE standard manages the carrier frequency and transmissions. Results are achieved by implementing the suggested system in MATLAB. An effective balance between noise and non-linearity can be achieved for a variety of bandwidths, according to experiments. It is possible to use properly biassed current and input signal power to lower system distortions and enhance EVM values.

The MIMO-LTE system's transmission challenges have been addressed using some of the earlier methods. To effectively evaluate the parameter, the frequency translation approach is introduced in DSB. However, this approach suffered from high implementation costs and a significant likelihood of channel fading. The photonic millimeter-wave data is prioritized in production and dissemination to improve the MIMO RoF system's transmission link. Due to significant data loss, this system's accuracy is too low. The author tested a system-based OFDM strategy in RoF, but this method was severely hampered by its poor capability, and failure could happen while transmitting data. To deal with the extensive data usage and high power consumption in C-RAN, the author suggested a VBSC-based information-theoretic approach. Nevertheless, this approach only performs well for a limited time and is inappropriate for real-time applications. The author presented a different strategy under the heading Framework of 5G Cellular Systems with Hybrid Supply and Energy Efficiency for C-RAN Structure. Due to high transmission requirements, this approach does not support MIMO

systems. The experimental analysis demonstrates the effectiveness of the suggested strategy, which addresses all the disadvantages mentioned above.

With the suggested method, the EVM value is less than 7.5 for QPSK modulation and less than 14 for QAM modulation. The EVM for MIMO1 and MIMO2 systems using QPSK modulation is 7.15. The EVM is lower for the existing ways and higher for the suggested approach while the number of iterations is increased to 100. The proposed approach's EVM for QAM modulation is less than 10, whereas the existing MIMO1 communication system's EVM is between 12 and 14. With 20 rounds, the suggested approach achieves the EVM of 9, which is useful for real-time applications. The SNR value decreases with fiber length for QPSK modulation of MIMO1 and MIMO2 signals. While using QAM, the SNR value significantly increases until the fiber length reaches 20, which starts to fall. The proposed technique achieves an SNR of around 1.5 dB and -1.5 dB for the current 20 km fiber length approach. The SNR for a current technique decreases because of the significant noise collection in a fiber.

The RoF MIMO communication system is modeled in the current methods, taking into account channel estimates, signal identification, aerial selection, etc., into account. Power limitations are a difficult problem that hasn't been solved in earlier studies. The suggested method examines the bias current and power restrictions for RoF MIMO communication. The suggested IAO algorithm simplifies the optimization issue by employing the optimality condition. The communication system performs better when the bias current and RF signal power are chosen optimally. Moreover, several bandwidth considerations are used to determine the trade-off between noise and nonlinearity.

4.6 Summary

The Multiple-Input Multiple-Output (MIMO) technology is combined with a radio-over-fiber (RoF) system. Wideband Long-Term Evolution (LTE) MIMO signals transmitted by the special system can support a wide range of services. It is possible to analyze the RoF fronthaul system in a MIMO system using several nonlinear effects. Transmission Parameters viz, Bias Current and Input Sgnal Power can be changed to reduce the non-linear effects of the ROF System. This study suggests that the MIMO RoF runs the BBU while optimizing the transmission settings included in this chapter. This procedure followed the IAO technique, which aims to minimize the nonlinear effects of a system while achieving the best standards for the bias currents and signal-input power of the two lasers. A distance of 10 km was used

for the experiments, and LTE-MIMO transmissions with different modulations and bandwidths were used. The carrier frequency and transmissions are governed by the LTE standard. The MATLAB tool is used to implement the suggested system. Research shows that at different bandwidths, rapid convergence is feasible, resulting in a fair balance between noise and nonlinearity. It indicates that this method may discover the ideal parameters in a limited number of iterations with adequate EVM precision. For the QPSK and QAM modulations, the maximum EVM of about 1.88 and 3.14, the SNR of about 0.134 and 3.146, and the computation complexity of 0.137s for 100 iterations are reached in the experimental result are also illustrated in this chapter.

The proposed MIMO work is extremely beneficial for increasing network efficiency in both wireless LAN and LTE systems. Even for tiny hand-held terminals, multiuser LTE can handle multi-stream transmission with extremely high data rates in a practical setting. Mobile communications and millimeter fiber transmission are two potential RoF uses. A millimeter fiber transmission system will address the electromagnetic interference and pollution problem better. The experimental results determined that suggested strategies produce superior results to alternative approaches.

CHAPTER 5

PHYSICAL LAYER SECURITY IN A GENERALIZED FREQUENCY DIVISION MULTIPLEXING-PASSIVE OPTICAL NETWORK USING OPTIMIZATION-BASED ENCRYPTION TECHNIQUE

5.1 Overview

One of the distinguishing aspects of fifth-generation (5G) applications is the Wide Bandwidth. While a large number of devices, such as those connected to the IoT, use the Internet, bandwidth turn into more limited for each device. Because bandwidth is a common type of data transfer in multimedia like music, photos, and movies, how to preserve bandwidth is a hot subject everywhere [94-95]. One of the benefits of bandwidth is that more information may be transmitted using the same bandwidth when it has been compressed. In the realm of communication, DSP (digital signal processing), like MIMO, OFDM, and GFDM, have been extensively employed. Additionally, Passive optical networks (PONs) emerge as the smartest option for the next-generation access network because of their straightforward design, energy-saving features, low price, and high transmission capacity. Furthermore, the OFDM passive optical network (OFDM-PON) has turned into one among the very promising options to satisfy the requests of following-generation networks because of its high spectrum efficiency, flexibility to arbitrary modulation constellations, and great tolerance to fiber dispersion [96-98].

Broadband service providers are actively evaluating the business potential and technological choices for the following generation of PON because 10-Gbps PON systems have been implemented effectively worldwide (NG-PON). The NG-PON2 has been standardized by the full-service access network (FSAN) [99]. The NG-PON2 must also be extremely adaptable, scalable, dependable, and effectual regarding bandwidth and consumption of energy. In addition, several multiplexing technologies, consisting of temporal division multiplexing (TDM), OFDM access (OFDMA), and wavelength division multiplexing (WDM), have been suggested for use in the access network. Although WDM-PON provides massive capacity, the system cost will rise significantly due to the need for many transceivers. In WDM-PON, each wavelength is permanent for one optical network unit (ONU), which results in imprecise granularity and resource waste. Raising the serial rate at a reduced cost per bit is the main issue for 25, 50, and 100-Gbps Ethernet PON. To make this possible, a new

suitable modulation layout should be considered to lessen the PON system's power requirements and complexity [100-101].

GFDM, or generalized FDM, is a gifted method for efficiently increasing transmission capacity. A 2D modular structure that spans both the time as well as frequency domains may be used in GFDM systems to propagate data. A pulse-shaping filter that can be adjusted is also employed to provide the system with a high degree of flexibility [102]. Due to advantages including multipath interference resistance, optical fiber dispersion resistance, and high spectrum utilization, GFDM-PON plays a crucial role in OFC (optical fiber communication), much as OFDM. To conduct contemporary coding methods, quadrature amplitude modulation (QAM) and non-return to zero (NRZ) may be effectively integrated with GFDM. Due to the expansion of Internet services and applications, GFDM technology is now regarded as an emerging technology frequently used to access optical transmission infrastructures. This GFDM method produces polarization mode dispersion (PMD), CD (chromatic dispersion), and inter-symbol interference (ISI). Additionally, because of its greater capacity and flexible bandwidth, coupled GFDM-PON has drawn the consideration of many researchers to improve data transmission in wireless communication systems. Additionally, GFDM-PON offers the advantages of optical and wireless OFDM systems.

Due to the diversity of network assaults and the data transfer involved in wireless communication, some questions concern network security. Additionally, as network threats get more sophisticated and challenging, they must be dealt with more effectively. Network security is currently a concern for governments everywhere. Data headers may readily be identified using conventional encryption at the top layer. Because it safeguards the data header, physical layer security draws more researchers to improve data transmission in online communications technology. Security of GFDM-PON is regarded as one of the key constituents of physical layer security to preserve the high unpredictability of motion trajectory and high initial value. Various encryption techniques have been developed to maintain network security in wireless communication networks. These include chaotic multi-level encryption, Brownian motion chaos, time-frequency confusion and phase masking, chaotic coding, constellation disruption, pilot assistance, digital filter multiple access (DFMA)-PON, and PAPR reduction. Some encryption methods are incompatible with probabilistic shaping approaches because of constellation dispersion. In light of this, an optimized-based encryption strategy that can ensure a sufficiently better level of security while lowering the cost of time and complexity of the system is suggested.

5.2 Proposed Methodology

This research suggests a method for enhancing PON's optical GFDM transmission while enhancing physical layer security. The proposed chaotic compressive sensing (CS) technique aims to compress the transmitted data. Transmission of bitstream utilizing CS is constrained by its failure to meet sparsity in both temporal and frequency domains. The sparsity of transferred data might be produced when transferring multimedia. In order to identify the data as multimedia, a sensor can then be utilized. If such is the case, then the CS procedure is utilized, and the sensor's output is recorded in the pilot as additional information and sent to the terminal simultaneously. A 2D logistic-sine-coupling map (2D-LSCM) is employed to encrypt the system during encryption processing to provide pseudo-random variables for the initial row of a measurement matrix. Hybrid Aquila-Harris hawk optimization (AHHO) with the best key selection is used for picture security. The discrete cosine transform (DCT) is employed to implement the CS method since data transmission is constrained at the physical layer. Combining GFDM-PON systems with this chaotic CS encryption method decreases bandwidth while enhancing security.

5.2.1 Physical Layer Security

The physical layer determines what occurs when an electromagnetic wave leaves the apparatus. To safeguard the data from eavesdroppers, one must leverage the physical characteristics of the channel to accomplish physical layer security (PLS). Typically, communication security has been achieved through techniques like shared secret keys. The upper layers of a network employ these tactics. Conversely, physical layer security uses the wireless channel's inherent unpredictability. Due to multipath propagation and the random variations in signal strength, Doppler, and delay domains, a wireless channel demonstrates this unpredictability. At both communications endpoints in the fundamental configuration, secret keys may be generated without explicit key exchange using the physical media's intrinsic unpredictability.

Determining the limits of completely secure communications, or communications with no risk of being intercepted, is another problem of physical layer security. Finding practical methods to raise secrecy rates is a related topic. It is also possible to increase security rates using beamforming, a method created to direct a signal toward the intended receiver(s) while concurrently suppressing it for unauthorized use.
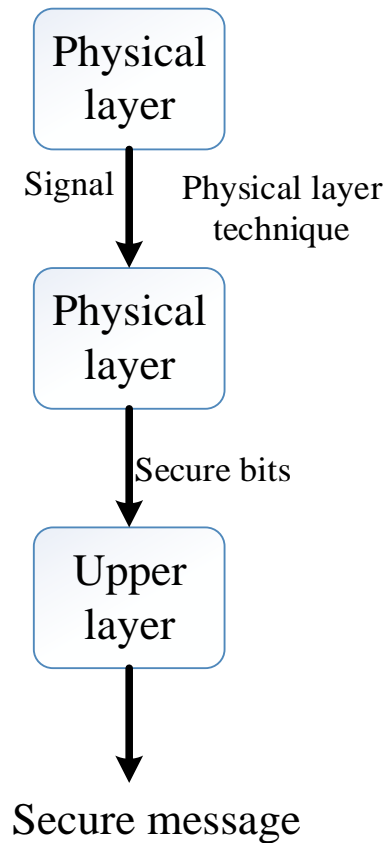
Figure 5. 1: Physical Layer Security

The PLS structure is seen in Figure 5.1. PLS is distinctive since it relies on the idea of information-theoretic security. To describe communication among two approved users in the presence of an unapproved user, PLS models a discrete memory-less wiretap channel. PLS techniques can effectively stop unapproved users from interrupting data signals. PLS can provide security even at the top tiers without encryption. Key-free encryption is made feasible by the use of suitable signaling and channel coding, as well as the exploitation of specific wireless channel peculiarities. PLS techniques have demonstrated their ability to maintain confirmed security in the face of almost infinite computational resources available to network hackers. Despite PLS's numerous benefits, it's vital to remember its serious drawbacks. Maximum security with a probability of one is practically unachievable since PLS is based mostly on average information. Furthermore, it is hard to do in real-world settings as the majority of PLS approaches need previous knowledge of the wiretap channel being used by the eavesdropper. Furthermore, utilizing PLS entirely in future wireless systems won't be viable because it needs a high data rate to offer security. To achieve security and resilience, PLS can be used with various higher-layer security methods in wireless communication networks.

5.2.2 Proposed chaotic CS-DCT approach

When signals are sparsely compressible (just a few nonzero coefficients exist in the time or frequency domain), the chaotic compression (CS) technique is applied. The CS method can be mathematically denoted as follows:

Assume an M-dimensional signal is

$$Y = (y_1, y_2, \ldots y_m)^T \tag{5.1}$$

Consider that V fulfils in the situation when Y is the l-sparse.

$$Y = v\mu \tag{5.2}$$

Where $\|\mu\|_0 = l(l << m)$ and μ is the vector with a I_0-norm. Assuming a $\phi = d \times c (d \leq c)$ measurement matrix exists. The CS sampling may be described as follows if the ith row of matrix be able to be signified as $\phi_i^T (1 \leq i \leq m)$ and S is used as the measurement vector:

$$S = \phi y + n = \phi v \mu + n = C\mu + n \tag{5.3}$$

Where ϕ and V regulate $C = \phi v$, and n stands for sampling noise. C must meet the Restricted Isometry Property (RIP) situation to correctly reconstruct the signal. A few matrices, including the Gaussian random matrix and random circular matrix (RCM), have been proven to satisfy the RIP requirement successfully. In this scenario, the measurement matrix is the RCM.

$$\begin{aligned} Q(j,1) &= \lambda(j-1,c) \\ Q(j,2:c) &= Q(j-1,1:c-1) \end{aligned} \tag{5.4}$$

Due to $l < d << c$, where $2 \leq j \leq d$, $\lambda > 1$. The restricted condition of only recovering y, μ is necessary to produce an infinite solution.

$$\min \|\mu\|_0 \ subject\ to \ \|q - C\mu\|_2 \leq \sigma_e \tag{5.5}$$

where σ_e it's energy. An approximation (a) and knowledge (s) may be found for the optimization answer I_0, which is an NP-hard issue.

(a) Chaotic CS encryption
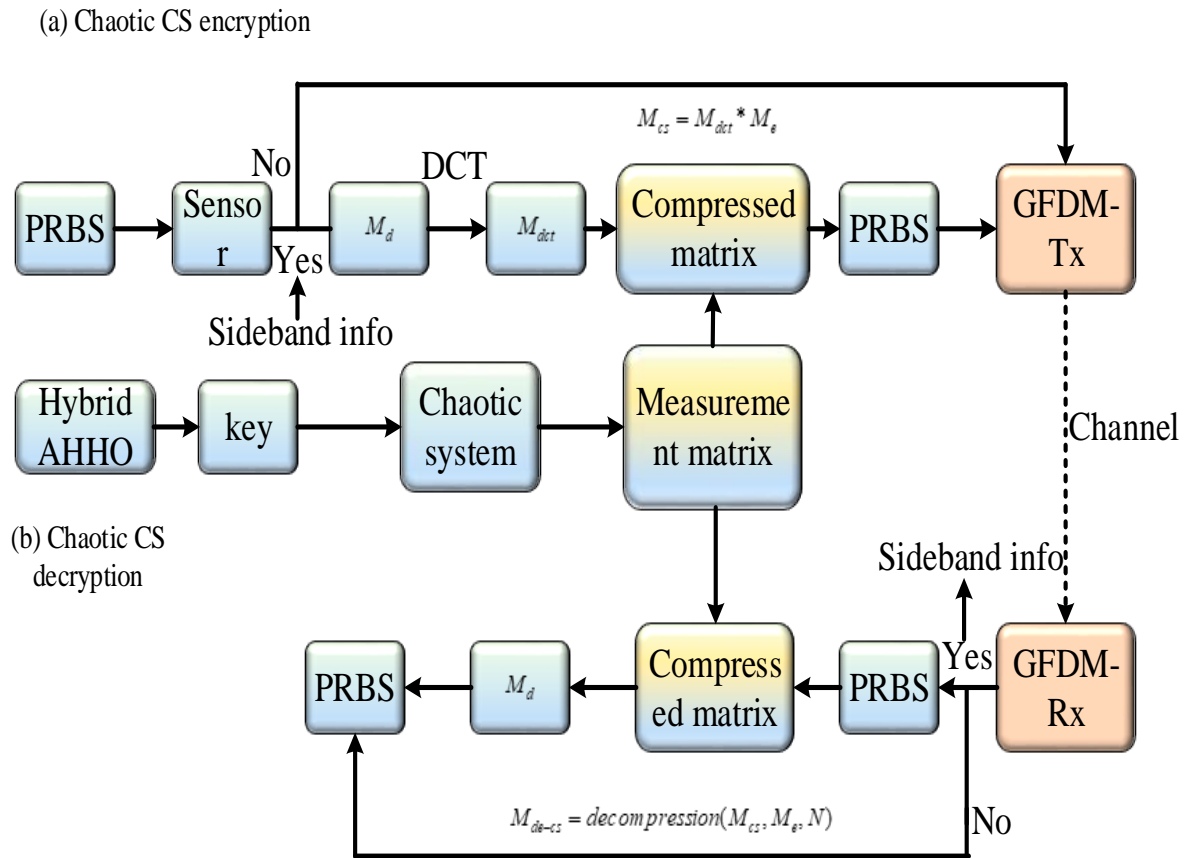
Figure 5. 2: Proposed method

Figure 5.2 presents the suggested system. The planned GFDM-PON system's schematic design shows how the transmitter and receiver data are processed. Figure 3 depicts the GFDM-structural PON's layout. A pseudo-random binary sequence (PRBS) is first created to imitate real data at the transmitter. Following serial to parallel (S/P) transformation, the PRBS is sent into the encoder while the mapper unit performs the capability of signal modulation. Modulation of constellation compression and coded modulation make up the encoder and mapper unit. With the use of CCM, a unique modulation format, a signal with uniform distribution may be converted into a signal with non-uniform distribution, making the modulated signal more reliable with and precisely according to the channel model. Different degrees of compressed signal constellations are able to be generated by varying compression factors to satisfy the wide range of user needs in various settings. Multi-carrier multiplexing is

implemented using GFDM modulation. After GFDM modulation, multiple CAP is used for modulation of carrier to implement IM/DD architecture. Following down-sampling and matching filtering at the receiver, related CAP and GFDM demodulation, decompression of constellation, and signal de-mapping are carried out to finish the reconstruction of the signal. The element of constellation compression is then modified by BER of the reconstructed signal, allowing for flexible channel support and enhancing the proposed system's transmission capabilities. The architecture of GFDM-PON is shown in Figure 5.3.
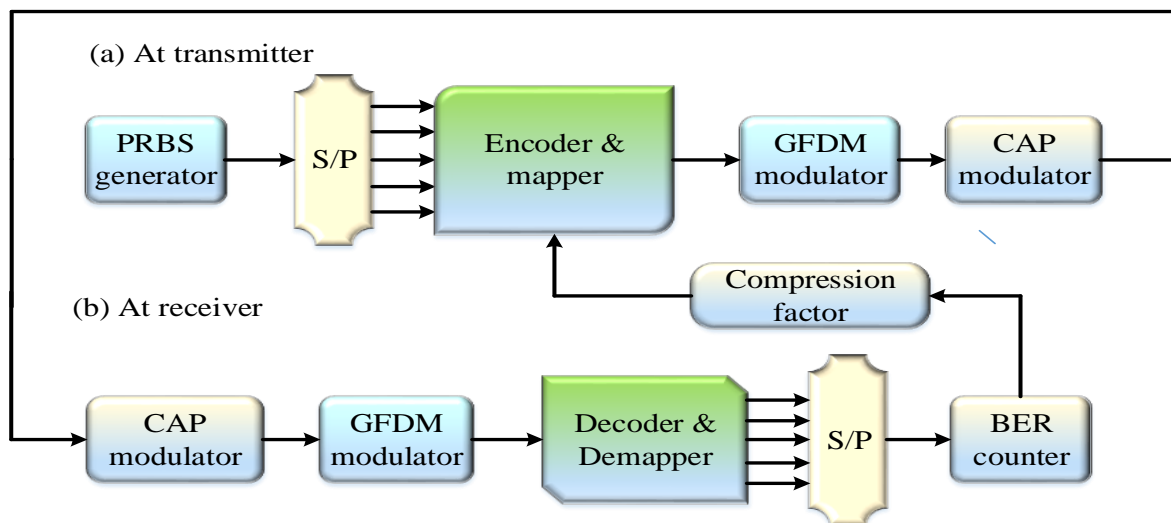
Figure 5. 3: GFDM-PON architecture

The data transmission of GFDM-PON can use the principle of a CS approach discussed above. The proposed plan is focused on making multimedia data smaller. An image is used as an illustration since it is more practical. The suggested approach for GFDM-PON is tested using a photograph of a tree with 256×256 size. Using the PRBS generator, the picture is transformed into a bitstream. A sensor picks up this bitstream to determine whether or not the data is multimedia. If the answer is no, the bitstream is immediately modulated using GFDM and sent; CS processing can be used if yes. The sideband information is configured as the sensor's output.

Once the sensor recognizes the bitstream of an image with a known dimension as multimedia, the CS processing starts. For the usage in pixels, bits are divided among 8-bit binary points. The information may then be transformed into a pixel matrix denoted by the letter Md. Meanwhile, M_d is transmitted to M_{dct} via the DCT, wherein the sparsity of the matrix can be determined. The M_{dct} is compressed using Equations (5.2) to (5.4) to produce a

compressed matrix (M$_{cs}$). Before sending, M$_{cs}$ must be transformed into a bit series and undergo modulation of OFDM. The measurement matrix Φ 's first row is produced in this case by a 2D-LSCM and may be written as;

$$\begin{cases} z_{j+1} = \sin\left(\pi\left(4\phi\, y_j\left(1 - y_j\right) + \left(1 - \phi\right)\sin\left(\pi z_j\right)\right)\right) \\ z_{j+1} = \sin\left(\pi\left(4\phi\, z_j\left(1 - z_j\right) + \left(1 - \phi\right)\sin\left(\pi y_{j+1}\right)\right)\right) \end{cases} \tag{5.6}$$

The preliminary values of the parameters $\left(y_1, z_1\right)$ and ϕ are preserved as key for chaotic system in such a case where $\phi \in [0,1]$ and the chaotic variables $\left(y_j, z_j\right)$ are in a chaotic state.

Image encryption techniques have become more focused due to the need for real-time, secure image communication over the Internet. The technique of modifying data to increase its security is known as encryption. A public key cryptosystem is an additional process CS encryption uses to encrypt data or images. The kind of operations carried out by the apps, together with other criteria used to choose the encryption plot, impact the plan's choice.

Create random encryption and decryption keys, then use the hybrid Aquila-Harris Hawk Optimization (HAHHO) algorithm to optimize them to create the best private and public keys. Complete the image security system's remaining components last.

5.2.3 2D-LSCM approach for encryption processing

To encrypt the system during encryption processing, the suggested work introduces 2D-LSCM, which generates pseudo-random variables for the initial row of a measurement matrix. This approach exhibits the best results in system encryption compared to existing technologies. Due to process complexity, poor life span, and failure to generate pseudo-variables, existing techniques are severely harmed. To secure an image from outside attack, the proposed 2D-LSCM technique has great stability and can produce pseudo-variables more precisely. The development of a 2D logistic sine coupling map is mostly based on the two earlier chaotic maps, such as the 1D logistic map and 1D sine mapping (2D-LSCM). In other words, it is produced by combining the Sine and Logistic maps and then increasing the dimension from one to two. According to estimates of chaotic performance, 2D-LSCM outperforms numerous recently created 2D chaotic maps in terms of ergodicity, the complexity of chaotic behavior, and chaotic interval.

5.2.3.1 Sine mapping

The sine map functions like a sine function, taking input from $[0, \pi]$ and converting it to a range $[0,1]$ that holds for the real result. This can be expressed numerically as,

$$z_{v+1} = S(z_v) = \gamma \sin(\pi z_v) \qquad (5.7)$$

Here, γ stands for the control factor, and the chaotic state of the map is indicated by a limit $\gamma \in [0.87,1]$.

5.2.3.2 Logistic mapping

The logistic map is a recurrence relation (or degree 2 polynomial mapping), which is sometimes cited as a prototypical demonstration of how complex, chaotic behavior may advance from incredibly straightforward nonlinear dynamical equations. The sigmoid function serves as the foundation for logistic mapping, which is mathematically expressed as,

$$z_{v+1} = L(z_v) = 4\sigma z_v (1 - z_v) \qquad (5.8)$$

5.2.3.3 Proposed 2D-LSC mapping

Better chaotic significance can be found in the current logistic and sine mapping, but it suffers from being too straightforward and having unstable chaotic intervals. Additionally, because of its chaotic usage, it might have unimaginable harmful ramifications. An improved chaotic property must be built to avoid the problems mentioned above. Unwanted eavesdropping attempts during chaotic modulation could harm the communication system. Coupling can be used to prevent random decay and the result distribution, length of chaotic orbits, and secrecy preservation. Modulation and coupling approaches can be created based on the logistic map and sine map and are mathematically controlled as,

$$\begin{cases} z_{v+1} = (\sin(4\pi \alpha \, y_v (1 - y_v)) + \beta) z_v (1 - z_v) \\ y_{v+1} = (\sin(4\pi \alpha \, y_{v+1} (1 - z_{v+1})) + \beta) y_v (1 - y_v) \end{cases} \qquad (5.9)$$

α and β stand in for the control parameters in this instance. The logistic mapping strategy is initially suggested to adjust the sine mapping by equation (3.9). The output of a logistic map and sine map was then produced as LSCM. To increase the behavior of chaotic

mapping, the dimension of 1D is finally expanded to 2D. A pseudo-variable is created using the LSCM technique to protect the system from outside attacks.

5.2.4 Hybrid Aquila-Harris hawk optimization for key selection

It is necessary to choose the optimal key for image encryption. This key is mostly in charge of effectively encrypting the image. The HAHHO algorithm is suggested as a potential solution to the problems that afflict traditional key selection methods, such as poor resistance, high optical fiber attenuation, etc. Aquila Optimization (AO) and Harris Hawk Optimization (HHO) are combined in this hybrid approach. This is a process that utilizes a symmetric key to provide both confidentiality and dependable security for encoding and decoding keys along with their corresponding images. In an asymmetric key (public key) algorithm, the private and associated keys are compared utilizing a key match. The key generation procedure still chooses additional parameters to register the public and private keys. The HAHHO method is used to optimize these produced keys. It is, therefore, possible to obtain the ideal public and private keys.

5.2.4.1 Aquila optimization

Laith A. [90] is the inventor of a recently created, cutting-edge optimization method known as AO. This method was modeled after the way Aquila hunted in nature. The suggested AO's optimization techniques are thus split into four groups: choosing the space for search with a great soar and vertical stoop, investigating inside separate search space with a short glide attack and a contour flight, taking advantage of a converged search space with slow descent assault and a minimal flight, and pouncing with a walk and grab prey.

By utilizing the equation to get a preliminary value for a group of X people, Y, AO was initialized.

$$Z_{ji} = \delta_1 \times \left(Ub_i - Lb_i \right) + Lb_i, \qquad j = 1, 2, \ldots, Y \quad i = 1, 2, \ldots, D_{jm} \qquad (5.10)$$

Where δ_1 stands for a seemingly random integer that belongs to $[0,1]$. The top and lower bounds at dimension i are indicated, respectively, by Ub_i and Lb_i. The test problem's dimension is designated as D_{jm}.

The area chosen at random: AO has two phases: exploration and exploitation, which are utilized to modify the present population. In exploration (Z_1), the Aquila determines the hunting position which is ideal by flying high with a vertical stoop after identifying the region of the prey. In this case, AO expansively discovers from a high height to pinpoint the location of prey in search space. Now exploration part begins when $t \leq \left(\dfrac{2}{3}\right) * T$ and has two approaches, the first of which is estimated by the expression below.

$$Z_1(t+1) = Z_{best}(t) \times \left(\dfrac{1-t}{T}\right) + \left(Z_N(t) - Z_{best}(t) * rand\right) \tag{5.11}$$

T represents the overall number of iterations. The factor $\left(\dfrac{1-t}{T}\right)$ is used to control the search throughout the exploration phase, $Z_{best}(t)$ representing the best individual thus far at iteration t. Additionally, the $Z_N(t)$ is calculated as an individual average across dimensions and is as follows:

$$Z_N(t) = \dfrac{1}{M} \sum_{i=1}^{M} Z(t) \ , \tag{5.12}$$

In the second exploration strategy, the Aquila rounds above target prey formulates the terrain, and attacks after being spotted from a great height. This technique involves contour flight with a brief glide attack. In this, the AO formulates the attack by closely examining the chosen location of A target prey. The AO modifies the current person using the Levy flight distribution, as presented in the following equation;

$$Z_2(t+1) = z_{best}(t) \times Levy(P) + Z_S(t) + (y - z) * rand \tag{5.13}$$

wherein Z_S represents a person who was picked randomly, $Z_2(t+1)$ is the result of a second search procedure (Z_2) for the solution of the next iteration t. $Levy(P)$ is the Levy flight distribution, which is described as;

$$Levy(P) = r \times \frac{v \times \sigma}{|u|^{\frac{1}{\alpha}}}, \quad \sigma = \left(\frac{\Gamma(1+\alpha) \times \sin\left(\frac{\pi\alpha}{2}\right)}{\Gamma\left(\frac{1+\alpha}{2}\right) \times \alpha \times 2^{\left(\frac{\alpha-1}{2}\right)}} \right) \tag{5.14}$$

Here, the constant values $r = 0.01$ and $\alpha = 1.5$ are used, while the random numbers v and u are drawn from the range [0, 1]. y and z are employed in equation (5.15) to replicate the spiral form as;

$$z = s \times \cos(\phi), \quad y = s \times \sin(\phi) \tag{5.15}$$

$$r = r_1 + U \times Q_1, \phi = -w \times P_1 + \phi_1, \quad \phi_1 = \frac{3 \times \pi}{2} \tag{5.16}$$

Where, $s = s_1 + V \times P_1$, random value is $s_1 \in [0, 20]$. Small values are denoted by $w = 0.005$ and $V = 0.00565$.

Two techniques are used to replicate an individual's ability for exploitation throughout the search process. In the first technique, the Aquila run down vertically with an initial attack to ascertain prey response after the prey region has been precisely designated, and they are arranged for the landing and attack. This tactic is called low flying with progressive descending attack. Here, AO takes advantage of the target's chosen location to approach its victim and attack. The first method is dependent on using the best answer (Y_{best}) and average location of each person (Y_M), and is constructed as follows;

$$Z_3(t+1) = (Z_{best}(t) - Z_N(t)) \times \beta - rand + ((Ub - Lb) \times rand + Lb) \times \tau \text{ the} \tag{5.17}$$

where $Z_3(t+1)$ is result of a third search technique Z_3 for the solution of t in the following iteration. The exploitation adjustment parameters are represented by β and τ, where $rand \in [0,1]$ is the random integer.

In the fourth technique Z_4, the Aquila approaches the target and then follows its stochastic motions while attacking it over the land. This strategy is called "walk and grab prey." Now the AO engages the prey in final combat in this final place. The second exploitation technique is dependent on the quality function, Z_{best} and $Levy$.

$$Z_4(t+1) = Qf \times Z_{best}(t) - (H_1 \times Z(t) \times rand) - H_2 \times Levy(E) + rand \times H_1 \quad (5.18)$$

where $Z_4(t+1)$ is the result of a 4th search procedure, which solves the problem t in the following iteration. In cases where balancing the search strategies is the primary goal, utilizing Qf is defined as,

$$Qf(t) = t^{\frac{2 \times rand() - 1}{(1-T)^2}} \quad (5.19)$$

The formula for N_1, which specifies different motions used to find the optimal solution, is

$$N_1 = 2 \times rand() - 1 \quad (5.20)$$

N_2 is reduced from two to zero and is described as;

$$N_2 = 2 \times \left(1 - \frac{t}{T}\right) \quad (5.21)$$

where *rand* stands for a random number.

5.2.4.2 Harris Hawk Optimization

In 2019 [103], Ali A. H. et al. unveiled HHO, a fresh meta-heuristic optimization technique. It was influenced by the impressively coordinated hunting behavior of the Harris' Hawk. Harris's hawk can exhibit a range of chase techniques depending on the prey's evasive movements and the habitat's dynamic character. These alternating behaviors help confuse the fleeing prey, and coordinated attempts can help Harris's hawk pursue the targeted prey until it becomes exhausted and becomes more vulnerable. The mathematical model is briefly summarized in the section below.

➢ **Exploration phase**

Harris' hawks would typically pause, wait, and survey the desert for prey. The Harris' Hawks are candidate answers in HHO, and in each stage, the best candidate answer is considered as planned prey or closely the best. The Harris hawks in HHO sit at random places and use one of two methods to wait for prey to appear. The random q value determines one of

two perching strategies, which are selected depending on the locations of other family members and the prey.

$$Z(t+1) = \begin{cases} Z_S(t) - rand\left|Z_s(t) - 2rand \times Z(t)\right| & p \geq 0.5 \\ (Z_{best}(t) - Z_N(t)) - rand(Lb + rand(Ub - Lb)) & p < 0.5 \end{cases} \quad (5.22)$$

Where p is an arbitrary value within 0 and 1, $Z(t+1)$ represents the hawks' location in iteration t, $Z_{best}(t)$ symbolizes the position of best, and $Z(t)$ represents the hawks' current position vector. $Z_S(t)$ is a hawk randomly chosen from the present population, and Z_N is the average location of a present population of hawks. The upper and lower limits of variables are represented by LB and UB.

➢ **The exploration to the exploitation stage transition**

The HHO algorithm switches from exploration to exploitation using a process dependent on the fleeing vitality of prey and then modifying the exploitative actions. Following is a description of the prey's energy, with a drop in energy as the prey flees.

$$E_p = 2E_0\left(1 - \frac{t}{T}\right) \quad (5.23)$$

Where E_p represents prey's escape energy, E_0 represents the energy's original state. In HHO, E_0 fluctuates at random with each repetition between (-1, 1). The rabbit is physically behind when the value of E_0 falls from 0 to -1, but the rabbit is physically gaining strength when the value of E_0 rises from 0 to 1. Throughout iterations, there is a diminishing tendency in the dynamic escape energy E_p. The algorithm executes the exploration phase $\left|E_p\right| \geq 1$ and the exploitation stage $\left|E_p\right| < 1$.

➢ *Exploitation stage*

Four diverse pursuing and attacking methods depending on the prey's escape energy and Harris' hawks' chasing strategies are introduced in this phase. In addition to the fleeing energy, the parameter is used to determine a strategy of chasing because it shows whether the prey will successfully escape before being attacked $(s < 0.5)$ or not $(s \geq 0.5)$.

(a) Soft besiege: The Harris' hawks gently surround prey to make it wearier before attacking, when $s \geq 0.5$ and $|E_p| \geq 0.5$, the prey still has enough energy to try to flee. The following behavior is modeled:

$$Z(t+1) = \Delta Z(t) - E_p |R_j Z_{best}(t) - Z(t)| \tag{5.24}$$

$$\Delta Z(t) = Z_{best}(t) - Z(t) \tag{5.25}$$

$$R_j = 2(1 - rand) \tag{5.26}$$

The power of the prey's random jump is indicated by R_j, where $\Delta Z(t)$ stands for the difference among the prey's location and its current location.

(b) Hard besiege: The Harris' hawks quickly encircle prey and then assault it when $s \geq 0.5$ and $|E_p| < 0.5$, when prey has a low fleeing energy. The following positions are updated in this scenario:

$$Z(t+1) = YZ_{best}(t) - E_p |\Delta Z(t)| \tag{5.27}$$

(c) Soft besiege with sequential fast dives: When $|E_p| \geq 0.5$ and $s < 0.5$, prey has sufficient energy to flee successfully; thus, the Harris' hawks engage in soft besiege by making a series of express dives around prey and attempting to gradually modify its direction and position. The following is a model for this behavior.

$$X = Y_{best}(t) - E |JY_{best}(t) - Y(t)| \tag{5.28}$$

$$X = Z + R \times LF(E) \tag{5.29}$$

$$Z(t+1) = \begin{cases} Y & \text{if } F(Y) < F(Z(t)) \\ X & \text{if } F(X) < F(Z(t)) \end{cases} \tag{5.30}$$

R is a random vector in this case. The updated position is only ever the best position between Y and X.

(d) Hard besiege with progressive fast dives: When r>1 and r2, the prey cannot flee due to lack of energy. In order to narrow the distance among themselves and the victim, the Hawks engage in a severe besiege. They then attack and kill the target. The following is how this behavior is mathematically represented:

$$\text{(e)} \quad X = Y_{best}(t) - E |JY_{best}(t) - Y(t)| \tag{5.31}$$

$$\text{(f)} \quad X = Z + R \times LF(E) \tag{5.32}$$

$$(g) \quad Z(t+1) = \begin{cases} Y & if \ F(Y) < F(Z(t)) \\ X & if \ F(X) < F(Z(t)) \end{cases} \tag{5.33}$$

The following position for a new iteration will be the only better position between Y and X.

5.2.4.3 Hybrid AHHO Algorithm for key selection

During the exploration point, the AO replicates hunting behavior for swiftly moving prey over a wide flying zone. Because of these characteristics, AO has a massive global search capability and a quick convergence speed. During the exploitation phase, the chosen search space is not, however, thoroughly explored. The Levy flight has a limited impact in late iterations, leading to premature convergence. Because of this, escaping local optima during the exploitation step of an AO algorithm is difficult even though it has great exploration capabilities and a quick convergence speed. The experimental results of an HHO approach reveal that the exploration phase has flaws, including inadequate population diversification and slow convergence speed. In the exploitation phase, four alternative hunting strategies are used to apply various location update algorithms depending on the energy and possibility of the prey's escape. Switching from exploration to exploitation is useful for adjusting to animal traits. The algorithm enters the exploitation stage as the amount of iterations rises and the prey's energy drops. In the optical line terminal, the Hybrid mentioned above, the AHHO method, is used for encryption (OLT).

The sensor's output and key may be stored as sideband data in the pilot and simultaneously transferred to ONU if the CS procedure is carried out. The pre-shared key began the decryption process when someone received data from the ONU. The compressed matrix (A_{dc}) is built using the received bitstream. To decompress (A_{dc}) and extract the data, the smooth l_0 norm $(SL0)$ technique is used. The standard Gaussian function is utilized as a smooth continuous function to estimate a lower amount of SL0, and it may be written as;

$$f_\sigma(x_j) = 1 - \exp(-x_j^2 / 2\sigma^2) \tag{5.34}$$

Where x_i is an jth element of vector r and σ is a parameter estimated by smoothness of f_σ, . Consider this:

$$F_\sigma(s) = m - \sum_{j=1}^{m} f_\sigma(x_j)$$

(5.35)

According to l_0's definition, the norm of l_0 r can be written as;

$$\|r\|_0 = \lim_{\sigma \to 0} F_\sigma(r)$$

(5.36)

Here, it can be observed that the value of $\|r\|_0$ is closer to the norm of I_0 when values of σ and F_σ are lower and greater, respectively. The best value's direction of decline is;

$$c = -\sigma^2 \nabla F_\sigma(r) = \left[r_1 \exp\left(-r_1^2/2\sigma^2, ..., r_m \exp\left(-r_m^2/2\sigma^2\right)\right)\right]$$

(5.37)

The flowchart of hybrid AHHO is provided in Figure 5.4.
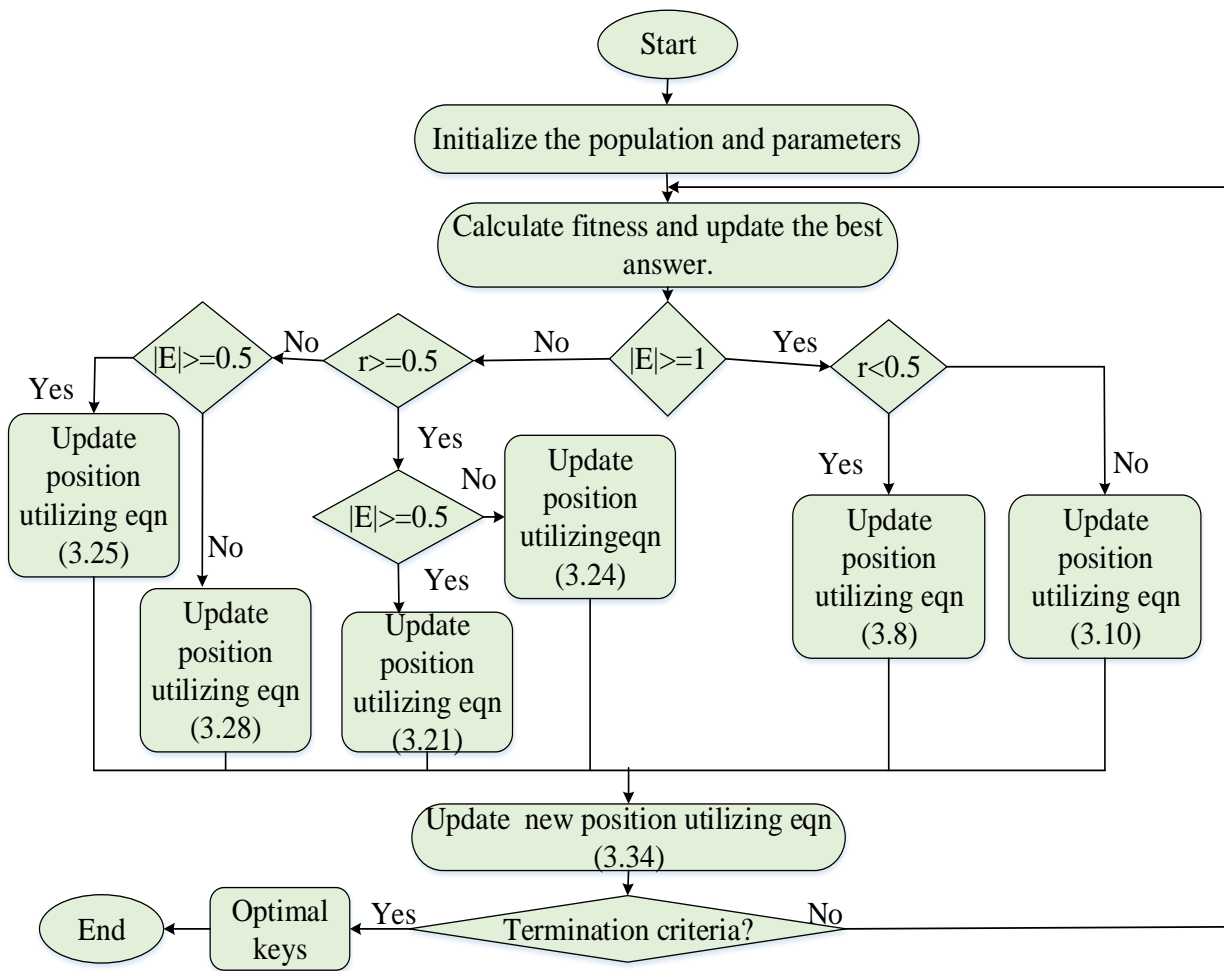
Figure 5. 4: Flowchart Hybrid AHHO algorithm

The pseudocode of Hybrid AHHO Algorithm is given as under:

Pseudocode of Hybrid AHHO Algorithm
Step 1: Initialize the population, number of iterations T, upper bound Ub_i, lower bound Lb_i
Step 2: Generate current candidate solution using equation (5.10).
Step 3: while ($t \leq \left(\dfrac{2}{3}\right) * T$)
Step 4: if ($rand \leq 0.5$)
Expanded exploration
Update the current solution using equation (5.11)
else
Narrowed exploration
Update the current solution using equation (5.13)
Step 5: if ($\lvert E_p \rvert < 1$)
Exploitation
Step 6: if $s \geq 0.5$ **and** $\lvert E_p \rvert \geq 0.5$ then
Soft besiege
Update the location vector using equation (5.24)
Step 7: else if $s \geq 0.5$ **and** $\lvert E_p \rvert < 0.5$ then
Hard besiege
Update the location vector using equation (5.27)
Step 8: else if $\lvert E_p \rvert \geq 0.5$ **and** $s < 0.5$ then
Soft besiege with progressive rapid dives
Update the location vector using equation (5.30)

Step 9: else if $\left| E_p \right| < 0.5$ **and** $s < 0.5$ then

Hard besiege with progressive rapid dives

Update the location vector using equation (5.33)

Step 10: return best individual $Z_{best}(t)$

5.3 Experiment Analysis and Discussion

MATLAB is used to accomplish the suggested method. Regarding BER and PAPR, the effectiveness of a suggested technique is evaluated. Chaotic compressed sensing (CS) and the DCT method compress the transmitted data. A 2D-LSCM is introduced to create seemingly random variables. A hybrid Aquila-Harris hawk optimization (AHHO) with the best key choice is also suggested for image security. The effectiveness of optimization is assessed in comparison to other existing optimizations, including Firefly optimization [104], Ant Bee Colony Optimization [105], and Ant Lion Optimization (ALO) [106]. The suggested method's effectiveness in GFDM-PON is evaluated by comparing its encryption and decryption times to those of existing OFDM-PON techniques. A 256*256 black-and-white pixel rugby ball image shown in Figure 5.5 is turned into a bit stream to test the proposed technique.

Figure 5. 5: Input image

Figure 5.6 shows images that are encrypted and decrypted. By comparing the real and decoded images, it can be seen that are nearly identical.
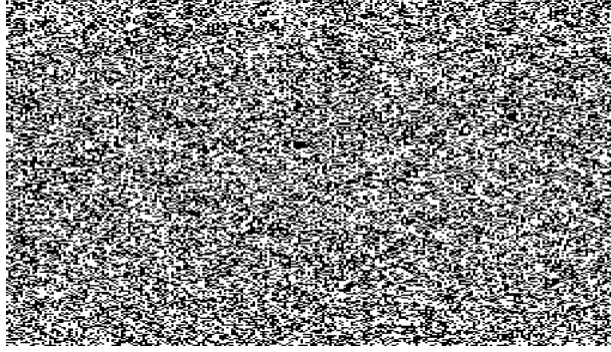
(a) Encrypted Image

(b) Decrypted Image

Figure 5. 6: Encrypted and decrypted image

This suggests a confidential transmission at the physical layer since ONU can extract essential information from its received signals. The Mean Structural Similarity (MSSIM) can be used to define this similarity coefficient. It is possible to gauge the effectiveness of image recovery using the MSSIM. The separation between windows Y and Z, which have the same size, is given as follows:

$$SSIM(Y,Z) = L(Y,Z) \times C(Y,Z) \times S(Y,Z) \tag{5.38}$$

Where structure (S), luminance (L), and contrast (C) are written as equations (5.39)-(5.41). The luminance information is represented by the average patch μ of each picture. The luminance comparison is as follows:

$$L(Y,Z) = \frac{2\mu_Y \mu_Z + C_1}{\mu_Y^2 + \mu_Z^2 + C_1} \tag{5.39}$$

Standard deviation σ is used to demonstrate contrast. The contrast-based comparison is thus:

$$C(Y,Z) = \frac{2\sigma_Y\sigma_Z + C_2}{\sigma_Y^2 + \sigma_Z^2 + C_2}$$

(5.40)

The standardization of each image with the related mean and standard deviation represents the structural element. The inner product of these signals can be used to compare the structure:

$$S(Y,Z) = \frac{\sigma_{YZ} + C_3}{\sigma_Y\sigma_Z + C_3}$$

(5.41)

Where σ_Z, σ_X and σ_{YZ} are the covariance of Y,Z and YZ, and μ_Y and μ_Z are averages of Y and Z. Their variance is represented by σ_Y^2 and σ_Z^2. $C_1 = 0.01d$, $C_2 = 0.03d$, $C_3 = C_2/2$, d are commonly used to describe a pixel values's dynamic range. Thus MSSIM can be expressed as,

$$MSSIM(Y,Z) = \frac{1}{N}\sum_{k=1}^{N} SSIM(Y_k, Z_k)$$

(5.42)

Where Y_k and Z_k represents contents of images in k^{th} the local window. The compression ratio (CR) is the percentage of input file size to reconstructed file size. Therefore, the kind of input patterns and their length, followed by the mapping and reordering process and the compression strategy, all impact the compression ratio. Bits per pixel (bpp) serve as the unit of CR. High CR provides better performance.

$$CR = \frac{size\ after\ compression}{size\ before\ compression}$$

(5.43)

The power of compression increases as the compression ratio decreases. Figure 5.7 shows a representation of a figure using various CRs. The CR value affects how much MSSIM is worth. As a result, the encryption process can significantly change the relevance of picture data and render it immune to statistical attacks.

CR = 0.25 : MSSIM =0.9527

CR = 0.50 : MSSIM =0.9434

(a)

(b)

CR = 0.75 : MSSIM =0.9387

(c)

Figure 5. 7: Recovery performance of (a) CR=0.25, (b) CR=0.5 and (c) CR=0.75

The CCDF (complementary cumulative distribution function) curves of PAPR with various CRs are shown in Figure 5.8. Here, the efficiency of the PAPR reduction has been assessed utilizing the CCDF. The CCDF calculates the likelihood that a signal's instantaneous power will exceed a predetermined level compared to its average power. The performance of PAPR under various circumstances (CR= 0.25, 0.5, and 0.75) is identical to the original signal, as shown in Figure 5.8. When CR=0.25, the curve of CCDF of PAPR looks somewhat superior to others since it has the least data.

Figure 5. 8: CCDF curves of PAPR at various CRs.

Assuming there are four ONUs and one transmits a real signal while the other three broadcast signals with CRs of 0.75, 0.5, and 0.25 when the suggested method is applied to the GFDM-PON system. The testing data is a picture of a ball, and the key for encryption is rightly inserted for the duration of decryption, much like the static security key allocation method. The CCDF achieves the same result as the real signal when the CR is at 0.25. The CCDF rapidly deviates from the original signal as the PAPR is raised. The CR at 0.5 and 0.75 deviates from the CCDF for the variable PAPR, similar to that at 0.25. The signal's original power level is 0.218 when the PAPR reaches 1. As the CR decreases from 0.75 to 0.5 to 0.25, the CCDF reaches values of 0.218, 0.329, and 0.303, respectively. When the PAPR reaches 10, the CCDF reaches values of 8.99, 8.99, 1.059, and 3.63, respectively, for the original CR of 0.75, 0.5, and 0.25. According to a detailed graph inspection, the discrepancy is caused by some optical fiber dispersion during signal transmission. Table 5.1 presents modifications in the relative values of CCDF curves for the PAPR with varying CRs.

Table 5. 1: Comparison values of CCDF curves of PAPR with various CRs

CCDF of PAPR		Original	CR=0.75	CR=0.5	CR=0.25
PAPR (dB)	1	0.218	0.218	0.329	0.303
	2	0.138	0.138	0.267	0.256
	3	0.084	0.084	0.169	0.169
	4	0.040	0.040	0.107	0.112
	5	0.013	0.013	0.045	0.051
	6	0.002	0.002	0.009	0.017
	7	0.0002	0.0002	0.0009	0.003
	8	4.13	4.13	0.000	0.0003
	9	9.77	9.77	2.22	8.27
	10	8.99	8.99	1.059	3.63

The bit error rate (BER) is a measure of bit mistakes per unit of time. By dividing the total number of bits supplied during the study period by the total number of bit errors, the bit error ratio, or BER, is determined. As a performance statistic with no units, the bit error ratio is typically expressed as a percentage.

Table 5. 2: Comparison values of BER performance

BER		Original	CR=0.75	CR=0.5	CR=0.25
Received optical power (dBm)	-25	0.317	0.318	0.183	0.226
	-23	0.181	0.182	0.119	0.147
	-21	0.046	0.045	0.048	0.062
	-19	0.003	0.003	0.006	0.009
	-17	0.000009	0.000009	0.00006	0.00013
	-15	1.2377	1.2337	1.485	1.0115

The comparison values of BER performance with various CRs are shown in Table 5.2. Performance is examined in terms of various compression ratios throughout the analysis. According to the analysis, the original signal is roughly matched by CR=0.75. According to

the graph, BER declines as received optical power rises. The BER reaches values of 0.317, 0.318, 0.183, and 0.226 for the original and 0.75, 05, and 0.25 for the CR when the received optical power is at -25dBm. Figure 5.9 modifies the signal's BER performance.
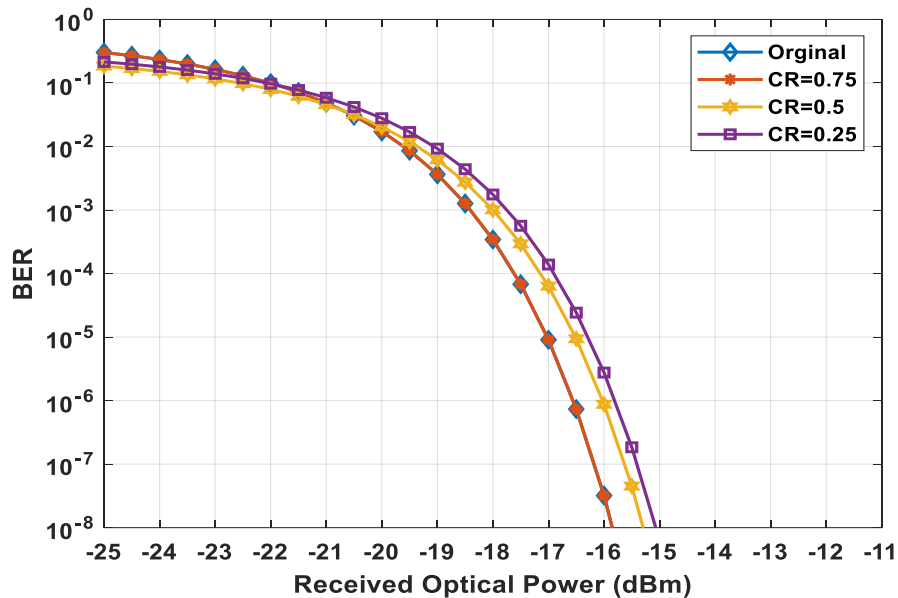
Figure 5. 9: The performance of BER for signal

The BER reaches 1.23, 1.23, 1.48, and 1.01 for the original and 0.75, 0.5, and 0.25 for the CR when the received optical power is at -15dBm. According to a thorough graph analysis, the proposed GFDM-PON technique has a low BER. It is because of a highly stable and advanced encryption technique. However, the current method has a significant error rate, brought on by short-lived, unstable encryption technology. The suggested Chaotic CS in GFDM-PON exhibits superior performance than other encryption algorithms in OFDM-PON, according to the examination of Table 5.3

Table 5. 3 Comparison of OFDM-PON techniques

	Encryption time (s)	Decryption time (s)	Amount of data (bits)
The proposed algorithm in GFDM-PON	0.0019	0.0720	524288
Chaotic CS in OFDM-PON [59]	0.00314	0.14756	524288
Chaos -DNA encrypting in OFDM-PON [107]	0.30059	0.30460	524288
Brownian motion - chaos in OFDM-PON [108]	0.09565	0.09167	524288

With 524288 bits, the suggested GFDM-PON achieves an encryption time of 0.0019 and a decryption time of 0.0720. Comparison graphs for decryption and encryption are given in Figures 5.10 -5.11.
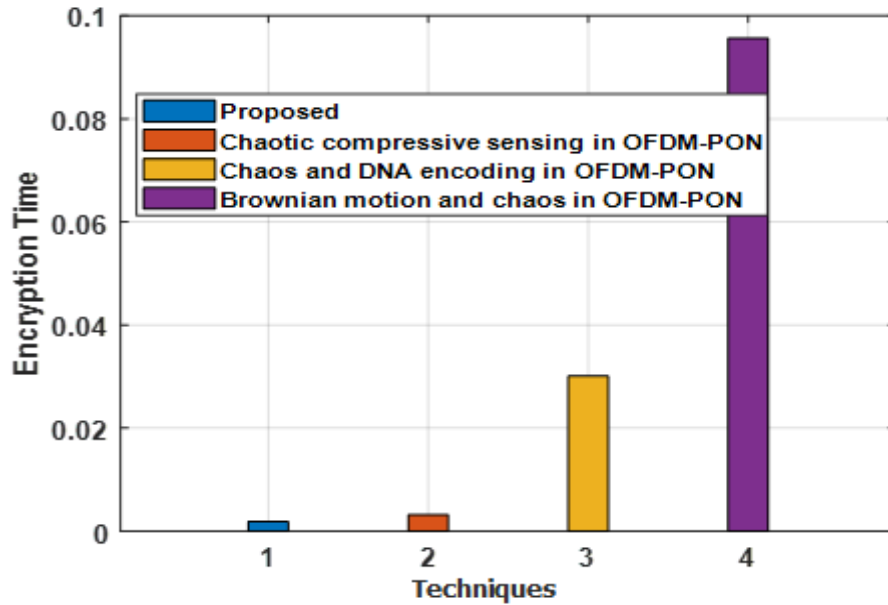
Figure 5. 10: Comparison of existing methods

Figure 5.10 displays the comparison of encryption time for various techniques. Existing techniques, such as chaotic CS in OFDM-PON, chaos-DNA encrypting in OFDM-PON, and Brownian motion-chaos in OFDM-PON achieve the encryption time obtained at around 0.00314, 0.30059, and 0.09565, respectively, while the bit amount is at 524288.
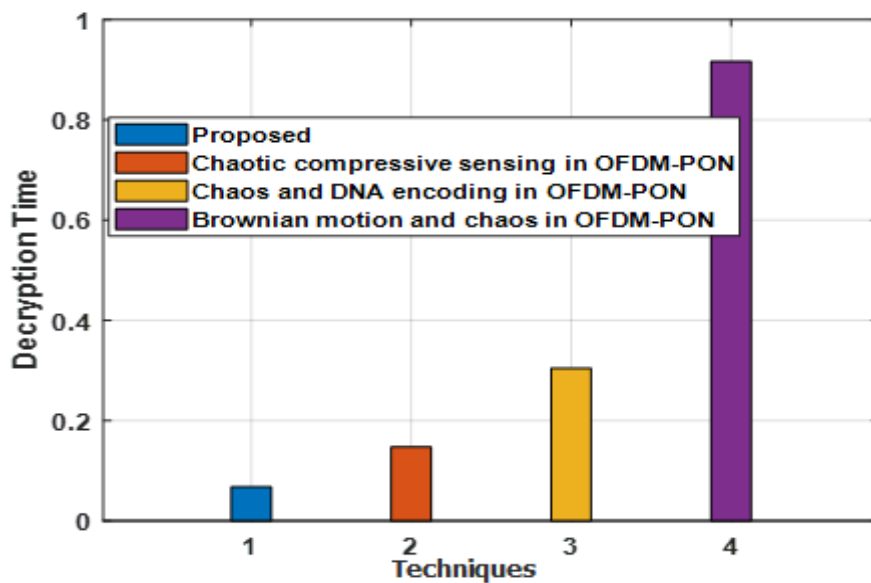
Figure 5. 11: Decryption time comparison graph

Figure 5.11 shows the comparison graph for decryption time for techniques such as chaotic CS, chaos-DNA encrypting, and Brownian motion-chaos in OFDM-PON. The proposed has a lower decryption time, while Brownian motion and chaos in OFDM-PON have a high decryption time. Both encryption and decryption take about the same amount of time. Because here, utilizing the SL0 technique in this case, the decryption process takes longer than encryption. The proposed chaotic CS algorithm also decreases the quantity of data and storage space while improving security. A thorough inspection of the graph shows that the current method achieves a longer encryption time. High optical fiber attenuation may lead to incapability as bit counts rise.

5.3.1 The comparison of a different optimization algorithm

The performance comparison across several optimizations is shown in Figure 5.11. For the best key selection in a suggested strategy, employ a hybrid AHHO algorithm. Because different optimizations, including Firefly, ABC, ALO, and WOA, are employed in the comparison. Figures 5.12-5.14 modify the graphical depiction of PSNR, MSE, and entropy. According to the research, the suggested methodology outperforms other current algorithms in MSE, PSNR, and entropy.

In comparison to the proposed strategy, the current approach achieves low entropy. Great entropy results in a system with high stability and the ability to process encryption effectively. The entropy representation is given in Figure 5.12.
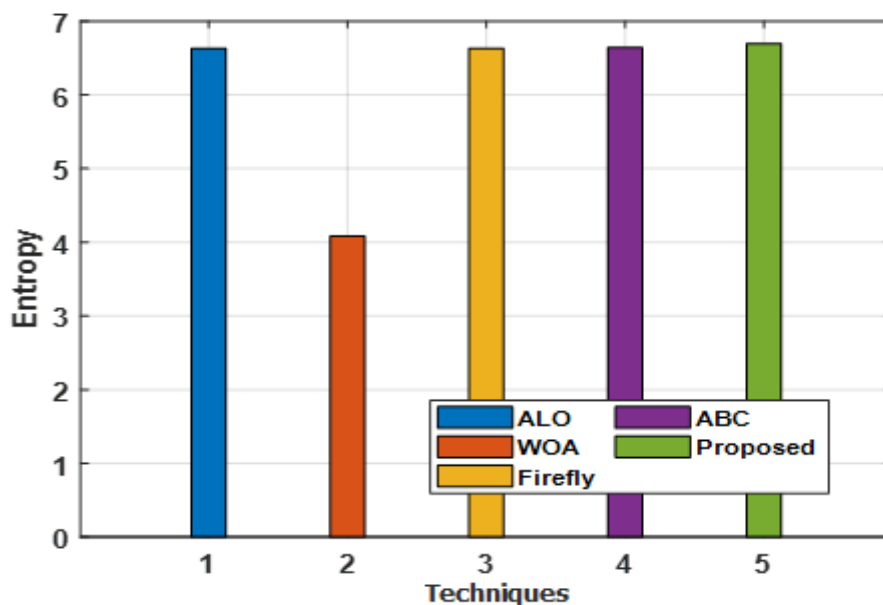
Figure 5. 12: Entropy Comparison Graph

Figure 5.12 gives the graphical representation of a comparison of proposed and existing techniques regarding entropy. According to the graph, the proposed method has slightly higher entropy than others, while WOA has the lowest entropy. PSNR comparison is given in Figure 5.13.
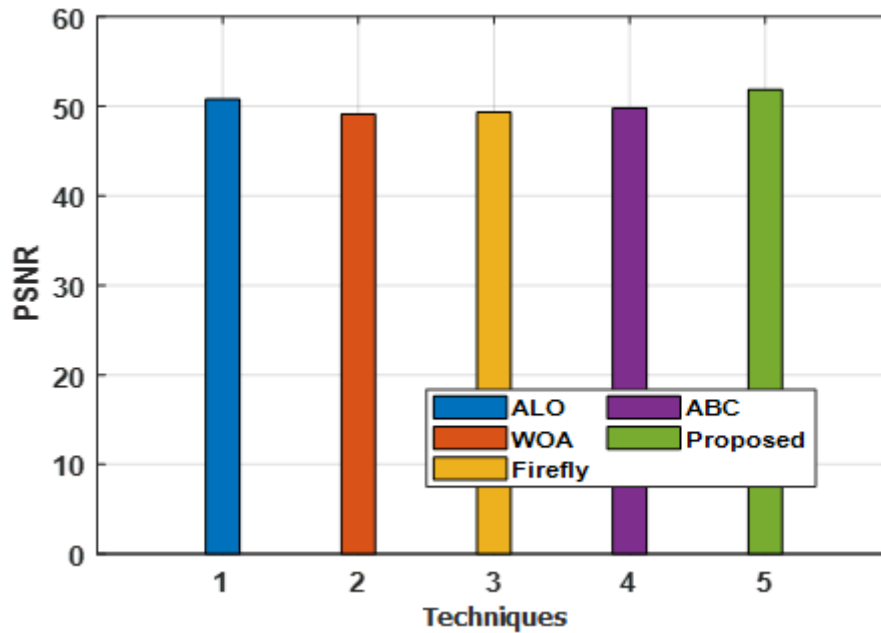
Figure 5. 13: PSNR Comparison Graph

Figure 5.13 shows the comparison of PSNR of various existing and proposed methods. PSNR value is higher for the proposed while PSNR values of others are slightly lesser than proposed. The proposed approach utilizes optical fiber more extensively, and this leads to a higher PSNR as compared to other approaches. Figure 5.14 shows the MSE comparison graph.
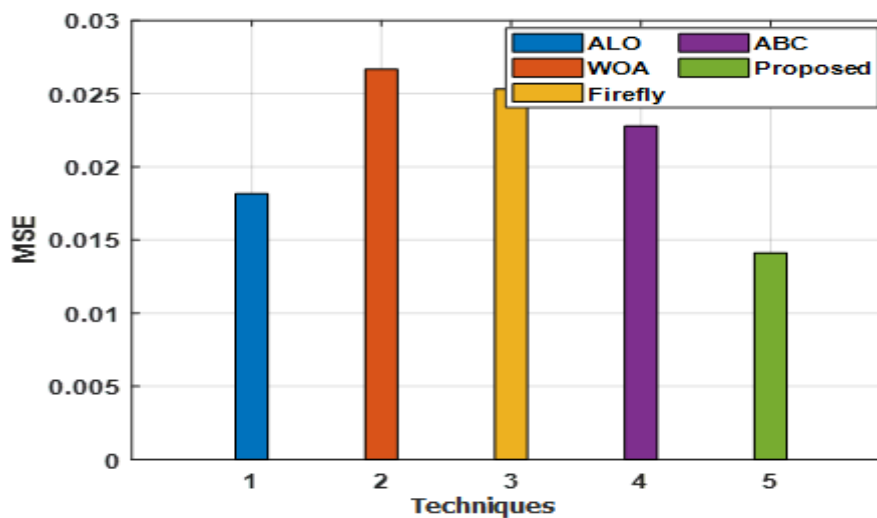
Figure 5. 14: MSE Comparison Graph

Figure 5.14 depicts the comparison values of MSE based on proposed and other existing techniques. MSE for the proposed method has the lowest value, while WOA has the highest value for MSE. The comparison for entropy, PSNR, and MSE is given in Table 5.4.

Table 5. 4 Comparison of proposed with various optimization algorithms in terms of entropy, PSNR, and MSE

Approaches	Entropy	PSNR	MSE
Proposed	6.695	51.863	0.01411
ALO [106]	6.6015	50.766	0.0181
WOA [109]	4.053	49.100	0.0266
Firefly [104]	6.6015	49.3241	0.0253
ABC [105]	6.6114	49.7855	0.02277

Entropy, PSNR, and MSE performance comparison figures for the proposed and existing algorithms are shown in Table 5.4. Entropy levels were reached for ALO, WOA, fireflies, ABC, and the proposed methods at 6.60, 4.05, 6.60, 6.61, and 6.69, respectively. ALO [106], WOA [109], firefly [104], ABC [105], and other current techniques, as well as the suggested ones, all achieved PSNRs of roughly 50.766, 49.100, 49.3, 49.7, and 51.863, respectively. Due to significant attenuation and noise, the current technique only achieves low PSNR. The PSNR must be extremely high for the system to perform effectively, which is what the suggested technique does. ALO, WOA, firefly, ABC, and the suggested technique achieved MSEs of around 0.018, 0.0266, 0.0253, 0.022, and 0.014, respectively. The significant inaccuracy and attenuation at the optical fiber are to blame for the previous method's extremely high MSE. Because optical fiber networks are highly capable, the suggested technique achieves minimal MSE. Figure 5.15 shows the graph of received optical power versus BER.
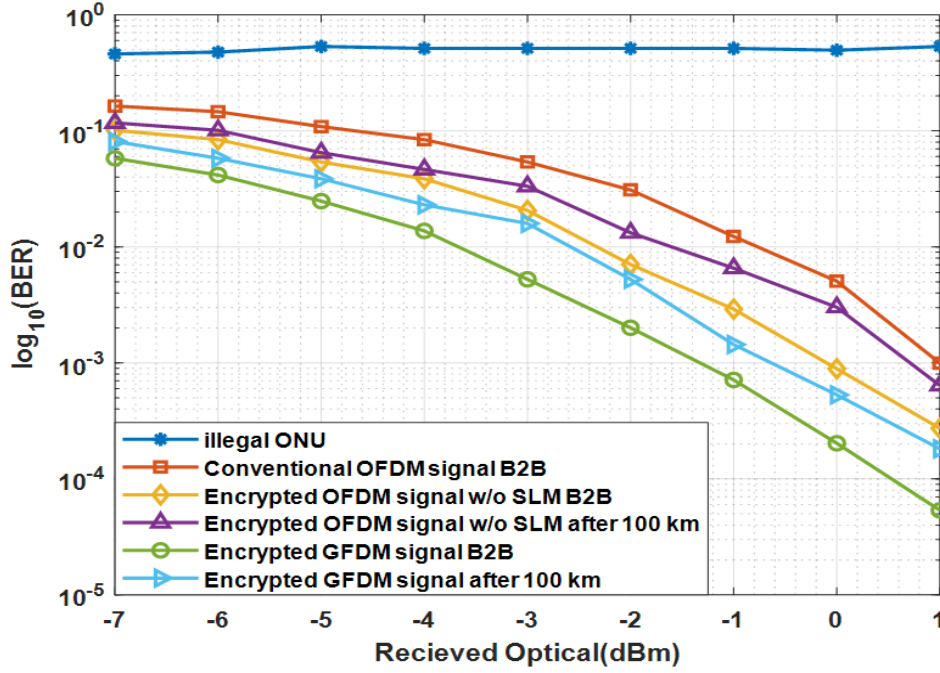
Figure 5. 15: Compares received optical power with BER with various encryption schemes.

The comparison of received optical power with BER for various encryption schemes is presented in Figure 5.15. The graph shows that the classic OFDM achieves higher BER than the suggested GFDM method. With a BER of 10, the performance of BER for a suggested technique is improved by roughly 1.5 dB. The BER performance of the existing method with frequency domain encryption was approximately 1.15 and 0.9 dB, worse than the suggested approach. Based on the developed method's penalty power among back-to-back with 100km optical fiber length, roughly 0.5dB at BER of 10.

5.3.2 Computational complexity of hybrid AHHO

This section describes the HAHHO's overall computational complexity. The three standards of solution initialization, fitness function calculation, and solution updating often serve as the foundation for the computational complexity of the approach. Locations produced by M hawks have a computational complexity of $O(M \times D)$, where D is issue dimension size. The complexity of computation in fitness assessment for an optimal solution during the iteration phase is $O(M)$. The computing difficulties of hawk position update and fitness comparison, respectively, are $O(3 \times M \times D)$ and $O(3 \times M)$ in the worst-case scenario. The suggested HAHHO method has a total computational complexity of $O(M \times D + (3 \times D + 4) \times M \times T)$, to put it simply.

5.3.3 Discussion

This research suggests a method for enhancing PON's optical GFDM transmission while enhancing physical layer security. The proposed chaotic compressive sensing (CS) approach aims to compress the transmitted data. Bitstream transmission with CS is constrained by its failure to satisfy sparsity in both domains i.e., frequency and temporal. The sparsity of data that transmitted might be produced when sending multimedia. In order to find data as multimedia, a sensor can then be utilized. If this is case, the CS method is utilized, and sensor's output is recorded in the pilot as side information and sent to the terminal simultaneously. A 2D-LSCM is employed to encrypt the system during encryption processing to produce pseudo-random variables for the initial row of a measurement matrix. Hybrid Aquila-Harris hawk optimization (AHHO) with the best key selection is used for image security. The DCT is employed to implement the CS method since data transmission is constrained in the physical layer. Combining GFDM-PON systems with this chaotic CS encryption method decreases bandwidth while enhancing security. The suggested work is employed in MATLAB, and the effectiveness is estimated against currently used OFDM-PON approaches. The outcome demonstrates that suggested method executes better than the OFDM-PON methods.

5.4 Summary

This chapter discussed a method to boost optical GFDM transmission in PON while enhancing the physical layer security. This chapter described the chaotic, CS, 2D-LSCM and optimization techniques, like AO, HHO and AHHO. Experiment results and discussion are also provided with graphical and tabular representation. Performance metrics, including BER, encryption-decryption times, entropy, MSE, PSNR, and CCDF are examined to demonstrate the suggested technique's effectiveness.

CHAPTER 6

EBOLA-OPTIMIZED JOINT SECURE COMPRESSIVE SENSING ENCRYPT AND SYMBOL SCRAMBLING MODEL FOR SECURITY IMPROVEMENT IN GFDM

6.1 Overview

Security issues threaten data integrity and provide several difficulties with fast advances and expansion of wireless communication networks, leading to the development of new encryption methods to prevent assaults. A collection of security measures for very complex behavior is established to safeguard multimedia data including text, music, and images from hackers who may employ multiple hacks at various levels in network systems [110, 111]. One of modern communication's most crucial study and design subjects is creating a secure connection. Traditional cellphone communication relies heavily on higher-layer cryptography for security, while tangible (lower-layer) data has not been properly safeguarded. Encryption at the higher and lower layers can be scrambled independently to increase security levels [112]. Using cryptography, two persons can converse through a safe wireless route without an attacker being able to decode the initial data.

Several countries are already introducing 5G wireless capabilities for Internet of Things (IoT) technologies, such as self-driving automobiles and smart cities. To deliver advantages like fast speeds, low latency, and extended battery life, the 5G network uses high-level technologies like beamforming, massive MIMO, and millimeter wave (mm-wave) [113]. Additionally, 5G technologies are supported by base station signal processing methods, including precoding. Precoding evenly distributes the various antenna components by mixing the incoming signals in a preset way. The OFDM system is the most popular 4G communication technique. Excellent reduced ISI, multipath interference resistance, and ease of implementation are only a few benefits of OFDM. Although OFDM uses rectangular pulse filters, the enormous sidelobes create intense out-of-band (OOB) radiation and a high peak-to-average power ratio (PAPR) [114, 115]. For the causes listed above, OFDM is inappropriate for 5G networks. GFDM is a workable waveform for 5G wireless technology since it overcomes the shortcomings of OFDM in meeting all criteria. GFDM is a modulation method of multicarrier that transmits data using non-rectangular pulse filters [116]. These filters can be used to get around issues with high OOB and PAPR values. It is a flexible system that may be modified

for different purposes. Last but not least, GFDM uses fewer cyclic prefixes (CP), which helps to increase spectrum efficiency.

The expanding request for wireless applications and the fast expansion in the amount of linked users have strained the volume of today's wireless communication infrastructures. The need for wireless applications is projected to rise due to their need for high throughput, excellent spectrum efficiency, and widespread connections with low latency [117] because of its inherently resilient characteristics to fiber dispersion, dynamic bandwidth allotment, and closely spaced subcarriers. To fulfill the demands of upcoming access networks, the OFDM-PON has shown to be a gifted option. The present way of protecting such data mainly relies on higher-layer encryption techniques, susceptible to technological attacks. To provide 100% coverage, the upcoming 5G cellular network will be required.

An innovative optical OFDM technique has been suggested as an alternative to attain the modulation with great spectral efficacy. OFDM-PON is the most noticeable among them when the low-bandwidth and optical sub-channels are analyzed. A top end security is necessary for wireless communications. Historically, the application layer has been where security in communications has been achieved by utilizing cryptographic encryption techniques that depend on computing resource constraints for decoding. Although MIMO includes spatial selectivity and directional gain for the transmitter, it lacks these features for the receiver, which is a drawback in multi-user wireless communication systems. Data confidentiality is protected by physical layer security (PLS), which utilizes information-theoretic methods. The inherent unpredictability of a transmission route serves as the foundation for physical layer security. The researchers will confront new challenges if the market transitions to 5G wireless communication.

Data collection and sampling are regarded as crucial components in digital systems. Compressive sensing is a sampling and sensing-based acquisition and reconstruction technique. Initially, the Shannon-Nyquist theorem-based conventional sensing models were used to sample the signals depending on the Nyquist rate. The receiver must modify its sampling rate to resemble the Nyquist rate to retrieve the information. The bandwidth specification of Nyquist theorem-based sampling contains a constraint. Nyquist sampling requires at least two times the signal bandwidth to recover a signal, which results in more samples and increases the cost of the acquisition process in big communication networks. Compared to standard approaches, compressive sensing recovers the signals with fewer

samples and measurement values. Compressive sensing is carried through three processes: sparse representation, encoding, and decoding. The goal of compressive sensing is to detect and reconstruct the signals with the highest possible accuracy using a sparse representation. The sparse signals are first sampled and then compressed using a measurement matrix. The receiver end has recovered the compressed signals using an appropriate recovery method. So in this work, a compressive sensing-based method with Ebola optimization is proposed to enhance security.

6.2 Proposed Methodology

In this, joint compressive sensing encryption is developed to overcome the challenges in a PON while transmitting secure data. This encryption method has four steps: compressed sensing, key generation, key selection, and symbol scrambling. Since it is regarded as an input, the pseudo-random binary sequence (PRBS) is categorized into sub-blocks at the transmitter side during the compressed sensing phase. These sub-blocks are then put into the sparse transform and measurement matrix, where they improve the compression rate and quality of the PRBS signal. Second, a key for secure data transfer across the PON channel is generated using the SHA-256 algorithm during the key generation phase. In the third phase, known as the key selection, the Ebola meta-heuristic algorithm is utilized to choose the best key from the results of the SHA-256 technique. Lastly, binary phase shift keying (BPSK) produces symbol scrambling to quantize and modulate the CS data. Finally, the sub-blocks are concatenated to create the original transmitted PRBS on the receiver side by performing the inverse procedure of the transmitter blocks. The framework of the suggested system is presented in Figure 6.1.
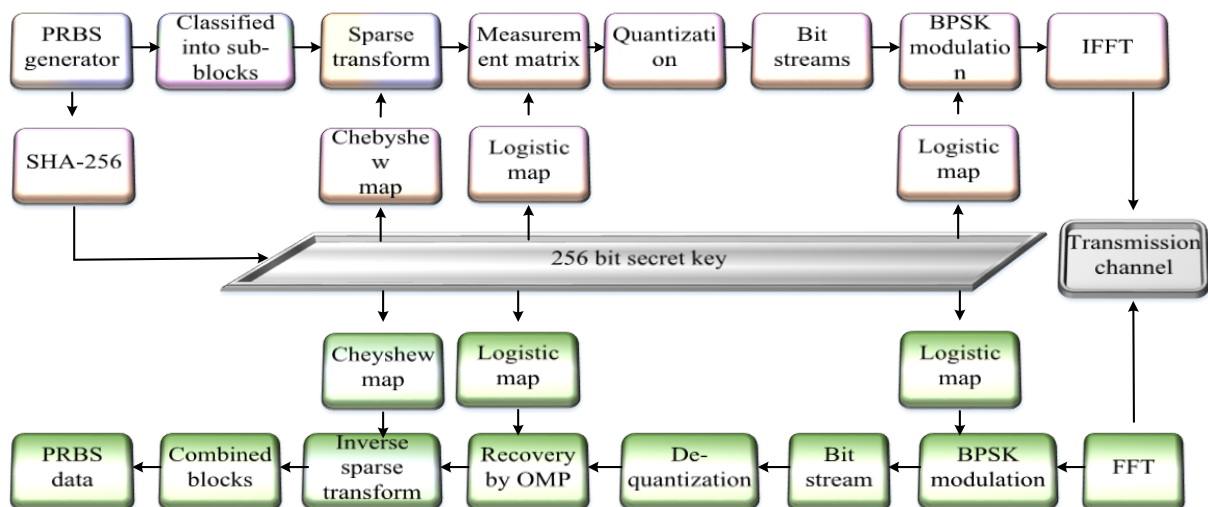

Figure 6. 1: Suggested method of the framework

143

The suggested framework consists of several blocks such as PRBS generator, sparse transform, measurement matrix, quantization, BPSK modulation, IFFT, FFT, OMP, inverse sparse transform, logistic maps, Chebyshev map, and SHA-256. So the main components are described below:

- **PRBS generator:** A periodic, deterministic signal called a PRBS comprises a stream of digital ones and zeros. A PBRS consists of a series of random binary integers. Because of this, the PRBS generator is just a random binary number generator. The value of one element in the sequence is unrelated to any other elements, making it "random". It is "pseudo" because, when considering random sequences, it is predictable and initiates repeating itself after N elements. The duration of each level, whether it is one or zero, is a multiple of the clock period of the PRBS generator. Throughout the pattern repeat time of the generator, the pattern of ones and zeros is random.

- **Measurement matrix:** One of the most crucial components of compressive sensing is the measurement matrix. It is utilized during the measurement process to sample just the elements that accurately depict the signal. The measurement matrix selection significantly impacts the accuracy and time of processing the sparse recovery procedure.

- **Quantization and dequantization:** The procedure of translating uninterruptedly infinite values to a more manageable collection of discontinuous finite values is known as quantization. This is a feature of analog-to-digital converters, which turn an analog signal into a sequence of digital values. The precision and quality of a quantized value are determined by the bit depth (amount of bits available). Dequantization also takes place in the proposed work.

- **BPSK modulation and demodulation:** A digital modulation method called binary phase-shift keying (BPSK) uses two phases of a reference signal (the carrier wave) to change or modulate two different phases of data. BPSK modulation is the most straightforward and reliable among all the PSK modulation techniques. It can only modulate at 1 bps.

- **IFFT and FFT:** A signal is transformed from frequency to time domain via the IFFT (Inverse FFT). A signal can be transformed from the time domain to the frequency domain using the FT (Fast Fourier Transform) algorithm. Leakage in the frequency spectrum will emerge from the FFT of a non-periodic signal. To reduce leakage, Origin offers several FFT windows.

- **OMP:** The most well-known greedy approach created to locate a sparse solution vector to a linear system of equations with insufficient data is called Orthogonal Matching Pursuit (OMP). OMP uses the projection method to determine the indices of a sparse solution vector's support. It is a sparse approximation approach that finds the "best matching" projection of multidimensional data onto an over-complete dictionary span.

- **Logistic map:** It constitutes a 1D discrete-time map with astonishing complexity despite its formal simplicity. One of the most significant and fundamental systems in the early study of deterministic chaos was its historical background.

- **Chebyshev map:** Chaotic characteristics, including a bigger parameter space, homogeneous data distribution, and semigroup structure, set the Chebyshev map apart. These qualities increase its acceptability in the design of a key agreement procedure. Some crucial characteristics of Chebyshev polynomials are function generating, orthogonality, recursive formula, and Parseval's identity.

- **SHA-256:** The SHA-256 algorithm is based on SHA-2 and transforms a character string into a 256-bit digest. In this specific piece, there are two innovations. The SHA-256 algorithm's compression function has been modified first. The second method involves hashing a single input text after appending the data from several textboxes to create a secured output.

6.2.1 Joint secure compressive sensing encryption

The theorem of Shannon-Nyquist sampling specifies the key method for the reconstruction of the signal from measurements and indicates that the sample rate must be at least twice the highest signal frequency. For a precise reconstruction in the discrete situation, the number of measurements must equal the signal length. Nevertheless, this method could need much storage space, a long sensing period, power, and several sensors. A new suggestion that goes beyond the conventional method is compression sensing (CS). It proves how a sparse signal may be rebuilt using fewer incoherent data. The fundamental principle of a CS technique is that most real-world signals have a compact depiction in a certain transform domain, where only a small subset of them are meaningful, and most are zero or inconsequential. Signal sparsity is used to describe this criterion. Another crucial criterion is the incoherent character of measurements (observations) in the signal collection domain. As a result, the key objective of CS is to estimate the original signal from a few linearly incoherent observations by using the sparsity feature.

So, one of the most intriguing recent developments in signal and image processing areas is compressed sensing (CS). It has been utilized in various applications, including astronomy, communication, and biological signal and image processing. The basic concept of CS is a unique sampling method that, under some circumstances, can result in a lower rate than the rate of standard Shannon sampling. The primary criterion for a successful CS is the input signal's compressibility or, more accurately, sparsity. A sparse signal contains fewer active (nonzero) components than its length. This characteristic may occur in the signal's sampling domain or with another basis, such as Fourier, Wavelet, Curvelet, or any other basis.

Measurement basis matrix (MBM) and sparse basis matrix (SBM) are two important matrices in the CS skeleton. DCT, Discrete Fourier transform (DFT), and discrete wave transform (DWT) are examples of common matrices that are used to function as an SBM. The two methods used as a measuring matrix are the partial Hadamard and the chaotic matrix. The Hadamard measurement matrix has the values 1 and -1 as its elements, also sides of this matrix are orthogonal. Matrix H of rank n is called a Hadamard matrix if its inverse and inversion are closely related. The chaotic map, in this case, creates the chaotic matrix.

6.2.1.1 Compressed sensing:

When dealing with sparse signals that a limited number of significant coefficients may adequately represent in a suitable transform basis, CS can be used to lower sampling rates. So, in addition to the conventional Nyquist rate, extremely tiny measurements are used to extract and rebuild the compressed or sparse signal from the region called ψ. The sparse or compressed signal is shown as $Q \subset r^m$. The following value Q is provided:

$$Q = \psi R \tag{6.1}$$

In Equation (6.1), $R \subset r^m$, where If R contains $l(l \ll n)$ non-zero entries, it is assumed that R has a value of l sparseness. The measurement vector is described below with the size $n(n < m)$ and the claimed value p.

$$p = \Theta q + mu = \Theta \psi R + mu = Yu + mu \tag{6.2}$$

Where, the matrix for sensing is $Y = \Theta \psi$, in that Θ is the matrix for measurement or matrix measurement (MM) which is created with the help of a chaotic map. Also, the vector for noise is denoted by mu. Matrix Y then satisfies the restricted isometry (RIP) constraint, which

identifies roughly orthonormal matrices, at least when applied to sparse vectors. It is a basic characteristic of a matrix that permits sparse recovery.

$$1 - \xi_L \leq \frac{\|Yu\|_2}{\|u\|_2} \leq 1 + \xi_L \tag{6.3}$$

In this equation (6.3), $\xi_L \in (0,1)$. The recreated signal u is created with the help of expression (6.2). There are two types of reconstructed signals viz., convex optimization and greedy techniques. This research focuses on secure compressed sensing and uses the traditional orthogonal matching pursuit (OMP) technique in terms of greedy methodology to learn the performance of a suggested secured strategy.

Here, the OMP has been utilized to get around the shortcomings of the matching pursuit algorithm. The orthogonalization concept is the foundation of OMP. It then determines the inner product between the measurement matrix and the residue, picks the index of the greatest correlation column, and extracts this column (in each iteration). The chosen set of atoms includes the extracted columns. A new approximation vector is then produced by the OMP's orthogonal projection over the subspace of previously chosen atoms, which is then utilized to update the residual. As the residual, in this case, is always orthogonal to the CS matrix's columns, no columns will be picked twice, and the number of picks grows during iterations.

6.2.1.2 Secure compressed sensing strategy

The study employs a secure block CS approach, which uses a matrix of chaotic measurement and a matrix based on chaotic for binary sequences. Block-compressed sensing (BCS) completes data capture and compression by using light measurement. BCS is the best method and can use its major benefit when working with high-dimensional images and films. This approach breaks the image into several tiny regions. It performs measurement and reconstruction on each region independently, dramatically decreasing computing complexity and freeing up storage space for the sensing matrix. The measuring matrix in BCS is compact, which is good for storing. After being achieved, the measurement value for each picture region may be supplied separately. The receiver can also independently recreate the picture region using the data to achieve real-time performance.

Several sub-blocks make up the actual binary sequence. Chaotic DCT is used to transform each block into an SB area. The resulting signal is then calculated using a chaotic DCT matrix. To decrease the computational complexity of CS, the actual binary sequence is divided into several

subblocks. Every sub-block is initially transformed into a disorganized DCT SB dependent on the DCT row scrambling. Using a map of logistics, chaotic sequences are created.

$$q(M+1) = \beta q(M)(1 - q(M)) \tag{6.4}$$

Here, $q(0)$ is represented as the initial value along with the value of $q(M)$ belongs to the range (0, 1). If the value of β, which is a parameter for control, is in the range of $3.5699 < \beta \le 4$, Equation (6.4) develops as a chaotic model. And lastly, it results in the generation of a chaotic vector with size M_C. According to the logistic map, $Q = [q(1), q(2), \cdots, q(M_C)]$ is the attained vector for chaotic. The mth element of α vector is stated as follows,

$$\alpha(M) = \mathrm{mod}\left(floor\left((q(M) + 100) \times 10^{10}\right), M_C\right) + 1 \tag{6.5}$$

$\beta_1 = [\beta(1), \beta(2), \cdots, \beta(M_B)]$ is used to convey the new chaotic integer scrambling vector that is produced. The *mth* row is signified as $E(n)$, and the usual DCT matrix is considered to be $E_1 = [E(1), E(2), \cdots, E(M_C)]$. After conducting row sampling on the DCT matrix E_1, by utilizing a row permutation vector β.

$$\psi_{chaos}^{DCT} = [E(\beta(1)), E(\beta(2)), \cdots, E(\beta(M_C))] \tag{6.6}$$

As a byproduct of the conventional DCT E_1, the chaotic DCT matrix that was created is referred to as the scrambling matrix D.

$$\psi_{chaos}^{DCT} = DE_1, \left(\psi_{chaos}^{DCT}\right)^t = E_1^{\ t} D^t \tag{6.7}$$

$$\psi_{chaos}^{DCT}\left(\psi_{chaos}^{DCT}\right)^t = DE_1 E_1^{\ t} = DJD^t = J \tag{6.8}$$

The matrix for chaotic DCT is ψ_{chaos}^{DCT}.

Similar to this, chaotic sequences are created from the Chebyshev map.

$$q(M+1) = \cos\left(K_e \times ar\cos(q(M))\right) \tag{6.9}$$

In this case, $q \subset (-1, 1)$, q_0, a starting value, and K_e are regarded as keys. Finally, using a variety of control settings and beginning values, multiple chaotic scrambling sequences C_1 are produced. The outcome of a chaotic DCT measurement matrix is supposed to be obtained X_{chaos}^{DCT}. Choose from M_C rows to N_C rows of a DCT matrix of size $M_C \times M_C$ to produce a partially chaotic DCT matrix. It functions as a $N_C \times M_C$ size Θ_{chaos}^{DCT} MM.

$$\Theta_{chaos}^{DCT} = \sqrt{\frac{M_C}{N_C}} SME_1 \tag{6.10}$$

Where, S stands for the subsampling matrix.

6.2.2 Key generation using SHA-256

Raw data is scrubbed through the process of hashing until it is impossible to recreate it in its real state. It takes a set of data and passes it through a function to numerically modify the plaintext. The function of hash generates a result or digests identified as a hash value. The plaintext is transformed into the appropriate hash digest using the hash function. The digest should never expose the original plaintext because they are designed to be irreversible. Hash functions always yield the same outcome while the input is unchanged, regardless of how frequently they are employed.

The Hash function is a key component of a signature authentication technique used extensively in electronic transactions. A tiny change in the input data can greatly impact the output data with this function. The collision-resistant, one-way cryptographic hash algorithms like SHA-256 take a plain text input of length (a multiple of 512) and produce a distinct hash result or digest with a fixed length of 256 bits (32 bytes). The maximum length of a message M that the SHA-256 can accept is 256 bits. The subsequent are several of the SHA-256 algorithm's distinguishing abilities:

- The cleartext must be fewer than 264 bits in length. The size must be in the contrast area to sustain the highest level of randomness in the digest.
- The 256-bit-long hash digest is a must for SHA-256, 512-bit long for SHA-512, etc. Bigger digests often imply more calculations at the expenditure of performance and storage.
- All hashing algorithms, containing SHA 256, are intended to be irreversible. In this case, neither should the digest return its original value after being hashed again, nor should the plaintext be obtained when the digest is present previously.

The SHA-256 function inputs a binary sequence and outputs a 256-bit key stream (BKS). At that moment, split 256 BKS K_{ey} into blocks of 8 bits. The following is the mathematical representation for K_{ey}.

$$K_{ey_1} = k_{e_1}, k_{e_2}, \ldots, k_{32} \tag{6.11}$$

Three distinct values are created depending on the SHA-256 key stream, and they are as follows:

$$u_1 = \frac{\left(k_{e_1} \oplus k_{e_2} \oplus \ldots \oplus k_{e_{16}}\right)}{256} \tag{6.12}$$

$$u_2 = \frac{\left(k_{e_{17}} \oplus k_{e_2} \oplus \ldots \oplus k_{e_{32}}\right)}{256} \tag{6.13}$$

$$u_3 = \frac{\left(k_{e_1} \oplus k_{e_2} \oplus \ldots \oplus k_{e_{32}}\right)}{256} \tag{6.14}$$

$\oplus$ defines the XOR operation in this case. The chaos model's three starting values are generated regarding the abovementioned values.

$$q_0 = q_0' + u_1/2 \tag{6.15}$$

$$r_0 = r_0' + u_2/2 \tag{6.16}$$

$$p_0 = p_0' + u_3/2 \tag{6.17}$$

Where, $q_0' r_0' p_0'$ are the actual initial values of a chaos system.

6.2.3 Optimal key selection using Ebola search optimization algorithm - ESOA

The EOSA metaheuristics uses the characteristics of the Ebola virus spread and the sickness it causes to determine how the exploration and exploitation stages of optimization could aid in solving various optimization issues in medicine.

The best optimum solution within the solution space is found through optimization, depending on certain predetermined restrictions. The ESOA updates each exposed individual's location using the equation (6.18)

$$m\left(K_i^{t+1}\right) = mK_i^t + \gamma G(K) \tag{6.18}$$

While γ represents the scale factor for each individual's displacement, mK_i^{t+1} and mK_i^t represent the updated and actual locations about time t and $t+1$. An individual's movement value is denoted by the $G(K)$.

$$G(K) = S_{rate} * Rand(0,1) + G(Inl_{best}) \tag{6.19}$$

$$G(S) = K_{rate} * Rand(0,1) + G(Inl_{best})$$ (6.20)

➢ **Exploitation phase:**

The infected person either remains where they are or is relocated within a range not exceeding S_{rate} within a distance of "0". The short distance movement, in this case, is designated as S_{rate}.

➢ **Exploration phase:**

Depending on the sick person migrating far from the typical neighborhood range K_{rate}, it is established. This leads to the conclusion that the more people in a group A are exposed to illness, the further the migration. S_{rate} and K_{rate} are controlled by the neighborhood parameter. If the value is $>= 0.5$, either a person leaves the neighborhood that spreads mega infection or arrives in the neighborhood that controls infection. Lastly, it determines which dual secret key from a 256-bit key stream is best for security.

➢ **Initialization**

The initial population is created using random number distribution, with all individuals starting at position '0'. Equation (6.21) is used to produce the individual. The upper and lower boundaries are symbolized as U_j and L_j, respectively, for the jth position. The range of K in population size ranges from $1,2,3...m$.

$$inl_j = L_j + Rand(0,1) * (U_j + L_j)$$ (6.21)

Among the group of infected people at a time t, choosing of best current solution is computed.

$$best(A) = \begin{cases} G_{best}, & fitness(C_{best}) < fitness(G_{best}) \\ C_{best}, & fitness(C_{best}) \geq fitness(G_{best}) \end{cases}$$ (6.22)

$best(A)$, C_{best} and G_{best}, respectively, at a time t are used to symbolize the best solution, the best solution as of that instant, and globally. The problem refers to the OF implements as $fitness$.

For this initialization, the fitness value was discovered along with the objectives for each created solution for both encryption and decryption.

The infected (I), susceptible (S), hospitalized (H), immunized (V), exposed (E), recovered (R), quarantine (Q), funeral (F), and deceased (D) categories should be updated. The goal of using

differential calculus in this research study is to determine how quickly I, S, H, V, E, R, Q, F, and D variables change over time T.

$$\frac{\partial S(T)}{\partial T} = \mu - (\gamma_1 I + \gamma_3 D + \gamma_4 R + \gamma_2 (PE))S - (\beta S + \Gamma I) \tag{6.23}$$

$$\frac{\partial I(T)}{\partial T} = (\gamma_1 I + \gamma_3 D + \gamma_4 R + \gamma_2 (PE)\tau)S - (\Gamma + u)I - (\beta)S \tag{6.24}$$

$$\frac{\partial H(T)}{\partial T} = \alpha I - (u + \omega)H \tag{6.25}$$

$$\frac{\partial R(T)}{\partial T} = uI - \Gamma R \tag{6.26}$$

$$\frac{\partial V(T)}{\partial T} = uI - (\pi + v)V \tag{6.27}$$

$$\frac{\partial D(T)}{\partial T} = (\beta S + \Gamma I) - \xi D \tag{6.28}$$

$$\frac{\partial Q(T)}{\partial T} = (\mu I - (uR + \Gamma D)) - \varepsilon Q \tag{6.29}$$

Scalar functions are used in the equation mentioned above.

> **Objective function**

In the present GFDM-PON secure data transfer, the PSNR value is measured as the goal function. The following is the objective function's mathematical expression:

$$OBJECTIVE = Max(PSNR) \tag{6.30}$$

> **Updating process for a new key**

Following calculating fitness, update I, S, H, V, E, R, Q, F, and D. To improve keys during the encryption and decryption phases, fresh keys are updated. The flowchart for the Ebola optimization technique is shown in Figure 6.2. The following is a possible writing of mathematical formula for this new key update:

$$New\_key\ update = Q + S + +V + H + I + E + R + F + D \tag{6.31}$$
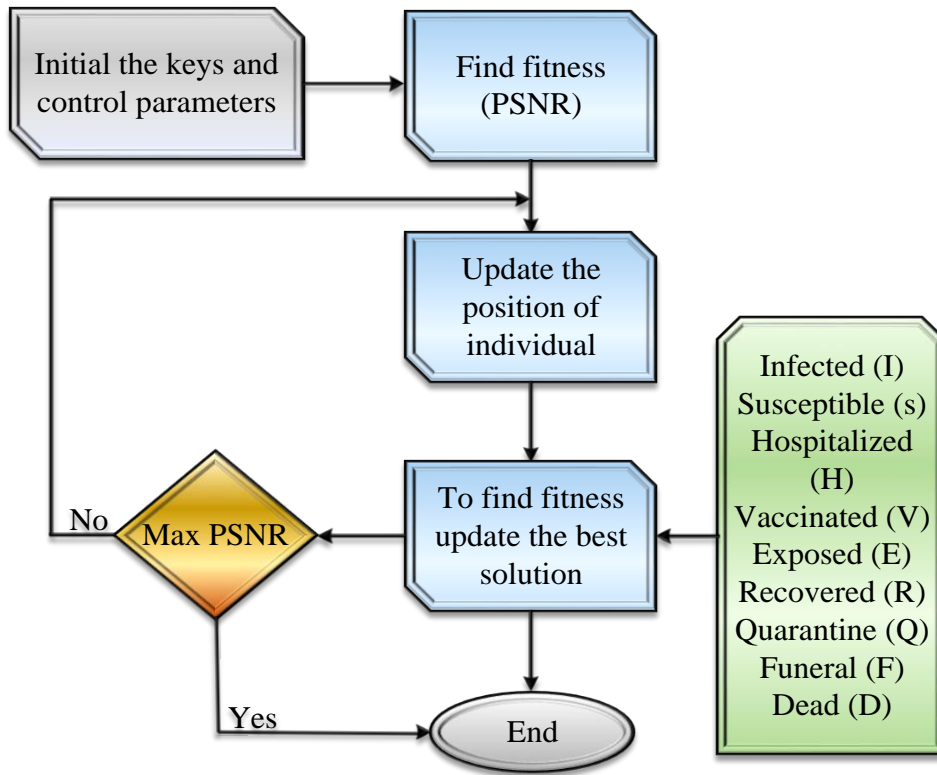
Figure 6. 2: Ebola optimization algorithm (EOA) Flowchart

The EOSA's pseudo code is shown below:

Algorithm 1: EOSA

Outcome: The best solution

Input: Objective function, ub, lb, psize, epoch, evdincub

Output: gbest solution

Step 1: $S, I, E, H, V, R, Q, solus \leftarrow non-zero$;

Step 2: $S \leftarrow formSusceptibleInDvD(psize, S)$ Equation (6.21)

Step 3: $j_{case} \leftarrow producedIndxCase(S)$;

Step 4: $c_{best}, g_{best} \leftarrow j_{case}$;

Step 5: while $E \leq epoch \wedge len(I) > 0$ **do**

Step 6: $Q \leftarrow rand(0, Eq. \times I)$;   Equation (6.29)

Step 7: $fracI = I - Q;$

Step 8: for $j \leftarrow 1$ **to** $len(fracI)$ **do**

Step 9: $\quad posi_j \leftarrow mov_{rate}(\ )$ $\qquad\qquad\qquad$ Equation (6.18)

Step 10: $\quad d_j \leftarrow rand(\ );$

Step 11: $\quad newI \leftarrow non - zero;$

Step 12: $\quad$ **If** $d_j > evdincub$ **then**

Step 13: $\qquad neighbourhood \leftarrow prob(posi_j);$

Step 14: $\qquad$ **If** $neighbourhood < 0.5$ **then**

Step 15: $\qquad tmp \leftarrow rand(0, Eq(6.24) \times I \times s_{rate});$

Step 16: $\qquad$ **End**

Step 17: $\qquad$ **Else**

Step 18: $\qquad tmp \leftarrow rand(0, Eq(24) \times I \times k_{rate});$

Step 19: $\qquad$ **End**

Step 20: $\qquad newI+ \leftarrow temp;$

Step 21: $\quad$ **End**

Step 22: $\qquad I+ \leftarrow newI;$

Step 23: $\quad$ **End**

Step 24: $\quad ho \leftarrow rand(0, Eq(6.25) \times I), H+ \leftarrow ho;$

Step 25: $\quad re \leftarrow rand(0, Eq(6.26) \times I), R+ \leftarrow re;$

Step 26: $\quad va \leftarrow rand(0, Eq(6.27) \times ho), V+ \leftarrow va;$

Step 27:	$de \leftarrow rand(0, Eq(6.28) \times I), D+ \leftarrow de;$
Step 28:	$I+ \leftarrow I - add(r,d);$
Step 29:	$S+ \leftarrow re;$
Step 30:	$S- \leftarrow de;$
Step 31:	$c_{best} = fitness(objfunc, I)$
Step 32:	**IF** $c_{best} > g_{best}$ **then**
Step 33:	$Object = Max(PSNR)$
Step 34:	$g_{best} = c_{best};$
Step 35:	$sols \leftarrow g_{best};$
Step 36:	**End**
Step 37: End	
Step 38: Return g_{best}, solus;	

6.2.4 Symbol scrambling scheme to modulate the CS data

To make the resultant binary sequence look more random, scrambling is a binary bit-level processing technique for the transmission rate signal. Employing an efficient digital modulation symbol scrambling technique increases the security of secure CS data. Imagine a scenario that $X = [X(0)X(1)\cdots X(m-1)]$ specifies a BPSK symbol m size vector, and chaotic function, which is derived from the logistic map, is designated as $G = [G(0)G(1)\cdots G(n-1)]$ of size n. The resulting G sequence is transformed into a binary sequence called A.

$$A(ke) = sign(G(ke) - 0.5) \tag{6.32}$$

The PBSK symbol vector $Y = [Y(0)Y(1)\cdots Y(n-1)]$ is then scrambled, and it may be obtained as shown below;

$$Z(ke) = X(ke)A(ke) \text{ (L)} \tag{6.33}$$

On the side of the receiver, the inverse scrambling operation is carried out.

6.2.4.1 Secure CS transmission model

A multi-carrier system called GFDM uses digital implementation to carry out the traditional filter band method. Low-complexity equalization is possible at the receiver side due to the use of cyclic prefix (CP) insertion. In GFDM, each block of $m = nk$ modulation symbols is sent using subsymbols of n and subcarriers of k. This waveform is non-orthogonal. The following is how the mathematical model for the transferred GFDM symbol is stated:

$$q[M] = \sum_{k=0}^{k_1-1} \sum_{n=0}^{n_1-1} s_{k,n} h\left[\langle M - Nk_1 \rangle_m\right] e^{-i2\pi \frac{k}{k_1} M} \tag{6.34}$$

Whereas $h[M]$ represents the transmitted prototype filter, $\langle (\cdot) \rangle_m$ denotes the m-operator modulo, and $s_{k,n}$ is the modulation symbols that are transmitted on the kth subcarrier and n^{th} sub symbol.

The GFDM matrix formula is provided by

$$q = As \tag{6.35}$$

Where, $s = (s_0 \ldots s_{n-1})^t$ and $s_N = (s_{0,N} \ldots s_{k-1,N})^t$.

The interplay between subsymbols and subcarriers, symbolized as A, in equation (6.35), demonstrates that the GFDM symbol is a linear modulation.

The obtained CS binary sequence is qualified and modulated using the BPSK modulation. The modulated transmission is changed through the wireless route. Afterward, the bit stream is transformed into a symbol stream that is categorized into sub-blocks using BPSK. Every sub-block is signified by an $X = [X(0)X(1)\cdots X(m-1)]$ of size m, and it is scrambled according to the equation (6.33). The resulting encrypted signal vector, denoted by the word Z, is converted into a GFDM time domain signal using an IFFT unit.

$$z = F^H Z \tag{6.36}$$

where F signifies the DFT matrix and the element (n,o) can be determined as;

$$F(n,o) = \frac{1}{\sqrt{m}} e^{-i\frac{2\pi NM}{m}} \quad n,o \in \{0,1,\ldots,m-1\} \tag{6.37}$$

The acquired time domain GFDM signal $s = (s_0 \dots s_{n-1})^t$ is given a cyclic precursor (CP) to eliminate the inter-symbol interference. The information must go through a power amplification device before being transmitted via a channel.

The noise of the detected signal is, at the recipient block,

$$R = F_1 \times s + G_a \qquad (6.38)$$

Where the additive white Gaussian noise is designated as $G_a = [g_0 g_1 \dots g_{m-1}]$ and the discrete impulse response of selective channel for wireless frequency is written as F_1. The quasi-static exponentially declining multipath Rayleigh fading structure is used in this proposed study. The following is the algebraic formula for this system:

$$f(t) = \sum_{j=0}^{j-1} f_j \xi(t - jT_s) \qquad (6.39)$$

f_j is a complicated Gaussian random variable in this instance.

$$f_i \sim cn(0, \theta_0 \exp(-jT_s / T_{RMS})) \qquad (6.40)$$

Here $\theta_0 = 1 - \exp(-T_R / T_{RMS})$. The root mean square (RMS) is written as T_{RMS}, and the receiver sampling number is marked as T_s. The frequency of channel reaction at k^{th} the subcarrier can be stated as;

$$F(k) = \sum_{j=0}^{j-1} f(j) \exp\left(-i \frac{2\pi kj}{m}\right) \qquad (6.41)$$

The channel reaction at j^{th} tap is represented by f_j in this instance.

Processing the output data $\Re$ is done using the FFT device. The information available at k^{th} the subcarrier is then stated as follows;

$$\Re(k) = F(k)Z(k) + H(k) \qquad (6.42)$$

Where, in frequency region, the complex Gaussian is represented by $H(k)$ with a zero mean and σ_k^2 variation.

As a result, the outgoing signal was equalized using minimal mean square error (MMSE) or zero-forcing (ZF). The formula for an equalized signal is;

$$\breve{Z}(k) = G(k)\Re(k) \qquad (6.43)$$

For ZF equalization $G(k) = \dfrac{1}{\breve{F}(k)} = \dfrac{\breve{F}*(k)}{\left|\breve{F}(k)\right|^2}$.

When equation (6.42) is substituted into equation (6.43), it results in the following equation (6.44).

$$
\begin{aligned}
\breve{Y}(k) \quad &= G(k)\big[F(k)Z(k) + H(k)\big] \\
&= G(k)F(k)Z(k) + G(k)H(K) \\
&= Z(k) + H(k)/F(k)
\end{aligned}
\tag{6.44}
$$

The equalized signal $\breve{Z}(k)$ is decoded using the chaotic encryption pattern U. When a signal $\breve{R}$ is received and decrypted, the equation is;

$$
\begin{aligned}
\breve{R}(k) \quad &= \breve{Z}(k)V(k) \\
&= \big[Z(k) + H(k)/F(k)\big]V(k) \\
&= \big[R(k)U(k) + H(k)/F(k)\big]U(k) \\
&= R(k) + H(k)U(k)/F(k)
\end{aligned}
\tag{6.45}
$$

The acquired decoded BPSK symbol stream is then converted into a bit stream and subjected to inverse quantization processing. To make a sub-block of sequence, the generated data is used. The real binary sequence is then created by integrating the complete sub-block sequence.

6.3 Results and Discussion

The current part defines the outcomes of a suggested approach to demonstrate the suggested model's efficacy compared to other strategies already in use. The performance metrics for this suggested method, including PSNR, CCDF, entropy, time of encryption, BER, time of decryption, and MSE, are evaluated and related to current methods using a MATLAB platform.

6.3.1 Performance metrics

PSNR and MSE are the two variables used to determine the quality of the restored data.

6.3.1.1 MSE

The average of the squared difference among observed and expected values is MSE. The analysis is less logical from the time when squared units are used instead of actual data units.

In this case, there will be less disparity among the recovered and real transferred signals if the MSE number is lower. The MSE algebraic formula is;

$$MSE = \frac{\sum_1^m [q-p]^2}{n*m} \qquad (6.46)$$

The quantity of rows and columns in the given signal is indicated as n and m, respectively, which q stands for the real signal and p for the recovered signal. In this, negative values for the differences are eliminated by squaring the differences, and it is assumed that MSE will not ever be less than or equal to one. Mostly regularly, it has a positive value. An error-free perfect model can only produce an MSE of 0. Squaring also amplifies the effect of greater errors. These formulas unfairly penalize bigger errors more than little errors. For the model to have fewer errors, this characteristic is crucial.

6.3.1.2 PSNR

The peak signal-to-noise ratio between two signals is determined with the help of the PSNR formula. Using this ratio, one may evaluate the original and created signals' quality. A greater PSNR value results in the highest possible signal fidelity. It may alternatively be described as the association among the maximum value (power) of a signal and distorted noise power that degrades the accuracy of its presentation. The following is a reference to the PSNR algebraic expression:

$$PSNR = 10 * \log_{10} \frac{M^2}{MSE} \qquad (6.47)$$

M stands for the signal's highest possible value.

The PSNR is frequently stated on the logarithmic dB scale because many signals have a very large dynamic range (the ratio between the highest and lowest attainable values of a variable quantity).

6.3.1.3 Entropy

The "amount of information" confined in a variable is calculated by entropy. This amount is now approximated depending on the amount of distinct values in the variable and the surprise level that this variable's value carries. Here, entropy is described as the probabilistic behavior of a data source in an input stream. The below equation (6.48) is an algebraic formula for entropy.

$$H(S) = \sum_{j=0}^{I-1} q_j \log_2 \frac{1}{q_j} \qquad (6.48)$$

In this case, q_j stands for the probability that the sign s_j will appear in S.

6.3.1.4 Bit compression ratio

Compression ratios (CRs) are percentages or ratios that express the difference between a file's real and last size after compression. This ratio relies on several variables, mostly the starting file's condition and compression technique utilized. The CR increases as the amount of resources needed to compress or decompress the data increases. Utilizing compression ratio, the suggested system's bit compression capacity is evaluated. The BCR is calculated using the following Equation (6.49).

$$\lambda = \frac{CR \times N_{ai}}{N_{actual\_bit}} \times 100\% \qquad (6.49)$$

Where n_{actual_bit} represents the real transmission bits and N_{ai} represents the necessary transmission bit.

6.3.2 Performance Analysis

The CCDF of PAPR for some known and suggested models is shown in Figure 6.3. Compared to the suggested GFDM system, the two current systems are the standard OFDM signal and the secure OFDM signal. The divergences signals may quickly rise based on CR values as varied as 0.25, 0.5, and 0.75.
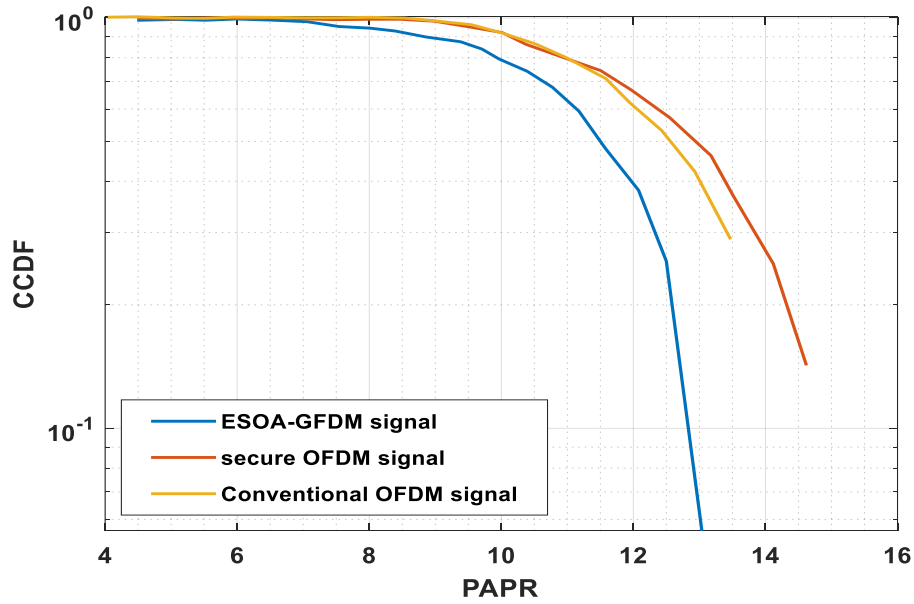
Figure 6. 3: A comparison of suggested and current CCDF values.

When the PAPR number is 4, the resultant CCDF values are 1.004402, 0.998001, and 0.987036. The achieved values of an initial signal are at 1.004402 when the PAPR value is 4. The obtained values for real and on the premise of changing CR values are 1.005161, 1.000994, and 0.987852, respectively, if the value of PAPR is 8. Figure 6.4 shows BER performance against optical power received.
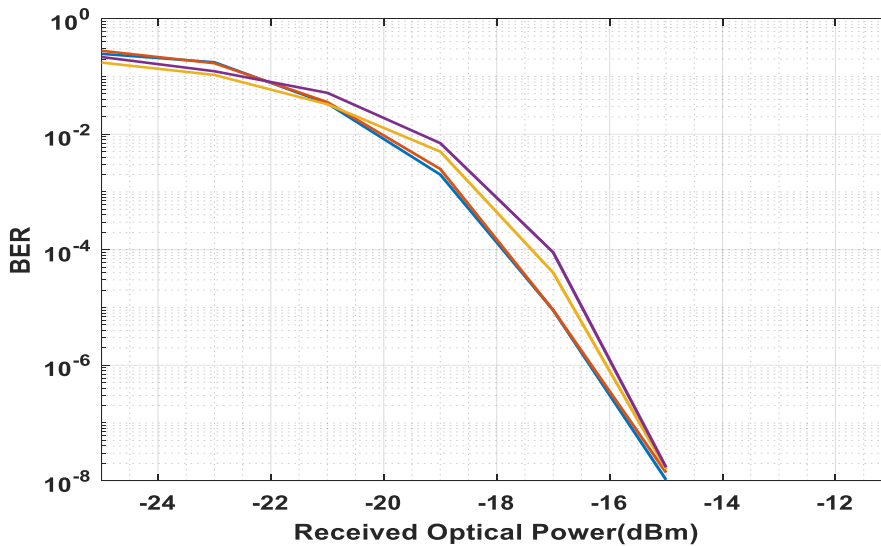
Figure 6. 4: Variations in BER values due to CRs

The performance of BER for a given signal with different CRs like 0.75, 0.5, and 0.25 is shown in Figure 6.4. The achieved BER measurements for the real CR at 0.25, 0.5, and 0.75 are 0.246, 0.217, 0.174, and 0.278, respectively, when the obtained optical power is -24dBm. The obtained values of BER are 1.71×10^{-8}, 1.59×10^{-8}, and 1.38×10^{-8} for the real, with CR values of

161

0.75, 0.5, and 0.25 if the received optical power is at -14. The suggested method obtains noticeably low BER values, as shown in Figure 6.4. Figure 6.5 displays the encryption time graph based on various OFDM-PON against the proposed GFDM-PON.
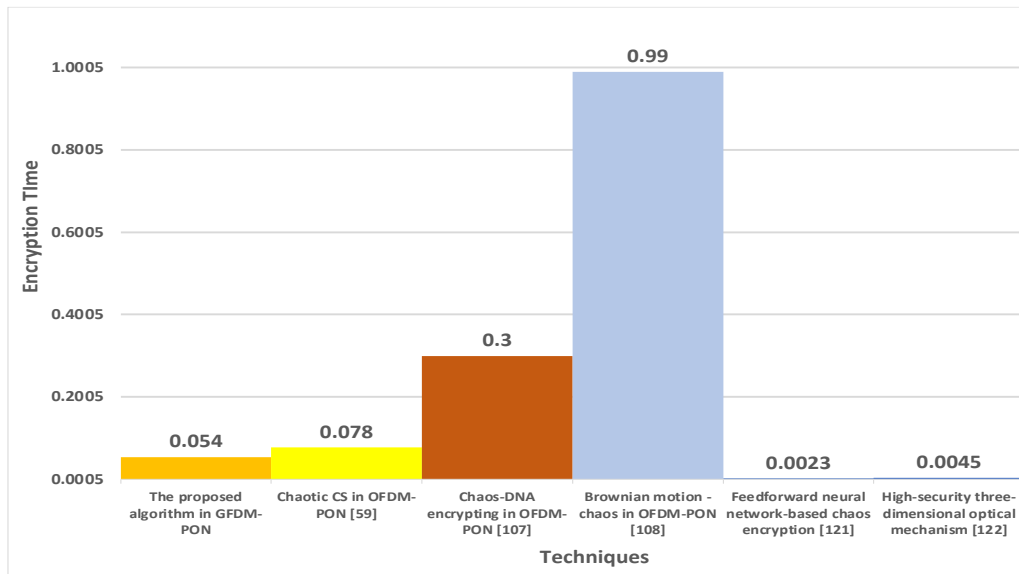

Figure 6. 5: Encryption time graph for various PON

Figure 6.5 shows the comparison graph for proposed GFDM-PON against Chaos-DNA encrypting, chaotic CS, Brownian motion-chaos, Feedforward neural network-based chaos encryption and High-security three-dimensional optical mechanism in OFDM-PONs. According to the graph, the proposed method has the lowest time for encryption, while Brownian motion and chaos take the highest time for encryption. Figure 6.6 shows the decryption time graph based on various OFDM-PON against the proposed GFDM-PON.
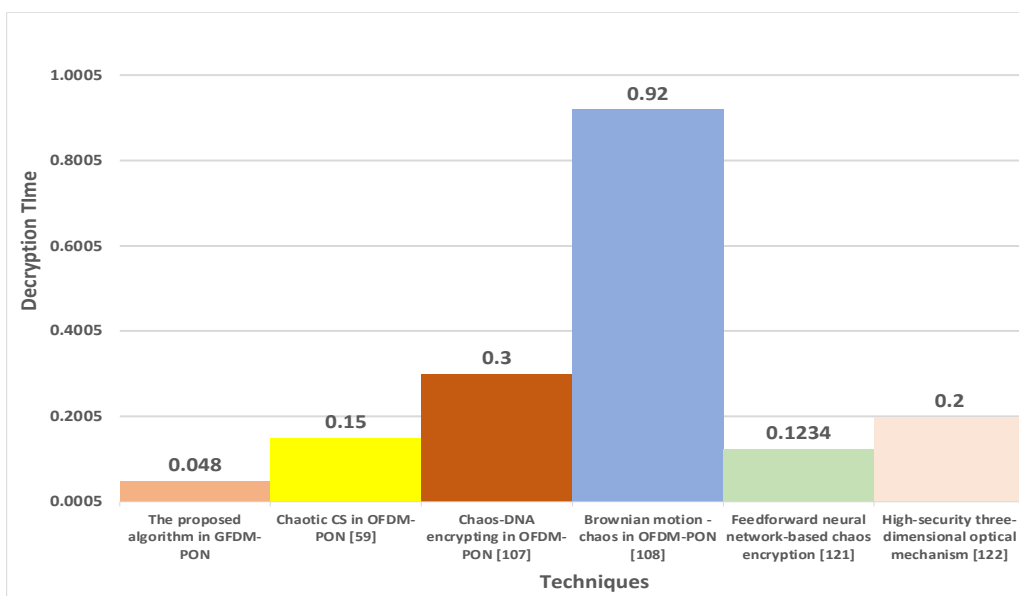

Figure 6. 6: Decryption time graph for various PON

The graphical representation of the time taken to decrypt data by various PON methods against the proposed GFDM is shown in Figure 6.6. According to the graph, the proposed takes less time than others, while Brownian motion-based OFDM-PON takes the highest time to decrypt data. Table 6.1 shows a comparison of ET and DT.

Table 6. 1 Encryption and Decryption Time Comparison

	Encryption time (s)	Decryption time (s)	Amount of data (bits)
The proposed algorithm in GFDM-PON	0.054	0.048	524288
Chaotic CS in OFDM-PON [59]	0.078	0.15	524288
Chaos-DNA encrypting in OFDM-PON [107]	0.30	0.30	524288
Brownian motion - chaos in OFDM-PON [108]	0.99	0.92	524288
Feedforward neural network-based chaos encryption [121]	0.0023	0.1234	524288
High-security three-dimensional optical mechanism [122]	0.0045	0.2000	524288

The ET and decryption times of various suggested and current systems, such as chaos and DNA encrypting, chaotic CS, and chaotic Brownian motion in OFDM-PONs, are shown in Table 6.1. If 524288 bits are regarded as a unit of data, the suggested system's ET and DT are 0.054 and 0.048, respectively. The current developed Chaos and DNA encrypting in OFDM-PON is 0.30, chaotic CS in OFDM-PON has an ET of 0.078, and earlier Brownian motion-chaos is 0.99. It also has an obtained decoding time of 0.15, realized Chaos-DNA encrypting is 0.30, and earlier Brownian motion-chaos is 0.92. Since the suggested model achieves maximum ET and DT compared to current methods, the GFDM-PON model is more efficient than the alternatives. Table 6.2 portrays the comparison in terms of performance measures.

Table 6. 2: Comparison of performance metrics among existing and proposed methods

Performance metrics	MSE	PSNR	Entropy	Decryption time	Encryption time
Proposed EOSA	0.004114	57.86319	9.495201	0.048	0.054
SOA [118]	0.008166	56.76692	9.411404	0.059	0.062
HOA [119]	0.012772	55.78557	9.401598	0.073	0.074
PSO [120]	0.015325	55.32411	9.401598	0.079	0.089

Comparing the suggested EOSA's PSNR, MSE, and entropy performance with some of the current Hive optimization algorithms (HOA), Spark optimization algorithms (SOA), and Particle Swarm Optimization (PSO) is shown in Table 6.2. It states unequivocally that the suggested EOSA outperforms the other three currently used methods in MSE, PSNR, and entropy values. The PSNR values obtained for the suggested EOSA and the current HOA, SOA, and PSO are 57.86319, 55.78557, 56.76692, and 55.32411, respectively. The suggested model gets a high PSNR value utilizing the ESOA method because maximum PSNR values result in high-quality data. Existing SOA, HOA, and PSO have achieved MSE values of 0.008166, 0.012772, and 0.015325, respectively. The obtained value is 0.004114, the lowest value compared to the suggested EOSA. This demonstrates how the suggested method improves data precision in the receiver block. The suggested approach has an entropy value of 9.495201, while the current HOA, SOA, and have 9.4015981598, 9.411404, and 9.401598, respectively. The highest entropy value of the suggested method allows for efficient encryption and decryption. The graph for PSNR is revealed in Figure 6.7.
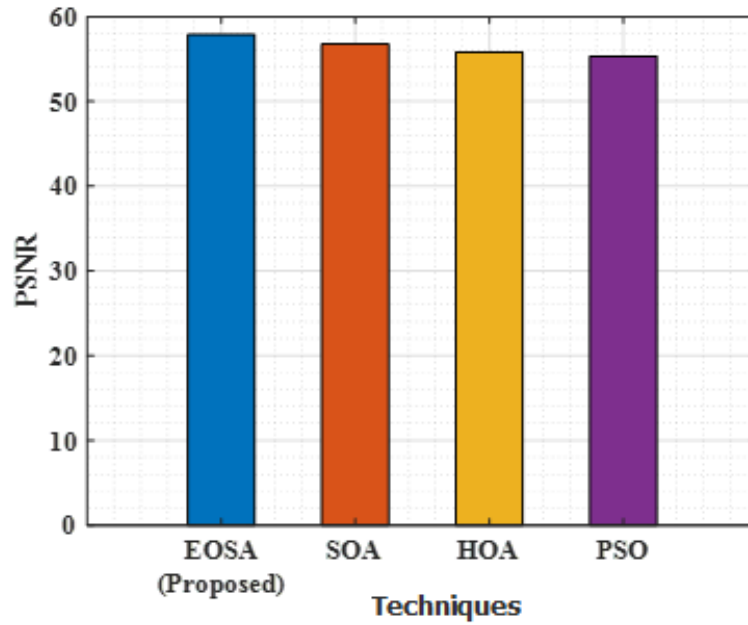
Figure 6. 7: PSNR Comparison Graph

Figure 6.7 illustrates the PSNR values of a suggested EOSA and several optimization techniques like SOA, HOA, and PSO. According to analyzing the graph, the proposed EOSA has the highest value of PSNR when compared to others, while PSO has the lowest PSNR value. Figure 6.8 shows the comparison graph in terms of MSE.
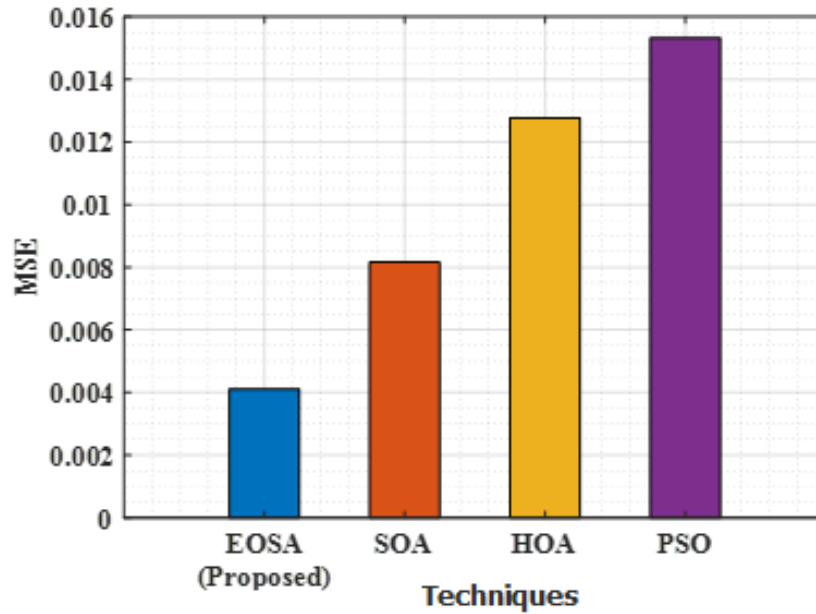

Figure 6. 8: MSE Performance Comparison Graph

The graphical representation of MSE for a proposed and existing optimization algorithm is shown in Figure 6.8. MSE for the proposed EOSA has the lowest value, while PSO has the

highest MSE value. Figure 6.9 displays the entropy comparison graph for suggested and various optimization techniques.
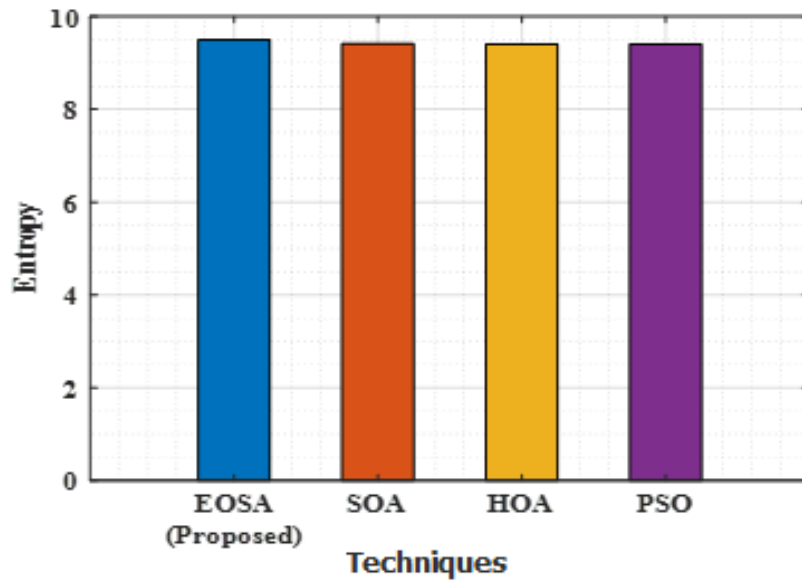
Figure 6. 9: Entropy Comparison Graph

Figure 6.9 shows the entropy comparison for suggested and existing SOA, HOA, and PSO techniques. The graph in terms of ET comparison is shown in Figure 6.5. The Entropy of a suggested method is marginally higher than others, while PSO has the lowest entropy among the existing techniques. The graph in terms of ET comparison is mentioned in Figure 6.10.
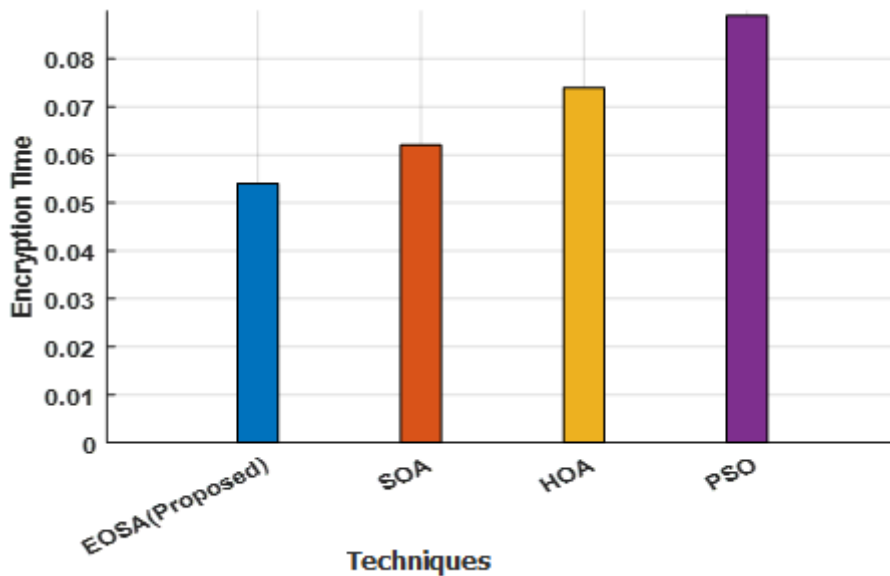
Figure 6. 10: ET Comparison Graph

Figure 6.10 shows how the proposed ET compares with other optimization methods. Compared to the current HOA, SOA, and PSO, which are 0.074, 0.062, and 0.089, the ET of a suggested

ESOA is minimal, or 0.054. Figure 6.11 demonstrates the graph of suggested and existing methods in terms of DT.
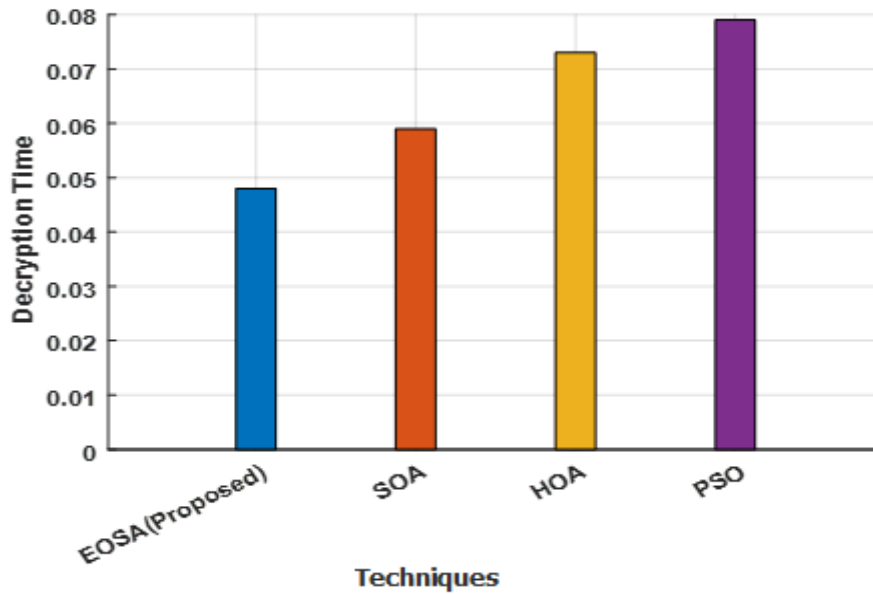
Figure 6. 11: DT Comparison Graph

Figure 6.11 also demonstrates the time essential to decode the data is 0.048, which is considerably less than the times required by the optimization methods that have already been put into place and whose obtained values are 0.059, 0.073, and 0.079. As a result, among all the compared methods, the suggested ESOA strategy is regarded as an efficient optimization algorithm. Figure 6.12 shows the graph based on a fitness function.
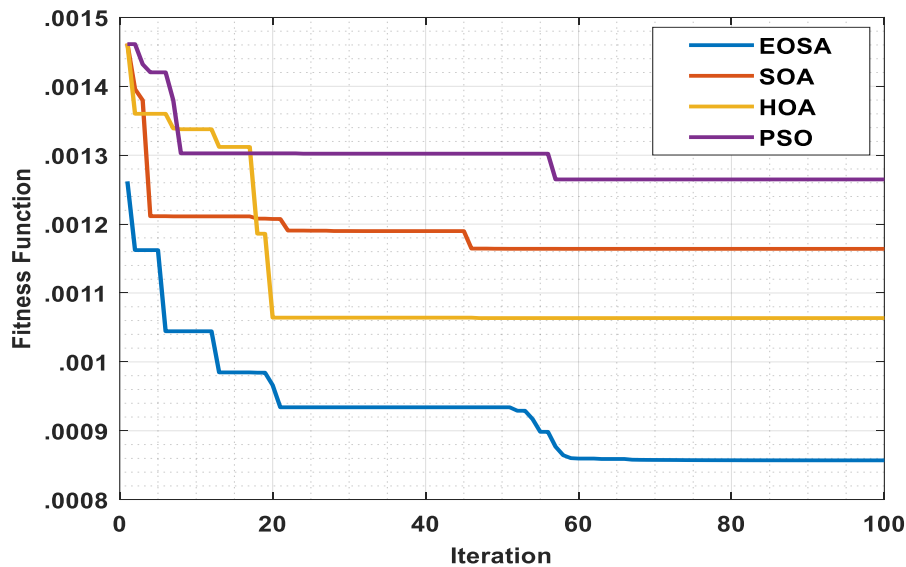
Figure 6. 12: Fitness function comparison graph

The suggested fitness function and earlier optimization methods are compared in Figure 6.12. The suggested EOSA methods accomplish the highest fitness function with the fewest iterations. However, more iterations are needed for the current SOA, HOA, and PSO to generate improved fitness functions. It makes the key selection procedure more time-consuming. However, the suggested algorithm consumes considerably less time and yields the greatest fitness value compared to other optimization algorithms.

Figures 6.13-6.15 display the measurement matrix distribution, including the initial row, initial column, and complete matrix. With various values ranging from 0-1, the suggested ESOA-GFDM signal's achieved quality is at its highest.
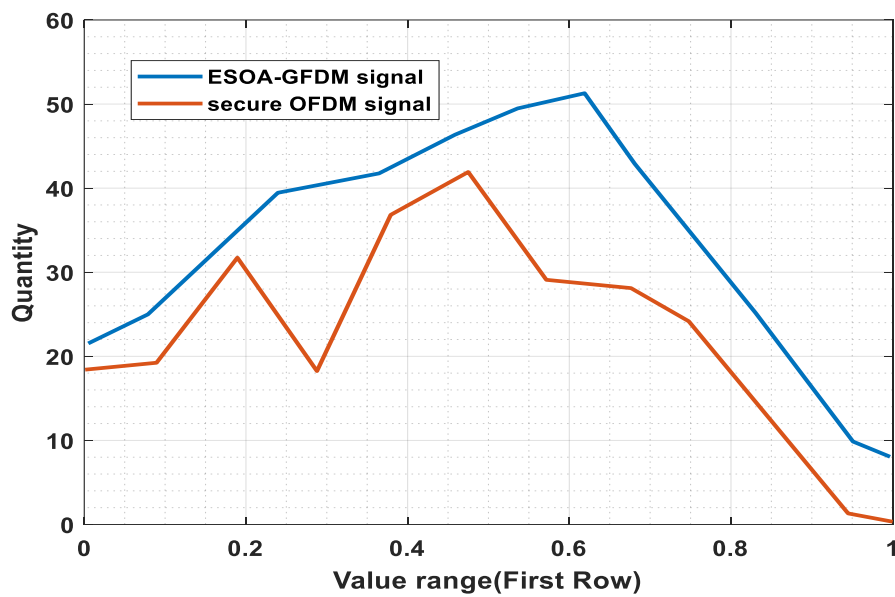
Figure 6. 13: MM distribution at the first row

The suggested approach yields a peak of 50 in the first row if the range is at 0.6, as shown in Figure 6.13. Figure 6.14 demonstrates the distribution of MM in the first column.
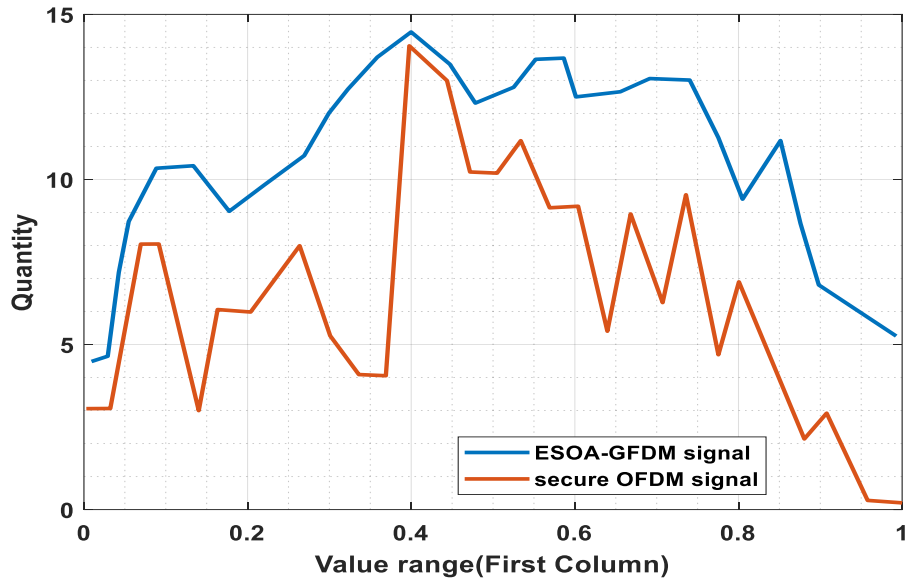
Figure 6. 14: MM distribution at the first column

In the initial column, the range of 0.4 is where the signal quality is at its highest with a quantity of 15 around. Figure 6.15 depicts the MM distribution for the full matrix for ESOA-GFDM and secure OFDM signals.
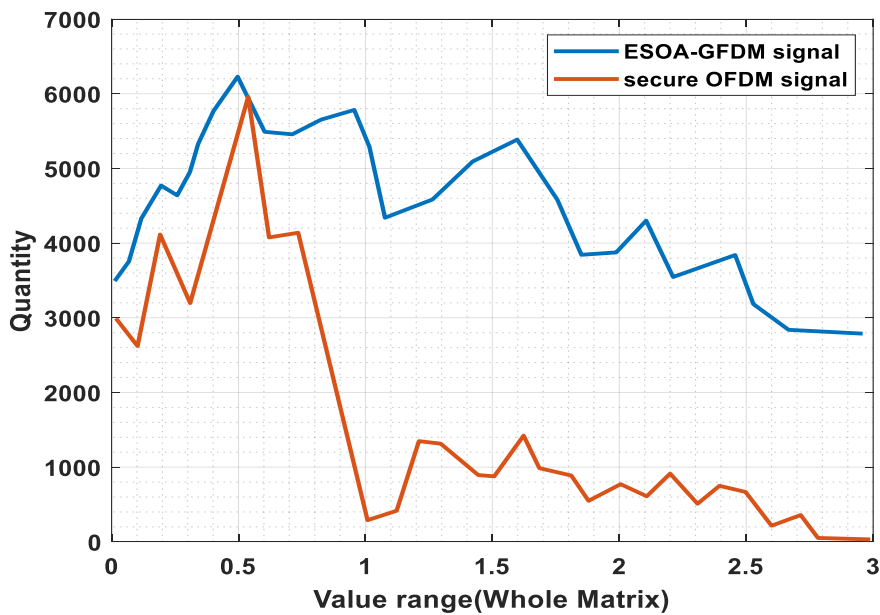
Figure 6. 15: MM distribution for full matrix

In conclusion, in the full matrix, the suggested ESOA-GFDM signal achieves a peak value at the magnitude of 0.5, and the quality of a generated signal is 6000, as shown in Figure 6.15.

The suggested ESOA-GFDM signal gets optimum quality compared to the current secure OFDM signal.

6.4 Summary

This chapter discussed how GFDM security is improved by adopting an Ebola-optimized JSCS encryption and model for symbol scrambling. This chapter clearly described each step in the proposed methodology, such as compressed sensing using SBM and MM, generation of a key using SHA-256, selection of optimal key using ESOA optimization, and scrambling of symbol using BPSK. Also, mathematical representations of these steps are provided. Additionally, the result of this methodology is provided with tabular and graphical representation for various performance metrics such as encryption and decryption time, BER, MSE, entropy, and PSNR.

CHAPTER 7

CONCLUSION AND FUTURE SCOPE

7.1 Conclusion

The first work is based on one of the technologies in the expanding 5G WC system: the MIMO-LTE RoF link. The main aim of this study is to improve the RoF Spatial Mux MIMO-LTE System's transmission performance. Each antenna in this situation broadcasts a 64-QAM, 800 GHz, 5G signal across a 70 km SSMF for dispersed applications. The MIMO system introduced bandpass sampling since it needs a lot of bandwidth to send the signal across the RoF link. Both D-RoF and A-RoF systems are considered in analyzing the suggested method's performance. Moreover, the MIMO system's transmission state is also examined. An optimization approach is also developed to further improve the bias current and power transmission in the MIMO RoF system. The D-RoF and A-RoF systems analyze performance indicators, including EVM, SNR, and EOP. The D-RoF and A-RoF in the experimental scenario had EVMs of 1.45% and 1.13%, EOPs of 51.19dB and 51dB, SNRs of 27dB and 26dB, and calculation times of 0.14s. The suggested MIMO system is a highly helpful wireless LAN network for boosting the LTE system's network performance. The RoF connection developed in this work aids in shielding data transmission from electromagnetic interference.

The second work suggests that the MIMO RoF operates the BBU while maximizing the transmission settings. The IAO method, which finds optimal standards for bias currents and provides signal power of two lasers while minimizing the nonlinear effects of the system, was used for this approach. The BBU and the RRH were separated by 10 km during the experiments, which used LTE-MIMO transmissions with various modulations and bandwidths in an IM/DD scheme. The LTE standard governs the carrier frequency and transmissions. MATLAB is used to implement the suggested system. An effective balance between noise and non-linearity may be established for a variety of bandwidths, according to experiments. It indicates that this method may discover the ideal parameters in a limited number of iterations with adequate EVM accuracy. For the QPSK and QAM modulations, the maximum EVM of approximately 1.88 and 3.14, the SNR of about 0.134 and 3.146, and the computation complexity of 0.137s for 100 iterations are reached in the experimental case. The suggested MIMO work is extremely beneficial for increasing network efficiency in both wireless LAN and LTE systems.

The third research suggests a method to enhance PON's optical generalized frequency division multiplexing (GFDM) transmission while enhancing physical layer security. The proposed chaotic compressive sensing (CS) technique aims to compress the transmitted data. Bitstream transmission utilizing CS is constrained by its failure to meet sparsity in both temporal and frequency domains. The sparseness of transmitted data might be produced when transferring multimedia. To identify data as multimedia, a sensor can be employed. If so, the sensor output is recorded as side information in the pilot and simultaneously sent to the terminal using the CS technique. During the encryption operation, the system is encrypted utilizing a 2D logistic-sine-coupling map (2D- LSCM), which creates pseudo-random variables for the first row of an MM. Hybrid Aquila-Harris hawk optimization (AHHO) with the best key selection is used for picture security. The DCT is employed to implement the CS method since data transmission is constrained at the physical layer. Using GFDM-PON systems with this chaotic CS encryption method decreases bandwidth while enhancing security. The suggested work is employed in MATLAB, and effectiveness is estimated against currently used OFDM-PON approaches. Entropy, MSE, PSNR, BER, encryption and decryption times, and others are performance indicators. To demonstrate the viability of the suggested approach, CCDF is examined.

The fourth work uses physical layer security data transfer for GFDM-PON and CS techniques. This technique mainly aims to compress and send data using the same bandwidth. Furthermore, to strengthen the suggested model's security using encryption by joint secure CS and scheme of symbol scrambling. Two chaotic DCT matrices are first employed for block-dependent CS data to serve as the basis of sparse and measurement matrices. The suggested approach achieves a higher PSNR value at a cheap computational cost. The produced BPSK signal from the CS block is then further encrypted using a chaotic sequence and sent through a wireless GFDM network. The presented model has a rather low obtained BER rating. An ideal key selection and key generation have been carried out to enhance PLS in the GFDM-PON. The optimization method utilized in this study to select the best key is the Ebola meta-heuristic approach. Finally, the GFDM-PON system's encrypted CS data is more securely sent due to the combined secure compressive sensing encryption and symbol scrambling technique.

7.2 Future scope

Future research will employ novel optimization methods to optimize the transmission parameter in terms of EVM more precisely. More emphasis will be placed on data encryption and decryption on GFDM-PON by the suggested systems. Keyless PLS has significant

benefits over traditional encryption, which has a number of real-world drawbacks. Low complexity, the lack of a requirement for key management infrastructure, the solution of the key distribution issue, and high appropriateness for contemporary dynamic communication technologies and low-power devices are a few of these.

REFERENCES

[1] Suseela V. & Mani. V. V. (2022). A survey on the integration of visible light communication with power line communication: Conception, applications and research challenges. *Optik*, 169582.

[2] Ons A., Kandaraj P. & Benoit P. (2022). Intelligent traffic management in next-generation networks. Future internet, 14(2), 44.

[3] Liam P. B., Amol D., Devika D. & Colm B. (2022). Role of analogue radio-over-fibre technology beyond 5g. In Optical Fiber Communication Conference (pp. Th1I-1). Optica Publishing Group.

[4] Muhammad U. H., Jian S., Sunish K. O. S., Ardavan R. & Adnan A. C. (2022). Experimental evaluation of hybrid fibre–wireless system for 5G networks. In *Telecom* (Vol. 3, No. 2, pp. 218-233). MDPI.

[5] Ramy R., Christi M., Samuel P. & Kamran E. (2022). A Silicon Photonics Automatically-Tunable mm-wave Remote Antenna Unit. In *2022 IEEE International Topical Meeting on Microwave Photonics (MWP)* (pp. 1-4). IEEE.

[6] Mohammed, H. A. (2022). 320 Gbps free space optic communication system deploying ultra-dense wavelength division multiplexing and polarization mode division multiplexing. *Journal of Optical Communications*, *43*(1), 137-145.

[7] Jia L., Yaqi H., Jie M., Jainfei L., Tianyi L. & Yang W. (2022). Precoding-enabled OFDM-ROF transmission system with self-pumping structure. *Optical Fiber Technology*, *73*, 103039.

[8] Fan L., Zibhin L., Mingzhu Y. & Xiaowu W. (2022). Architectures and key DSP techniques of next generation passive optical network (PON). In *2022 Optical Fiber Communications Conference and Exhibition (OFC)* (pp. 1-3). IEEE.

[9] Dinesh A., Hardeep S. S., Vinay B. & Jagdeep K. (2022). Enhanced spectrum slicing: wavelength division multiplexing approach for mitigating atmospheric attenuation in optical communication. *Optical and Quantum Electronics*, *54*(4), 258.

[10] Muhammad U. H. (2022). Practical Demonstration of 5G NR Transport Over-Fiber System with Convolutional Neural Network. In *Telecom* (Vol. 3, No. 1, pp. 103-117). MDPI.

[11] Wei X., Jing S., Sun, Furong L. & Yan Y. (2022). Reverberation Chamber Techniques for Determining the Adjacent Channel Leakage Power Ratio of Wireless Devices. *IEEE Transactions on Microwave Theory and Techniques*.

[12] Ahmed, SS., Al-Raweshidy H. & Alkhayyat A. (2022). Distributed remote antenna unit with selection-based of (RoF-IoT) paradigm: Performance improvement.

[13] Marwa M. K., Sameer A. S. L., Hadi F. H., Raed K. A. & Adnan H. A. (2021). Analyzing the BER and optical fiber length performances in OFDM RoF links. Indonesian Journal of Electrical Engineering and Computer Science, 23(3), 1501-1509.

[14] Fawziya A., Hamed. A. & Rajagopal N. (2023). The performance of millimeter-wave over fiber using electro absorption modulator and avalenche photodiode. *Optik*, *273*, 170331.

[15] Kristjan V. B., Andraz D., Matjaz V. & Bostjan B. (2022). Stabilization concept for maintaining maximum suppression of the undesired sideband in a radio-over-fiber link using a single add/drop micro-ring resonator. In *2022 International Workshop on Fiber Optics in Access Networks (FOAN)* (pp. 16-19), IEEE.

[16] Jiang Y., M. Jiao, Lei, C., Yao J., Yuan W., Gong P. & Xie L. (2022). Frequency response measurement method of photodetector based on multiple harmonics. *IEEE Photonics Technology Letters*.

[17] Wu Z., Wang Q., Hu C., Yu Z. & Wu W. (2022). Modeling and assessment of five-frequency BDS precise point positioning. *Satellite Navigation*, *3*(1), 8.

[18] Schrenk, B. & Stephanie, M. V. (2022). Reclaiming Light Dropped During Optical Modulation to Bias Avalanche Photodetectors. *Journal of Lightwave Technology*.

[19] Memon K. A., Butt R. A., Mohammadani, K. H., Das B., Ullah S., Memon S. & Noor U. A. (2020). A bibliometric analysis and visualization of passive optical network research in the last decade. *Optical Switching and Networking*, *39*, 100586.

[20] Chia-Yi W. (2022). *Frequency-synchronous distributed antenna systems enabled by sigma-delta-over-fiber for 5G and beyond* (Doctoral dissertation, Ghent University).

[21] Li W., Wenli C., Kai C., Renjun H. & Wenjian Z. (2022). The Research on the Signal Generation Method and Digital Pre-Processing Based on Time-Interleaved Digital-to-Analog Converter for Analog-to-Digital Converter Testing. *Applied Sciences*, *12*(3), 1704.

[22] Wang, R., Fan, Y., Tan, J., Shi, F., Zhai, W., Tan, Q. & Gao, Y. (2022). A linearized optical single-sideband modulation RoF link with tunable optical carrier-to-sideband ratio. *Optics Communications*, *511*, 127991.

[23] Sachin K., Gopi T., Harikeerthana, N., Munish K. G., Vidit G., Grzegorz M. K. & ChuanSong W. (2023). Machine learning techniques in additive manufacturing: a state of the art review on design, processes and production control. *Journal of Intelligent Manufacturing*, *34*(1), 21-55.

[24] Kosuke N., Hsuan Y. K., Shota I., Kazuki T. & Ryo I. (2022). Multiple beam-steering for 5G multi-user MIMO mobile fronthaul based on IFoF and RoF transmission. *Optics Continuum*, *1*(5), 1165-1175.

[25] Yegon, G. K., Waswa, D. W., Isoe, G. M., Rotich, S. K., Gibbon, T. B. & Leitch, A. W. R. (2022). Signal Transmission Performance at 1550nm Using Directly Modulated VCSEL over G. 652 and G. 655 fiber links. In *Proceedings of the Sustainable Research and Innovation Conference* (pp. 179-185).

[26] Lana L. E., Salih M. S. A. (2022). REVIEW ON RADIO OVER FIBER SYSTEMS FOR CAPACITY ENHANCEMENT. *Journal of Duhok University*, *25*(2), 482-506.

[27] Md. A. S., Khatun, Mehmuda K., Tanisa A., Antara A. P., Partha C. & Tanupriya C. (2022). Performance analysis of OFDM system on multipath fading and inter symbol interference (ISI) using AWGN. In *Computational Intelligence in Pattern Recognition: Proceedings of CIPR 2021* (pp. 25-36). Springer Singapore.

[28] Bryce M. & Dan F. (2022). Quantitative Stimulated Raman Scattering Microscopy: Promises and Pitfalls. *Annual Review of Analytical Chemistry*, *15*, 269-289.

[29] Muhammed S. A., Mustafa M. H., Bakr A. T., Ahmed S. M. & Emad M. E. (2022). Performance of Effect for XPM and FWM in Fiber Optics. In *Proceedings of International Conference on Emerging Technologies and Intelligent Systems: ICETIS 2021 Volume 2* (pp. 345-355). Springer International Publishing.

[30] Yingge C., Leonardo S., Xinyue L. & Francois L. (2022). Optically powered gas monitoring system using single-mode fibre for underground coal mines. *International Journal of Coal Science & Technology*, *9*(1), 26.

[31] Mohsin M., Imran A. T. & Pablo O. (2022). Coded-GFDM for reliable communication in underwater acoustic channels. *Sensors*, *22*(7), 2639.

[32] Prem S. & Ekant S. (2022). FBMC: A Waveform Candidate for Beyond 5G. In *A Glimpse Beyond 5G in Wireless Networks* (pp. 89-118). Cham: Springer International Publishing.

[33] Khalid H. M., Monir H., Rizwan A. B., Kamran A. M. & M. Mujtaba S. (2022). ONU migration using network coding technique in Virtual Multi-OLT PON Architecture. *Optical Fiber Technology*, *68*, 102788.

[34] Yifan Z., Choaqin G., Wei L. & Guiyu G. (2022). Design and simulation of optical network architecture based on point-to-multipoint direct communication between optical network units for data center. *Photonic Network Communications*, *44*(1), 1-9.

[35] Shahryar S., Shila K. S., Mehrdad P. & Ali R. A. (2022). Toward a Modern Last-Mile Delivery: Consequences and Obstacles of Intelligent Technology. *Applied System Innovation*, *5*(4), 82.

[36] Juan, P. H., Chueh, C. Y. & Wang, F. K. (2022). Distributed MIMO CW Radar for Locating Multiple People and Detecting Their Vital Signs. *IEEE Transactions on Microwave Theory and Techniques*.

[37] Vincenzo D. M., Claude M., Adriana M., Cosimo C., Jeoffray V., Philippe P., Marc G., Emmanuel M., Youcef O., Aziz B. & Sylvain G. (2022). Pulsed X-Ray Radiation Response of Ultralow Loss Pure-Silica-Core Optical Fibers. physica *status solidi (a)*, *219*(2), 2100519.

[38] Dongdong Z., Fan L., Wei W., Mingzhu Y. & Qi S. Zhaohui L. (2022). Modified gerchberg-saxton algorithm based electrical dispersion pre-compensation for intensity-modulation and direct-detection systems. *Journal of Lightwave Technology*, *40*(9), 2840-2849.

[39] Tehseen M., Muhammad A. M., Inayatul H., Iram R., Inam U., Muhammad A. K., Deepak A., Mohamed T. B. O. & Habeeb H. (2022). The Role of ML, AI and 5G Technology in Smart Energy and Smart Building Management. *Electronics*, *11*(23), 3960.

[40] Azhar A. S., Subhi R. M. Z., Ahmed S. A., Rizgar R. Z., Mohammed A. M. S. & Omar A. (2020). Evolution of mobile wireless communication to 5G revolution. *Technology Reports of Kansai University*, *62*(5), 2139-2151.

[41] Muhammad F., Bilal M. K., Rabia B., Rupert C.D.Y., Cory B. & Syed S. H. Z. (2020). Multibillion packet lookup for next generation networks. *Computers & Electrical Engineering*, *84*, 106612.

[42] Jianjun Y., Xinying L. & Xiaodan P. (2020). Broadband radio-over-fiber technologies for next-generation wireless systems. In *Optical Fiber Telecommunications VII* (pp. 979-1038). Academic Press.

[43] Jimmy J. N., Hervé G., Ljupco J., Kemal A., Miha S., Ziming Z., Nuno P., Michal G., Haibin Z., Urban K., Zhong F. & Ales S. (2017). Secure real-time monitoring and management of smart distribution grid using shared cellular networks. *IEEE Wireless Communications*, *24*(2), 10-17.

[44] Luiz F. F. D. A., Jose R. D. S., Luiz Ausgto M. P., Arismar C. S. JR., Luciano L. M., Joel J. P. C. R., Ricardo A. L. R. & Antonio M. A. (2020). Control Networks and smart grid teleprotection: Key aspects, technologies, protocols, and case-studies. *IEEE Access*, *8*, 174049-174079.

[45] Thiago R. R., Simon R., Bruno C., Chris V., Diego P. G., Evangelos P., Evangelos G., Konstantinos N., Michael K., Dimitrios K., Eugenio R., Izabela S., Mykhaylo D., Dimitrios K., George K., Salvador S., Nikos P. & Idelfonso T. M. (2021). Transition technologies towards 6G networks. *EURASIP Journal on Wireless Communications and Networking*, *2021*(1), 1-22.

[46] Agnese C., Aldo M. & Luigi Z. (2020). Distributed dynamic strain sensing based on brillouin scattering in optical fibers. *Sensors*, *20*(19), 5629.

[47] Kumar, S., Sharma, S. & Dahiya, S. (2021). Wdm-based 160 gbps radio over fiber system with the application of dispersion compensation fiber and fiber bragg grating. *Frontiers in Physics*, *9*, 691387.

[48] Lim, C., Nirmalathas, A., Novak, D., Waterhouse, R. & Yoffe, G. (2000). Millimeter-wave broad-band fiber-wireless system incorporating baseband data transmission over fiber and remote LO delivery. *Journal of lightwave technology*, *18*(10), 1355-1363.

[49] Paredes-Páliz, D. F., Royo, G., Aznar, F., Aldea, C. & Celma, S. (2020). Radio over fiber: an alternative broadband network technology for IoT. *Electronics*, *9*(11), 1785.

[50] Vibhakar S., D., Taneja, M. K. & Gaur, M. A. (2015). Performance Evaluation Of Bandwidth Scheduling Techniques In Passive Optical Networks. International Journal of Engineering and Computer Science, Vol. 4 No. 10 (2015).

[51] Jothi, O., Ataro, E. & Musyoki, S. (2022). Performance Evaluation of a SCM-OFDM Radio over Fiber System for the Mobile Fronthaul.

[52] Singh, M., Pottoo, S. N., Malhotra, J., Grover, A. & Aly, M. H. (2021). Millimeter-wave hybrid OFDM-MDM radio over free space optical transceiver for 5G services in desert environment. *Alexandria Engineering Journal*, *60*(5), 4275-4285.

[53] Elbir, A. M., Mishra, K. V., Shankar, M. B. & Ottersten, B. (2021). A family of deep learning architectures for channel estimation and hybrid beamforming in multi-carrier mm-wave massive MIMO. *IEEE Transactions on Cognitive Communications and Networking*, *8*(2), 642-656.

[54] Yichuan L., Salman G., Butt, Muhammad. F. U. B. & Muhammad E. (2021). Analog radio over fiber aided C-RAN: optical aided beamforming for multi-user adaptive MIMO design. *Frontiers in Communications and Networks*, *2*, 725976.

[55] M. Vinoth K. & Vinod K. (2020). Relative investigation of methods to generate millimeter wave in radio-over-fiber communication. In *Micro-Electronics and Telecommunication Engineering: Proceedings of 3rd ICMETE 2019* (pp. 567-574). Springer Singapore.

[56] Jaswinder K. & Vishal S. (2019). MIMO-OFDM-radio over fiber system incorporating higher-order space-time block codes. *Microwave and Optical Technology Letters*, *62*(1), 37-45.

[57] Anastasios V., Petros N. & Georgios P. (2020). A Hybrid Link-TDMA MAC Protocol for Conventional and Radio over Fiber WLANs. *Wireless Communications and Mobile Computing*, *2020*, 1-15.

[58] Weile Z., Aijun W. & Dongjuan S. (2020). Multidimensional optimization of a radio-over-fiber link. *IEEE Transactions on Microwave Theory and Techniques*, *69*(1), 210-221.

[59] Tingwei W., Chongfu Z., Yuhang C., Mengwei C., Huan H., Zhi Z., Heping W., Xiong Z. & Kun Q. (2021). Compressive sensing chaotic encryption algorithms for OFDM-PON data transmission. Optics express, 29(3), 3669-3684.

[60] R. Anil K. & K. Satya P. (2021). Performance analysis of GFDM modulation in heterogeneous network for 5G NR. *Wireless Personal Communications*, *116*, 2299-2319.

[61] Rizwana A. & Anand S., (2020). Optical GFDM: an improved alternative candidate for indoor visible light communication. *Photonic Network Communications*, *39*, 152-163.

[62] Siva V., Kishor V. & Ventaka V. M. (2020). Low complex implementation of GFDM system using USRP. *IET Communications*, *14*(13), 2060-2067

[63] Mohammad U. H. & Ghulam M. (2022). Fibre wireless distributed antenna systems for 5G and 6G services. *Electronics*, *12*(1), 64.

[64] Adnan H. A., Alaa D. F. & Maham K. N. (2020). Analysis of a framework implementation of the transceiver performances for integrating optical technologies and wireless LAN based on OFDM-RoF. *International Journal of Electrical and Computer Engineering*, *10*(4), 4252.

[65] Meet K., Anu S. & Reecha S. (2021). Performance analysis of a full-duplex TWDM-PON using OFDM modulation with red LED visible light communication System. *Wireless Personal Communications*, *119*, 2539-2559.

[66] Jinnan Z., Bo L., Jianxin R., Yaya M., Shuaidong C., Rong T., Xiumin S., Yu B., Xiangyu W., Feng W., Yongfeng W., Lilong Z., Tingting S. & Rahat U. (2022). High-security multi-level constellation shaping trellis-coded modulation method based on clustering mapping rules. *Optics Express*, *30*(9), 15401-15415.

[67] Mrinmoy S., Asok K. & Bansibadan M. (2021). PAPR reduction using twin symbol hybrid optimization-based PTS and multi-chaotic-DFT sequence-based encryption in CP-OFDM system. *Photonic Network Communications*, *41*, 148-162.

[68] Joarder J. S., Saifur R. S., Sheikh U., Sujoy K. J. & Masanori H. (2022). Uav-aided transceiver design for secure downlink ow-dfts-ofdm system: A multi-user mmwave application. *IEEE Access*, *10*, 34577-34590.

[69] Syamsuri Y., Rawa M. M., Zuraidah Z., Che B. M. R., Azwan M. & Siti B. A. A. (2021, May). Modulation index and phase imbalance of dual-sideband optical carrier suppression (DSB-OCS) in optical millimeter-wave system. In *Photonics* (Vol. 8, No. 5, p. 153). MDPI.

[70] Mohit B. & Manoj S. (2022). A Low Cost all Optical Photonic Technique Based on Brillouin Scattering for mm-Wave Generation. In *Journal of Physics: Conference Series* (Vol. 2327, No. 1, p. 012039). IOP Publishing.

[71] Xiaorong X., Minghang S., Wei-Ping Z., Wei F. & Yingbiao Y. (2022). Bidirectional Link Resource Allocation Strategy in GFDM-based Multiuser SWIPT Systems. *KSII Transactions on Internet and Information Systems (TIIS)*, *16*(1), 319-333.

[72] Deepthi, S. & Visalakshi, P. (2021). Enhanced Optical OFDM: A novel approach for SISO and MIMO Visible Light Communication system in indoor environment. *Optical and Quantum Electronics*, *53*, 1-24.

[73] Joarder J. S., Shaikh E. U., Md. Rabiul I., Md. Mahbubar R., Abbas Z. K. & M. A. Parvez M. (2021). Gyre precoding and t-transformation-based gfdm system for uav-aided mmtc network. *Electronics*, *10*(23), 2915.

[74] Zhiyi W., Yaoqiang X., Sitao W., Yuansiyi Y., Bingshuai W., Yating C., Zhihua Z., Jing H. & Liang Y. (2021). Probabilistic shaping based constellation encryption for physical layer security in OFDM RoF system. *Optics Express*, *29*(12), 17890-17901.

[75] Yaoqiang X., Tian X., Zhiyi W., Linrong J., Sitao W. & Jing H. (2023). Secure RoF system based on key nested polar code and feedback neural network. *Optics Express*, *31*(26), 43075-43088.

[76] Archa C. & Joseph Z. (2021). Design and analysis of full duplex RoF system with efficient phase noise cancellation from a coherent RoF system. *Journal of Optical Communications*, *44*(s1), s1395-s1408.

[77] Muhammad U. H., Muhammad Y. D., Sunish K. O. S. & Muhammad I. (2024, June). Experimental Analysis of A-RoF Based Optical Communication System for 6G O-RAN Downlink. In *2024 35th Irish Signals and Systems Conference (ISSC)* (pp. 1-6). IEEE.

[78] Shakir S. A., Hamed A. & Rajagopal N., H. & Nilavalan, R. (2024). Investigating delay of the media access control protocols for IoT-RoF using quantum entanglement. *IET Networks*.

[79] Ji W., Yun H., Shi X. & Yin, P. (2023). The Distributed Antenna System and Wireless Positioning Mechanism Based on Optimized Radio-Over-Fiber technology.

[80] Govind V. & Rajesh K. (2021). "Autocorrelation energy and aquila optimizer for MED filtering of sound signal to detect bearing defect in Francis turbine." *Measurement Science and Technology* 33, no. 1 (2021): 015006.

[81] Abdulmohsen A., Asif I. K., Fahad A., Yoosef B. A., Md M. A. & Sana Q. (2022). "Modeling of Remora Optimization with Deep Learning Enabled Heavy Metal Sorption Efficiency Prediction onto Biochar." *Chemosphere* (2022): 135065.

[82] Yang Y., Yunqiang W., Hongji Y., Mohammad K. & Mokhtar M (2022). "Nodes clustering and multi-hop routing protocol optimization using hybrid chimp optimization and hunger games search algorithms for sustainable energy efficient underwater wireless sensor networks." *Sustainable Computing: Informatics and Systems* 35 (2022): 100731.

[83] Mehdi H. A. & Abbas A. S. (2019). "PAPR reduction in OFDM systems: An efficient PTS approach based on particle swarm optimization." *ICT Express* 5, no. 3 (2019): 178-181.

[84]. Alice F, Hadi S., Hayssam D., H., Tareq Y. A. & Mohammad S. A. (2020). Ultramassive MIMO Systems at Terahertz Bands: Prospects and Challenges. *IEEE Vehicular Technology Magazine*, *15*(4), pp.33-42.

[85]. Md. F. H., Ayman U. M., Topojit D., Farjana B. M. & Khondoker Z. I. (2019). Recent research in cloud radio access network (C-RAN) for 5G cellular systems-A survey. *Journal of Network and Computer Applications*, *139*, pp.31-48.

[86]. Ping Y., Yue X., Ming X. & Shaoqian L. (2019). 6G wireless communications: Vision and potential techniques. *IEEE Network*, *33*(4), pp.70-75.

[87]. Robin C. & Robert A. (2020). Massive MIMO systems for 5G and beyond networks—overview, recent trends, challenges, and future research direction. *Sensors*, *20*(10), p.2753.

[88]. Shunliang Z., Xuejun C., Weihua Z. & Yongming W. (2019). Green 5G enabling technologies: an overview. *IET Communications*, *13*(2), pp.135-143.

[89] Mateo C., Carro P. L., Garcia-D. P., De Mingo J. & Salinas I. (2019). RoF spatialMux MIMO-LTE fronthaul system transmission parameter selection with nelder-mead optimization algorithm. *IEEE/MTT-S International Microwave Symposium-IMS*, pp. 1046-1049. IEEE.

[90] Laith A., Dalia Y., Mohamed A. E., Ahmed A. E., Mohammed A. A. A. & Amir H. G. (2021). Aquila Optimizer: A novel meta-heuristic optimization Algorithm. *Computers & Industrial Engineering*, *157*, p.107250.

[91] Sankalap A. & Satvir S. (2013). The firefly optimization algorithm: convergence analysis and parameter selection. *International Journal of Computer Applications*, *69*(3).

[92] Mehak K. & Sankalap A. (2018). Chaotic grey wolf optimization algorithm for constrained optimization problems. *Journal of computational design and engineering*, *5*(4), pp.458-472.

[93] Dervis K. & Bahriye B. (2007, June). Artificial bee colony (ABC) optimization algorithm for solving constrained optimization problems. In *International fuzzy systems association world congress* (pp. 789-798). Springer, Berlin, Heidelberg.

[94] Nyale D. & Duncan C. (2022). A Review of the Effects of Fifth-Generation Mobile Networks (5G) on the Fourth Industrial Revolution (Industry 4.0) and the Digital Transformation of Businesses. International Journal of Computer Applications Technology and Research.

[95] Shalini D., Ashish K. & Rajani S. (2022). Advanced security model for multimedia data sharing in Internet of Things. *Transactions on Emerging Telecommunications Technologies* (2022): e4621.

[96] Muhammad K. A. K., Farman A., Muhammad I., Fazal M., Faisal A., Asar A., Suliman K., Saifur R., Grzegorz P. & Adam G. (2021). Mitigation of Phase Noise and Nonlinearities for High Capacity Radio-over-Fiber Links." *Electronics* 10, no. 3 (2021): 345.

[97] Mahmoud A. H. (2022). Performance Analysis of Gigabit Passive Optical Network for the Real-Time Support of Higher Education in Somaliland, Case study: University of Hargeisa. PhD diss., 2022.

[98] Qingan D., Li Z., Huixin L., Junkai L., Xiaohan G., Xudong C., Zhenfei D., Qunying Y. & Jun L. (2022). Design and Performance Analysis of Hybrid Multidimensional OAM-DM-WDM-OFDM-PON System with High-Capacity and Long-Distance Transmission. In *Photonics*, vol. 9, no. 7, p. 448. MDPI, 2022.

[99] Snehpreet K. (2021). Comparison between RCORD Based FTTH Network & Traditional GPON Based FTTH Network.

[100] Abdulai S. (2022). Digital Orthogonal Filtering-enabled Flexible Transmission Systems and Network Architectures for Fixed and Wireless Network Convergence." PhD diss., Bangor University, 2022.

[101] Jiakai Y. (2021). Software-defined networking control for x-haul optical networks in testbed experiments and emulation. PhD diss., The University of Arizona, 2021.

[102] Kelvin C. (2021). High mobility in OFDM based wireless communication systems."(2021).

[103] Ali. A. H., Seyedali M., Hossam F., Ibrahim A., Majdi M. & Huiling C. (2019). Harris hawks optimization: Algorithm and applications. *Future generation computer systems*, *97*, pp.849-872

[104] Shuang L., Zhiyi F., Geng S. & Jin Z. (2020). A physical layer security approach based on optical beamforming for indoor visible light communication. *IEEE Communications Letters* 24, no. 10 (2020): 2109-2113.

[105] Jitendra K. S. & Narander K. (2020). Fuzzy Ant Bee Colony For Security And Resource Optimization In Cloud Computing. In 2020 5th International Conference on Computing, Communication and Security (ICCCS), pp. 1-5. IEEE, 2020.

[106] Sivanantham, E. (2020). "Neighbour Selection Framework For Security Enabled Wireless Networks Networks Using Ant Lion Optimization Approach."

[107] Zhang, Chongfu, Wei Z., Chen C., Xiujun H. & Kun Q. (2018). "Physical-enhanced secure strategy for OFDMA-PON using chaos and deoxyribonucleic acid encoding." Journal of Lightwave Technology 36, no. 9 (2018): 1706-1712.

[108] Tingwei W., Chongfu Z., Chen C., Haodong H., Hanhan W., Shaohua H. & Kun Q. (2018). Security enhancement for OFDM-PON using Brownian motion and chaos in cell. Optics express 26, no. 18 (2018): 22857-22865.

[109] Hongqing H. & Lin Z. (2020). Secure Radio Frequency DCS Watermark-Aided Physical Layer Authentication Design for NB-IoT Systems. In *International Conference on Security and Privacy in Digital Economy*, pp. 33-49. Springer, Singapore, 2020.

[110] Jin H. P., Shailendra R., Sushil K. S., Mikail M. S., Abir E. A., Tae W. K., Yi P. & Jong H. P. (2021). A comprehensive survey on core technologies and services for 5G security: Taxonomies, issues, and solutions. *Hum.-Centric Comput. Inf. Sci* 11, no. 3 (2021).

[111] Kholoud Y. N., Mohammed A. A., Mehedi M., N. Z. J., Jehad A. & Mohammed B. (2021). A survey on security threats and countermeasures in IoT to achieve users confidentiality and reliability. *Materials Today: Proceedings* (2021).

[112] Zhenlong M., Jinqing L., Xiaoqiang D., Yaohui S. & Zefei L. (2021). Double image encryption algorithm based on neural network and chaos. *Chaos, Solitons & Fractals* 152 (2021): 111318.

[113] Fantin I.R.E. & Appadurai M. (2022). Internet of things-based smart transportation system for smart cities. In *Intelligent Systems for Social Good: Theory and Practice*, pp. 39-50. Singapore: Springer Nature Singapore, 2022.

[114] Muddasar N., Giuseppe D. P. & Antonio C. (2021). Application of reinforcement learning and deep learning in multiple-input and multiple-output (MIMO) systems." *Sensors* 22, no. 1 (2021): 309.

[115] Chaitanya B. (2021). Enhanced method to reduce papr in MiMo-OFDM system using STBC-DPC/THP." PhD Diss., Andhra University, 2021.

[116] Mohammed J. M. A. & Saad S. H. (2022). Securing Physical Layer of 5G Wireless Network System over GFDM Using Linear Precoding Algorithm for Massive MIMO and Hyperchaotic QR-Decomposition. International Journal of Intelligent Engineering and Systems 15(5):579-591, 2022.

[117] Mohammed S. A., Chatti S., T. V. R., Piyush K. S., Surendra K. S., Papiya D. & Musah A (2022). 5G-Telecommunication Allocation Network Using IoT Enabled Improved Machine Learning Technique. *Wireless Communications and Mobile Computing* 2022 (2022).

[118] H. Yu (2021). Apriori algorithm optimization based on Spark platform under big data. Microprocessors and Microsystems vol. 80, pp. 103528, 2021.

[119] Yao L., Xuening C., Yuezhen Z., Shuo D., Jianmai S. & Zhing L. (2021). HIVE: Route Optimization Problem of Automatic Delivery System with Mobile Depot and Multiple Drones. In 2021 IEEE 23rd Int Conf on High Performance Computing & Communications; 7th Int Conf on Data Science & Systems; 19th Int Conf on Smart City; 7th Int Conf on Dependability in Sensor, Cloud & Big Data Systems & Application (HPCC/DSS/SmartCity/DependSys), pp. 1338-1345, 2021.

[120] Feng W., Heng Z. & Aimin Z. (2021). A particle swarm optimization algorithm for mixed-variable optimization problems. Swarm and Evolutionary Computation vol. 60, pp. 100808, 2021.

[121] Ling X., Xi F., Yang Z., Zifang Y. & Ding D. (2022). Feedforward Neural Network-Based Chaos Encryption Method for Polarization Division Multiplexing Optical Ofdm/Oqam System. SSRN Electronic Journal, 2022.

[122] Jie C., Bo L., Jianxin R., Yaya M., Xiangyu W., Shuaidong C., Linong Z., Ying L., Zeqian G., Shuyu Z., Dongdong X., Lei J. & Juntao Z. (2023). High-security three-dimensional optical transmission mechanism utilizing time-frequency-space interleaving disruption. Optics Express, vol. 31, no. 23, pp. 38640–38640, Oct. 2023.